BATHYMETRIC AND SUBSTRATE CONTROLS ON SUBMARINE MASS-TRANSPORT EMPLACEMENT PROCESSES AND CHANNEL-LEVEE COMPLEX EVOLUTION

Andrea Lucía Ortiz Karpf

Submitted in accordance with the requirements for the degree of

Doctor of Philosophy

The University of Leeds

School of Earth and Environment

September 2016

The candidate confirms that the work submitted is her own, except where work which has formed part of jointly-authored publications has been included. The contribution of the candidate and the other authors to this work is explicitly indicated below. The candidate confirms that appropriate credit has been given within the thesis where reference has been made to the work of others.

The work in Chapter 5 was published on of the 2nd of August, 2016. The version in Chapter 5 has been slightly modified from the published version following the external examiner's comments.

Ortiz-Karpf, A., Hodgson, D. M., Jackson, C. A.-L., McCaffrey, W. D. (2016). Mass-Transport Complexes as Markers of Deep-Water Fold-and-Thrust Belt Evolution: Insights from the Southern Magdalena Fan, Offshore Colombia. *Basin Research*, p. 1-24, doi:10.1111/bre.12208

As the primary author, I was responsible for seismic mapping, analysis and interpretation, and writing of the manuscript. The contribution of the other authors was limited to discussion on the data and editorial suggestions.

In August 2016, the work in Chapter 6 was accepted for publication the Journal of Sedimentary Research pending major revisions. The reviewer's suggestions have not been incorporated into the version in Chapter 6.

As the primary author, I was responsible for seismic mapping, analysis and interpretation, and writing of the manuscript. The contribution of the other authors was limited to discussion on the data and editorial suggestions.

The work in Chapter 7 of the thesis was published as follows:

Ortiz-Karpf, A., Hodgson, D.M., McCaffrey, W.D. (2015). The role of mass-transport complexes in controlling channel avulsion and the subsequent sediment dispersal patterns on an active margin: the Magdalena Fan, offshore Colombia. *Marine and Petroleum Geology*, v. 64, p. 58–75.

As the primary author, I was responsible for seismic mapping, analysis and interpretation, and writing of the manuscript. The contribution of the other authors was limited to discussion on the data and editorial suggestions.

This copy has been supplied on the understanding that it is copyright material and that no quotation from the thesis may be published without proper acknowledgement.

The right of Andrea Lucía Ortiz-Karpf to be identified as Author of this work has been asserted by her in accordance with the Copyright, Designs and Patents Act 1988.

© 2016 The University of Leeds and Andrea Lucía Ortiz-Karpf.

ACKNOWLEDGEMENTS

This thesis is dedicated to Juan Carlos Mendoza:
Thank you for making this possible.

I would like to thank my supervisor Dave Hodgson for the guidance and all the interesting discussions, but above all, for being an amazing person; I couldn't have landed in better hands and this wouldn't have been possible without your trust and support. I thank Bill McCaffrey for all the inspirational discussions, it was a privilege to listen to (and try to absorb) your knowledge and experience, and drink your fabulous coffee. I also thank Chris Jackson for the constructive and honest feedback which helped to considerably improve the manuscripts, you're a natural!

I would also like to thank Jaime Castillo, Jaime Martinez and Orlando Otálora for going through all the administrative procedures to provide me with the seismic data, you saved me. I also thank Equión-Energía Limited, Shell, Ecopetrol and Petrobras for allowing me to use the data and Colciencias for providing the funding for the first two years of my PhD.

To the Brazilians: Thank you for being our family in Leeds. Things would have been a lot harder and lonelier without you.

To Natalia Rendón and Natalia Angarita: Thank you for being my guardian angels, I feel so lucky to have such amazing and unconditional friends.

To my friends from the Spanish Playgroup: Thanks for all the support, for listening and sympathising and for making things a lot easier to figure out.

To Aurélia, Catherine, Cathey, Hannah, Janet, Luz, Menno, Michelle, Miquel, Riccardo, Sarah, Menno and Yvonne: thank for making me believe that I am actually a super-woman. We've had great times together and you will always be in my heart. I wish you the best in the next phase and hope you that you all become very happy grown-ups.

Thanks to Pato and Caro for your hospitality in London; special thanks to Pato for being my 24/7 Petrel-emergency help line! To Pedro, for leading the way and for being an excellent conference buddy.

Thanks to my mum who still comes to the rescue every time she is needed and to Tío Mono for his love and generosity.

To Joaquín and Lucas: you are my greatest motivation; thank you for making it all better with a smile.

ABSTRACT

Mass-transport complexes (MTCs) can significantly modify the seascape by eroding the substrate and depositing thick hetherolithic packages that can behave as hydrocarbon seals or reservoirs. MTC erosion can affect the integrity of underlying reservoir units, and affect subsequent sediment dispersal. Moreover, the irregular seabed profiles resulting from MTC erosion and emplacement can affect the distribution and architecture of subsequent sediments. This study uses a 1900 km^2 3D seismic volume from the southern Magdalena Fan, offshore Colombia to investigate: i) the relationship between changes in the size, distribution and provenance of the MTCs and the evolution of tectonic structures; ii) the relationship between and the distribution of MTCs, the geometries of their basal erosion surfaces and their internal characteristics, with the morphology and composition of the seabed, and iii) the effects of MTC-related bathymetric irregularities on the architecture and development of channel-levee complex sets and avulsion lobes.

The size, distribution and provenance of MTCs changed through time with the oldest MTCs being smaller (9-100 km^2 in area) and sourced and from local collapse of the growing anticlines. Younger MTCs are larger (more than 200-300 km^2) and sourced from the shelf, postdating the main phase of folding and faulting in the study area. These changes were used to propose a model of the tectono-stratigraphic evolution of the study area, demonstrating that MTCs can be used to constrain the timing and style of tectonic deformation in time and space. Additionally, the local morphology of the MTC basal surfaces reflects compositional changes in the underlying units, with deeper erosion occurring above channel axes deposits and more subtle slope changes across different levee units. MTC dispersal was influenced by a combination of structural and depositional relief: channel-levee complex sets channelized, diverted or blocked the subsequent mass-flows depending on the orientation of the channel-levee complex sets with respect to the direction of the flow, and the height of the levees with respect to flow thickness. Within the largest MTC, the distribution of the seismic facies was influenced by the underlying bathymetry, with internal contraction occurring updip of bathymetric highs, erosion and bypass above higher gradient slopes, and increased disaggregation towards the margins. Moreover, MTC erosion left behind an erosional remnant ridge upon which a younger channel-levee complex-set developed irregular levee geometries that led to levee collapse and channel avulsion. Map-view geometries and seismic-amplitude extractions suggest that the initial avulsion lobes were mud-prone and evolved

to form sand-prone lobes. The distribution, morphology and evolution of the avulsion lobe complexes were influenced by megaclasts protruding on the MTC top surface.

This study demonstrates that: i) the architecture, geometries and distribution of MTCs, channel-levee complex sets and avulsion lobes are strongly influenced by bathymetric irregularities on the seabed at various scales; ii) flow-pathways, geometries, distribution and internal characteristics of MTCs can be affected by the properties of the substrate; iii) the stratigraphic evolution of the Magdalena Fan is characterised by the interaction between MTCs and channel-levee complex sets. The learnings from this study can be applied to deeper intervals that are less well imaged and to other margins dominated by MTCs and channel-levee complex sets.

TABLE OF CONTENTS

ACKNOWLEDGEMENTS ii

ABSTRACT iii

1 **Introduction** 1

1.1 Rationale 1

1.2 Data and Study area 4

1.3 Research Questions 6

1.4 Thesis Outline 10

2 **Submarine Slope Systems** 13

2.1 Slope Depositional Systems 13

2.2 Processes and Products 14

2.2.1 Submarine Sediment Gravity Flows 14

2.3 Depositional Elements on the slope. 22

2.3.1 Mass-Transport Complexes. 22

2.3.2 Submarine Channels 28

2.3.3 Avulsions Lobes. 33

2.4 Types of Continental Slope Profiles and Bathymetric Controls on Slope Sedimentation. 35

3 **Regional Setting** 42

3.1 Tectonic Setting. 42

3.2 Stratigraphy 46

3.2.1 Basement 46

3.2.2 Upper Cretaceous-Palaeocene 46

3.2.3 Palaeocene-Lower Eocene 48

3.2.4 Mid-Eocene-Mid-Oligocene 49

3.2.5 Late Oligocene-Late Miocene 49

3.2.6 Late Miocene-Recent 50

3.3 The Magdalena Fan 51

4 **Methodology** 59

4.1 Framework mapping 59

4.2 Seismic Facies 59

4.2.1 General seismic facies 60

4.2.2 MTC seismic facies association 64

4.2.3 Kinematic Indicators 67

4.2.4 Definition of Seismic Units 70

5 **Mass-Transport Complexes as Markers of Deep-Water Fold-and-Thrust Belt Evolution: Insights from the Southern Magdalena Fan, Offshore Colombia** 71

5.1 Introduction 71

5.2 Regional Setting 74

5.3 Data and Methods 74

5.4 Structural Elements ..... **Error! Bookmark not defined.**

5.5 Seismic Stratigraphy 80

5.5.1 Southern Region 82

5.5.2 Central Region 88

5.5.3 Northern Region 92

5.6 Interpretation..... 95

5.6.1 MTC provenance and timing of emplacement.....**Error! Bookmark not defined.**

5.6.2 Tectono-stratigraphic Evolution 98

5.7 Discussion 101

5.7.1 Changes in MTC distribution, source and size in response to structural uplift 101

5.7.2 Evolution and chronostratigraphic significance of MTC basal surfaces. 103

5.8 Conclusions 105

6 **Influence of Seabed Morphology and Substrate Composition on Mass-Transport Flow Processes And Pathways** 106

6.1 Introduction 106

6.2 Data 107

6.3 Geological Setting 107

6.4 Methodology 110

6.5 Seismic stratigraphy 111

6.5.1 Pre-MTC Stratigraphy 111

6.5.2 MTCs 117

6.6 Discussion 128

6.6.1 Substrate and Bathymetric Controls on Flow Pathways and Deposit Geometry .. ……128

6.6.2 Substrate and Bathymetric Controls on the Distribution of the Seismic Facies of C1..... **Error! Bookmark not defined.**

6.7 Implications of Flow-Seabed Interactions 137

6.8 Conclusions 140

7 **The Role of Mass-Transport Complexes in Controlling Channel Avulsion and the Subsequent Sediment Dispersal Patterns on an Active Margin: the Magdalena Fan, Offshore Colombia**…. 142

7.1 Introduction 142

7.2 Geological setting 143

7.3 Study area and data 146

7.4 Seismic units 147

7.4.1 Seismic Unit A: Channel-levee complex-set (CLC) 1 150

7.4.2 Seismic Unit B: Erosional remnant 150

7.4.3 Seismic Unit C: Channel-levee complex-set (CLC) 2 152

7.4.4 Seismic Unit D: MTC 153

7.4.5 Seismic Unit E: Channel-levee complex-set (CLC) 3 157

7.4.6 Seismic Unit F: Avulsion Lobes 160

7.4.7 Seismic Unit G: Channel-levee complex-set (CLC) 4..... **Error! Bookmark not defined.**

7.5 Discussion ..... **Error! Bookmark not defined.**

7.5.1 Possible causes for shelf/slope instability: **Error! Bookmark not defined.**

7.5.2 Channel avulsion 165

7.5.3 Evolution of the avulsion lobe complex-set 168

7.5.4 Implications 172

7.6 Conclusions 173

8 **Discussion and Conclusions** 175

8.1 How does seabed bathymetry influence the emplacement processes and architecture of MTCs, channel-levee complex sets and avulsion lobes? 175

8.1.1 Bathymetric Effects on Channel-levee Complex Sets and Avulsion Lobes. 175

8.1.2 MTCs 178

8.2 How can MTC emplacement influence the evolution of subsequent deep-water systems? 182

8.3 How does substrate composition influence the evolution, facies and geometries of MTCs? 184

8.4 How can MTCs be used as a record of the style and timing of dynamic seabed deformation? 188

8.5 Interaction of Controls 190

8.6 Recommendations for Future Work 191

8.6.1 MTCs as markers of seabed deformation 191

8.6.2 Relationship between MTC-related relief and channel avulsions 191

8.6.3 Relationship between bathymetry and substrate heterogeneities with the internal characteristics of MTCs 191

8.6.4 Detailed Architecture and Evolution of the Channel-levee Complex-Sets. 192

9 **LIST OF REFERENCES** 193

APPENDIX A: Quantitative Seismic Facies Analysis 220

LIST OF FIGURES

Figure 1.1. Location of the study area……5

Figure 2.1 Spectrum of gravity flows and deposit types……15

Figure 2.2. Mass-flows……17

Figure 2.3. Outcrop examples of slumps and debrites……19

Figure 2.4. Turbidity current structure and overspill……... 20

Figure 2.5. Facies associations of low density and high density turbidites……22

Figure 2.6. Examples of the seismic character of MTCs……25

Figure 2.7. Schematic representation of the characteristic domains and features of MTCs……..……28

Figure 2.8. Hierarchical definition of channel-levee complexes and channel-levee complex sets……..……30

Figure 2.9. Architecture of channel-levee complex sets……31

Figure 2.10. Attribute extractions of channel-levee complexes in East Kalimantan, Indonesia……34

Figure 2.11. Seabed profile from the Gulf of Mexico showing different types of accommodation on non-graded slopes……..37

Figure 2.12. Examples of the interaction between submarine channels and structurally-deformed slopes……...……39

Figure 2.13. Variations in external levee geometry depending on the relative timing between deformation and sedimentation……...……40

Figure 3.1. Main physiographic and tectonic features of the Caribbean region……..43

Figure 3.2. Compilation of images from published studies showing variations in the tectonic and depositional styles along the Sinú Fold Belt ……....44

Figure 3.3. Chronostratigraphic chart……47

Figure 3.4. Map showing the key structural elements and drainage systems of northern Colombia……52

Figure 3.5. Pleistocene-Holocene evolution of the Magdalena Fan…….....53

Figure 3.6. Characteristics of the Magdalena fan basinwards of the continental slope……54

Figure 4.1. Seismic facies composing channel-levee complex sets……61

Figure 4.2. Examples of facies 4 and 5……62

Figure 4.3. Example of seismic facies 6……63

Figure 4.4. Examples of MTC facies 1 and 5……65

Figure 4.5. Examples of MTC facies 2 and 3……65

Figure 4.6. Example of MTC seismic facies 4……..66

Figure 4.7. Example of large folded megaclasts……..67

Figure 4.8. Example of the morphology of lateral scarps and their relationship with flow direction.……...……..68

Figure 4.9. Examples of grooves on the basal surface of an MTC……...69

Figure 5.1. Location and tectonic setting……..75

Figure 5.2. Subregional structural setting……77

Figure 5.3. Structural elements……...79

Figure 5.4. MTC Regions……81

Figure 5.5.Maps showing the areal distribution, morphology and seismic facies of MTCs S1-S6……...85

Figure 5.6. MTCs S1-S4……..86

Figure 5.7. MTC S5……..87

Figure 5.8. MTCs S4 and S6……...88

Figure 5.9. MTC C1……..90

Figure 5.10. MTCs underlying C1……91

Figure 5.11. MTCs N1 and N2……94

Figure 5.12. Summary of interpreted chronostratigraphy and provenance……..…..97

Figure 5.13. Schematic representation of the tectono-stratigraphic evolution……..100

Figure 6.1. Geological setting……...108

Figure 6.2. Structural elements……109

Figure 6.3. Substrate Map……115

Figure 6.4.Seismic cross sections showing the morphology of the basal surfaces and the configuration of the substrate……..……116

Figure 6.5 MTCs in the study area……...118

Figure 6.6. Bounding surfaces of C1……...120

Figure 6.7. Downdip changes in the morphology of C1……123

Figure 6.8. Thickness and variance maps of C1……124

Figure 6.9. Uninterpreted and interpreted sections along the centre of C1…….....125

Figure 6.10. Seismic cross-sections showing examples of the seismic facies in C1..126

Figure 6.11. Grooves at the base of C1……...128

Figure 6.12. Types of interactions between MTCs and channel-levee complex sets..133

Figure 6.13. Distribution of megaclasts with respect to the grooves on the basal surface of C1……...135

Figure 7.1. General location and tectonic setting of the study area……144

Figure 7.2. Subregional setting and study area…….....145

Figure 7.3. Areal distribution of seismic units……151

Figure 7.4. Seismic units……152

Figure 7.5. Architecture of the MTC in Unit D……....154

Figure 7.6. Characteristics of the MTC in Unit D……...155

Figure 7.7. Megaclasts protruding on the MTC top surface……156

Figure 7.8. Down-flow changes in architecture through the middle reach of CLC3….158

Figure 7.9. Down-flow changes in architecture through the lower reach of CLC3…...159

Figure 7.10. Seismic line to indicate the stratigraphy of the avulsion lobe deposits that overlie CLC3……....161

Figure 7.11. North-facing perspective views of RMS amplitude extractions of Unit F.162

Figure 7.12. Changes in the response of CLC4 to the underlying bathymetric anomalies……..164

Figure 7.13. Schematic line drawings summarising the evolution of the CLC3 levee collapse and the initiation of avulsion……...168

Figure 7.14. Cartoon highlighting the interaction between the avulsion lobe deposits and the underlying bathymetric anomalies……..171

Figure 8.1. Channel location and evolution in the study area……...177

Figure 8.2. Schematic diagram illustrating the effect of substrate composition on mass-flow emplacement processes and the distribution, geometries and characteristics of the resulting deposits……...187

Figure 8.3. Influence of the interaction between gravity flows and the underlying seabed on the resulting deposits……..190

Figure A.1. Pseudo-horizons in MTC C1 used to compute interval attribute extractions. ……..220

Figure A.2. Polygons subdivided by equally-spaced lines in in which attribute values were extracted every 100 m……..…....221

Figure A.3. Ternary diagrams showing normalised values of variance, RMS amplitude and dip for facies 1, 2 and 3. …..……..221

LIST OF TABLES

Table 5.1. MTC seismic facies……78

Table 5.2. Summary table showing the main characteristics of the MTCs and their classification……...82

Table 6.1. MTC seismic facies classification……..112

Table 7.1. Seismic facies classification……...149

1 Introduction

1.1 Rationale

Sediment gravity flows are the main mechanism of sediment transport from the continental shelf to deep-ocean basins, and deposit large volumes of sediment on the continental slope (e.g. Booth et al., 2003; Prather, 2003; Steffens et al., 2003; Mayall et al., 2010; Talling et al., 2012; Talling, 2014). Turbidity currents and mass-flows are a hazard to near-shore and submarine infrastructure and to coastal communities (Barley, 1999; Piper et al., 1999; Masson et al., 2006; Hsu et al., 2008; Romero-Otero, 2009; Talling, 2014). Turbidity currents deposit sand that can form valuable hydrocarbon reservoirs (Weimer and Pettingill, 2007). Mass-transport complexes (MTCs), the product of mass-flows, can act as seals to hydrocarbon reservoirs or less commonly, as reservoirs in their own right (e.g. Gamboa et al., 2010; Omosanya and Alves, 2013; Alves et al., 2014). Due to their erosive power, mass-flows can significantly modify the seascape, controlling subsequent sediment-dispersal patterns and affecting the presence and continuity of underlying reservoirs (Masson et al., 1997; Prior et al., 1984; Gee et al., 2006; Heniö and Davies, 2006; Lamarche, 2008; Alves and Cartwright, 2009; Morley, 2009; Joanne et al., 2013).

The main conduit of turbidity currents are submarine channel-levees systems, which have been studied in depth. Outcrop studies of exhumed systems provide detailed knowledge of the main sedimentological characteristics and depositional processes of channel-fills and levee successions (e.g. Mutti, 1992; Cronin et al., 2000; McCaffrey et al., 2002; Kane et al., 2007; Kane and Hodgson, 2011; Hodgson et al., 2011; Hubbard et al. 2014). Experimental studies provide important insights into the dynamic behaviour of channelized turbidity currents (e.g. Keevil et al., 2006, 2007; Kane et al., 2008; Straub et al., 2008; Janocko et al., 2013), and modern systems and three-dimensional seismic

interpretation contribute to our understanding of their morphology, large-scale architectures, and stacking patterns (e.g. Abreu et al., 2003; Deptuck et al., 2003, 2007; Posamentier and Kolla, 2003; Mayall, et al., 2006, 2010; Cross et al., 2009; Maier et al., 2011; Covault et al., 2014; Jobe et al., 2015). MTCs have been comparatively less-studied; outcrop and core studies have provided insights into their sedimentological structure and depositional processes (e.g. Jones, 1939; Woodcock, 1976; Farrell, 1984; Elliot and Williams, 1988; López-Gamundí, 1993; Shanmugam et al., 1994; Draganits et al., 2008; Strachan et al., 2008; Tripsanas et al., 2008; Armitage et al., 2009; Van der Merwe et al., 2011; Alves and Lourenço, 2010; Buttler and McCaffrey, 2010, Eggenhuisen et al., 2010; Dykstra et al., 2011; Festa, 2015; Gamboa and Alves, 2015; Sobiesiak et al., 2016). Experimental studies have contributed to our understanding of the dynamic evolution of submarine mass-flows (e.g. Mohrig et al., 1999; Marr et al., 2001; Ilstad et al., 2004; Elverhøi, 2005), and studies based on bathymetric surveys and 3D seismic have significantly increased our knowledge of the geometries and internal configurations of MTCs (e.g. McAdoo et al., 2000; Frey-Martinez et al., 2005, 2006; Moscardelli et al., 2006; Bull et al., 2009; Posamentier and Martinsen, 2008; Alves, 2010; Romero-Otero et al., 2010; Gamboa et al., 2011; Omosanya and Alves, 2014; Scarselli et al., 2013; Alves et al., 2014).

The effects of bathymetry on sediment gravity flows have been widely recognised and extensively studied on submarine channels and intraslope lobes (e.g. Clark and Pickering, 1996; Haughton, 2000; Booth et al., 2003; Prather, 2003; Gee and Gawthorpe, 2006; Heniö and Davies, 2006, 2007; Clark and Cartwright, 2009, 2011, Kane et al., 2010; Mayall et al., 2010; Vinnels et al., 2010; Jones et al., 2012; Jolly, 2014; Spychala et al., 2015). These studies are mostly focused on the effect of large-scale bathymetric perturbations such as tectonic and gravity-driven structures and diapirs. Only few studies consider the effect of more subtle erosional and depositional geometries, with most concentrating on the effects of MTC-related bathymetric irregularities on overlying

turbidites (e.g. Brami et al., 2000; Gee et al., 2007b; Moscardelli et al., 2006; Jackson and Johnson, 2009; Alves, 2010; Alves and Cartwright, 2010; Clark and Cartwright 2011, 2012; Dykstra et al. 2011; Olafiranye et al., 2013; Alfaro and Holz, 2014; Kneller et al., 2015).

Bathymetric effects on MTCs, although recognised in several studies (e.g. Frey-Martinez et al., 2006; Moscardelli et al., 2006; Gamboa et al., 2010; Vinnels et al., 2010; Clark and Cartwright, 2012; Jones et al., 2012; Alves et al., 2014b; Dalla Valle et al., 2015) have not been explicitly studied. Previous studies have documented the effect of large-scale structures and diapirs on the sediment-flow pathways and distribution of MTCs (e.g. Pickering and Corregidor, 2005; Heniö and Davies, 2006, Moscardelli et al., 2006; Gee et al., 2007b; Morley, 2009; Romero-Otero et al., 2010; Clark and Cartwright, 2012; Vinnels et al., 2010; Alves et al., 2014b; Festa et al., 2015; Pérez et al., 2016). Some have also recognised MTCs as important components of growth sequences and recognised their potential for constraining tectonostratigraphic models (Clark and Cartwright, 2012; Alves et al., 2014b; Festa et al., 2015; Pérez et al., 2016). However, few studies have analysed the relationship between changes in the distribution and characteristics of MTCs with the style and timing of dynamic seabed deformation (Clark and Cartwright, 2012; Alves et al., 2014). The effect of small-scale bathymetry, caused by the depositional relief of underlying sedimentary packages, such as channel-levee complexes and contourites on MTCs, has also been noted but not investigated in detail (e.g. Manley and Flood, 1988; Damuth and Embley, 1981; Frey-Martinez et al., 2006; Romero-Otero et al., 2010; Talling et al., 2012).

The variety of deposits that comprise submarine slope successions, including channel-levee complexes, MTCs and contourites (Nakajima et al., 1998; Migeon et al., 2001; Piper and Normark, 2001; Skene et al., 2002; Frey-Martinez et al., 2006; Jackson and Johnson, 2009; Alves, et al., 2010; Alves and Cartwright, 2010; Gamboa et al., 2010; Vinnels et al., 2010; Kneller, et al., 2015; Ducassou et al., 2015) can result in

compositional heterogeneities on the seabed and shallow subsurface. These heterogeneities potentially affect the ability of the overriding flows to erode and determine the volume and type of substrate entrained This has implications on the dynamic evolution of the flows and on the characteristics of the resulting deposits (Dykstra et al., 2011; Iverson, 2012; Day et al., 2015). However, the role of substrate character (e.g. composition, texture, compaction, heterogeneity) on the morphology, composition and internal structure of MTCs has not been studied in detail.

Consequently, the main objective of this thesis is to investigate the role of bathymetric irregularities of different scales on the distribution, emplacement processes and evolution of MTCs, channel-levee complex sets and avulsion lobes, and to investigate the role of substrate heterogeneities on MTCs.

1.2 Data and Study area

This study is based on a 3D seismic survey located in the Colombian Caribbean continental margin (Fig 1.1). It has an area of 1900 km^2 and is Post-Stack Depth-Migrated (PSDM) and has a bin spacing of 12.5 x 12.5 m. The study concentrates on Upper Pleistocene strata, in the interval between the seabed and c. 1000 m below. In this interval, the maximum frequency is 45 Hz and the dominant frequency is 30 Hz, which by assuming a sediment velocity of 1900 m/s, yield a vertical resolution of c. 10-15 m and a horizontal resolution of c. 15 m. These values were provided by Equión-Energía Limited and extracted from their proprietary velocity model which is calibrated to nearby wells.

The seismic survey images the southern portion of the Magdalena Fan. The southern part of the seismic volume images the northern tip of the Southern Sinú Fold Belt (Fig. 1.1B-C). The northern part of the survey images a portion of the undeformed, central part of the fan (Fig. 1.1B-C). In the southeastern part of the seismic survey, the slope is deformed by imbricate fold and thrust anticlines; to the northwest, the morphology of the

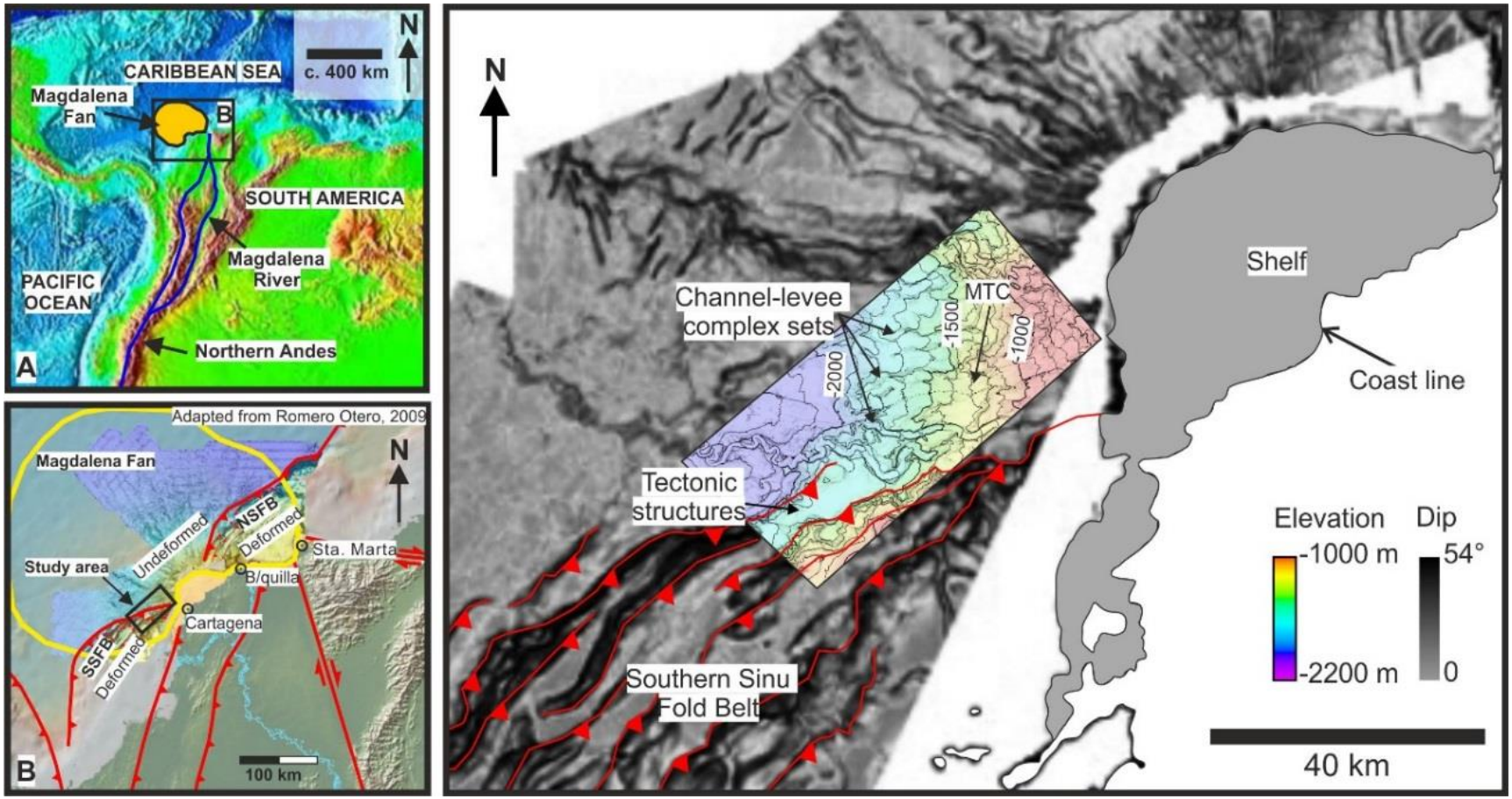

Figure 1.1. Location of the study area. **A.** The study area is located in the Caribbean Sea offshore, Colombia, northern South America; satellite image from NOAA. **B.** Map showing the location of the Magdalena Fan and the location of the seismic survey that defines the study area; modified from Romero-Otero, 2009. **C.** Dip map of the seabed in the southern Magdalena; the greyscale map is taken from Romero-Otero (2009), the coloured map defines the study area and is a dip map coloured by elevation. Note that the bathymetry is dominated by imbricate anticlines to the SE and channel-levee complex sets and MTCs to the NW.

slope is defined by the depositional relief of multiple channel-levee complexes and MTCs (Fig. 1.1C). A detailed description of the geological setting is provided in Chapter 3.

1.3 Research Questions

The specific objectives of this thesis are framed by four research questions that will be returned to towards the end of the thesis in Chapter 7.

1.3.1 How does seabed bathymetry influence the emplacement processes and architecture of MTCs, channel-levee complex sets and avulsion lobes?

Rationale: The interaction between channel-levee systems and dynamic or static structural relief has been well-documented on many continental margins including offshore Angola (Gee and Gawthorpe, 2006; Mayall et al., 2010; Jones et al., 2012), the Niger delta (Jolly, 2014), the Gulf of Mexico (e.g. Booth et al., 2003; Prather, 2003), NW Borneo (e.g. Morley, 2009), the Nile Delta slope (e.g. Clark and Cartwright, 2009, 2011, 2012; Georgiopoulou and Cartwright, 2013), and the Colombian Caribbean (e.g. Ercilla et al., 2002; Romero-Otero, 2009; Romero-Otero et al., 2010; Vinnels et al., 2010). The effects of seabed topography on mass-transport complexes (MTCs) have also been documented in the Amazon Fan (e.g. Damuth and Embley, 1981; Manley and Flood. 1988), offshore Trinidad (e.g. Moscardelli et al., 2006), the Nile Delta slope (Clark and Cartwright, 2012), offshore Israel (Frey-Martinez et al., 2006), offshore Brazil (e.g. Gamboa et al., 2010), and the Colombian Caribbean Margin (Ercilla et al., 2002; Romero-Otero, 2009; Romero-Otero et al., 2010; Vinnels et al., 2010; Alfaro and Holz, 2014), amongst others. The effect of erosional and depositional relief, however, has received little attention. Most studies concentrate on the effects of irregular relief of MTCs on subsequent turbidite sedimentation and on the creation of accommodation within slide scars (e.g. Brami et al., 2000; McGilvery et al., 2004; Moscardelli et al., 2006; Jackson and Johnson, 2009; Alves, 2010; Olafiranye et al., 2013; Kneller et al., 2015). There is, therefore, a lack of studies that explicitly investigate the interaction of bathymetric

irregularities at a range of scales on of the type and evolution of gravity flows, and their products.

In the study area, the presence of tectonic structures, high-relief channel-levee complex sets and MTCs (Fig. 1.1) enables the investigation of the effects of the interaction between turbidity currents and mass-flows with bathymetric features of different scales. This is important because bathymetric fluctuations affect flow uniformity leading to changes in erosion and depositional patterns (Kneller and Branney, 1995), thereby determining the facies distribution. The effect of bathymetric irregularities on a given flow is a function of the properties of the flow and the scale of the bathymetric features (McCaffrey and Kneller, 2004); therefore different types of flow have different responses to underlying bathymetry. Understanding the effects of different scales of bathymetric fluctuation on different types of turbidity currents and on mass-flows can improve our ability to predict reservoir and seal presence, quality and continuity.

1.3.2 How does MTC emplacement influence the evolution of subsequent deep-water systems?

Rationale: MTCs can create accommodation that can focus subsequent turbidity current pathways (e.g. May et al., 1983; Mutti et al., 1988; Brami et al., 2000; Lowe, 2004; Moscardelli et al., 2006; Jackson and Johnson, 2009; Kertznus, 2009; Alves, 2010; Olafiranye et al., 2013; Kneller 2015; Kneller et al., 2015), modify regional sediment dispersal patterns by capturing updip drainage (Piper and Behrens, 2003; Haflidason et al., 2004; Kertznus, 2009; Loncke et al., 2009), degrade deepwater fold-and-thrust belts (e.g. Heniö and Davies, 2006; Clark and Cartwright, 2009; 2012; Vinnels et al., 2010; Romero-Otero, 2010; Geersen et al., 2011; Alfaro and Holz, 2014; Idárraga-García and Vargas 2014; Vargas and Idárraga-García 2014; Festa et al., 2015, Yarbuh and Contreras, 2015), and create bathymetric irregularities that affect the architecture of subsequent deposits (e.g. Brami et al., 2000; Moscardelli et al., 2006; Jackson and Johnson, 2009; Alves, 2010; Olafiranye et al., 2013; Kneller et al., 2015). Although the

importance of MTC emplacement on the evolution of deep-water depositional systems is widely recognised, there is still a paucity of studies that document the range of effects that MTCs can have on the subsequent depositional architecture and that consider the longer-term impact of MTC emplacement on the evolution of submarine fans. In the study area, MTCs were deposited coeval with tectonic deformation (Ercilla, 2002; Romero-Otero, 2009; Vinnels, 2010). Degradation of the deep-water fold and thrust belt and MTC emplacement modified the seascape both locally and sub-regionally. This enables the investigation of the different spatial and temporal scales at which MTCs can affect the evolution of deep-water systems.

1.3.3 How does substrate composition influence the evolution, facies and geometries of MTCs?

Rationale: Mass-flow emplacement processes can result in significant erosion, entrainment and degradation of the seascape (e.g. Prior et al., 1984; Gee at al., 2006; Weimer and Slatt, 2007; Lamarche et al., 2008; Posamentier and Martinsen, 2011; Joanne et al., 2013). Substrate entrainment is an important factor that influences the dynamic evolution of mass-flow transport processes and depositional character (e.g. Dykstra et al., 2011; Iverson, 2012; Day et al., 2015; Sobiesiak et al., 2016). It is widely accepted that the capacity of a flow to erode, depends on both the characteristics of the flow and the slope over which it propagates (Alves and Lourenço, 2010; Dykstra et al., 2011; Iverson, 2012; Day et al., 2015). The composition of the substrate influences the volume and type of material entrained, and consequently the rheological evolution and characteristics of the resulting deposits (e.g. Dykstra et al., 2011; Iverson, 2012). This is particularly important for MTCs, which can derive up to 50% of the deposited material from substrate erosion (e.g. Prior et al., 1984; Gee at al., 2006; Lamarche et al., 2008; Joanne et al., 2013). The interaction between mass-flows and the seabed therefore has important implications on the presence and continuity of underlying reservoirs and on the ability of MTCs to constitute hydrocarbon reservoirs or seals. Compositional and

volumetric changes in gravity flows can also affect their runout distance which is a key parameter to assess the risk that these flows pose to submarine infrastructure. Despite the importance of substrate properties on the distribution and characteristics of MTCs it has not been studied. In the study area, MTCs that overlie erosional surfaces incise into several stratigraphic packages composed of channel-levee complex sets and older MTCs. This enables the investigation of the influence of substrate heterogeneities on the distribution, morphology, and internal characteristics of MTCs.

1.3.4 How can MTCs be used as a record of the style and timing of dynamic seabed deformation?

Rationale: Several studies, have investigated the interaction between channel-levee complex sets and growing structures (e.g. Clark and Pickering, 1996; Haughton, 2000; Prather, 2003; Heniö and Davies, 2006; 2007; Gee and Gawthorpe, 2006; Gee et al., 2007; Clark and Cartwright, 2019; 2012; Mayall et al., 2010; Kane et al., 2010; Jones et al., 2012; Jolly, 2014). Changes in the distribution, morphology and architecture of channel-levee complex sets alongside dynamic seabed deformation has been used to infer their timing with respect to structural growth (Clark and Cartwright, 2009, 2011; Mayall et al., 2010; Jones et al., 2012; Jolly, 2014). Conversely, although MTCs have also been recognised as important agents in the degradation of deep-water fold and thrust belts (e.g. Heniö and Davies, 2006; Clark and Cartwright, 2009; 2012; Vinnels et al., 2010; Romero-Otero, 2010; Geersen et al., 2011; Alfaro and Holz, 2014; Alves et al., 2014b; Idárraga-García and Vargas 2014; Vargas and Idárraga-García 2014; Festa et al., 2015, Yarbuh and Contreras, 2015), few have investigated the relationship between three-dimensional changes in the distribution, source and scale of MTCs with structural growth, and whether systematic responses to seabed deformation can be used to constrain the tectonostratigraphic evolution of active continental margins (Geersen et al., 2011; Clark and Cartwright, 2012; Festa et al., 2015; Pérez et al., 2016). The study area for this thesis is located in the northern tip of the Southern Sinú Fold Belt (Fig. 1.1), where

the youngest and structurally simplest structures along the trend developed (Martinez et al., 2015). Here, several stacked MTCs are contained in the shallow stratigraphy. Given that the deformation is less advanced than in other areas along the fold belt, primary tectonostratigraphic relationships can be interpreted with confidence. This provides an excellent opportunity to investigate the occurrence of changes in the distribution, provenance and characteristics of MTCs that could be related to dynamic seabed deformation and used to constrain the tectonostratigraphic evolution.

1.4 Thesis Outline

The thesis contains three manuscripts, Chapters 5 is published in *Basin Research*, Chapter 7 is published in *Marine and Petroleum Geology*, and Chapter 6 is has been accepted for publication in the *Journal of Sedimentary Research* pending major revisions.

Chapter 2: Submarine Slope Systems. This chapter contains an introduction to the processes and deposits typical of submarine slope settings and a literature review on previous studies that have investigated the effect of bathymetry and substrate on slope deposits. It summarises the morphological characteristics of continental slopes, the classifications and products of submarine gravity flows and the characteristics of channel-levee complex sets, avulsion lobes and MTCs and their typical seismic signature based on previous seismic-based studies. It also provides a summary of the current understanding of the effects of MTC emplacement on deep-water systems and the influence of substrate and bathymetry on channel-levee complex sets, MTCs and avulsion lobes.

Chapter 3: Regional Setting. This chapter contains an introduction to the geological setting of the Colombian Caribbean margin and a review of previous studies in the Magdalena Fan.

Chapter 4: Methodology. This chapter outlines the seismic mapping and interpretation methods used. It also contains two seismic facies classifications which were used to interpret sedimentary subenvironments. It also describes the kinematic indicators used to interpret the emplacement directions of MTCs.

Chapter 5 Mass-transport complexes as markers of deep-water fold-and-thrust belt evolution: Insights from the southern Magdalena Fan, Offshore Colombia. Chapter 5 contains a version of the manuscript published in *Basin Research,* in August 2016. Chapter 5 has been slightly modified from the published version following the suggestions of the external examiner. In this chapter a package containing stacked and laterally coalescing MTCs is described in detail. The geometries of the MTCs, kinematic indicators and stratigraphic relationships are used to infer provenance and relative timing of MTC emplacement with respect to structural uplift. This is then used to propose a model for the tectonostratigraphic history of the study area. The applicability of this approach to other settings and the chronostratigraphic significance of MTC composite basal surfaces are discussed.

Chapter 6: Bathymetry and substrate as controls on mass-transport flow processes and pathways. This chapter contains the initial submitted version of a manuscript that has been accepted for publication in the *Journal of Sedimentary Research* pending major revision. Here, the stratigraphic units that underlie the MTCs described in Chapter 5 are characterised. Relationships between the composition and bathymetric expression of these substrate units and the characteristics of the MTCs that overlie them are explored. The effect of bathymetric fluctuations, caused by structural and depositional relief, on the flow-pathways and internal characteristics of MTCs are also documented and discussed.

Chapter 7: The role of mass-transport complexes in controlling channel avulsion and the subsequent sediment dispersal patterns on an active margin: The

Magdalena Fan, offshore Colombia. This chapter contains the final version of a manuscript published in *Marine and Petroleum Geology* in January 2015. The nomenclature of the structures and the MTC regions have been modified from the published version for consistency with chapters 5 and 6. This chapter describes the stratigraphy directly overlying the MTC package and documents the influence of MTC-related bathymetric irregularities on the architecture and evolution of subsequent channel-levee complex sets and avulsion lobes.

Chapter 8: Discussion and conclusions. This chapter discusses how the results presented in chapters 5 to 7 contribute to answering the research questions outlined in Section 1.3, and contribute to our understanding of deep-water slope systems. The implications of these findings are considered and possible future research is suggested.

2 Submarine Slope Systems

2.1 Slope Depositional Systems

Clastic sediments in deep-water settings are commonly emplaced by *sediment gravity flows* derived from gravitational failures at the shelf-edge or slope, continuous *underflows* fed by rivers (hyperpycnal flows), and/or oceanographic processes such as storms, tides and currents (e.g. Piper and Normark, 2009; Meiburg and Kneller, 2010; Leeder, 2011; Talling, 2014). Commonly, these gravity flows travel downslope through submarine canyons, leveed channels, and gullies that form conduits on the slope that feed sand-rich fans on the basin floor (Reading, 1996; Leeder, 2011). Different triggers operate on different types of margins; in deltaic margins, for example, delta-lip failures due to low tides or river floods, or plunging hyperpycnal flows are common triggers (Talling, 2014). In river-fed canyons, slope failures in the canyon head or margins, plunging hyperpycnal flows and large storm waves are more common. Collapse of the outer shelf and submarine slope, which tends to generate mass-flows (e.g. Piper and Normark, 2009; Talling, 2014), can be caused by gas hydrate dissolution (e.g. Maslin et al., 2004; Grozic, 2010), sea level fluctuations (e.g. Manley and Flood, 1988; Maslin et al., 1998, 2004; Minisini et al., 2007; Masson et al., 2010), seismic activity (e.g. McAdoo et al., 2000; Frey-Martinez et al., 2005; Minisini et al., 2007; Alfaro and Holz, 2014), high sediment input (e.g. Manley and Flood, 1988; Maslin et al., 1998, 2004; Beauboeuf and Friedman, 2000; McGilvery et al., 2004; Dugan and Stigall, 2010; Masson et al., 2010), and oversteepening of the slope due to structural uplift and salt and mud diapirism (McGilvery et al., 2004; Frey-Martinez et al., 2005; Moscardelli et al., 2006; Moscardelli and Bull, 2008; Vinnels et al., 2010; Alfaro and Holz, 2014). Different triggering mechanisms and resulting flows and deposits may operate on any given continental margin at different points and times (Talling, 2014).

2.2 Processes and Products

2.2.1 Submarine Sediment Gravity Flows

Submarine sediment gravity flows are sediment-fluid mixtures that translate downslope under the action of gravity and the density contrast with the ambient fluid (Kuenen, 1950; Middleton and Hampton, 1973), and are classified based on their rheology and grain support mechanisms (e.g. Lowe, 1976; Shanmugam et al., 1994; Stow et al., 1996; Mulder and Alexander, 2001; Talling et al., 2012; Fig. 2.1). Rheological classifications distinguish plastic or cohesive and fluidal or non-cohesive flows. Plastic flows have a shear strength and mobilize once normal stress is exceeded by shear stress. Plastic flows are laminar and deposit en-mass or freeze (e.g. Stow et al., 1996; Shanmugam, 2002; Talling et al., 2012). Fluidal flows have no shear strength, and when decelerating, they drop sediment out of suspension and tend to aggrade (e.g. Stow et al., 1996; Shanmugam, 2002; Talling et al., 2012).

2.2.1.1 Mass-Flows

Mass-flows are produced by mass-wasting and are classified based on their rheology and the degree of disaggregation of the failed material into slides, slumps and debris flows (e.g. Lowe, 1976; Nemec, 1990; Shanmugam et al., 1994; Mulder and Alexander, 2001). Slides comprise rotated coherent blocks in which the internal stratification remains intact. Slumps are characterised by plastic deformation, folding and contortion of the contained strata (Dott, 1963; Nemec, 1990; Shanmugam et al., 1994). Slides and slumps have runout distances from metres to a few kilometres (e.g. Mulder and Alexander, 2001; McGilvery et al., 2004). Debris flows are cohesive, plastic, highly concentrated laminar flows that can travel for hundreds of kilometres (e.g. Mulder and Alexander, 2001; McGilvery et al., 2004; Talling, 2013). In debris flows, clasts are supported by matrix strength (cf. Nardin et al., 1979; Lowe, 1982; Mulder and Alexander, 2001; Talling et al., 2012; Fig. 2.1). However, the term debris flow is also often used for laminar, weakly cohesive flows in which grain collision is the main clast-support mechanism (e.g.

Shanmugam et al., 1994; Manica, 2012; Talling, 2012). Importantly, mass-flows can undergo transformations during translation by incorporating sediment through erosion, entraining ambient fluid (water) and through disaggregation of the failed mass, transforming from slides, through slumps to debris flows (Shanmugam et al., 1994; Stow et al., 1996; Locat and Lee, 2005; Strachan, 2008; Omosanya and Alves, 2013; Fig. 2.2). Because slides, slumps and debris flows form a process continuum, the properties and behaviour of flow types between end members can vary locally and temporally; thus the same flow may be behave as a slump or a debris flow at different points or at different times (e.g. Strachan, 2008).

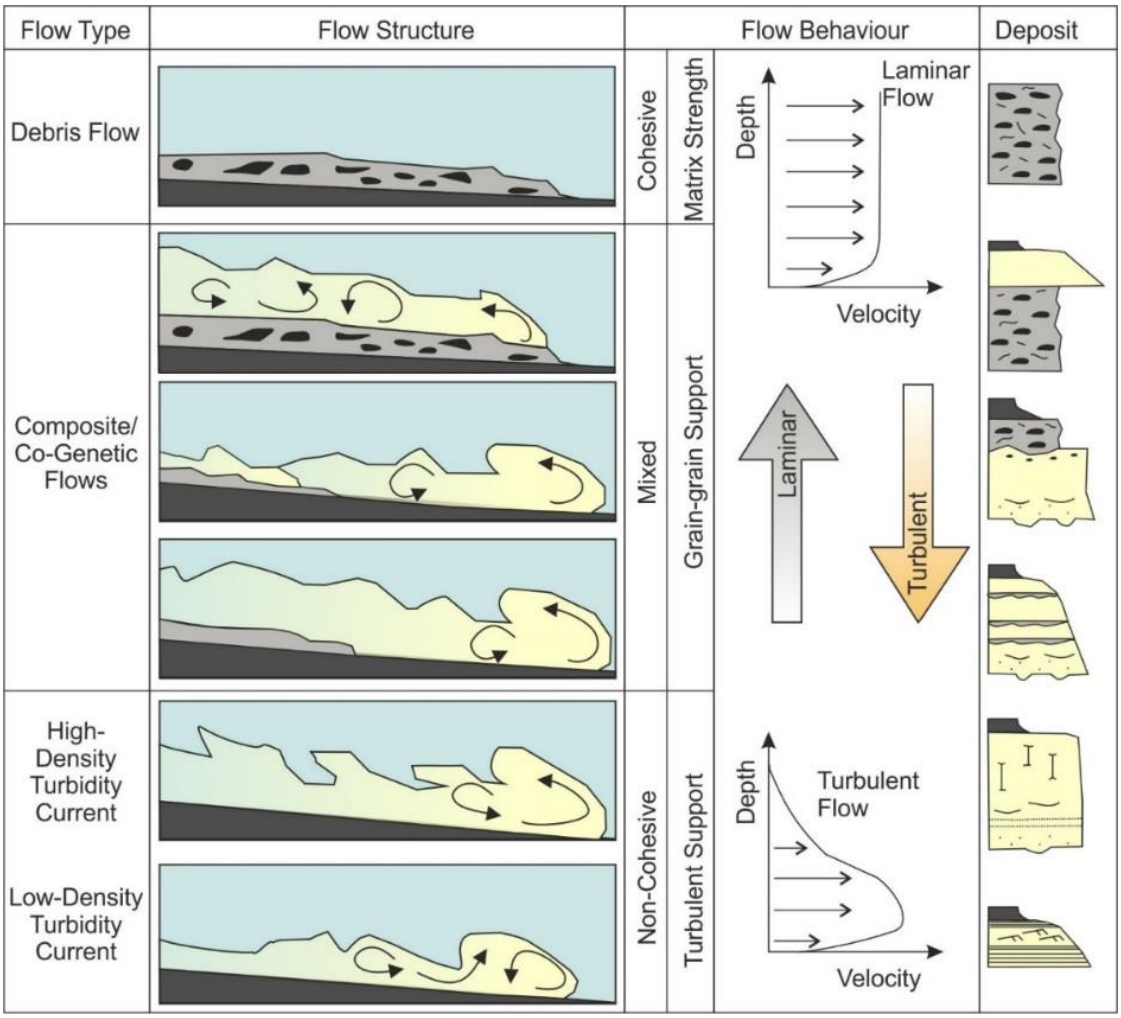

Figure 2.1 Spectrum of gravity flows and deposit types. Modified from Haughton et al (2009).

Debris flows cover a wide spectrum of rheologies, viscosities, densities, and transport mechanisms. Although they usually contain ungraded particles of variable grain sizes

within a viscous matrix, they can also be composed entirely of mud (*mud flows*; Mulder and Alexander, 2001; Talling, 2013). Sedimentation by debris flows occurs en-masse by freezing (Mulder and Alexander, 2001; Talling et al., 2012, Talling, 2013) although some studies suggest that less cohesive debris flows can develop surges and progressively aggrade (Major, 1997). Although clasts within debris flows are mostly randomly distributed, some degree of grain-size segregation can occur (e.g. Mulder and Alexander, 2001; Johnson et. al., 2012; Talling et al., 2012). Mixing along the upper surface of debris flows can lead to the formation of a more dilute suspension that travels above the main flow (Mulder and Alexander, 2001; Ilstad et al., 2004; Talling et al., 2012). Also, large blocks can be segregated towards the front and margins of the flow, with the matrix remaining unsorted (Johnson et. al., 2012; Talling et al., 2012). Segregation of larger clasts towards the margins can lead to the construction of levees (e.g. Johnson et al., 2012). Inverse grading can also be achieved through kinetic sieving (Legros, 2002; Talling et al., 2012). The behaviour and dynamic evolution of a debris flows are strongly influenced by the clay content; the addition of relatively small volumes of clay can significantly increase the viscosity and yield strength while damping turbulence (Coussot, 1997; Baas et al., 2004; Ilstad et al., 2004; Talling, 2012). Muddy, highly-cohesive debris flows have a higher yield strength and can therefore support coarser clasts; mixing is inefficient and grain-size segregation and the development of a fine-grained suspension at the top are hence less likely to occur (Ilstad, 2004; Talling et al., 2012). Less cohesive debris flows can support only smaller clasts and they mix more efficiently enabling grading and the development of a finer sediment suspension at the top; they are also more likely to develop turbulence transitioning to hybrid flows (Ilstad, 2004; Haughton et al., 2009; Talling et al., 2012) or turbidity currents (Nemec, 1990; Lowe, 1976; Shanmugam et al., 1994; Haughton et al., 2009; Talling, 2013; Fig. 2.1). The development of *hydroplaning,* a process in which a layer of ambient fluid is entrained beneath the frontal part of the debris flow, minimising basal friction may facilitate long runout distances (e.g. Mohrig et al., 1999; Ilstad et al., 2004; Elverhøi et al., 2005).

Erosion by debris flows occurs mostly through progressive scouring; the rates of sediment entrainment are sensitive to pore-pressure increase that develop in the underlying sediments as they are overridden by the debris flow, sometimes leading to liquefaction (Iverson, 2012). The development of increased pore-pressure depends on the weight of the overriding debris flow and on the momentum transferred from the flow to the substrate resulting in compressional loading and shear deformation (Iverson, 2012). The behaviour of the substrate depends on its porosity, permeability and water saturation; saturated, loosely packed beds are more prone to liquefaction (Iverson, 2012).

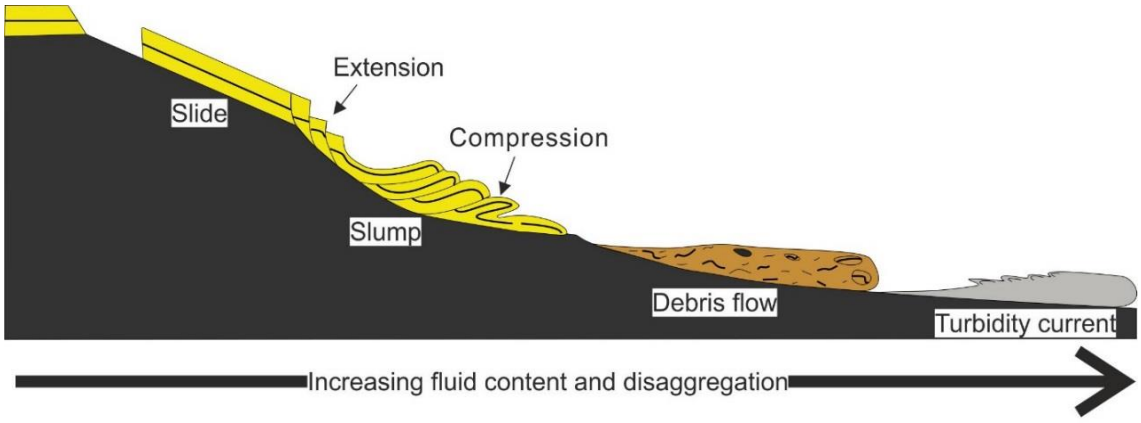

Figure 2.2. Mass-flows. Modified from Shanmugam et al. (1994).

2.2.1.1.1 Slides

Slide deposits are lithified blocks that have been displaced along a detachment surface with minimal internal deformation. They occur at all scales (e.g. Shanmugam et al., 1994; Stow et al., 1996)

2.2.1.1.2 Slumps

Slump deposits can be a few centimetres to hundreds of meters thick (Stow et al., 1996) and are characterised by pervasive deformation with the primary stratification still being recognisable (Fig. 2.3). Generally, they are characterised by extensional deformation updip and contractional deformation towards the toe with the degree of deformation increasing down-flow as the folds become asymmetric and sometimes recumbent (Elliot

and Williams, 1988; Farrell and Eaton, 1988; Strachan, 2002; Bull et al., 2009; Fig. 2.2). When the folding is simple, the orientation of the axes of the folds can be used to infer flow direction (Jones, 1939; Woodcock, 1976; Stow et al., 1996; Bull et al., 2009), but they must be used in conjunction with other kinematic indicators.

2.2.1.1.3 Debrites

Because debris flows comprise a spectrum of rheologies and flow types, the characteristics of their deposits vary significantly. In general, they are described as massive, chaotic, and poorly sorted with clasts that float in a finer-grained matrix (Stow et al., 1996; Fig.2.3). High-strength cohesive debrites (*sensu* Talling et al., 2012) have relatively high content of cohesive mud, are relatively thick (tens of metres thick) and are usually continuous to the failure location (Talling et al., 2012). They commonly contain large blocks that can be up to a few kilometres wide (e.g. Prior et al., 1984; Bull et al., 2009; Alves, 2010; Alves and Cartwright, 2010; Alves and Lourenço, 2010; Gamboa, et al., 2011; Jackson, 2011; Talling et al., 2012; Kneller et al., 2015; Alves, 2015; Gamboa and Alves, 2015). These *megaclasts* are often internally folded (e.g. Jackson, 2011; Alves, 2015; Gamboa and Alves, 2015) and can be supported by buoyancy or clast-to-clast interactions (Mulder and Alexander, 2001; McGilvery et al., 2004). Low-strength cohesive debrites (*sensu* Talling et al., 2012) contain comparatively less cohesive mud within the matrix and are characterised by smaller clasts (Talling et al., 2012).

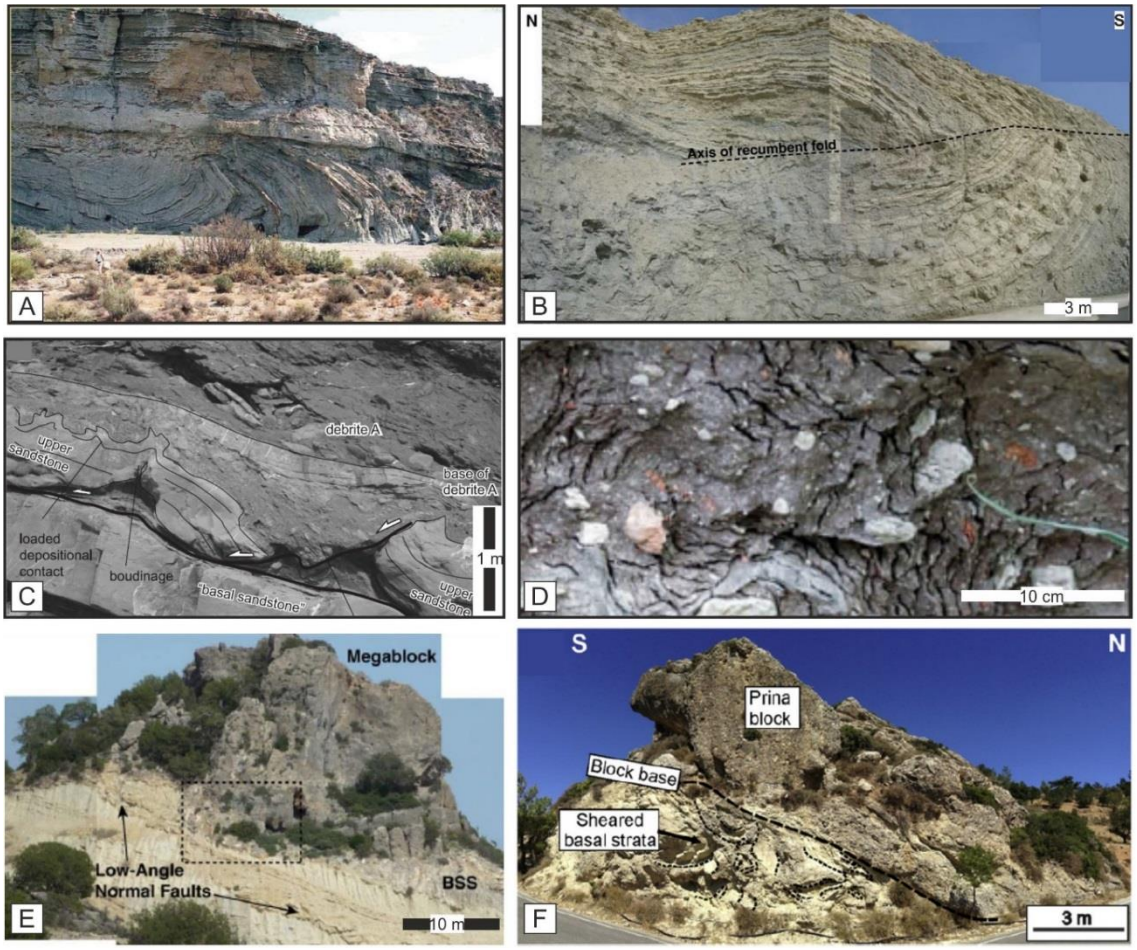

Figure 2.3. Outcrop examples of slumps and debrites. **A.** Slump folds from the El Gordo Megabed in the Tabernas Basin, Spain; taken from Weimer and Shipp (2004). **B.** Slump fold from the Makrilia Formation in SE Crete; taken from Alves and Lourenço (2010). **C.** Debrite from the Rupe-Rosa section in the Apennines, Italy; taken from Butler and McCaffrey (2010). **D.** Debrite from the Voghera sector in the Apennines, Italy; taken from Festa et al. (2015). **E.** Example of a megaclast in the Makrilia Formation, SE Crete; taken from Alves and Lourenço (2010). **F.** Example of a megaclast from the Prina Series, SE Crete; taken from Gamboa and Alves (2015).

2.2.1.2 Turbidity Currents

Turbidity currents are sediment-water mixtures in which turbulence is the main mechanism for clast support (Middleton and Hampton, 1973; Mulder and Alexander, 2001; Talling, 2012; Meiburg and Kneller, 2014; Fig. 2.1). They move downslope due to their excess density with respect to the ambient seawater (Middleton and Hampton, 1973; Talling, 2012; Meiburg and Kneller, 2014). They are characterised by double-shear boundaries; at the base is the flow-sediment interface, and at the top the flow-ambient fluid interface (Leeder, 2011). The friction at these boundaries causes mixing, turbulence, drag and the formation of Kelvin-Helmholtz instabilities along the upper

boundary (Meiburg and Kneller, 2010; Birman et al., 2009). The drag caused by the Kelvin Helmholtz instabilities is greater at the upper boundary than at the basal boundary leading to a velocity profile in which the maximum time-averaged velocity occurs close to the seabed (Meiburg and Kneller, 2010; Hansen et al., 2015). Turbidity currents are hence highly density stratified with the coarsest fraction traveling close to the seabed and the finer portion traveling towards the top as suspended load (Hiscott et al., 1997, Pirmez and Imran, 2003, Peakall et al., 2000; Meiburg and Kneller, 2010; Fig. 2.4). The frontal part of the flow carries the coarsest fraction and is characterised by a thicker *head* with a steep leading edge. Behind the head is the thinner *body* in which sediment is carried in suspension; towards the rear is the *tail* which thins rapidly and is more diluted (Stow et al., 1996; Fig. 2.4). A cloud of suspended sediment settles after the flow has passed.

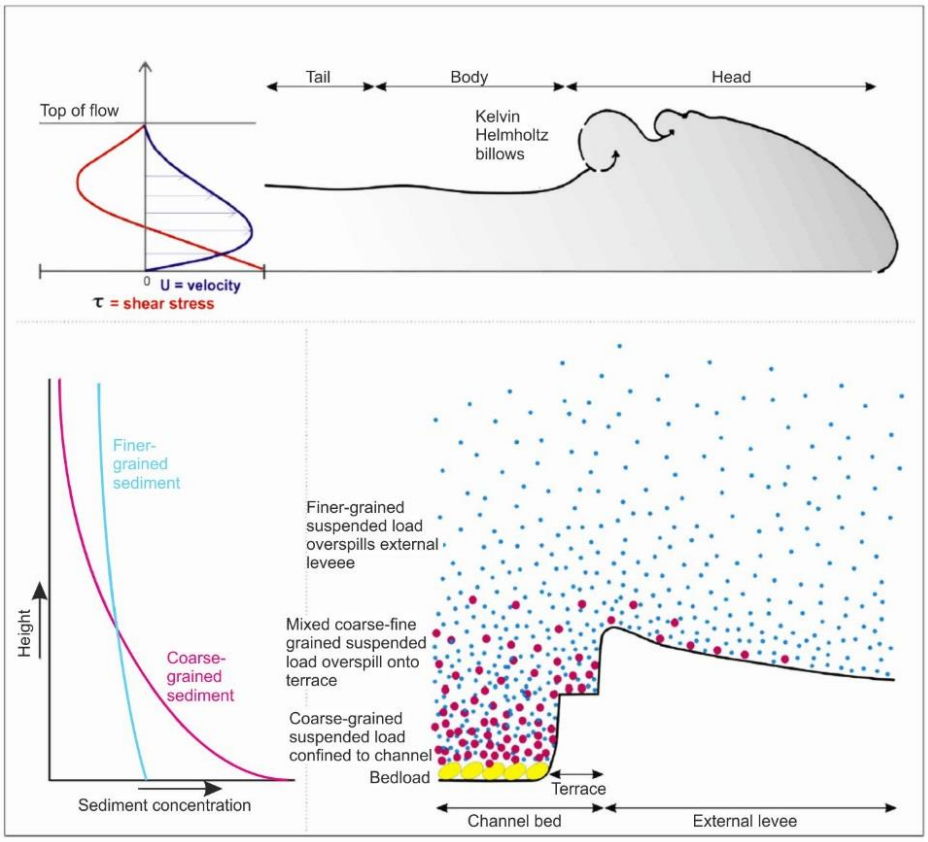

Figure 2.4. Turbidity current structure and overspill; taken from Hansen et al (2015).

Sedimentation takes place when the flow decelerates, and this occurs mostly from the body and tail of the flow in a layer-by-layer fashion as coarser grains preferentially settle (Talling et al., 2012). The velocity of the flow can change in time and space and is strongly influenced by slope and lateral confinement (Kneller and Branney, 1995; Kneller, 1995; Stow et al., 1996; McCaffrey and Kneller, 2004). A flow in which acceleration remains constant through time is said to be *steady*. An *unsteady* flow that decelerates through time is said to be *waning*, while a flow that accelerates through time is said to be *waxing. Flow uniformity* refers to spatial changes in acceleration, *non-uniform* flows that accelerate are said to be *accumulative* because they tend to erode, and those that decelerate are *depletive* because they tend to deposit (Kneller and Branney, 1995). Turbidity currents can transition to debris flows through turbulence suppression, this process is called *flow transformation* (e.g. Fisher 1982; Haughton et al., 2009; Talling, 2013). Weakly cohesive flows that exhibit both laminar and turbulent behaviours are termed *hybrid sediment gravity flows* (Fig. 2.1; Haughton et al., 2009; Talling, 2013).

2.2.1.2.1 Turbidites

Turbidites are the product of the sedimentation by turbidity currents. Individual beds can range in thickness from a few millimetres to several metres, and grain-sizes can range from mud to gravel. The Bouma sequence (Bouma, 1962) describes five divisions (Ta-Te) that are normally graded from medium sand-size particles to silt and clay (Fig. 2.5). Facies associations depend on the grainsize distribution within the parent flow; *low density turbidites,* composed of fine sand, silt and clay usually form Bouma's Tc, Td and Te divisions (Leeder, 2011; Fig. 2.5), while *high density turbidites* are composed mainly of coarse grained sand and gravel (e.g. Lowe, 1982; Reading, 1996). Hindered settling towards the base of high-density turbidity currents due to grain interactions result in facies that are dominated by traction structures (Fig. 2.5). Because coarse sand and gravel cannot be fully supported by turbulence (Mulder and Alexander, 2001; Manica,

2012), high-density turbidites have also been classified as *concentrated density flows* (Mulder and Alexander, 2001).

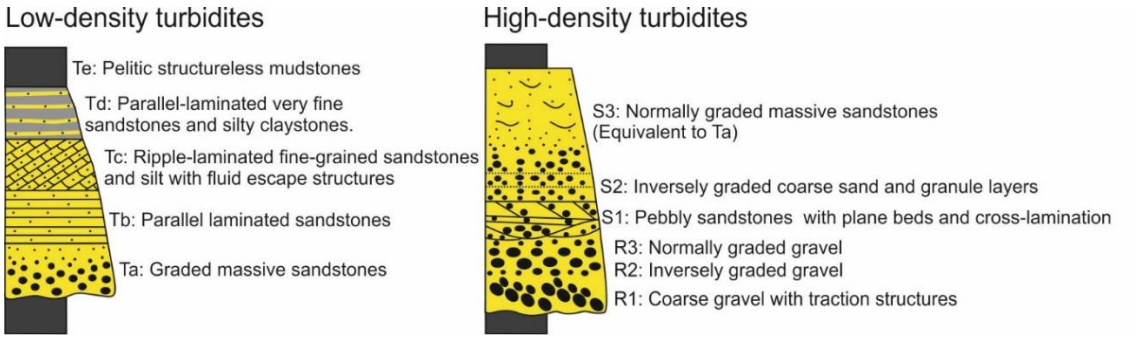

Figure 2.5. Facies associations of low density and high density turbidites. Low density turbidites after: Leeder (2011) and references therein. High density turbidites after Lowe (1982) and Reading (1996).

2.2.1.3 Hybrid Sediment Gravity Flow Deposits

Deposits that show evidence both cohesive, laminar flows and non-cohesive, turbulent flows are termed *hybrid sediment gravity flow deposits* (Haughton et al., 2009; Talling et al., 2012; Talling, 2013) and comprise beds that transition upwards from high-density turbidites to debrites, beds that change vertically from debrites to high-density turbidites, and beds with intercalated bands of debrites and high-density turbidites (Haughton et al., 2009; Talling, 2013; Fig. 2.1).

2.3 Depositional Elements on the slope

2.3.1 Mass-Transport Complexes

The term *mass-transport complex* was introduced by Weimer (1990) to describe packages made of chaotic, hummocky and subparallel reflections observed in seismic datasets in the Mississippi Fan, Gulf of Mexico. Those packages, which occur at the base of depositional sequences, are overlain by channel-levee complexes and were interpreted to be composed by “disorganised slides, debris flows and turbidites” (Weimer, 1990). In 2004, the term was re-defined to include all seismic-scale (tens to thousands of km^2) products of mass-transport processes (slides, slumps and debrites) regardless of their sequence-stratigraphic context (Weimer and Shipp, 2004). This definition does

not specify whether mass-transport complexes (MTC) refer to the deposits of single or multiple flows. The term *mass-transport deposit (MTD)* is also widely used in the literature to refer to the deposits of mass-flows. Some authors use the term MTD to refer to deposits emplaced by a single mass-flow (e.g. Minisini et al., 2007; Gamboa et al., 2010; Dykstra et al., 2011; Alves et al., 2013), and the term MTC to refer to a deposit composed of more than one MTD (e.g. Gamboa et al., 2010; Alves et al., 2013). However, the definition of the term MTD is unclear and its use across the literature is inconsistent. For example Moscardelli et al. (2006) and Moscardelli and Wood (2008) use the term MTC to describe seismic packages resulting form mass-flows offshore Trinidad; subsequently, Moscardelli and Wood (2015) use the term MTD to refer to the same deposits and others that were originally described as MTCs in the literature. Due to the inconsistent use of the term mass-transport deposit (MTD), and the fact that given the limitations of the seismic dataset used (10-15 m vertical and lateral resolution), it is not possible to determine with confidence whether the deposits are the result of single or multiple flows, in this thesis the term mass-transport complex (MTC) will be used to describe all seismic packages interpreted to have resulted from mass-wasting processes, in accordance with Weimer and Shipp (2004).

MTCs can occur at various scales; larger ones can occupy areas of hundreds to thousands of square kilometres and are often sourced from the shelf-break and are termed *shelf-attached* (Moscardelli and Wood, 2008, 2015). Smaller MTCs cover areas of up to a hundred square kilometres, are sourced by local collapse of steep areas of the slope including anticline flanks, salt domes and canyon walls, and are classified as *detached MTCs* (Moscardelli and Wood, 2008, 2015). The seismic expression of MTCs varies. Some MTCs contain relatively continuous reflections that are folded and sometimes contorted, while others contain imbricate thrusts and folds (e.g. Brami et al., 2000; Moscardelli et al., 2006; Bull et al., 2009; Posamentier and Martinsen, 2011; Alfaro and Holz, 2014; Fig. 2.6F-G); these are respectively termed *slump folds* and *thrust-and-*

fold systems by Bull et al. (2009). MTCs containing the features are sometimes interpreted as slumps (e.g. Frey-Martinez et al., 2005, 2006; Bull et al., 2009; Posamentier and Martinsen, 2011) and are characterised by extensional deformation updip and contractional deformation towards the toe of the deposits in the form of folding and thrusting (Lewis, 1971; Frey-Martinez et al., 2005, 2006; Posamentier and Martinsen, 2011). Other MTCs are characterised by discontinuous and chaotic reflections that commonly contain packages of continuous to semi-continuous, coherent parallel reflections; they are usually interpreted as debrites with blocks or megaclasts (e.g. McGilvery et al., 2004; Alves and Cartwright, 2009; Gamboa et al., 2011; Jackson, 2011; Omosanya and Alves, 2013; Alves, 2015; Fig. 2.6B). Megaclasts can reach c. 200-400 m in thickness and up to c. 10 km^2 in area (e.g. Alves, 2010; Jackson, 2011), and contain planar or folded reflections (e.g. Gamboa et al., 2011; Jackson, 2011; Omosanya and Alves, 2013; Alves, 2015; Gamboa and Alves, 2015; Fig. 2.6C-E). Commonly, MTCs contain both semi-continuous, folded and/or faulted reflections and chaotic reflections (e.g. Posamentier and Kolla, 2003; Moscardelli et al., 2006; Olafiranye et al., 2013; Fig. 2.6A). Offshore Trinidad, Moscardelli et al. (2006) interpreted the occurrence of thrusts and folds within an overall chaotic MTC as the result of lateral confinement between mud volcanos. Lateral and vertical variations in the amplitude, continuity and internal deformation of the reflections reflect the heterogeneity of the deposits (Gamboa et al., 2010; Dykstra et al., 2011; Alves et al., 2014).

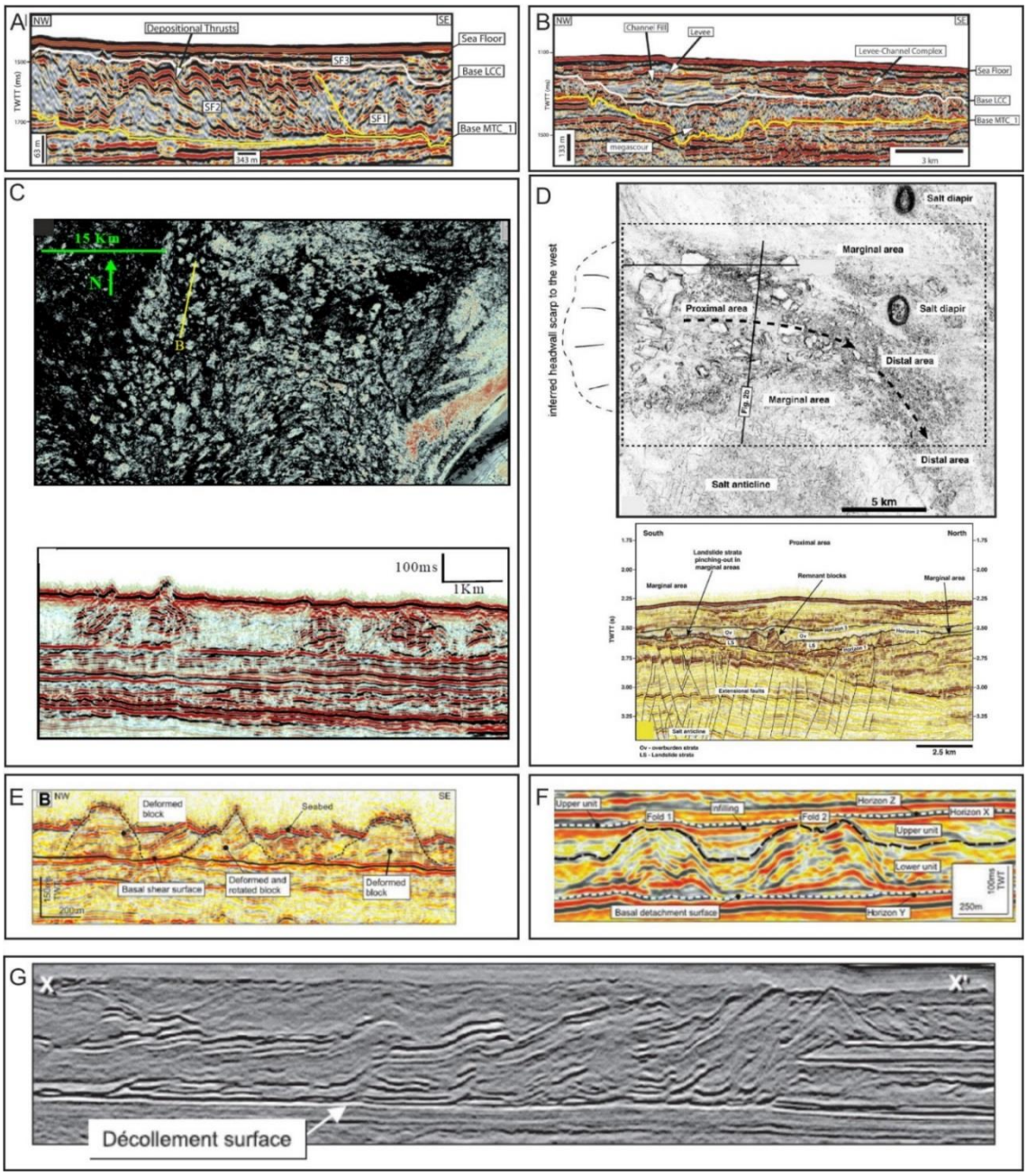

Figure 2.6. Examples of the seismic character of MTCs. **A.** Seismic line from offshore Trinidad showing an MTC composed of thrusted and folded semi-continuous reflections to the NW (SF2), and lower-amplitude chaotic reflections to the SE (SF1); taken from Moscardelli et al. (2006). **B.** MTC from offshore Trinidad composed of relatively low-amplitude chaotic reflections; taken from Moscardelli et al. (2006). **C.** Example of an MTC containing megaclasts within a debritic matrix; the map at the top is an RMS amplitude extraction. Taken from McGilvery et al. (2004). **D.** Example of an MTC offshore Brazil, containing megaclasts within a debritic matrix; the map at the top is a coherence slice. Taken from Alves and Cartwright (2009). **E.** Deformed megaclasts in a debritic matrix offshore Norway; taken from Bull et al. (2009). **F.** Folded semi-continuous reflections interpreted as slump folds in Bull et al. (2009). **G.** Example of a slump in the Gulf of Mexico; taken from Posamentier and Martinsen (2011).

Simplified MTC models define a headwall domain, a translational domain, and a toe domain (e.g. Prior et al., 1984; Weimer and Slatt, 2007; Frey-Martinez et al., 2005; Bull et al., 2009; Fig. 2.7). The orientation of some of the features that occur within these domains can sometimes be used to infer the direction of flow emplacement and are known as *kinematic indicators* (*sensu* Bull et al., 2009) The *headwall domain* is the upslope portion of the MTCs, which is dominated by extension (e.g. Bull et al., 2009; Weimer and Slatt, 2007; Frey-Martinez, 2005, 2006; Posamentier and Martinsen, 2011; Fig. 2.7). Here, the *headwall scarp* is characterised by a steep upward-cutting and commonly composite erosion surface that has an arcuate map-view geometry (Bull et al., 2009). When retrogradational failure occurs, several down-stepping headwall scarps can develop (e.g. Piper and Behrens, 2003; Haflidason et al., 2004; Bull et al., 2009; Kertznus, 2009; Loncke et al., 2009; Georgiopoulou et al., 2010). *Crown cracks,* which are small-scale normal faults, are also characteristic of the headwall domain (Frey-Martinez et al., 2005; Bull et al., 2009).

The *translational domain* is characterised by *lateral margins* that are sub-parallel to the flow direction (Prior et al., 1984; Weimer and Slatt, 2007; Frey-Martinez, 2005; Bull et al., 2009; Fig. 2.7). The base of the MTC is often characterised by a *basal glide plane* or décollement, also referred to as the *basal shear surface* (e.g. Bull et al., 2009; Frey-Martinez, 2005; Alves and Lourenço, 2010; Posamentier and Martinsen, 2011). It is commonly parallel to the underlying stratigraphy although it can locally develop *ramps* that cut across stratigraphic levels (Trincardi and Argnani, 1990; Frey-Martinez et al., 2005; Bull et al., 2009; Omosanya and Alves, 2013). Alternatively, MTC basal surfaces can be irregular and highly erosive (e.g. Weimer and Shipp, 2004; Moscardelli et al., 2006; Joanne et al., 2013; Olafiranye et al., 2013). Irregularities in the basal surface can sometimes be related to *in situ* remnant blocks or deep, narrow erosional scours also known as *slots* (Frey-Martinez, 2005; Moscardelli et al., 2006; Bull et al., 2009). V-shaped scours in the basal surface that are linear in map-view and trend parallel to the

flow direction, and diverge downslope are interpreted to be formed by erosion by large blocks transported at the base of debris flows; they are knows as groves or striations (Posamentier and Kolla, 2003; Gee et al., 2006; Draganits et al., 2008; Bull et al., 2009; Talling et al., 2012). Large blocks are referred to as *megaclasts* (e.g. Jackson et al., 2011; Olafiranye et al., 2013) or alternatively they are termed *translated blocks* when found within the translational domain or *outrunner blocks* when found beyond the downdip limit of the MTC (Prior et al., 1984; Nissen et al., 1999; Bull et al., 2009; Alves, 2015). They can sometimes be aligned parallel to the direction of the flow (Bull et al., 2009). Differential compaction between the MTC matrix and the megaclasts can lead to increased relief at the top of MTCs (Alves, 2010; Alves and Cartwright, 2010). The irregularities on MTC top surfaces can interact with the overlying deposits affecting their geometries and architectures (e.g. McAdoo et al., 1997; Brami et al., 2000; Posamentier and Kolla, 2003; Moscardelli et al., 2006; Jackson and Johnson, 2009; Alves, 2010; Alves and Cartwright, 2010; Olafiranye et al., 2013; Alves, 2015; Kneller et al., 2015).

The *toe domain* is dominated by compression due to the arrest of the flowing mass, which generates a back-stepping compressional wave forming contractional features such as imbricate thrust and fold systems and pressure ridges (Prior et al., 1984; Weimer and Slatt, 2007; Frey-Martinez et al., 2005; 2006; Moscardelli et al., 2006; Bull et al., 2009; Alfaro and Holz, 2014; Fig. 2.7). Pressure ridges are positive parallel arcuate ridges orientated perpendicular to flow (e.g. Posamentier and Kolla, 2003; Moscardelli et al., 2006; Bull et al., 2009; Alfaro and Holz, 2014). Thrusts in the fold and thrust systems generally dip landward and can therefore be used as directional indicators (Frey-Martinez et al., 2005; Bull et al., 2009; Alfaro and Holz, 2014); folds verge in the down-flow direction while fold axes are perpendicular (Jones, 1939; Woodcock, 1976; Bull et al., 2009).

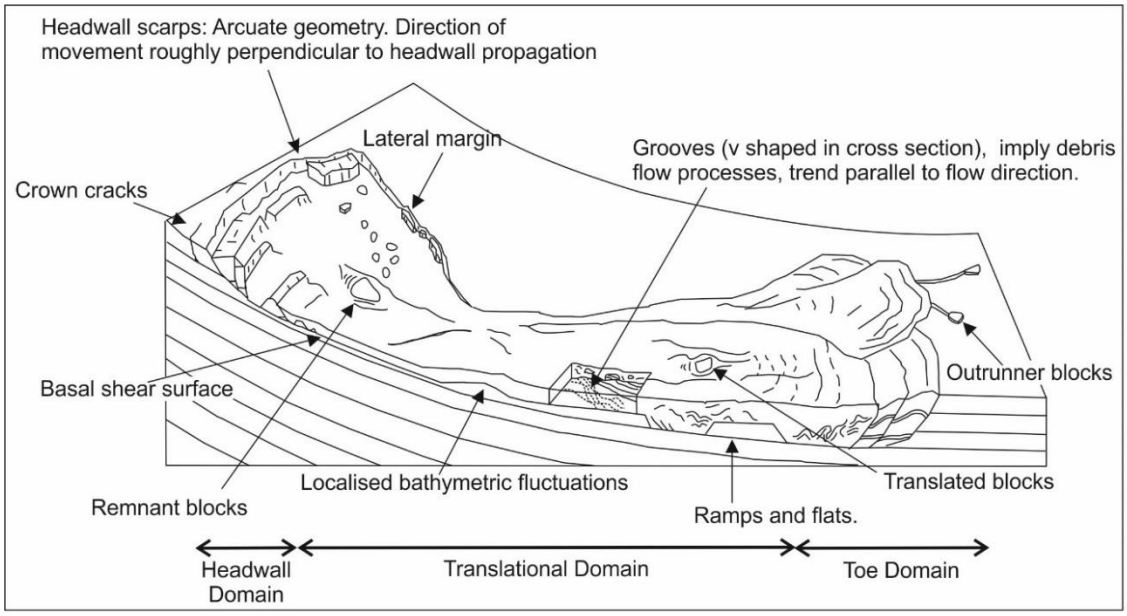

Figure 2.7. Schematic representation of the characteristic domains and features of MTCs. From Bull et al. (2009).

2.3.2 Submarine Channels

Submarine channels are conduits that transport sediment gravity flows from the shelf break to the basin floor. These conduits can be confined by entrenchment through erosion of the slope, by the construction of external levees (*sensu* Kane and Hodgson, 2011), or through a combination of both processes (e.g. Mayall et al., 2006; Janocko et al. 2013; Hodgson et al., 2016). This study concentrates on levee-bounded channels.

2.3.2.1 Channel-levee complex-sets

The internal fill of submarine channels is complex and can include high and low density turbidites, MTCs and hemipelagites (Mayall et al., 2006). They are characterised by cross-cutting stratigraphy and multiple erosion surfaces of different orders (Mayall et al., 2006; Sprague et al., 2005; Hodgson et al., 2011). Numerous hierarchical classifications exist (e.g. Mutti and Normark, 1987; Mutti, 1992; Pickering et al., 1995; Sprague et al. 2005; Mayall et al., 2006); this study follows the classification proposed by Sprague et al. (2005) and Di Celma et al. (2011). *Channel-levee complex sets* are characterised by a composite confining surface (Hodgson, et al., 2011; 2016) that is variably sinuous in plan-view (e.g. Clark et al., 1992; Posamentier and Kolla, 2003; Mayall, 2006; Wynn et

al., 2007; Armitage et al., 2012) and is bounded on either side by wedge-shaped external levees (*sensu* Kane and Hodgson, 2011; Fig. 2.8). It is filled by genetically-related *channel-complexes* that are seismically mappable channelized features (Sprague, et al., 2005; Fig. 2.8). In the present study, the conduits of channel-levee complex sets are 100-200 m thick and 1-2 km wide and the bounding levees are c. 200 m high and over c. 4 km wide. Channel-complexes are up to 100 m thick and c. 300-500 m wide. The fill of channel complexes commonly comprises sandstone packages that tend to concentrate towards the channel axis, fine grained sandstones and siltstones that dominate the channel margins and chaotic sandy or muddy facies that represent MTCs (Hodgson et al., 2011; Fig. 2.9A). On seismic data, the sand-prone channel axes are imaged as stacked high-amplitude discontinuous reflections (Deptuck et al., 2003, 2007; Posamentier and Kolla, 2003; Mayall et al., 2006; Catterall et al., 2010; McHargue et al., 2011; Armitage et al., 2012; Fig. 2.9B-C); the channel margins are lower-amplitude packages with little internal reflectivity or parallel internal reflections (Deptuck et al., 2003, 2007; Posamentier and Kolla, 2003; Mayall et al., 2006; Fig. 2.9B-C). In contrast, MTCs appear as massive, low-amplitude packages and are usually found towards the base of channel complexes (Posamentier and Kolla, 2003; Mayall et al., 2006). The relative proportion of seismic facies may vary considerably between channel complexes. Channel-complexes can stack vertically, or laterally with variable offset distances. Lateral stacking can occur consistently in a specific direction or shift through time (Clark and Pickering., 1996; Mayall et al., 2006), it can also vary along the length of a single channel resulting in complex channel architectures (Mayall et al., 2006; Catterall et al., 2010).

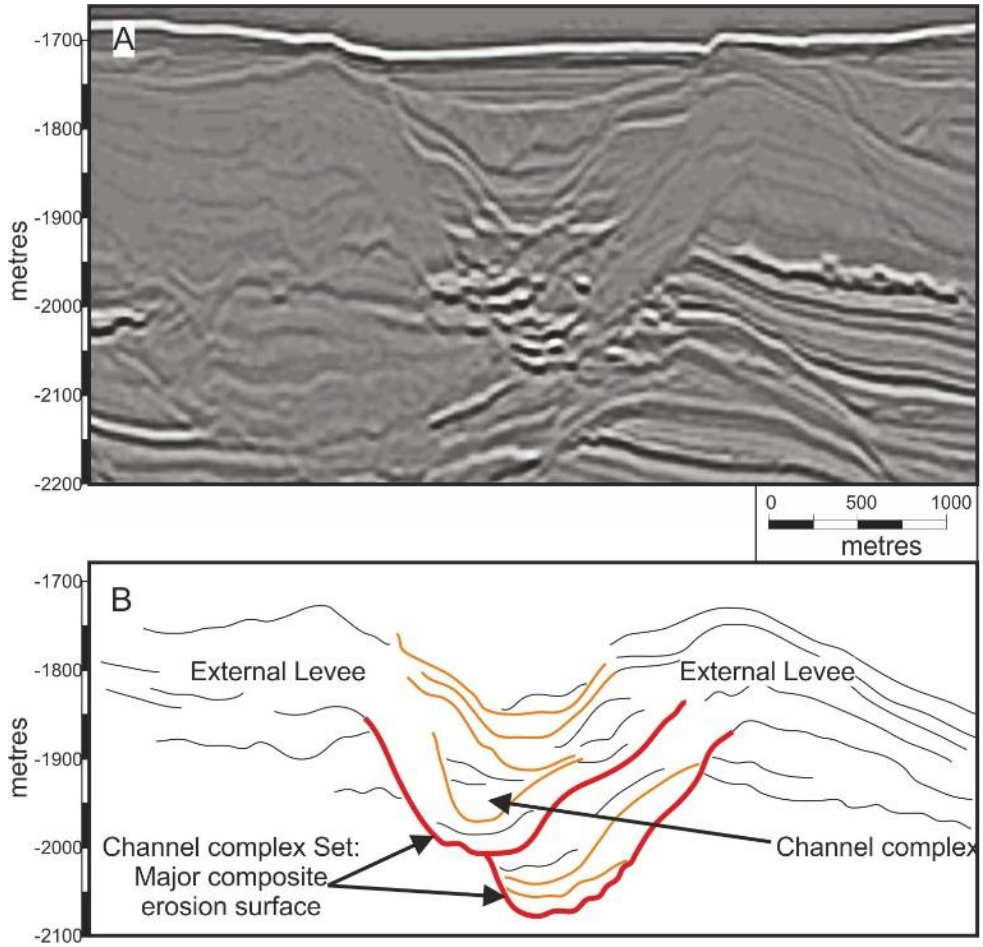

Figure 2.8. Hierarchical definition of channel-levee complexes and channel-levee complex sets. Modified from Stevenson et al. (2015).

2.3.2.1.1 External Levees

External levees are large constructional wedges of fine-grained sediment that form through deposition of low-density turbidity currents that spill out of adjacent channels (e.g. Skene et al., 2002; Deptuck et al., 2003; Babonneau et al., 2004; Kane et al., 2010b; Nakajima and Kneller, 2012; Morris et al., 2014; Hansen et al., 2015; Fig. 2.4). On seismic reflection data, levees appear as high-relief wedges that thin away from the channel complex-set and are characterised by parallel, low-amplitude reflections that dip at higher angles towards the top (e.g. Posamentier and Kolla, 2003; Deptuck et al., 2003; Catterall et al., 2010; Armitage et al., 2012; Figs. 2.8 and 2.9).

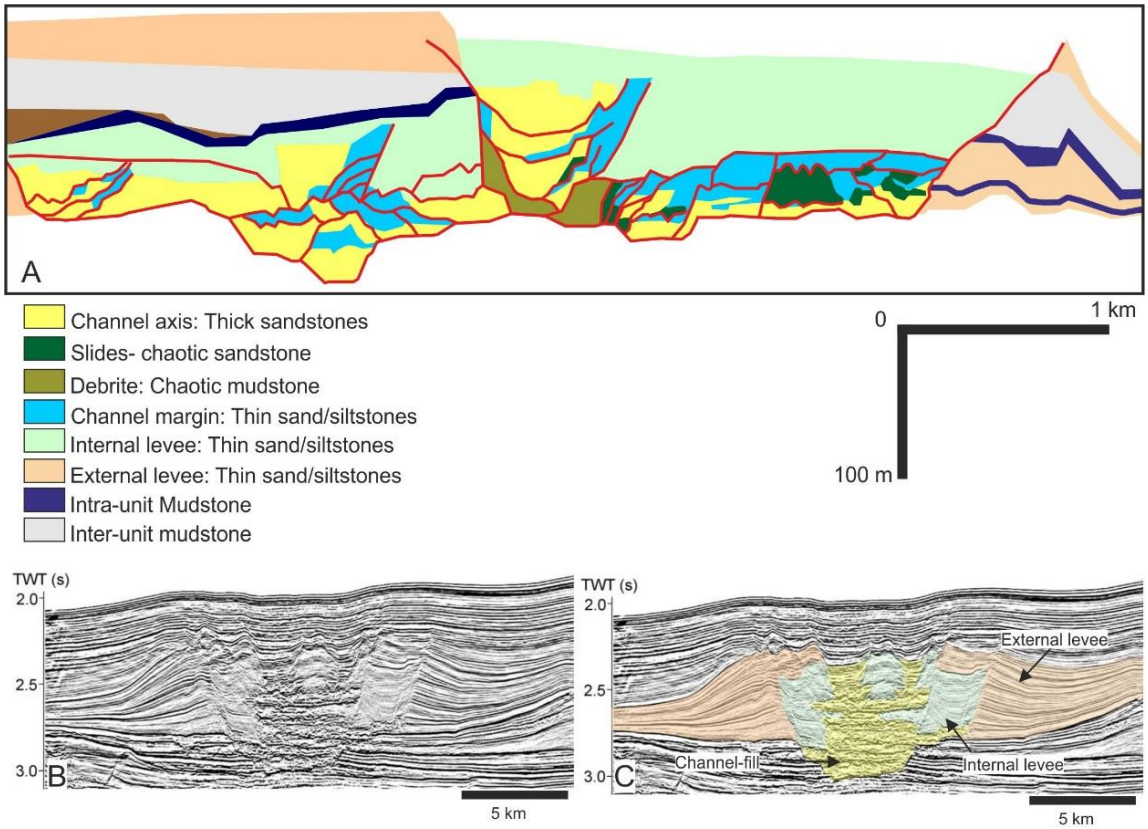

Figure 2.9. Architecture of channel-levee complex sets. **A.** Schematic correlation panel based on c. 200 closely-spaced logged sections in Units C and D of the Fort Brown Formation in the Karoo Basin, southwestern South Africa. Taken from Hodgson et al., 2011. **B** and **C.** Uninterpreted and interpreted seismic cross-section across a channel-levee complex set in the Indus Fan, note the wedge-shaped packages of continuous parallel reflections that bound the channel belt on either side, interpreted as external levees; the high-amplitude discontinuous reflections of the channel axis and the contrasting lower-amplitude, semi-continuous, parallel reflections of the internal levees. Taken from Deptuck et al. (2003).

The stratified flow can exceed the height of the channel due to the density contrast between the turbidity current and sea water, resulting in considerable over-spill that creates high-relief levees (Kane et al., 2010b; Straub and Mohrig, 2008; Fig. 2.4). Typically, external levees comprise interbedded mudstone and siltstone that vary in proportion as a function of distance to the channel axis and the flow thickness relative to the height of the levee (Straub and Mohrig, 2008; Kane et al., 2010b; Nakajima and Kneller, 2012; Morris et al., 2014; Hansen et al., 2015). Overall, bed thickness and grain size decreases upwards and laterally away from the channel axis (e.g. Gervais et al., 2001; Pirmez and Imran, 2003; Dennielou et al., 2006; Hodgson et al., 2011; Morris et al., 2014; Hansen et al., 2015). Levee relief is inversely related to grain size, with finer grained levees being higher (Hiscott et al., 1997; Pirmez and Imran, 2003). Despite the

relatively steep levee back slope, over spilling flows are likely to decelerate quickly beyond the levee crest due to water entrainment and thickening (Pirmez and Imran, 2003; Kane et al., 2010b). These strongly depositional flows become progressively diluted and dissipate in a near exponential manner that is reflected in the resulting levee geometry (e.g. Skene et al., 2002; Straub and Mohrig, 2008; Nakajima and Kneller, 2012; Talling et al., 2012). The grain size in a particular level within a levee is a function of the relief between channel base and levee crest and flow height; higher levees will only allow the finer grained portion of the flow to over-spill, while lower relief channels are likely to over spill coarser grained material (Hiscott et al., 1997, Pirmez and Imran; 2003). Therefore, levee topography influences the grain size distribution further along the channel (Pirmez and Imran, 2003).

Levee thickness decays systematically away from the channel, and downslope as flows become progressively sandier (e.g. Pirmez and Flood, 1995; Babonneau et al., 2002; Skene et al., 2002; Straub and Mohrig, 2008). Thickness decay away from the channel has been documented to conform to exponential, logarithmic or power law functions (Birman et al., 2009; Skene et al., 2002; Kane et al., 2010b; Nakajima and Kneller, 2013). However, levee geometries may vary as a result of local collapse into or away from the channel conduit (Catterrall et al., 2010; Sawyer et al., 2014; Hansen et al., 2015), through the formation of sediment waves (e.g. Armitage et al., 2012) and cyclic steps and/or as a result of the interaction with adjacent channels (Hansen et al., 2015). Also, bathymetric fluctuations on irregular slopes can result in variable levee geometries (Catterall et al., 2010; Nakajima and Kneller, 2012; Chapter 7).

2.3.2.1.2 Internal Levees and Terrace deposits.

Internal levees (*sensu* Kane and Hodgson et al., 2011) are formed when low-density turbidity currents overspill channel complexes but remain confined by the external levees that bound the channel-levee complex set (Fig. 2.9). They are characterised by thin-bedded, fine-grained sediments (Kane and Hodgson, 2011). In seismic they appear as

low-amplitude packages that may contain parallel internal reflections that terminate abruptly against the composite confining erosion surface of the channel-levee complex set (e.g. Deptuck et al., 2003; Catterall et al., 2010; Armitage et al., 2011; Fig. 2.9B-C). They can have a variety of polygonal shapes in plan-view and can have wedge-shapes or flat tops in cross-section (Deptuck et al., 2003). Hansen et al. (2015) introduce the term *depositional terraces* to denote confined overbank deposits that have a flat top instead of being wedge-shaped. This study uses the term internal levee to refer to all forms of confined overbank irrespective of their shapes because it is not possible to differentiate the two types in the dataset used.

2.3.3 Avulsions Lobes

Avulsion lobes form when an external levee is breached leading to channel avulsion (e.g. Flood et al., 1991; O'Byrne et al., 2007; Pirmez et al., 1997; Posamentier and Kolla, 2003; Kolla, 2007). Commonly, they are connected to the parent channel by a thin and shallow channel conduit at an *avulsion node* which is the locus of a change in channel orientation (e.g. Posamentier and Kolla, 2003; Kolla, 2007; Armitage et al., 2012; Saller, et al., 2012; Fig. 2.10). Avulsion lobes can be sand-rich (e.g. Posamentier and Kolla, 2003; Kolla, 2007; Armitage et al., 2012; Terlaky and Arnott, 2014; Terlaky et al., 2016) and on seismic reflection data have been associated with high-amplitude seismic reflection packages (HARPS) found towards the base of channel-levee complexes (Flood et al., 1991; O'Byrne et al., 2007; Pirmez et al., 1997). In the Amazon fan, stacked splays exceed thickness of 50 m (Pirmez et al., 1997). In the Kaza Group, Canada, they are characterised by structureless medium- and coarse-grained sandstones with 20-30% mud matrix and erosional bases that transition laterally to medium-coarse grained sandstones with 30-50% matrix (Terlaky and Arnott, 2014; Terlaky et al., 2016).

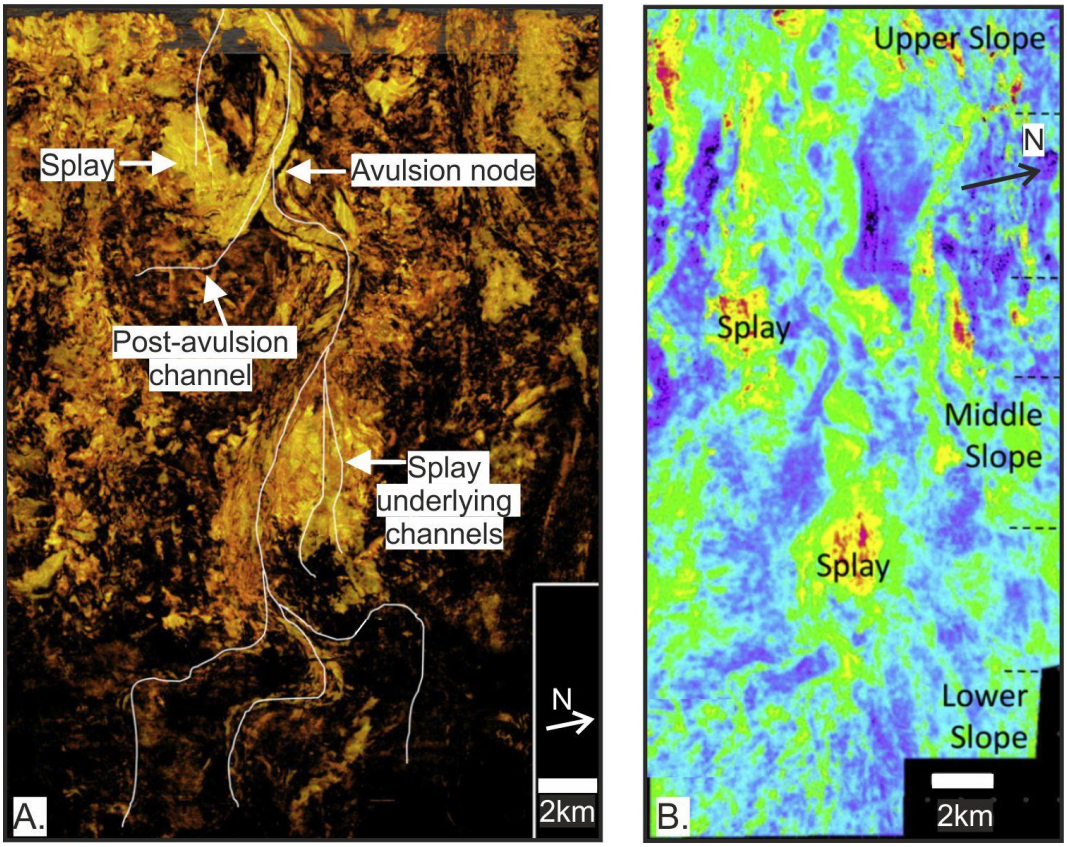

Figure 2.10. Attribute extractions of channel-levee complexes in East Kalimantan, Indonesia. Taken from Saller et al. (2012) **A.** Optical stack of absolute amplitudes of a channel-levee complex set. Yellow colours represent higher amplitudes interpreted to be sand-prone and black represents lower amplitudes interpreted as mud-prone **B.** Average amplitude extraction of a channel-levee complex set. High amplitudes are red and yellow and interpreted to be sand-prone, lower amplitudes are blue and purple and are interpreted to be mud-prone.

Channel avulsion is a fundamental process in the evolution and growth of submarine fans because it leads to the formation of new channel conduits thereby imposing changes in sediment dispersal patterns through time (Pirmez and Flood, 1995; Manley and Flood, 1988). Avulsions can be triggered by changes in the morphology of channel-levee complex (i.e. sinuosity and axial gradient), changes in the cross-sectional area of the channel conduits due to in-channel aggradation, levee erosion by MTCs, channel plugging and levee slumping (Posamentier and Kolla, 2003; Kolla, 2007; Armitage et al., 2012; Brunt et al., 2013). Changes in sinuosity, axial gradient or reduced cross-sectional area cause channel-levee complexes to become unstable and increase the probability of avulsion (Kolla, 2007). The relationship between the degree of instability of a given channel-levee complex and the magnitude of the flows determines its probability to

avulse. Stable channel-levee complexes are likely to require high-volume turbidity currents to breach the levee and cause avulsion, while unstable channel-levee complexes do not necessarily require large volume flows to force a breach (Kolla, 2007).

Most documented cases of channel avulsion have focussed on passive margins and have interpreted the most common trigger mechanism to be increased in-channel aggradation and/or peak volume flows (Armitage et al., 2012; Kolla, 2007). In the Niger delta slope, channel avulsions were associated with turbidity currents that were oversized with respect to the cross-sectional area of the channel conduits and was shown to be more common in channels in which in-channel aggradation had progressively reduced the channel's cross-sectional area (Armitage et al., 2012). Radial avulsion patterns have been documented in the Niger Delta slope and the Southern Zaire fans and are interpreted to have developed in response to axial gradient changes (Armitage et al., 2012; Kolla, 2007). In the Indus and Bengal fans, increased in-channel aggradation occurred in response to axial gradient changes and increased sinuosity, leading to avulsion (Kolla, 2007). In the De Soto Canyon, Gulf of Mexico, the Amazon Fan, and the Axial and Northern Zaire fans, peak volume flows were identified as the main causal mechanism (Posamentier and Kolla, 2003; Kolla, 2007). Levee collapse or failure is recognised as a possible mechanism for avulsion but few cases have been documented and has been previously considered as a random process (Kolla, 2007).

2.4 Types of Continental Slope Profiles and Bathymetric Controls on Slope Sedimentation

An *equilibrium profile* is a hypothetical slope in which neither erosion or sedimentation occur (Pirmez et al., 2000). Real slope profiles usually differ from the hypothetic equilibrium profile leading to areas erosion or sedimentation on the slope (Ross et al., 1994; Pirmez et al., 2000; Prather, 2003). Equilibrium profiles are also termed *at grade* and are characterised by a long-term equilibrium between erosion, sedimentation and subsidence that leads to margin progradation (Ross et al., 1994). *Above-grade* slopes

occur when upper slope gradients are steeper than the equilibrium profile, resulting in margins dominated by erosion, mass-wasting and sediment bypass (Ross et al., 1994). The concept of *slope readjustment* (Dailly, 1983; Ross, 1994) implies that submarine slopes are dynamic and that sedimentary systems respond to changes in basin physiography in an attempt to return to a graded or equilibrium profile (Ross, 1994; Pirmez, 2000; Prather, 2003). Adams and Schlager (2000) found that geometry of most continental slopes can be described by either exponential, Gaussian or linear equations. Linear slope profiles are characterised by a constant slope, where sediments rest at an angle of repose; downslope sediment transport only occurs when sedimentation surpasses a critical angle. Exponential slopes are characterised by an exponential decrease in slope towards the basin, resulting in net degradation in the upper slope and net sedimentation at the toe. Gaussian profiles are characterised by a sharp shelf-slope break and a progressively declining slope downdip. Gaussian slopes can develop in areas of high-sediment input where the shelf-slope break remains fixed through time, or where sea-level changes or ocean currents modify the slope.

Prather (2003) defined three types of slopes and associated styles of accommodation: 1) above-grade slopes with well-developed ponded accommodation (e.g. NW Gulf of Mexico), 2) above-grade slopes with stepped or terraced profiles (e.g. Niger delta slope, lower Congo and NW Borneo), and 3) graded slopes with minor bathymetric anomalies (e.g. eastern Gulf of Mexico; Fig. 2.11). The types of accommodation (i.e. ponded, healed-slope and slope accommodation, *sensu* Prather, 2003; Fig. 2.11), result from the interplay between seabed deformation and sediment supply. Because the configuration of the slope affects flow uniformity, and hence the erosional and depositional behaviour of turbidity currents (Kneller and Branney, 1995; McCaffrey and Kneller, 2004), it has an important influence on the distribution and architecture of the overlying deposits (Prather, 2003; Steffens et al. 2003).

Examples of out-of-grade slopes along passive tectonic margins include northwestern Gulf of Mexico, Niger delta, Lower Congo, Angola and Brazil. These are dominated by gravity-driven deformation above mobile substrates, composed of salt (Gulf of Mexico, Lower Congo, Angola and Brazil) and over-pressured shale (Niger delta slope; Booth et al., 2003; Steffens et al., 2003; Gee and Gawthorpe, 2006; Clark and Cartwright 2009, 2011; 2012; Gamboa et al., 2010; Mayall et al., 2010; Jones et. al., 2012; Jolly, 2014). Seabed deformation has resulted in the segmentation of the slope and development of ponded, healed-slope and slope accommodation types (*sensu* Prather, 2003; Fig. 2.11 and 2.12). Steffens et al. (2003) found that the slopes of the Gulf of Mexico and Angola are comparatively gentler compared to the Niger delta slope. Examples of out-of-grade slopes in active tectonic margins include offshore NW Borneo, and the southern Caribbean, offshore Colombia (Fig. 2.12). Here, contractional tectonic deformation leading to the development of deep-water fold-and-trust belts and mud diapirism have resulted in steeped slope profiles with some ponded and healed slope accommodation and tortuous sediment conduits (Ercilla et al., 2002; Gee et al., 2007b; Morley, 2009; Romero-Otero, 2009; Vinnels et al., 2010; Cadena et al., 2015).

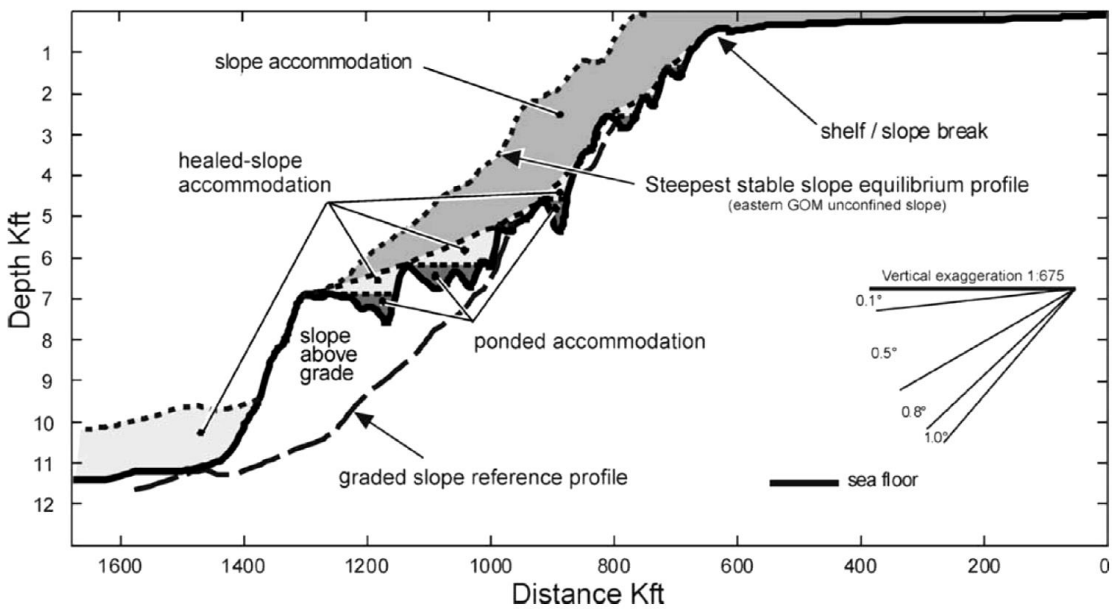

Figure 2.11. Seabed profile from the Gulf of Mexico showing different types of accommodation on non-graded slopes, namely ponded, healed-slope and slope accommodation. Taken from Prather (2003).

Previous studies have found that the erosional and depositional patterns of submarine channels change in response to dynamic seabed deformation (e.g. Haughton, 2000; Prather, 2003; Heniö and Davies, 2006; 2007; Gee and Gawthorpe, 2006; Gee et al., 2007; Clark and Cartwright 2009, 2011, 2012; Mayall et al., 2010; Kane et al., 2010; Jones et al., 2012; Alves et al., 2014b; Jolly, 2014; Fig. 2.12). Submarine channels can shift away from growing structures resulting in lateral aggradation (e.g. Mayall, 2010; Clark and Cartwright, 2009, 2011; Kane et al., 2010; Jones et al., 2012); become ponded in salt withdrawal or piggy-back basins (e.g. Ercilla et al., 2002; Booth et al., 2003; Prather, 2003; Gee and Gawthorpe, 2006; Morley, 2009; Romero-Otero, 2009; Hesse et al., 2010; Vinnels et al., 2010; Jones et al., 2012), and/or be blocked or deflected by structural highs (e.g. Clark and Pickering, 1996; Gee and Gawthorpe, 2006; Clark and Cartwright, 2009, 2011; Mayall et al., 2010; Vinnels et al., 2010; Jones et al., 2012). The effect that structural growth has on a particular submarine channel depends on the erosional power of the flows, the rate of seabed deformation and the orientation of the structures with respect to the flows (Mayall et al., 2010). Changes in the underlying bathymetry can also result in changes in sinuosity and the development of knickpoints (Heniö and Davies, 2007; Romero-Otero, 2009); they have also been related to submarine channel avulsion (Armitage et al., 2012; Kolla, 2007; see Section 2.3.3).

Therefore, the stacking patterns of channel complexes and the geometries of channel-levees can be used to infer the timing of seabed deformation with respect to sedimentation (Clark and Cartwright, 2009; 2011; Jones et al., 2012; Alves et al., 2014b; Jolly, 2014; Fig. 2.13). Moreover, changes in the stacking patterns and the distribution of submarine channels through time can be used to infer the timing and rate of seabed deformation and to reconstruct the tectono-stratigraphic history (Clark and Cartwright, 2012; Jones et al., 2012; Alves et al., 2014b; Jolly, 2014).

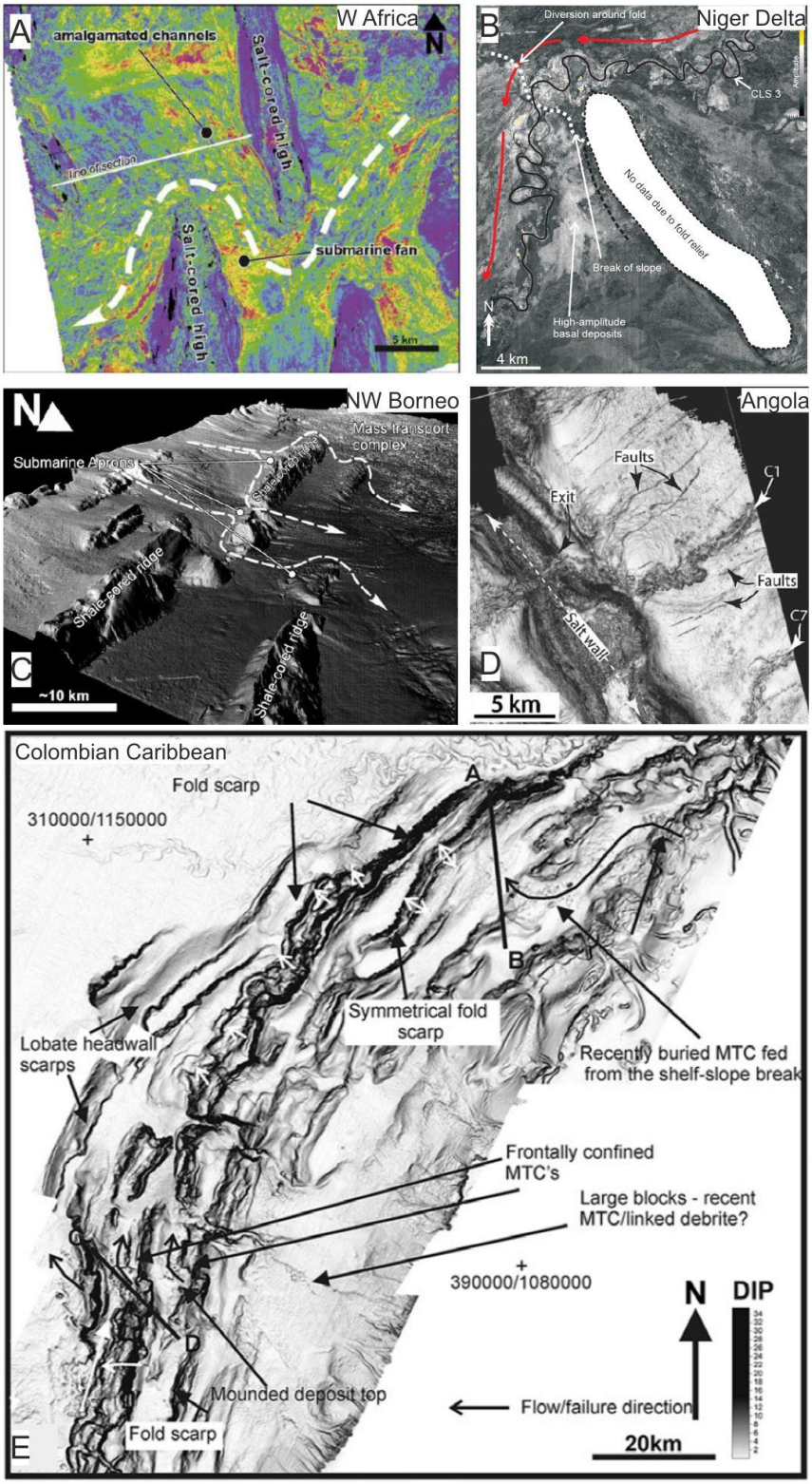

Figure 2.12. Examples of the interaction between submarine channels and structurally-deformed slopes. **A.** Horizon slice through a growth package offshore West Africa showing tortuous corridors around salt-cored structures, taken from Prather (2003). **B.** Amplitude map at the base of a channel-levee complex set showing diversion around a fold in the Niger delta slope, taken from Clark and Cartwright (2012). **C.** Tortuous paths between shale-cored ridges in offshore NW Borneo, taken from Prather (2003). **D.** Variance extraction from offshore Angola showing convergence of channels as they pass through and exit in a salt wall, taken from Gee and Gawthorpe, 2006. **E.** Seabed dip map on the Southern Sinú Fold Belt in the Colombian Caribbean showing the tortuous sediment conduits across the fold belt, taken from Vinnels et al. (2010).

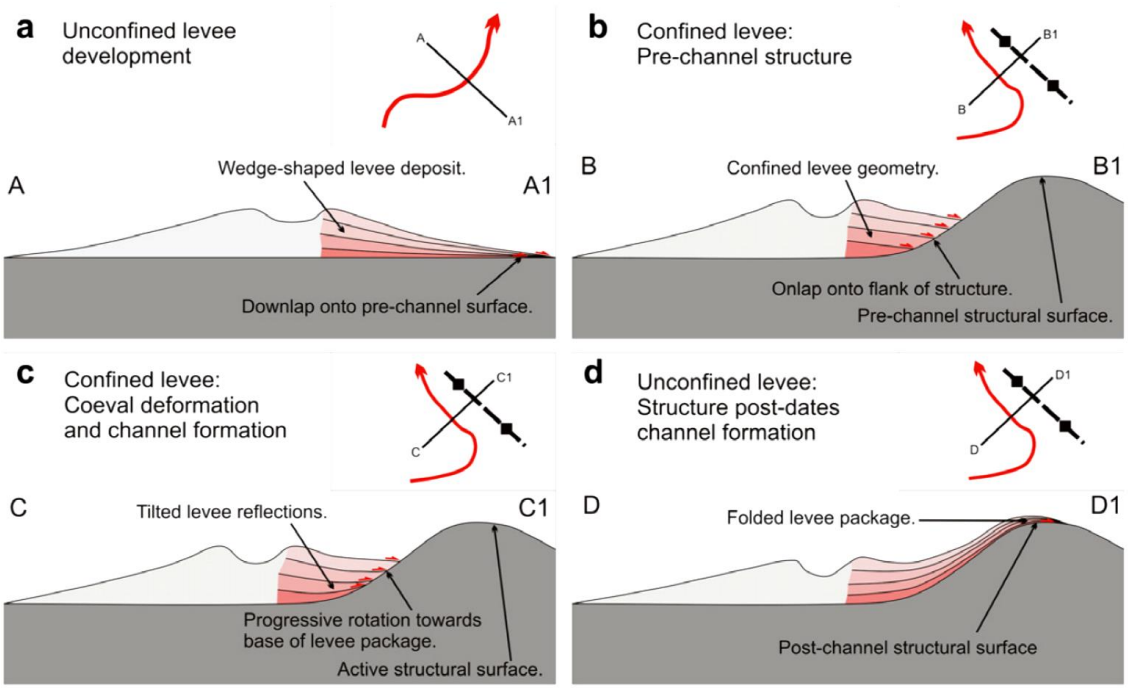

Figure 2.13. Variations in external levee geometry depending on the relative timing between deformation and sedimentation; taken from Clark and Cartwright (2011).

The effect of slope bathymetry on slope lobes has also been widely documented (e.g. Prather et al., 1998; Booth et al., 2003; Prather, 2003; Spychala et al., 2015). The development of ponded mini-basins can confine turbidity currents leading to the development of slope lobes. These usually onlap the flanks of the mini-basins and heal the slope allowing younger flows to reach other mini-basins downdip; a depositional pattern commonly known as fill-and-spill (e.g. Prather, 1998). As such, accommodation styles transition from ponded to healing and to slope accommodation (*sensu* Prather, 2003).

Similarly to submarine channels and lobes, the distribution, geometries and internal architecture of MTCs is influenced by the underlying bathymetry (e.g. Frey-Martinez, 2006; Moscardelli et al., 2006; Gamboa et al., 2010; Vinnels et al., 2010; Clark and Cartwright, 2012; Jones et al., 2012; Alfaro and Holz, 2014; Alves et al., 2014b; Dalla Valle et al., 2015; Fig. 2.14). In the Borneo fold-and-thrust belt, MTCs sourced from the steep flanks of imbricate anticlines are common and are sometimes confined within piggy-back basins that develop between thrust-cored anticlines (Gee et al., 2007b;

Morley, 2009). Degradation of the anticlines and healing of the ponded accommodation (*sensu* Prather, 2003) can connect otherwise isolated piggy-back basins (Gee et al., 2007b; Morley, 2009). The recurrence of this process can eventually link the shelf to the open slope through tortuous conduits (Gee et al., 2007b; Morley, 2009). Similar processes are documented in the Sinú Fold Belt, offshore Colombia (e.g. Ercilla et al., 2002; Romero-Otero et al., 2009; Vinnels et al., 2010; see Chapter 3). Therefore, the lateral and vertical distribution of MTCs and their characteristics can change through time in response to seabed deformation (Clark and Cartwright, 2012; Festa et al., 2015; Pérez et al., 2016). This is demonstrated by Clark and Cartwright (2012), who studied the distribution and architecture of MTCs and submarine channels and use it to reconstruct the evolution of the Bobo fold in the Niger Delta fold-and-thrust-belt. Alves et al. (2014b) demonstrate the effect of fold degradation on the kinematic evolution of thrust-cored anticlines in the Nankai Trough, Japan, and relate recurrent mass-wasting to a period of increased instability related to contraction and shortening. In the Northern Apennines, Festa et al. (2015) show that the spatial distribution of MTCs along the Ligurian accretionary wedge changed through time, accompanied with a relative increase in MTC size and thickness. Festa et al. (2015) integrated these observed changes with regional geological knowledge in order to constrain the tectonic evolution. In a recent regional study, Pérez et al., (2016) measured the dimensions of 1020 MTCs in several basins along the Scotia-Antarctic plate-margin and used changes in vertical and spatial MTC densities to infer periods of increased slope instability that could be related to major tectonic events and help constrain the regional tectonic evolution.

3 Regional Setting

3.1 Tectonic Setting

In the northwestern corner of South America, the Nazca, South American, Cocos and Caribbean plates interact (e.g. Duque-Caro, 1979; 1984; Flinch, 2003; Cediel et al., 2003; Cerón et al., 2008; Fig. 3.1). Oblique subduction of the Caribbean Plate beneath the South American Plate is interpreted to have started in the Late Cretaceous following a Late Jurassic-Early Cretaceous period of rifting and a prolonged period of subsidence through most of the Cretaceous (Escalona and Mann, 2011 and references therein; Alfaro and Holz, 2014b). Between the Late Cretaceous and the Neogene, east-to west collision of the Caribbean Plate against the South American Plate progressed from Colombia to eastern Venezuela (Escalona and Mann, 2011). This resulted in the formation of a continuous and diachronous offshore fold-and-thrust belt that extends from the Panama Arc to northern Venezuela, which is regionally known as the South Caribbean Deformed Belt (SCDB) (e.g. Pindell et al., 1988; Escalona and Mann, 2011; Bernal-Olaya, 2015). The southern part of the SCDB is located offshore Colombia and is locally known as the Sinú Fold Belt (Fig. 3.2). The Sinú Fold Belt, and the onshore San Jacinto Fold Belt, are NNE-SSW orientated accretionary prisms that developed during the Cenozoic. The accretionary prisms comprise imbricate thrusts sheets that are transferred to the north by a series of strike-slip fault zones (Duque-Caro, 1979; Pindell, 1994; Meschede and Frisch, 1998; Cediel et al., 2003; Pindell and Kennan, 2009; Escalona and Mann, 2011; Bernal-Olaya, 2015; Martinez et al., 2015; Fig. 3.2).

The San Jacinto Fold Belt is the innermost and oldest accretionary prism, and is separated from the Sinú Fold Belt by the Sinú Fault (Fig. 3.2). The formation of the San Jacinto Fold Belt has been interpreted as Cretaceous-Eocene (Ruiz et al., 2000) or Palaeocene-Oligocene (Flinch, 2003) and is composed of oceanic basement rocks and Cretaceous-Neogene sedimentary rocks (e.g. Duque-Caro 1979,1984; Flinch, 2003;

Guzmán, 2007; ANH and ATH, 2009; Herrera et al., 2009; Alfaro and Holz, 2014). The Sinú Fold Belt is located offshore and extends along the entire Colombian Caribbean margin. The structural style of the Sinú Fold Belt changes along strike (Fig. 3.2). There is a more compressional regime in the Southern Sinú Fold Belt, characterized by west-verging asymmetric fault bend and fault propagation folds (e.g. Flinch, 2003; Vence, 2008; Vinnels et al., 2010). In the Bahia Basin, there is a more transpressive regime characterized by symmetric, unfaulted detachment folds and positive flower structures (Galindo, 2013). In the Guajira Offshore Basin, there is a transtensional regime (e.g. Vence, 2008; Bernal-Olaya, 2015). The Sinú Fold Belt is interpreted to represent the latest phase of accretion, which took place in the Miocene-Recent and is associated to the Andean Orogeny (e.g. Duque-Caro, 1979; Ruiz et al., 2000; Flinch, 2003).

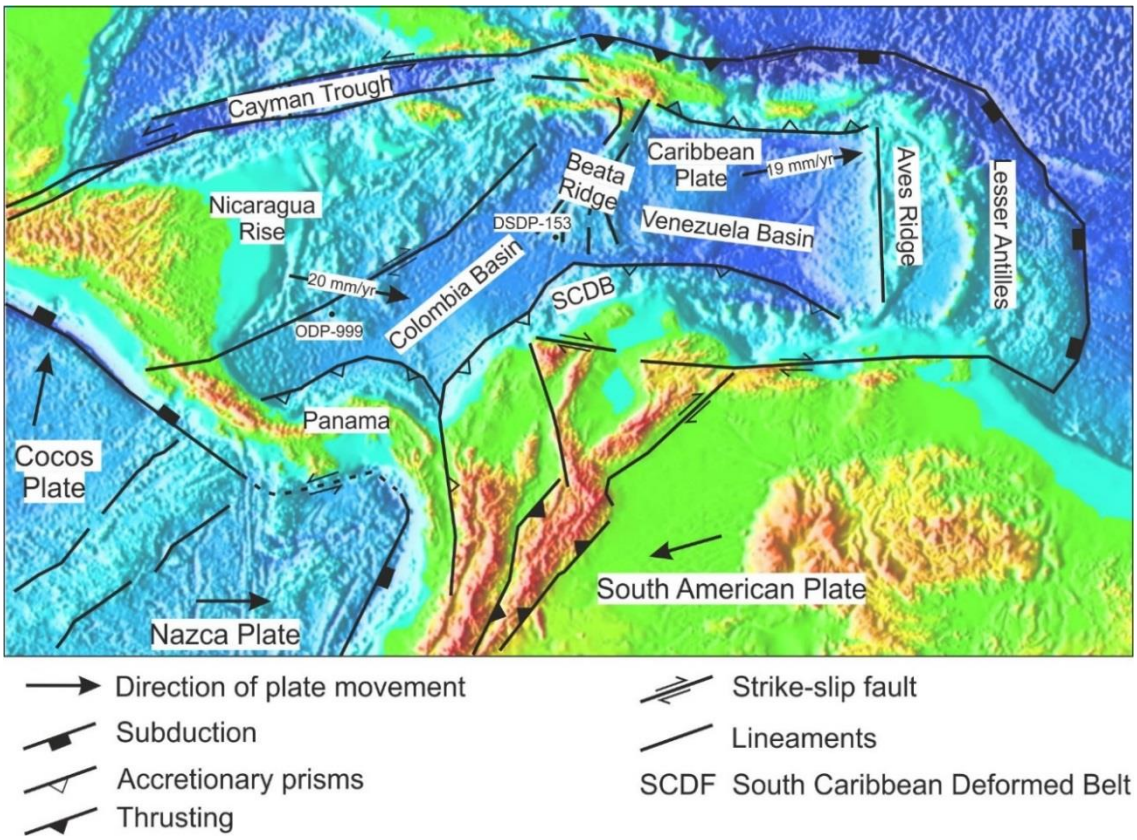

Figure 3.1. Main physiographic and tectonic features of the Caribbean region. The western estimated rate of displacement of the Caribbean Plate was taken from DeMets et al. (2000) and the one to the east from Trenkamp et al. (2002); satellite image from NOAA.

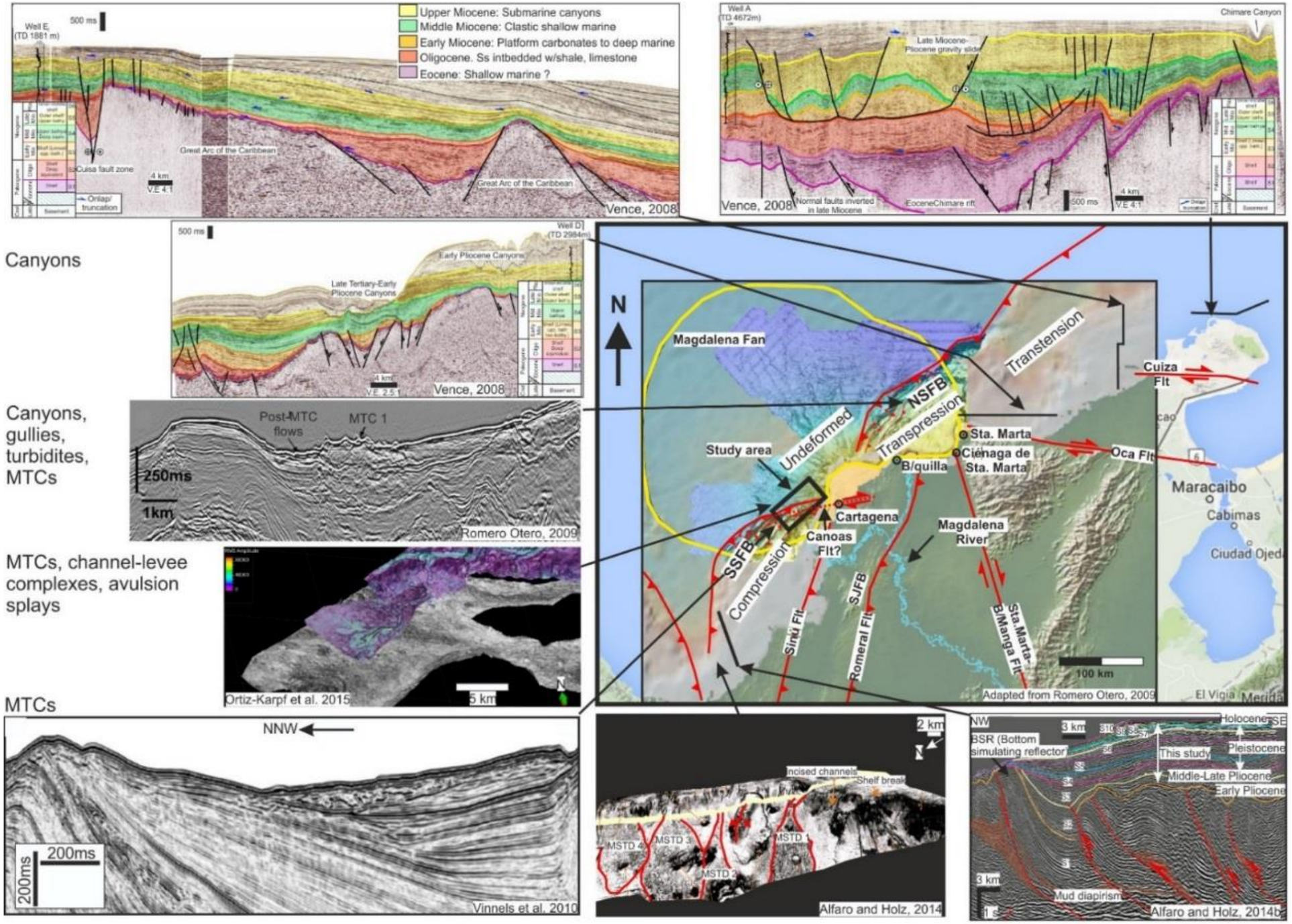

Figure 3.2. Compilation of images from published studies showing variations in the tectonic and depositional styles along the Sinú Fold Belt; SSFB: Southern Sinú Fold Belt, NSFB: Northern Sinú Fold Belt. The map, modified from Romero–Otero (2009), shows the main structural elements, the outline of the Magdalena Fan according to Kolla and Buffler (1984) and the study area.

Deformation of both the Sinú and San Jacinto fold belts occurred in pulses and is diachronous, being older towards the south and younger towards the north (e.g. Alfaro and Holz 2014b; Bernal-Olaya, 2015; Martinez et al., 2015). To the west of the city of Cartagena, the Sinú Fold Belt is interrupted as the deformation front bends to the east and an area of subdued deformation underlies the present-day position of the Magdalena Fan (Fig. 3.2); the accretionary prism continues to the NE of the Magdalena Fan (Fig. 3.2). In this study, the segment of the fold belt located to the SW of the undeformed area is referred to as the Southern Sinú Fold Belt while the portion to the NE is referred to as the Northern Sinú Fold Belt (Fig. 3.2). The study area is located 26 km northwest of the city of Cartagena, on the northern tip of the Southern Sinú Fold Belt (Fig. 3.2).

Several models have been postulated to explain the partitioning of the Sinú Fold Belt. According to Breen (1989), sedimentation of the Magdalena Fan on both the subducting and subducted plates reduces the surface slope and prevents the sediment wedge from sliding forward on the detachment surface. As a result, deformation shifts from the toe towards the interior of the upper plate. Based on gravimetric data, Ruiz et al. (2000) document a change in the nature of the underlying crust, which is interpreted as entirely oceanic crust in the accretion zone and both continental and oceanic in the transpressional and transtensional zone. These regions are interpreted to be separated by the Canoas Fault (Fig. 3.2), which acts as a right-lateral transfer zone that offset the thrust belt creating the space that was occupied by the Magdalena Fan (Ruiz et al., 2000). This model was later supported by observations from 3D seismic data, which demonstrated the absence of an accretionary wedge underlying the Magdalena Fan (Martinez et al., 2015). However, the presence of the Canoas Fault was not corroborated by later studies using bathymetric (Romero-Otero, 2009) and 3D seismic interpretation (Martinez et al., 2015). Alternatively, Martinez et al. (2015) interpret a transpressive regime along the Southern Sinú Fold Belt, and propose that the shift in the deformation

front to the east responds to the cumulative effect of a series of E-W-trending strike-slip faults instead of one major fault.

3.2 Stratigraphy

This section describes the stratigraphy of the Sinú-San Jacinto Basin, which is mostly based on onshore outcrop (e.g. Guzmán, 2007; Herrera et al., 2009) and slim-hole studies (ANH and Universidad de Caldas, 2009). Most of these studies have been carried out in the San Jacinto Fold Belt. Due to frequent lateral facies changes and contentious biostratigraphic dating, several contradictory chronostratigraphic studies in the Sinú-San Jacinto basin exist (e.g., Duque-Caro, 1990; Duque-Caro et al., 1996; Guzmán, 2007; Herrera et al. 2009; ANH-ATG, 2009). Two seismic-based studies that integrate previous field-based studies and well data with seismic-stratigraphic analyses have proposed chronostratigraphic models for the Sinú-San Jacinto basin (Alfaro and Holz, 2014; Martinez et al., 2015).

3.2.1 Basement

In the San Jacinto area, the basement is made of mafic igneous rocks consisting of Upper Cretaceous gabbro, basalt and pillow lavas, intruded by Palaeocene monzodiorite, monzonite, syenite and gabbro (Flinch, 2003). These are overlain by a volcaniclastic unit known as the Barroso Formation (Flinch, 2003).

3.2.2 Upper Cretaceous-Palaeocene

The Cansona Formation has traditionally been described as thin beds of chert with fine-grained sandstones, siliceous siltstones and grey, reddish, black and green shales (e.g. Guzmán, 2007; Niño, 2005). More recently, Herrera et al., 2009 and AHN and ATG (2009) described the Cansona Formation as being primarily composed of thin beds of dark grey, siliceous and calcareous mudstones and shales, with low proportions of chert. In the basal section, they also described lithic sandstones and conglomerates with

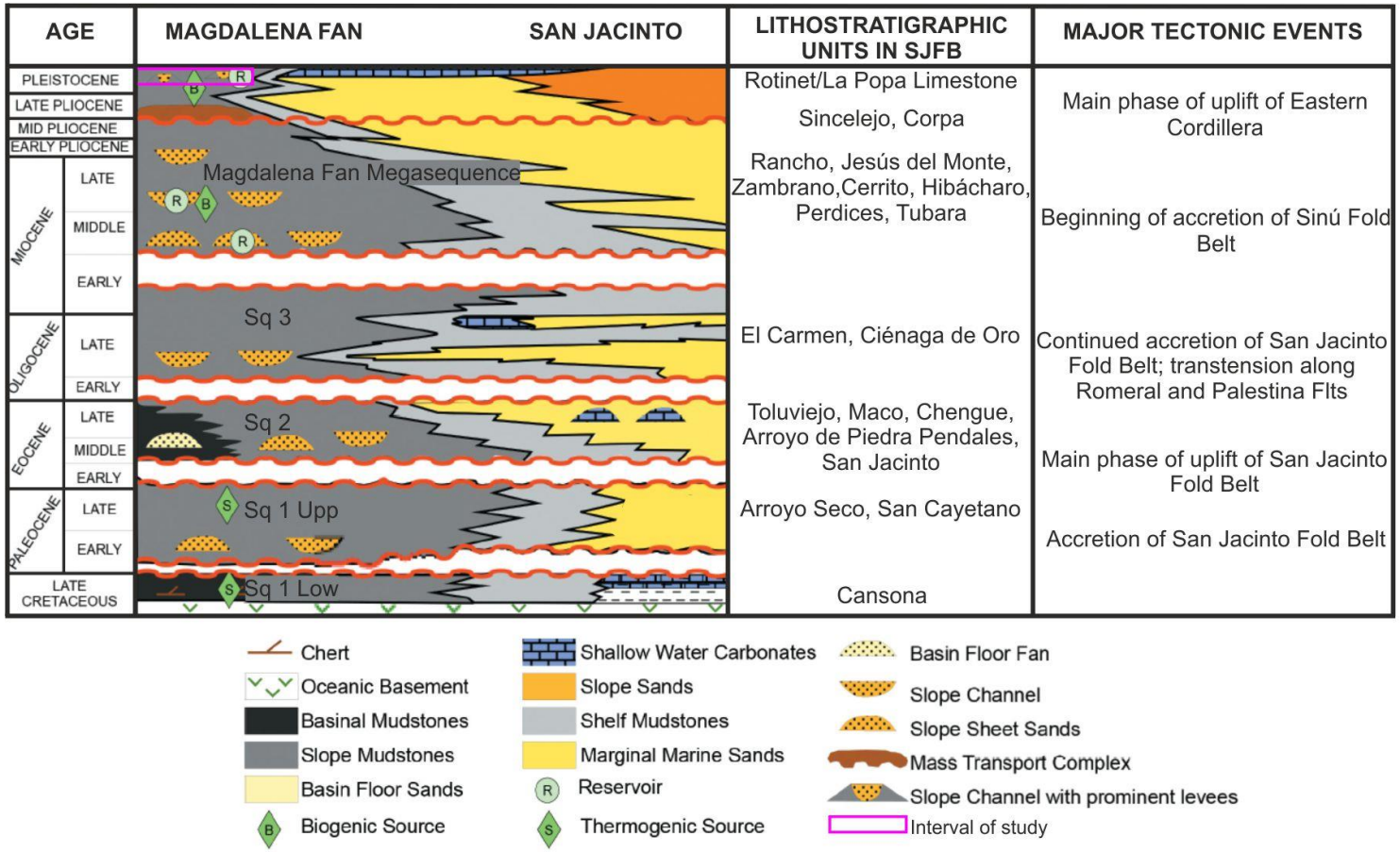

Figure 3.3. Chronostratigraphic chart showing the possible correlation between the seismic sequences defined offshore in the study area, the lithostratigraphic units described in the San Jacinto Fold Belt (SJFB), and major regional tectonic events. Modified from Martinez et al. (2015).

glauconite and fragments of bivalves, interdigitated with mudstones. These contrasting descriptions have led the Cansona Formation to be interpreted as deposited in deep-marine by Guzmán, (2007) and Niño (2005), and in shallow marine settings by Herrera et al. (2009) and ANH and Universidad de Caldas (2009). The latest interpretation matches the findings of the ODP and DSDP wells (see Fig. 3.1 for location) where limestones, marls and chalks were reported in the Upper Cretaceous sediments (Edgar, 1973). Martinez et al. (2015) correlate the Cansona Formation with the basal part of seismic sequence 1, defined in the seismic volume used in this study (Fig. 3.3). It is described as a seismic package containing relatively high-amplitude reflections that fill basement lows and onlap basement highs. This interval is affected by normal faults that also displace the basement but do not propagate into the overlying packages. It is interpreted to represent the latest syn-rift phase (Martinez et al., 2015).

3.2.3 Palaeocene-Lower Eocene

This interval has been attributed to the San Cayetano Formation by Flinch (2003) and Guzmán (2007- Fig. 3.3). It is composed of interbedded basaltic lithic sandstones, siltstones and claystones, with rare conglomerates and chert towards the top, and interpreted as turbidites (Flinch, 2003; Guzmán, 2007). Towards the southern area of the San Jacinto Fold Belt it has been defined as the Arroyo Seco Formation, described as sequence of normally graded litharenites, commonly calcareous, or with high content of organic matter, alternated with carbonaceous mudstones (Herrera et al., 2009; ANH and Universidad de Caldas, 2009). Mud-prone levels consist of variably bioturbated, dark calcareous mudstones, occasionally interbedded with sandstone and limestone (Herrera et al., 2009; ANH and Universidad de Caldas, 2009). Polymictic, generally grain-supported conglomerates with a calcareous, coarse sand matrix, are also reported (ANH and Universidad de Caldas, 2009). Following these observations, Herrera et al. (2009) and ANH and Universidad de Caldas (2009) interpret the Arroyo Seco Formation as deposited in a transitional, deltaic environment. Contained in the San Cayetano and

Arroyo Seco formations, Cardona et al. (2012) found lithic clasts containing heavy minerals such as kyanite, garnet and schist; they were interpreted as being sourced from an accreted and uplifted intra-oceanic arc. Martinez et al. (2015) correlate the Arroyo Seco Formation with the upper part of seismic sequence 1 (Fig. 3.3), which is not affected by normal faults and has less lateral thickness changes than the basal part of the sequence.

3.2.4 Mid-Eocene-Mid-Oligocene

This interval is characterised by lateral facies variations between clastic sandstones and conglomerates, interpreted to have been deposited by fan deltas (Guzmán 2007), and bioclastic limestones with skeletal fragments of molluscs, red algae, echinoids, macro-foraminifera, and oncolites (Guzmán, 2007; Herrera et al., 2009) deposited in shallow-marine environments. This interval is interpreted as a carbonate platform locally interrupted by point-sourced fluvio-deltaic systems (Guzmán, 2007; Cardona et al, 2012; Alfaro and Holz, 2014b). Due to frequent lateral facies variations, several lithostratigraphic units comprise the Mid-Eocene to Mid-Oligocene sequence, including the Maco, Chengue, Toluviejo, Arroyo de Piedra, Pendales and San Jacinto formations (Fig. 3.3). Martinez et al. (2015) correlate this interval to their seismic sequence 2 (Fig. 3.3), which is characterised high-amplitude reflections that downlap against an unconformity that truncates seismic sequence 1.

3.2.5 Late Oligocene-Late Miocene

This interval contains the El Carmen Formation (Fig. 3.3), also known as the Porquera Formation (Guzmán, 2007), which is composed of dark grey claystones with planktonic foraminifera and is a tested source rock in the Lower Magdalena Valley. At a similar chronostratigraphic level, Herrera et al. (2009) and ANH and Universidad de Caldas (2009) describe comparable mudstones as the El Floral Formation. Offshore, Martinez et al. 2015 correlate the El Carmen Formation with a low-amplitude onlapping package, which they interpret as a transgressive sequence (sequence 3; Fig. 3.3). Similarly, Alfaro

and Holz (2014b) interpret this interval to represent a regional relative sea-level rise. The upper part of this interval locally contains the Ciénaga de Oro Formation which is composed of lithic sandstones with undulated and flaser lamination, containing fragments of bivalves, gastropods, leafs and carbonaceous material (ANH and Universidad de Caldas, 2009). It is interpreted to have been deposited in a fluvially-influenced transitional to shallow marine environment (ANH and Universidad de Caldas, 2009).

3.2.6 Late Miocene-Recent

This interval is characterised by progressive shallowing (Guzmán, 2007; Alfaro and Holz, 2014b; Martinez et al., 2015-Fig. 3.3). In the San Jacinto Fold Belt, Late Miocene units contain shallow marine and transitional sandstones and conglomerates (Flinch, 2003; Guzmán, 2007; Herrera et al., 2009). Lithostratigraphic units include the Rancho, Jesús del Monte, Zambrano, Cerrito, Hibácharo, Perdices and Tubará formations (Guzmán, 2007-Fig. 3.3). Pliocene and Pleistocene units are composed of siltstones with muscovite, coal and plant fragments and root marks, lithic sandstones with internal erosion surfaces, and conglomerates with volcanic clasts (Herrera et al., 2009). Lithostratigraphic units comprise the Sincelejo, Corpa and Rotinet formations (Guzmán, 2007). Offshore, this interval is dominated by the Magdalena Fan which is interpreted to have been established in the Mid-Late Miocene (Duque-Caro, 1979, 1984; Kolla and Buffler, 1984; Breen, 1989; Ruiz et al., 2000; Romero-Otero, 2009; Alfaro and Holz, 2014b; Martinez et al., 2015). Martinez et al. (2015) defined this interval as the Fan Megasequence; it is characterised by continuous progradation from frontal lobes, to channel-levee complex sets and mass-transport complexes (MTCs) (Martinez et al., 2015). Northeast of the city of Cartagena (Fig. 3.2), the Pleistocene is represented by the reefal limestones of the La Popa Formation (Guzmán, 2009). This study concentrates in the shallow stratigraphy of the southern Magdalena Fan (Fig. 3.3), which was drilled to the northeast of the study area by the Cartagena wells and dated as Pleistocene-

Recent based on planktonic foraminifera (Rincon et al., 2007). Given that the latest phase of activity of the Magdalena Fan in the study area occurred during the Late Pleistocene (Romero-Otero, 2009; see section 3.3), this is the likely age of the study interval.

3.3 The Magdalena Fan

The Magdalena Fan has an area of 68,000 km^2 (Romero-Otero et al., 2009) and is fed by the Magdalena River (Fig. 3.4), which is 1,600 km long with a drainage basin area of 260,000 km^2 (Restrepo and Kjerfve, 2000). The sedimentation of the Magdalena Fan is inferred to have started in the Middle Miocene following the Oligocene-Miocene Proto-Andean Orogeny (Duque-Caro, 1979; Kolla and Buffler, 1984; Alfaro and Holz, 2014b; Martinez et al., 2015). Since the Miocene, repeated avulsions of the Magdalena River have led to the river mouth being positioned in multiple locations between the cities of Cartagena and Santa Marta (Fig. 3.4). Based on multibeam bathymetry and 2D seismic (Fig. 3.4), Romero-Otero (2009) investigate the stacking patterns of channel-levee complex sets, and the influence of tectonics on major lateral shifts in the position of the fan. Romero-Otero (2009) reconstructed the recent (Pleistocene to Holocene) history of the Magdalena Fan and identified eleven different positions of the Magdalena River mouth and its corresponding delta (Fig. 3.5). Nine shifts occurred during the Plio-Pleistocene, with the last major changes taking place in the Late Pleistocene, when onshore uplift caused the river to avulse from just north of the city of Cartagena to the Ciénaga de Santa Marta. Subsequently, it switched to the west in the Holocene to its present-day river mouth position (Fig. 3.4 and 3.5). According to this interpretation, the interval investigated in this study (Fig. 3.3) was likely deposited during the Late Pleistocene (Fig. 3.5).

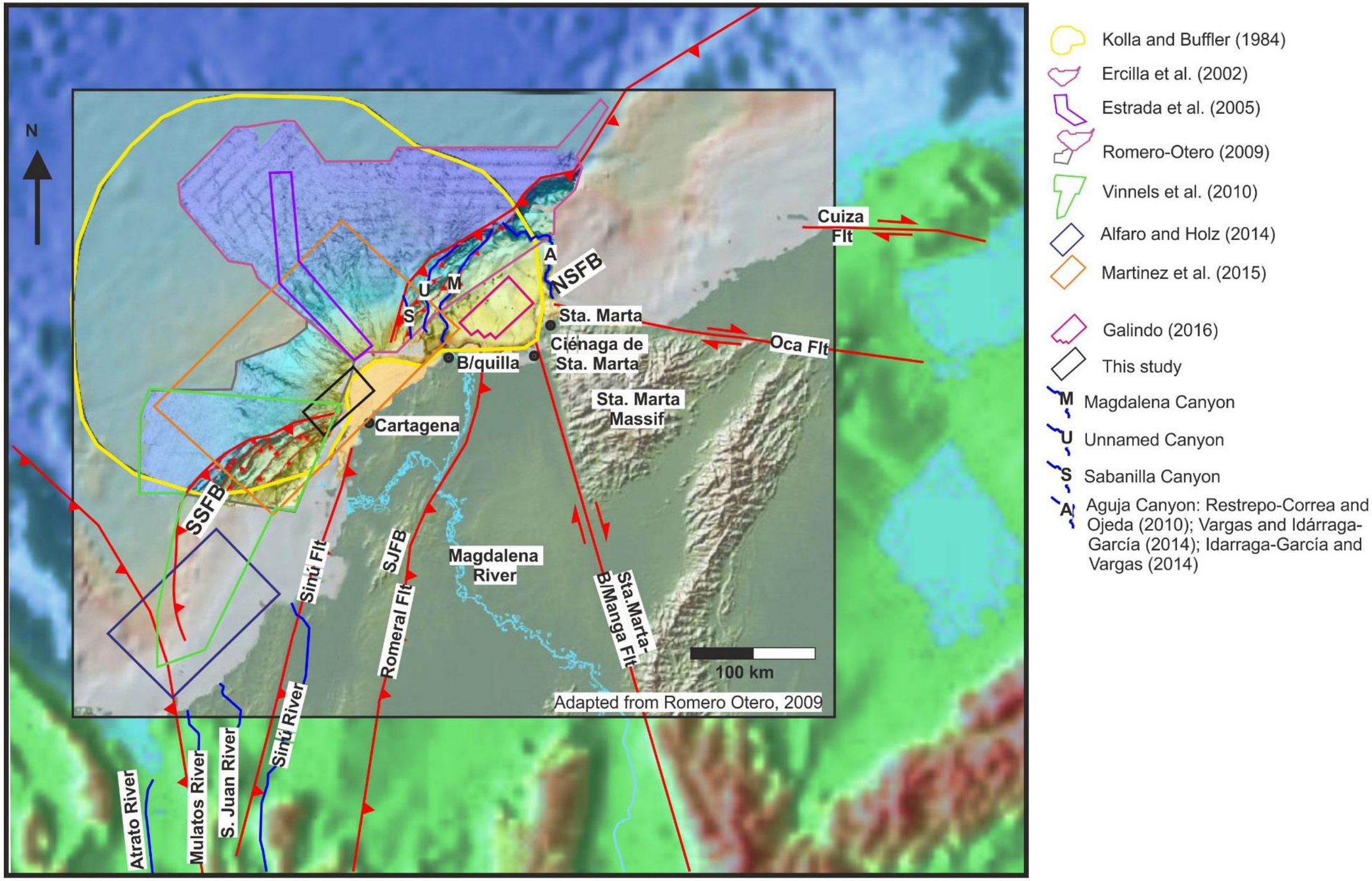

Figure 3.4. Map showing the key structural elements and drainage systems of northern Colombia, and the location of the Magdalena Fan. Coloured polygons show the location of previous studies with respect to this study (black polygon). Modified from Romero-Otero (2009).

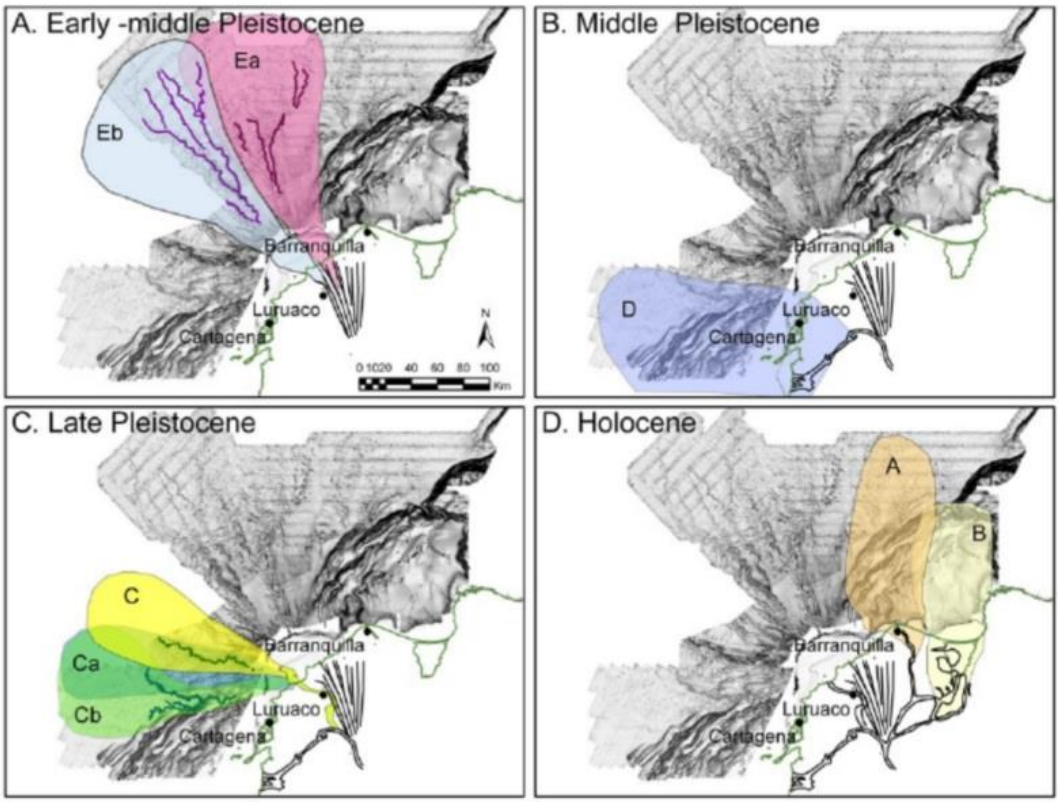

Figure 3.5. Pleistocene-Holocene evolution of the Magdalena Fan. From Romero-Otero (2009).

Kolla and Buffler (1984) used multichannel seismic and piston cores to characterise the morphology of the fan and subdivided it, in the down-flow direction, into upper, middle and lower fan areas (Fig. 3.6). The upper fan, located basinward of the continental slope, is composed of well-developed channel-levee complexes and sediment waves that contrast with the updip slope, which is characterised by an irregular seafloor with canyons and slumps. In the middle fan, the number of channel-levee complex sets increases and the height of their levees to decreases gradually downslope (Kolla and Buffler, 1984). In the lower fan, few channels are documented and the fan has a relatively flat morphology. Here, turbidites composed of Ta, Tb intervals and composed of medium to fine grained sands were observed in piston-cores (Kolla and Buffler, 1984).

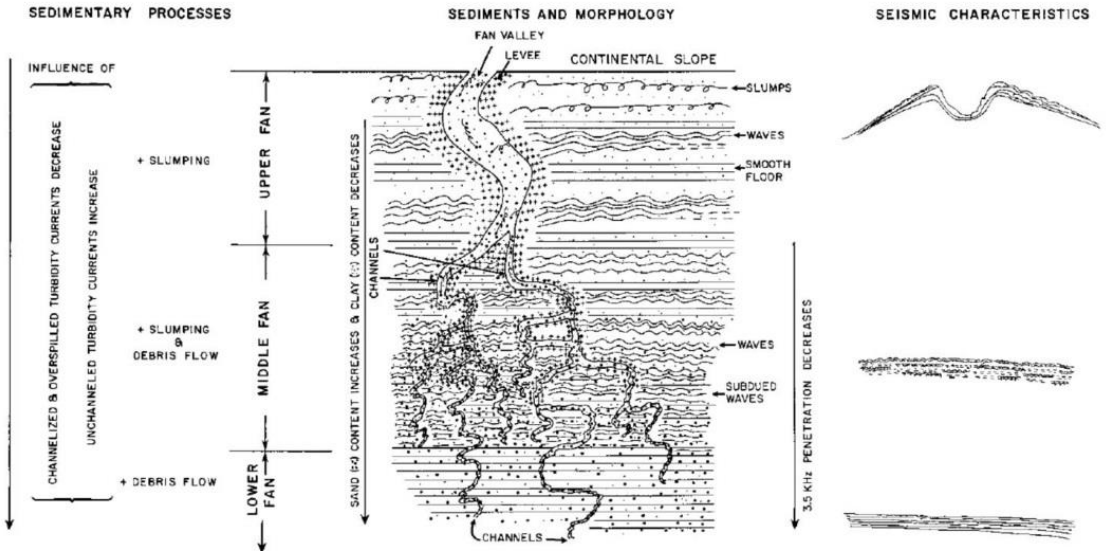

Figure 3.6. Characteristics of the Magdalena fan basinwards of the continental slope. From Kolla and Buffler (1984).

Currently, the Magdalena River, discharges c. 150 MT of sediment per year into the Caribbean Sea, making it the largest direct sediment contributor, and one of the world's top ten rivers in terms of sediment load (Restrepo and Kjerfve, 2000; Restrepo and López, 2008). These sediments create a 1,690 km^2, wave-dominated delta (Restrepo and López, 2008) deposited on a narrow (c. 2 km) shelf that is connected to the basin floor by three active submarine canyons known as the Sabanilla, Magdalena and Unnamed canyons (Romero-Otero, 2009; Fig. 3.4). The slope in the Magdalena Fan is predominantly above-grade (Cadena et al., 2015). In the deformed areas it is characterised by Gaussian slope profiles (*sensu* Adams and Schlager, 2010) with ponded accommodation (*sensu* Prather, 2003) and tortuous sediment flow-pathways (Ercilla et al., 2002; Romero-Otero, 2009; Vinnels et al., 2010; Cadena et al., 2015). In the relatively undeformed central part of the fan, slope profiles are exponential (*sensu* Adams and Schlager, 2010) and characterised by steep upper slope gradients (2.5-3.5º- Romero-Otero, 2009) that result in mass-wasting, bypass and erosion (Cadena et al., 2015). Cadena et al. (2015) interpret that through erosion and sedimentation, the Magdalena Fan is transitioning from and out-of-grade slope to a graded slope.

The present day sediment flow-pathways are located in the Nothern Sinú Fold Belt and traverse four piggy-back basins connected through a series of knick-points (Fig. 3.4). These piggy-back basins are primarily filled by MTCs that were sourced from the frontal limbs of growing anticlines (Romero-Otero, 2009; Romero-Otero et al., 2010). Piston cores along the present-day sediment flow pathways show that turbidites are composed of 40-80% fine to very fine sandstones, which are variably sorted and contain abundant plant debris; the remaining 20-60% is composed of silt and mudstones (Romero-Otero, 2009). Romero-Otero (2009) analysed the cable breaks reported since the 1950s, which are interpreted to have been caused by gravity flows, and correlated them to river flood-stages and seasonally enhanced long-shore drift.

To the east of the active fan, north of the Santa Marta Massif, the Aguja Canyon, a sinuous feature that is not directly fed by the Magdalena delta develops (Fig. 3.4). Restrepo-Correa and Ojeda (2010) used multibeam bathymetry to describe its morphology in detail, which is characterised by steep canyon walls, abrupt changes in orientation and various knickpoints. Restrepo-Correa and Ojeda (2010) interpret pulses of slip along the Oca Fault (Fig. 3.4) and mud diapirism as important controls on the evolution and morphology of the Aguja Canyon. Vargas and Idárraga-García (2014) also used multibeam bathymetry to identify and date 31 submarine landslides on the flanks of the Aguja Canyon. The landslides are dated from 1 to 631 ky and possible causal mechanisms are seismicity and slope oversteepening due to mud diapirism (Vargas and Idárraga-García, 2014).

Ercilla et al. (2002), used multibeam bathymetry and high resolution seismic profiles to characterise the morphology and depositional patterns of the northern Magdalena Fan (Fig. 3.4). They divide the fan in two provinces characterised by Gaussian and exponential slope morphologies: deformed-constructional and undeformed-erosive. The deformed-constructional provinces overlie uplifted areas of the accretionary prism where sediment transported by canyons and gullies is deposited within the fold belt, hence the

term constructional. The undeformed-erosive province is located in the central undeformed area and is similar to passive margin fans and is characterised by large MTCs, channel-levee complex sets and sediment waves (Ercilla et al., 2002). This area is classified as erosive because the primary depositional geometry of the channel-levee complex sets has been degraded and modified by MTCs and sediment waves (Ercilla et al., 2002). Estrada (2005) used part of the same bathymetric survey to quantitatively characterise the morphology of a Mid-Late Pleistocene, sinuous channel-levee complex set in the central part of the fan (Fig. 3.4). Measurements of the thalweg and levee profiles, used to compute a channel relief profile, show that although there is a general decrease in channel and levee relief downslope, they are highly irregular, particularly in the updip area (Estrada et al., 2005). Estrada et al. (2005) also document two major avulsions and the development of associated knick-points that favoured local erosion and bypass. Based on the height of the levees, Estrada et al. (2005) infer that genetically-related turbidity currents were relatively thick and contained a large volume of silt and mud. They propose that turbidity currents became sandier downdip due to overspilling, thus explaining the downdip reduction in levee thickness.

The southern part of the fan, which is no longer actively fed by the Magdalena River, is in the Southern Sinú Fold Belt (Fig. 3.4). This region corresponds to the southern part of the area studied by Romero-Otero and the northern part of the area studied by Vinnels et al. (2010; Fig. 3.4). Here, changes in gradient, related to growth of the tectonic structures are interpreted to have been a major influence on the morphology of the channel-levee complex sets (Romero-Otero, 2009). Increased sinuosity, resulting in repeated channel avulsion and northward migration of the channel-levee complexes in response to structural uplift during the Pleistocene is documented (Romero-Otero, 2009). Abandonment of syn-tectonic channel-levee complexes that became folded by the growing anticlines and the creation of new channel conduits also occurred (Romero-Otero et al., 2009). Further south, sediments in the Southern Sinú Fold Belt are mainly

sourced from rivers that drain volcanic terranes and are small in comparison to the Magdalena River, the largest of which is the Sinú River (Vinnels et al., 2010; Fig. 3.4). Here the slope is characterised by imbricate thrust anticlines and piggy-back basins, creating tortuous corridors. Based on multi-beam bathymetry and 2D seismic, Vinnels et al. (2010) define sediment routes that do not pass directly across structurally deformed areas, routes that traverse the fold belt and reach the Colombia Basin, and routes that pass through the fold belt but do not connect to the Colombia Basin. Mass-wasting is a common process; MTCs are mostly detached (*sensu* Moscardelli and Wood, 2008), tend to occur within piggy-back basins and are sourced from local collapse of the steep flanks of the anticlines. Degradation of the flanks of the anticlines and filling of the piggy-back basins can connect otherwise isolated sub-basins (Romero-Otero, 2009; Vinnels et al., 2010). The recurrence of this process, can eventually create through-going tortuous conduits that connect the shelf to the open slope in the foreland (Vinnels et. al., 2010). The study by Vinnels et al. (2010) demonstrates the complexity of the sediment dispersal patterns across the deformed seabed and highlight the effect of bathymetric irregularities on turbidite and MTC sedimentation.

As mentioned above, MTCs are recognised along the entire Magdalena Fan. In the deformed areas of the fan detached MTCs (*sensu* Moscardelli and Wood, 2008) are most common and are triggered by instability of the steep frontal flanks of the anticlines or steep canyon walls (Ercilla et al., 2002; Romero-Otero, 2010; Vinnels et al., 2010). In the undeformed areas shelf-attached MTCs (*sensu* Moscardelli and Wood, 2008) are more frequent and are possibly triggered by seismic activity or abandonment of the delta front and the downdip fan (Romero-Otero et al., 2010); these tend to concentrate in inter-channel lows. In the undeformed area, detached MTCs also occur as a consequence of local levee collapse. Idárraga-García and Vargas (2014) used high-resolution bathymetry to characterise submarine landslides in the Magdalena Fan and the Sinú Fold Belt. They interpret the landslides in the Sinú Fold Belt to be more cohesive,

comprising slumps and blocky debris flows with runout distances between 11 km, while those in the Magdalena fan are interpreted as “disintegrative,” meaning that they leave no deposit within or at the base of the scar (Idárraga-García, 2014). Dating of the landslides shows that in the Sinú Fold Belt MTCs to span between 12 and 1030 ky, while in the Magdalena Fan MTCs span from 14 to 9,760 ky.

As shown above, most of the previous studies that investigate sedimentation patterns in the area of influence of the Magdalena Fan have used bathymetric and 2D seismic data (Kolla and Buffler, 1984; Ercilla et al., 2002; Estrada et al., 2005; Romero-Otero, 2009; Restrepo-Correa and Ojeda, 2010; Romero-Otero et al., 2010; Vinnels et al., 2010; Idárraga and Vargas, 2014; Vargas and Idárraga, 2014). Since 2007, however, eleven 3D seismic surveys have been acquired along the Colombian Caribbean margin, exponentially improving the understanding of the tectonic and sedimentary environments. Yet, few studies have been published. Alfaro and Holz (2014) characterised the sediment dispersal patterns in the westernmost area of the Southern Sinú Fold Belt which is affected by folding, thrusting and mud diapirism, and is primarily fed by the Atrato, Mulatos, San Juan and Sinú rivers (Fig. 3.4). The deposits identified are mostly composed of slumps and debrites confined within piggy-back basins, with some intervening turbidites (Alfaro and Holz, 2014). Mud diapirism, high fluvial sediment supply and gas hydrate dissolution are interpreted as possible triggering mechanisms. Martinez et al. (2015) propose a model for the tectonostratigraphic evolution of the Magdalena Fan area, integrating the seismic survey used in this study with 2D seismic, well data and outcrop studies and postulate a possible oil play involving source rocks from the Upper Cretaceous and Palaeocene. More recently, Galindo (2016) developed a PhD thesis that investigated the structural evolution of the Bahía Basin. This is hence the first study to characterise the sediment dispersal patterns and depositional geometries of the Magdalena Fan in detail using 3D seismic data.

4 Methodology

4.1 Framework mapping

Seismic interpretation was performed using Petrel®. Key stratigraphic horizons were defined based on reflection terminations such as truncation, onlap and downlap and changes in the seismic character. These horizons were mapped on a relatively coarse grid, with a line-spacing of 25 to 50 depending on the lateral continuity of the reflections. Horizons were auto-tracked using the 3×3 validated option and interpolated by creating surfaces. Basic attribute extractions such as RMS amplitude and variance taken on isoproportional slices (cf. Zeng et al., 1998) were produced and analysed to gain a general understanding of the depositional patterns.

4.2 Seismic Facies

Seismic facies were defined based on the amplitude, continuity, and configuration of the seismic reflections, the geometry of seismic units, and their stratigraphic relationship with other seismic facies. Seismic facies and facies associations were then used to interpret sedimentary sub-environments such as channel-levee complexes, MTCs, lobes, etc. The interpretation of these seismic facies and facies associations is based on comparison with previously published and widely cited seismic based studies of deep-water systems (e.g. Mitchum et al., 1977; Pirmez et al., 1997; Abreu et al., 2003; Deptuck et al., 2003; Posamentier and Kolla, 2003; Gee et al., 2007; Cross et al., 2009; Catterall et al., 2010), and on the broader understanding of the regional setting.

Two seismic facies classifications were defined, the first one is a general seismic facies classification that includes all the major sedimentary subenvironments identified in the interval of interest; the second one is a detailed subdivision of the MTC seismic facies association. Chapters 5 to 7 contain individual classifications depending on the seismic

facies that are relevant to each chapter; those classifications are extracted from the following descriptions.

4.2.1 General seismic facies

4.2.1.1 Facies 1: Parallel discontinuous

This is a common seismic facies type in which the reflections are parallel, yet discontinuous (i.e., can only be traced for a maximum of c.1 km) (Fig. 4.1). They may be flat, inclined, wavy or concave. Amplitudes are variable but generally high, especially towards the base of the package. In map view the seismic facies is elongate with sinuous, high and low amplitude threads, and is bounded on either side by the wedge-shaped, continuous facies (Fig. 4.1).

This seismic facies type is interpreted to represent the fill of slope channel complex sets (e.g., Abreu et al., 2003; Deptuck et al., 2003; Posamentier and Kolla, 2003; Mayall et al., 2006; McHarghe et al., 2011).

4.2.1.2 Facies 2: Parallel wedge-shaped

Parallel, continuous, inclined, low-amplitude reflections commonly form packages of 50-300 m thick that thin progressively until they pinch out over a maximum distance of 4 km, resulting in a wedge-shaped geometry (Fig. 4.1). This facies is commonly found on either side of the parallel, discontinuous facies and it commonly displays basal downlap. Locally, the basal reflections onlap older sedimentary packages, or the reflections are truncated and overlain by younger deposits. In map view the wedge shapes are elongate, trending parallel to the channel fill facies (Fig. 4.1).

The wedge-shaped geometry, basal downlap and the spatial relationship with channel-fill facies supports an interpretation for this seismic facies as external levees (e.g., Deptuck et al., 2003; Posamentier and Kolla, 2003; Catterall et al., 2010; Nakajima and Kneller, 2013).

4.2.1.3 Facies 3: Confined, sub-parallel wedge-shaped

Seismic facies 3 comprises sub-parallel continuous reflections that can be traced for 1-2 km in cross-section. They thin towards, and are confined by, an incision surface (Fig. 4.1A). Thicknesses of individual packages is c. 100 m. Individual reflections dip gently into the confining surface, at an angle that decreases upwards. Amplitudes are generally low and in map view they are elongate. This facies is found between the parallel discontinuous channel-fill facies and the confining surface, trending parallel to both in map view (Fig. 4.1B). Packages are sometimes down-thrown and rotated across discontinuities that dip towards the channel fill facies.

This facies is interpreted as being representative of internal levees (sensu Kane and Hodgson 2011) or terrace deposits (e.g. Deptuck et al., 2003; Babonneau et al., 2004; Hansen et al., 2015).

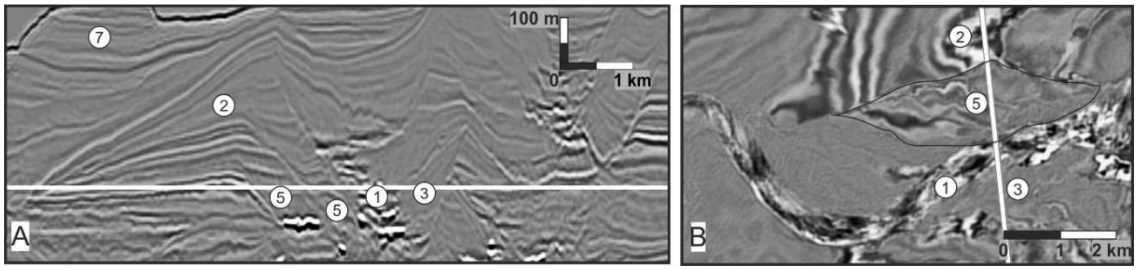

Figure 4.1. Seismic facies composing channel-levee complex sets. **A.** Seismic cross-section showing examples of facies 1, 2, 3 and 5 which are interpreted to compose channel-levee complex sets and seismic facies 7 which is interpreted as background sedimentation. **B.** Depth slice showing the map view appearance and areal distribution of facies 1, 2, 3 and 5 which are interpreted to compose channel-levee complex sets.

4.2.1.4 Facies 4: Chaotic

Composed of chaotic, discontinuous reflections in which troughs can be traced for a maximum of 500 m and peaks typically are only continuous for c. 100-200 m. The internal character is chaotic with individual reflections dipping in different directions and at different angles. It overlies erosional basal surfaces and the tops are often irregular (Fig. 4.2). Facies 4 ranges from c. 50-200 m in thickness with areal extents of tens to hundreds of kilometres and steep lateral margins. Commonly, irregularities on the top surface

coincide with discrete areas of coherent and/or deformed reflections that cover areas up to 7 km^2, with maximum thicknesses exceeding 250 m.

The chaotic facies is interpreted to represent mass transport complexes (MTCs) that can comprise deposits from a range of cohesive mass flow processes including debris flows, slumps and slides (e.g. Weimer, 1990; Weimer and Shipp, 2004; Moscardelli et al., 2006; Bull et al., 2009). The discrete protruding areas are interpreted as megaclasts (e.g. Gamboa et al., 2011; Jackson, 2011; Olafiranye et al., 2013; Omosanya and Alves, 2013; Alves, 2015; Gamboa and Alves, 2015).

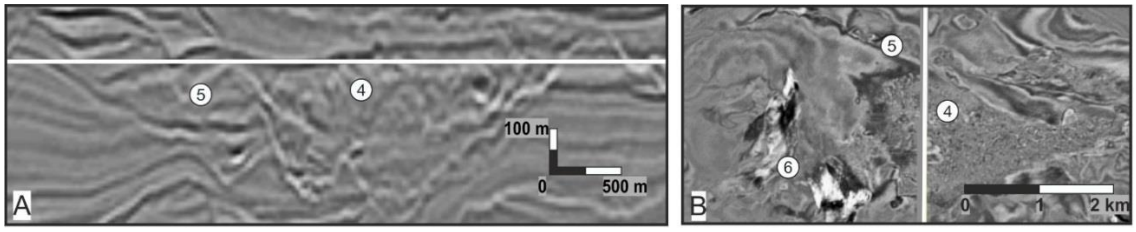

Figure 4.2. Examples of seismic facies 4 and 5. **A.** Seismic cross-sections showing seismic facies 4 which is chaotic and interpreted as MTCs. Seismic facies 5 is composed of parallel rotated reflections that are interpreted as slides from the lateral walls of the MTCs when they are adjacent to facies 4. **B.** Depth slice showing the map view appearance of facies 4, 5 and 6.

4.2.1.5 Facies 5: Sub-parallel rotated

This seismic facies is characterized by sub-parallel reflections that are rotated with respect to adjacent, overlying and underlying reflections along discontinuities that sometimes exhibit listric geometries (Fig. 4.1A and 4.2A). Amplitudes are variable and rotated packages are elongate in map view (Fig. 4.1B and 4.2B). When located adjacent to the channel-fill facies, within the channel confining surface, packages are rotated across a discontinuity that dips towards the channel axis and are approximately 100 m thick and 700-1500 m wide in cross-section (Fig. 4.1A). Locally, individual reflections and packages have wavy geometries. Rotated seismic packages are also found in association with chaotic seismic facies (Fig. 4.2A). They overlie normal faults that dip in the direction of the chaotic facies. They are about 3 km wide in cross section and 100 m thick.

The rotated packages are interpreted as coherent blocks of substrate that have been affected by post-depositional sliding above décollement surfaces. When adjacent to channel fill facies and within the channel's confining erosion surface, they are interpreted as slides of internal levee, or inner external levee deposits (*sensu* Kane and Hodgson, 2011). When associated with chaotic facies they are interpreted as blocks of substrate at the margins of MTCs

4.2.1.6 Facies 5: Parallel, variable amplitude reflections

Found as single cycle events or in packages of a few reflections. They are parallel and continuous over c. 3-7 km in cross-section, and downlap onto underlying surfaces and onlap onto older adjacent packages (Fig. 4.3A). Maximum thickness ranges between 15 and 80 m and decreases away from a central point, resulting in a convex shape. Amplitudes are also higher towards the centre and display a range of lobate geometries in map view that are up to 2 km wide and 10 km^2 in area. In map view, high amplitudes can be traced to the lobes along narrow elongate pathways that are less than 100 m wide (Fig. 4.3B).

This seismic facies is interpreted as lobe complexes fed by channelized conduits.

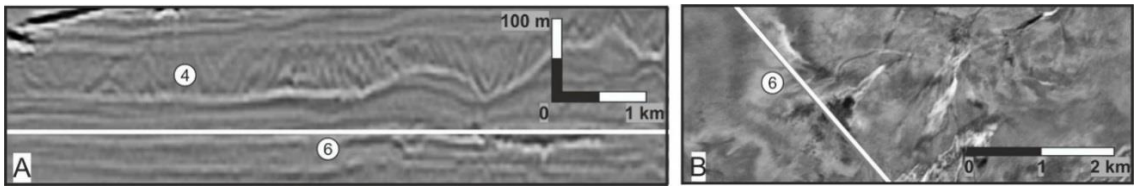

Figure 4.3. Example of seismic facies 6. **A.** Seismic cross-section showing examples of seismic facies 4 (chaotic) and 6 which is composed of parallel, variable amplitude reflections with a convex shape. **B.** Depth slice showing the lobate geometries of facies 6 and the channelized features that connect to the lobes.

4.2.1.7 Facies 6: Parallel, dim amplitude, continuous reflections

Parallel and dim reflections are commonly found to drape or onlap pre-existing bathymetry (Fig. 4.1A). Reflections can be continuously traced for over 10 km.

This seismic facies is interpreted as representative of background sedimentation, likely consisting of siliciclastic suspension fallout.

4.2.2 MTC seismic facies association

The MTC seismic facies was further subdivided based on the amplitude, continuity and deformation of the seismic reflections, in order to capture its heterogeneity. A quantitative evaluation of the MTC seismic facies within the largest MTC, measuring variance, amplitude and dip values for each of the seismic facies, in accordance with the methodology proposed by Alves et al. (2014), was performed in order to test the seismic facies classification defined using visual inspection; this is included in Appendix 1.

4.2.2.1 MTC facies 1

Facies 1 generally contains relatively low-amplitude, chaotic reflections that have an erosional base and an irregular top (Fig. 4.4). These packages often contain facies 5; thicknesses are normally ≥50 m.

Facies 1 is interpreted to represent debrites (cf. Posamentier and Kolla, 2003; Olafiranye et al., 2013). The discontinuity and chaotic character of the reflections are interpreted to indicate that the material within the debrites was highly disaggregated (cf. Alves et al., 2014).

4.2.2.2 MTC facies 2

Facies 2 is composed of variable amplitude, semi-continuous reflections that are deformed by folds that are c. 200-300 m wide (Fig. 4.5A). They overly erosional surfaces and have irregular tops and commonly contain facies 5. Thickness is normally c. 100 m.

Facies 2 is interpreted to represent debrites (cf. Posamentier and Kolla, 2003; Olafiranye et al., 2013) in which the material was less disaggregated in comparison to facies 1 (cf. Alves et al., 2014).

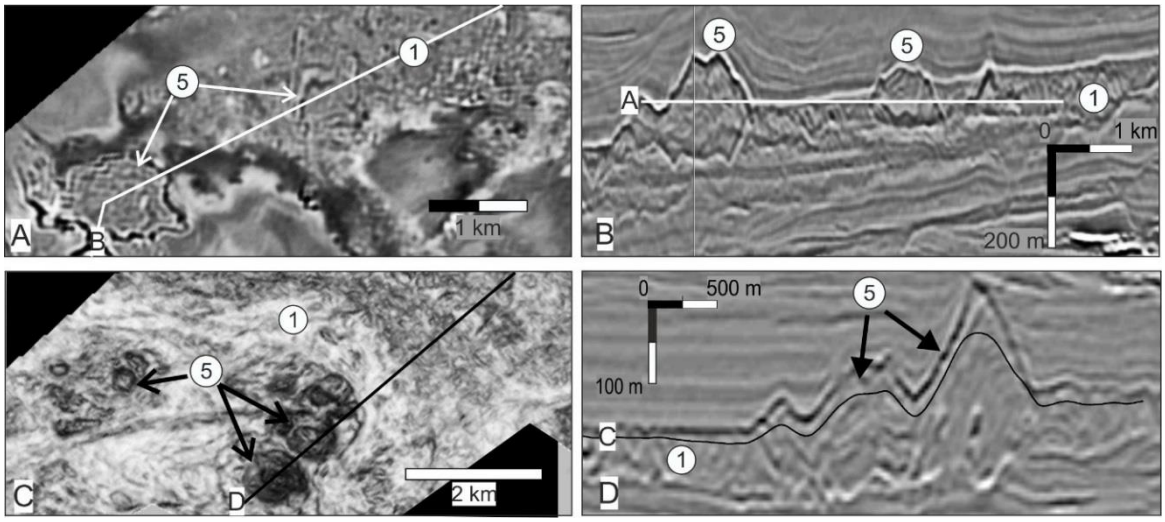

Figure 4.4. Examples of MTC seismic facies 1 and 5. **A.** Depth slice showing the map view appearance of MTC seismic facies 1 (debrites) and 5 (megaclasts). **B.** Cross-sectional view of the megaclasts in A. Note the contrast with MTC seismic facies 1. **C.** Variance extraction in the uppermost interval of an MTC showing megaclasts. **D.** Cross-sectional view of the megaclasts in A.

4.2.2.3 MTC facies 3

Facies 3 is characterised by variable amplitude, semi-continuous reflections that affected by imbricate are thrusts that bound folds that are c. 400-500 m wide and more than c. 200 m high (Fig. 4.5B). Facies 3 is interpreted as imbricate fold and thrust systems (*sensu* Bull et al., 2009) developed in response to contraction (cf. Frey-Martinez et al., 2006; Moscardelli et al., 2006; Dykstra et al., 2011).

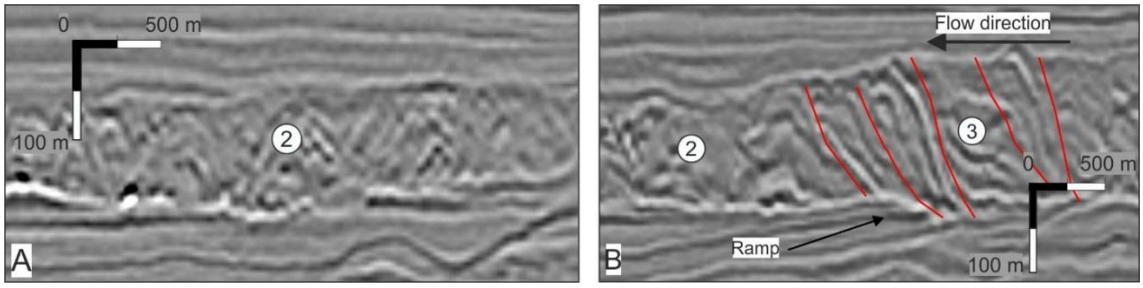

Figure 4.5. Examples of MTC seismic facies 2 and 3. **A.** Seismic cross-section showing MTC seismic facies 2; note the folded semi-continuous to discontinuous reflections. B. Seismic cross-section showing MTC seismic facies 2 (debrites) and 3 (imbricate thrust and fold systems). The vergence of the thrusts and folds can be used as an indicator of emplacement direction.

4.2.2.4 MTC seismic facies 4

Facies 4 is characterised by low-amplitude packages with few internal reflections that overlie erosional surfaces and have undulated tops (Fig. 4.6). Thicknesses are between c. 50 and 100 m. Facies 4 is interpreted as mud-prone debrites (cf. Posamentier and Kolla, 2003; Talling et al., 2012).

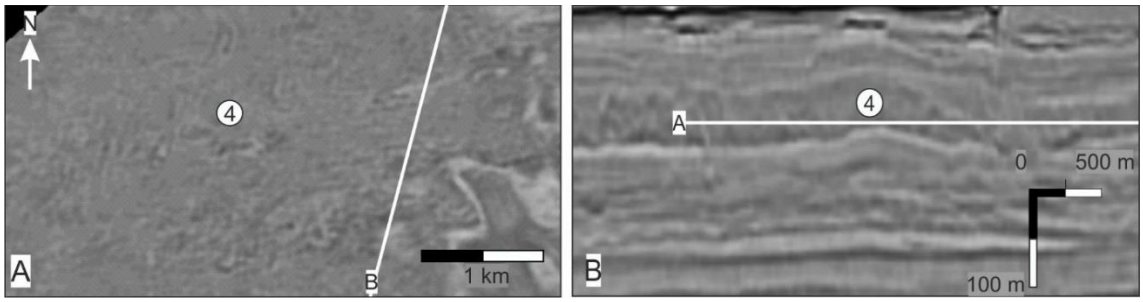

Figure 4.6. Example of MTC seismic facies 4. **A.** Depth slice showing the low-amplitude reflection-free character of MTC seismic facies 4 which is interpreted as mud-prone debrites. **B.** Seismic cross-section showing the appearance of MTC seismic facies 4.

4.2.2.5 MTC seismic facies 5

Discrete packages of coherent, parallel reflections set within a matrix dominated by facies 1 or 2. These coherent reflections occur in packages that are predominantly up to 200 m thick and cover areas of up to 1.6 km^2 (Fig. 4.4). In most cases these packages are folded. Based on these characteristics and by comparison to features described elsewhere, facies 2 is interpreted to be megaclasts transported within the MTC parent flow and deposited within the MTC itself (*sensu* e.g. Prior et al., 1984; Bull et al., 2009; Alves, 2010; Alves and Cartwright, 2010; Alves and Lourenço, 2010; Gamboa, et al., 2011; Alves, 2014; Jackson, 2011; Talling et al., 2012; Kneller et al., 2015; Alves, 2015; Gamboa and Alves, 2015). Some of these packages are considerably larger, with areas of 5-7 km^2 and thicknesses in excess of 250 m. They are composed of parallel reflections that are folded into symmetric, asymmetric, recumbent and isoclinal folds and are associated with facies 1 and 2 (Figure 4.7). Given the lateral continuity of the reflections and the scale of the folds (up to 7 km^2), the larger packages, rather than representing megaclasts, could instead be interpreted as slump folds (cf. Bull and Cartwright, 2010;

Posamentier and Martinsen, 2011). However, due to their association with facies 1 and 2 and because differentiating between these two hypotheses is not critical to the overall objective of this study, they are preferably interpreted as megaclasts (cf. McGilvery et al, 2004; Bull et al, 2009; Frey-Martinez, 2010; Jackson, 2011; Posamentier and Martinsen, 2011; Olafiranye et al, 2013; Alves, 2015).

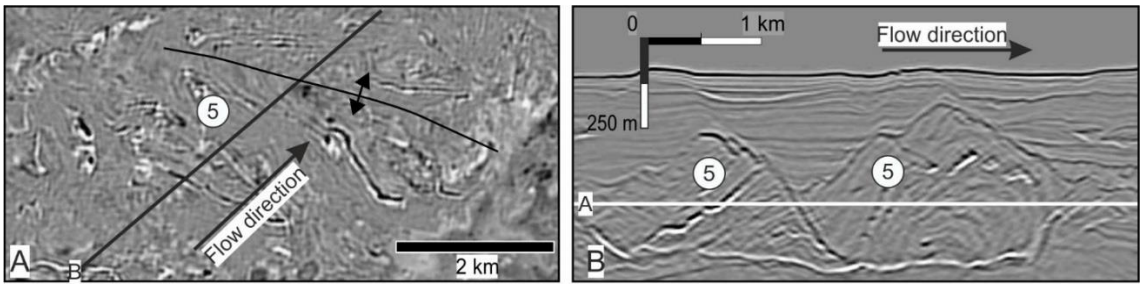

Figure 4.7. Example of large folded megaclasts. **A.** Depth slice showing the axis of a fold in a megaclast. **B.** Seismic cross-section showing asymmetric to recumbent fold within a megaclast. Fold vergence can be used to infer emplacement direction.

4.2.3 Kinematic Indicators

In order to interpret the emplacement direction of MTCs, kinematic indicators (*sensu* Bull et al., 2009) were analysed. These were identified at the basal surfaces and within the MTCs, using depth and thickness maps, variance and amplitude extractions, depth slices and seismic cross-sections.

4.2.3.1 Lateral scarps

Lateral scarps are orientated broadly parallel to the MTC flow direction, and generally decrease in height in the down-flow direction (cf. Bull et al., 2009) (Fig. 4.8).

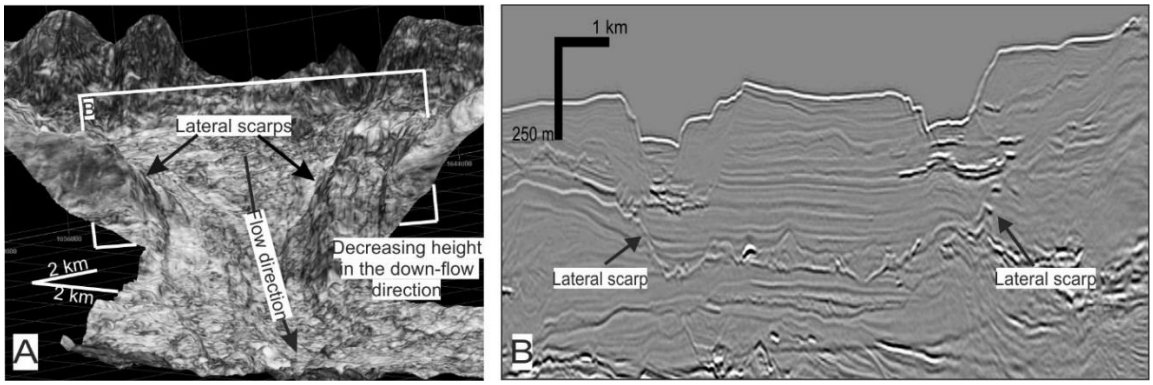

Figure 4.8. Example of the morphology of lateral scarps and their relationship with flow direction. **A.** Perspective view of the basal surface of an MTC in the study area. **B.** Seismic cross-section showing the morphology of the basal surface and the lateral scarps.

4.2.3.2 Ramps

Ramps form when the basal surface of the MTC cuts to a higher or lower stratigraphic level (Bull, et al., 2009; Alves, 2015). Ramps often strike perpendicular to the flow but this is not always the case (Alves, et al., 2014b); therefore they must be used in conjunction with other kinematic indicators to establish the flow direction. In this study, ramps were found to cut to higher stratigraphic levels (Fig. 4.5) and to be orientated perpendicular or highly oblique to the orientation of the lateral walls.

4.2.3.3 Grooves

Grooves are v-shaped erosional marks on the basal surface left by blocks being dragged at the base of MTCs (Posamentier and Kolla, 2003; Gee et al., 2005; Draganits et al., 2008; Bull et al., 2009; Alves, 2014). In map view, the grooves generally diverge down slope (Posamentier and Kola, 2003; Gee et al., 2005; Draganits et al., 2008). In the study area, grooves are particularly well imaged in variance extractions on the basal surfaces of MTCs where they form lineaments that are parallel to the flow direction and diverge in the down-slope direction (Fig. 4.9).

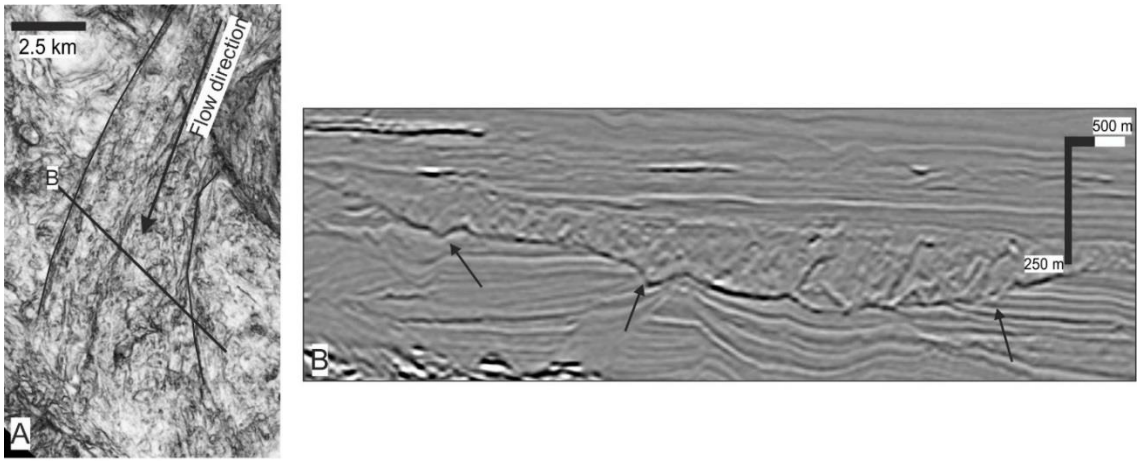

Figure 4.9. Examples of grooves on the basal surface of an MTC. **A.** Variance extraction at the base of an MTC in the study area. The darker lineaments are interpreted as grooves (*sensu* Bull et al., 2009). **B.** Seismic cross-section showing the v-shaped grooves.

4.2.3.4 Imbricate thrust and fold systems

Previous studies have documented thrust and fold systems near the toes of MTCs, interpreting them to form in response to updip-propagating contractional stress waves caused by the deceleration or cessation of the flow front (McGilvery and Cook, 2003; Frey-Martinez, 2005; Moscardelli et al., 2006; Bull et al., 2009). Flow direction is generally perpendicular to the strike of the thrusts and folds verge in the down-flow direction (Bull et al., 2009). In the study area the faults and folds in the imbricate thrust and fold systems have a consistent vergence that was used to infer flow direction (Fig. 4.5B).

4.2.3.5 Folded Megaclasts

Most of the megaclasts in the study area are folded, and in most cases fold vergence is unclear. However, the folds within the larger megaclasts (up to 7 km^2 in area) are asymmetric allowing fold vergence to be used as an indicator of emplacement direction (cf. Jones, 1939; Woodcock, 1976; Bull et al., 2009; Fig.4.7).

4.2.3.6 Alignment of Megaclasts

Megaclasts can sometimes be aligned parallel or perpendicular to the flow direction (cf. Bull et al., 2009). In the study area, megaclasts are often found in groups or clusters, sometimes they are aligned parallel to the orientation of the lateral scarps.

4.2.4 Definition of Seismic Units

Detailed top and base horizons for the channel-levee complex sets and MTCs were mapped using a line spacing of 10-20 lines depending on the continuity of the reflections. The horizons were auto-tracked using the 5×5 validated option and then interpolated by creating surfaces. The resulting surfaces were thoroughly inspected and edited manually to remove interpolation or interpretation errors. Root mean square (RMS) amplitude and variance extractions were performed on the bounding surfaces and systematically within the deposits to visualise the internal architecture of channel-levee complexes and MTCs. In general, amplitude extractions were more useful to characterise channel-levee complex sets and variance extractions were more useful for characterising MTCs.

5 Mass-Transport Complexes as Markers of Deep-Water Fold-and-Thrust Belt Evolution: Insights from the Southern Magdalena Fan, Offshore Colombia

The work in this chapter is published in:

Ortiz-Karpf, A., Hodgson, D. M., Jackson, C. A.-L., McCaffrey, W. D. (2016). Mass-Transport Complexes as Markers of Deep-Water Fold-and-Thrust Belt Evolution: Insights from the Southern Magdalena Fan, Offshore Colombia, Basin Research, p. 1-24, doi:10.1111/bre.12208

5.1 Introduction

Mass-transport complexes (MTCs) were originally defined using seismic reflection data (Weimer, 1990) and they include a spectrum of deposit types (slides, slumps and debrites; e.g. Dott, 1963; Nemec, 1990; Shanmugam et al., 1994; Moscardelli et al., 2006; Moscardelli and Wood, 2008; Manica, 2012). Moscardelli and Wood (2008) define relatively small gravitational failures caused by local oversteepening of the submarine slope as *detached MTCs*; these are typically thin (<100 m) and may cover only a few tens of square kilometres. Large failures of the shelf edge, which may be caused by earthquakes, gas-hydrate dissolution, increased sediment supply or sea-level change (e.g. Manley and Flood, 1988; Beaubouef and Friedmann, 2000; Maslin et al., 2004; Frey-Martinez et al., 2005; Grozic, 2010; Masson et al., 2010) are termed *shelf-attached MTCs* (Moscardelli and Wood, 2008). Shelf-attached MTCs can reach thousands of square kilometres in area and be hundreds of metres thick (Moscardelli and Wood, 2008, 2015).

Commonly, submarine fold-and-thrust belts in both active and passive tectonic margins are degraded by mass-wasting events and are thus flanked by MTCs (e.g. Heniö and Davies, 2006; Clark and Cartwright, 2009, 2011, 2012; Vinnels et al., 2010; Romero-

Otero, 2010; Geersen et al., 2011; Alfaro and Holz, 2014; Idárraga-García and Vargas 2014; Vargas and Idárraga-García 2014; Festa et al., 2015, Yarbuh and Contreras, 2015). Previous studies focused on salt-or-shale-based passive margins, prone to thin-skinned deformation, have considered the relationship between MTC emplacement and structural evolution. For example, Heniö and Davies (2006) use 3D seismic data from the Niger Delta to examine the three-dimensional degradation of compressional folds created by gravity tectonics. Clark and Cartwright (2012) analysed the distribution and architecture of channel-levee complexes and MTCs within a growth package in a fold in the deep-water fold-and-thrust-belt in the Western Niger Delta in order to reconstruct the three-dimensional, sequential development of structural relief.

On tectonically-active continental margins, recurrent mass-wasting is commonly caused by seabed oversteepening due to structurally induced seabed deformation and/or by seismic activity (e.g. Moore et al., 1976; Torelli et al., 1997; Goldfinger et al., 2000; Frey-Martinez et al., 2005, 2006; Minisini et al., 2007; Lamarche, 2008; Cattaneo et al., 2010; Dan et al., 2010; Romero-Otero et al., 2010; Geersen et al., 2011; Alfaro and Holz, 2014; Alves, 2014b; Festa et al., 2015; Pérez et al., 2016). Several studies on active margins have investigated the mechanisms for slope failure and provide detailed descriptions of the deposits resulting from fold degradation (e.g. Trincardi and Argnani, 1990; Moscardelli and Wood, 2008, 2015; Rogers and Goodbred, 2010; Romero-Otero, et al., 2010; Alfaro and Holz, 2014; Idárraga-García and Vargas 2014; Vargas and Idárraga-García 2014). However, few relate MTC emplacement to the tectono-stratigraphic evolution of the basin margin. For example, Geersen et al. (2011) relate a series of large-scale slope collapses with the regional tectonic history and present a two-dimensional model for the evolution of mass-failures offshore Chile. Festa et al. (2015) present a detailed outcrop study that investigates the relationship between the distribution of MTCs and the tectonostratigraphic evolution of the northern Apennines. Pérez et al. (2016) document variations in the dimensions, and vertical and spatial distribution of MTCs in

several basins with different deformation styles along the Scotia-Antarctica plate margin, and relate them to the regional tectonic evolution. However, there is still a paucity of detailed, three-dimensional analyses that link the timing, location and character of MTCs with the growth of individual structures within developing deep-water fold-and-thrust belts. Furthermore, the evolution and chronostratigraphic significance of the basal surfaces underlying MTCs in areas of recurrent mass-wasting has not been studied previously.

This study is based on detailed mapping of the near-seabed, likely Pleistocene stratigraphy (Ortiz-Karpf et al., 2015), imaged in a 3D seismic reflection survey from the southern Magdalena Fan, offshore Colombia (Fig. 5.1). The seismic survey is located at the northern tip of the Southern Sinú Fold Belt, imaging the transition between imbricate thrust-cored anticlines to the south and a relatively undeformed area to the north (Fig. 5.1B). Here, several MTCs were deposited at a time when the Magdalena Fan was prograding under the influence of high sediment supply and the Southern Sinú Fold Belt was propagating outboard to the NW (e.g. Romero-Otero et al., 2009; Martinez et al., 2015). Due to the location of the study area within the fold-and-thrust belt and to the relatively recent tectonic deformation of the near-seabed sediments, the degree of deformation is less advanced than in other areas along the fold-and-thrust belt (Vinnels et al., 2010; Romero-Otero et al., 2010; Alfaro and Holz, 2014; Martinez et al., 2015); the primary tectono-stratigraphic relationships and internal characteristics of the deposits are therefore well-preserved. The high-resolution of the data and its tectono-stratigraphic setting therefore enable: i) the examination of variations in the distribution, source and size of the MTCs in response to growth of the deep-water fold-and-thrust belt, and ii) the investigation of the evolution and chronostratigraphic significance of MTC basal erosion surfaces.

5.2 Regional Setting

The Magdalena Fan is located in the Caribbean Sea, on the northern coast of Colombia, northern South America (Fig. 5.1). The margin is tectonically active due to Cretaceous-to-Recent oblique subduction of the Caribbean Plate beneath the South American Plate (Duque-Caro, 1979; Pindell, 1994; Meschede and Frisch, 1998; Cediel et al., 2003; Pindell and Kennan, 2009). Plate convergence has resulted in the formation of imbricate thrust belts, which have been active onshore since the Late Paleocene (Flinch, 2003) and offshore since the Middle-Late Miocene (Cediel et al., 2003; Martinez et al., 2015). The offshore Sinú Fold Belt is dominated by a series of thrust-cored anticlines that are younging to the north (Bernal-Olaya, 2015; Martinez et al., 2015) and have experienced episodic growth during the Plio-Pleistocene (Kolla and Buffler, 1984; Duque-Caro, 1979, 1984; Cediel et al, 2003; Flinch, 2003). The Sinú Fold Belt is divided into two regions of active deformation (Southern and Northern Sinú Fold Belts, Fig. 5.1B). The Magdalena Fan, which is believed to have been active since the Late Miocene (Duque-Caro, 1979, 1984; Kolla and Buffler, 1984; Breen, 1989; Romero-Otero, 2009), is located in a relatively undeformed area between the fold belts, extending offshore into the Colombia Basin (Fig. 5.1B). Submarine fan sedimentation was coeval with subduction-induced structural uplift and tectonic activity (Kolla and Buffler, 1984; Vinnels et al., 2010; Romero-Otero 2009; Romero-Otero et al., 2010; Alfaro and Holz, 2014; Ortiz-Karpf et al., 2015).

5.3 Data and Methods

This study uses a three-dimensional seismic reflection survey covering the northern tip of the Southern Sinú Fold Belt and the southern part of the undeformed area that is mantled by the Magdalena Fan (Fig. 5.1B). The seismic survey was acquired in 2008 and covers an area of 1900 km^2. It is Post-Stack Depth-Migrated (PSDM) and has a bin spacing of 12.5 x 12.5 m. This study focuses on the shallow stratigraphy (up to c. 1,000 m below seabed) where the maximum frequency is 45 Hz and the dominant frequency

is 30 Hz. By assuming a sediment velocity of 1900 m/s, which seems reasonable given the relatively shallow depth of burial, these frequency and velocity values yield a vertical resolution of c. 10-15 m and a horizontal resolution of c. 15 m. The water bottom is defined by a positive reflection event, which is represented by a black reflection in the seismic images. Although a few wells have been drilled to the NE of the study area, they were not available for this study.

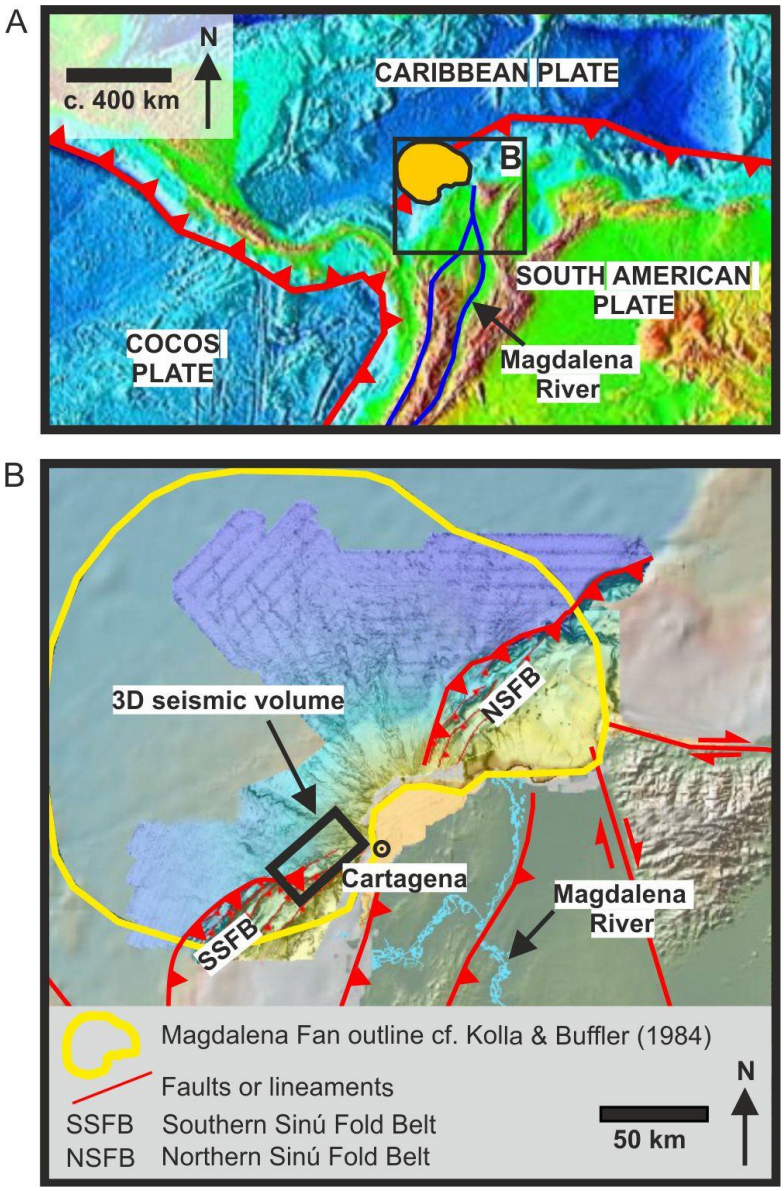

Figure 5.1. Location and tectonic setting. **A.** The Magdalena Fan is located in the Caribbean Sea, off the northern coast of Colombia, South America where the Caribbean Plate obliquely subducts beneath the South American Plate. The yellow polygon outlines the Magdalena Fan (cf. Kolla and Buffler, 1984), map from NOAA. **B.** The Magdalena Fan is in the Sinú Fold Belt, which is divided into the Southern Sinú Fold Belt (SSFB) and the Northern Sinú Fold Belt (NSFB), separated by an area of subdued deformation. Adapted from Romero-Otero (2009).

Ortiz-Karpf et al. (2015; Chapter 7) studied the stratigraphic interval of interest, defining seven seismic facies that were used to infer a number of sedimentary sub-environments (i.e. channel-fill, levees, lobes and MTCs; Chapter 4). These sub-environments were then grouped into seven seismic units. Ortiz-Karpf et al. (2015) interpret that seismic Unit D, which is located 300-500 m below the seabed, is dominated by MTCs. In the study described here, Unit D and older, underlying MTCs and their bounding surfaces were characterised and mapped in greater detail, and the chronology of MTC emplacement was assessed with respect to the development of the deep-water fold-and-thrust belt. Based on the amplitude, continuity and configuration of the seismic reflections, and their external geometry, three MTC seismic facies can be defined (Table 5.1). Seismic attribute extractions, including amplitude, dip, variance and chaos were performed and integrated with variance and amplitude depth slices to define lateral facies changes and create seismic facies maps. Kinematic indicators such as the orientation of the lateral scarps, onlap patterns, fold and thrust vergence, grooves and megaclasts alignment (sensu Bull et al., 2009) were interpreted from maps and cross-sectional views. These kinematic indicators were used to infer MTC flow directions and to link individual MTCs back to their source areas, thus enabling the investigation of the relationship between fold-and-thrust belt growth, seabed deformation and MTC emplacement.

5.4 Structural Elements

In order to relate the characteristics of the MTCs to the structural evolution, it is necessary to establish the structural framework of the study area. This section describes the structures whose growth led to or controlled emplacement of the MTCs.

Towards the northern tip of the southern Sinú Fold Belt, NE-SW-striking thrusts bend towards the east, resulting in an overall rotation of the deformation front towards the continent (Figs. 5.1B and 5.2). Within the study area, two thrust sheets are imaged (Fig. 5.2). Basinwards three more thrust sheets are present to the SW of the seismic volume (Fig. 5.2). In the study area, the western and eastern thrust sheets are each associated

with large anticlines, herein referred to as the *downdip anticline (DA)* and *updip anticline (UA)* respectively (Fig. 5.2). These anticlines are separated by a narrow syncline, herein referred to as the *syncline* (Fig. 5.3).

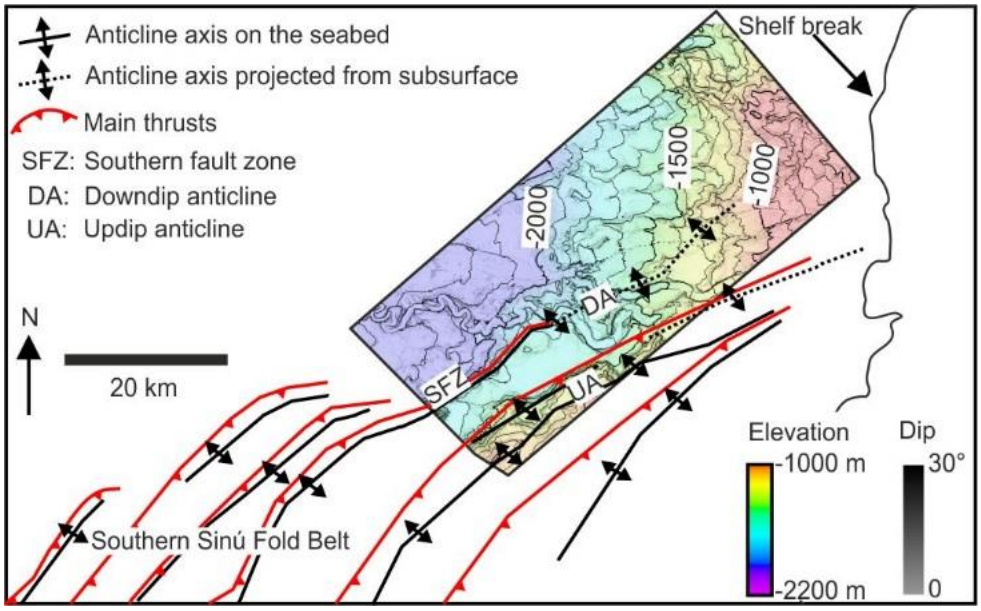

Figure 5.2. Subregional structural setting. Seabed dip map coloured by subsurface elevation within the seismic volume. The main thrusts and anticlinal axis in and around the study area are from Romero-Otero (2009). The study area is in the northern tip of the Southern Sinú Fold Belt and images two thrust sheets, the downdip anticline (DA) and updip anticline (UA).

The DA is divided into a northern and southern domain, which are separated by a saddle (Fig. 5.3A). The southern downdip anticline (SDA), is asymmetric, with its steepest flank dipping to the NW. The anticline is cored by the *southern fault zone (SFZ)*, which comprises three sub-parallel thrust faults that strike SW-NE and dip to the SE (Fig. 5.3A and C). The relief of the anticline increases to the SW, and the displacement, strike and lateral separation of the underlying faults vary. Towards the NE, the faults curve towards the east (Fig. 5.3A), become steeper, and lose displacement before ultimately tipping out. Towards the northern tip of the SFZ, the DA becomes progressively more symmetric, and its axis rotates towards the east (Fig. 5.3A). Here the anticline plunges slightly to the NE to form the saddle (Fig. 5.3D) separating it from the northern downdip anticline (NDA). Towards the NE the anticline becomes broad and symmetric (Fig. 5.3A and B). The NDA is unfaulted and it does not have a seabed expression because it has been greatly eroded (Fig. 5.3B).

A

Seismic Facies	Description	Interpretation
1	Variable amplitude, semi-continuous to chaotic reflections in packages that have an erosional base and irregular top (B-C). Packages are 50-100 m thick and are sometimes locally deformed by thrusts and 200-300 m wide folds.	The chaotic character of facies 1 suggests that the contained material is at least partially disaggregated (cf. Alves et al., 2014) and, based on these characteristics, facies 1 is interpreted to represent debrites (cf. Posamentier & Kolla, 2003; Olafiranye et al., 2013).
2	Discrete packages of coherent, parallel reflections set within a matrix dominated by facies 1 (B-C). These coherent reflections occur in packages that are predominantly up to 200 m thick and cover areas of up to 1.6 km^2. In some cases these packages are folded or faulted. Some of these packages are considerably larger, with areas of 5-7 km^2 and thicknesses in excess of 300 m. They are composed of parallel reflections that are folded into symmetric, asymmetric, recumbent and isoclinal folds and are associated with facies 1 (D-E).	Megaclasts transported within the MTC parent flow (e.g. Olafiranye et al., 2013; Jackson, 2011; Ortiz-Karpf et al., 2015). Due to the lateral continuity of the reflections and the scale of the folds, the larger packages could be alternatively interpreted as slump folds (cf. Bull & Cartwright, 2010; Posamentier & Martinsen, 2011). However, differentiating between these two hypotheses is not critical to the overall objective of this study and they are also interpreted as megaclasts (cf. McGilvery et al., 2004; Bull et al., 2009; Frey-Martinez, 2010; Jackson, 2011; Posamentier & Martinsen, 2011; Olafiranye et al., 2013; Alves, 2015). The geometry of the folds can be used to infer the MTC flow direction, with the fold axes interpreted to be orientated broadly perpendicular to flow direction and the folds verging in the down-flow direction (cf. Jones, 1939; Woodcock, 1976; Bull et al., 2009). When the folds are symmetric, only the azimuth of the flow can be determined.
3	Variable amplitude, semi-continuous reflections that are folded and disrupted by reverse faults (F). Thrust imbricates which commonly bound asymmetric anticlines are well developed in facies 3. The folds are 400-500 m wide and c. 200 m high.	Imbricate thrust and fold systems (*sensu* Bull et al., 2009) in contractionally deformed MTCs (e.g. McGilvery et al., 2004; Frey-Martinez et al., 2005; 2006; Alfaro & Holz, 2014). Flow direction is generally perpendicular to the strike of the faults and folds verge in the down-flow direction (Bull et al., 2009).

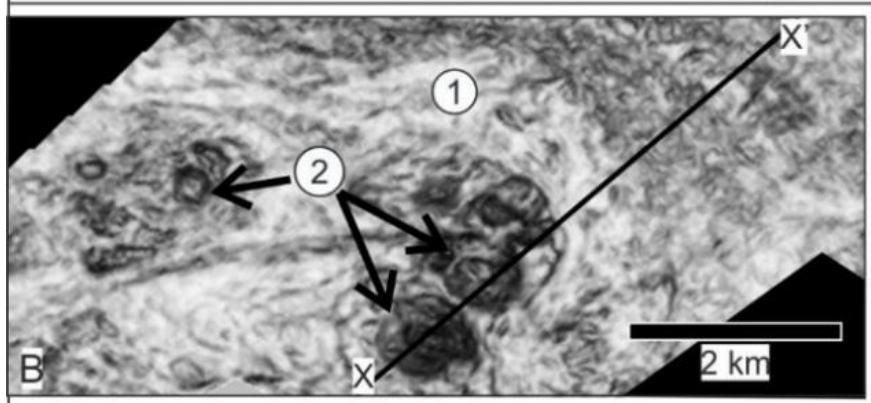

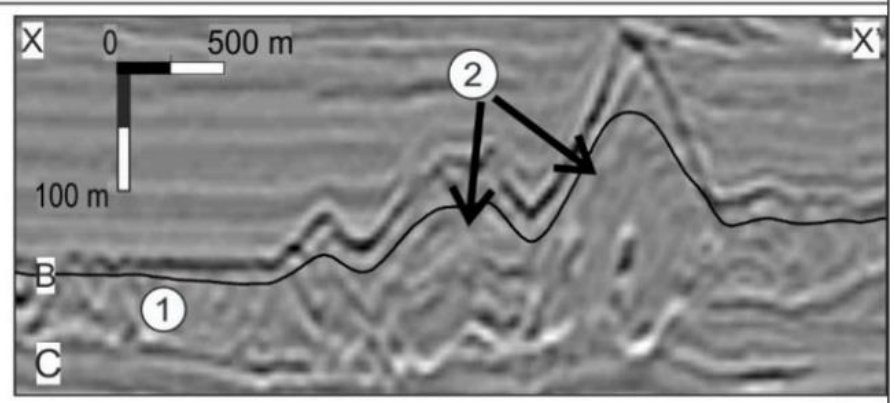

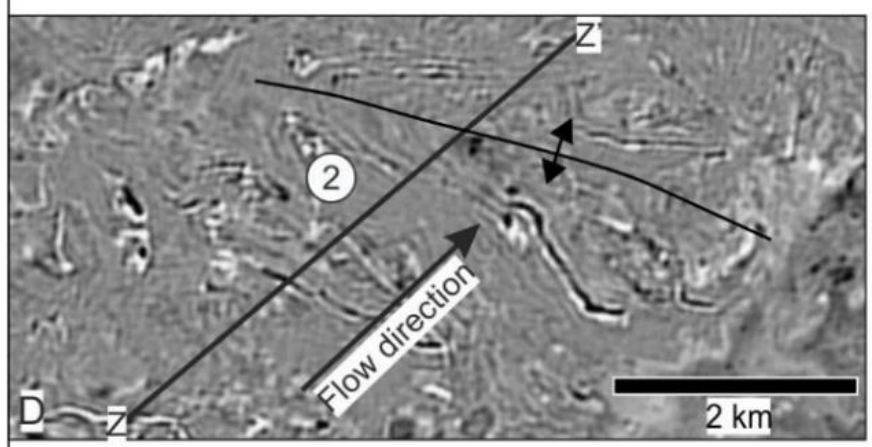

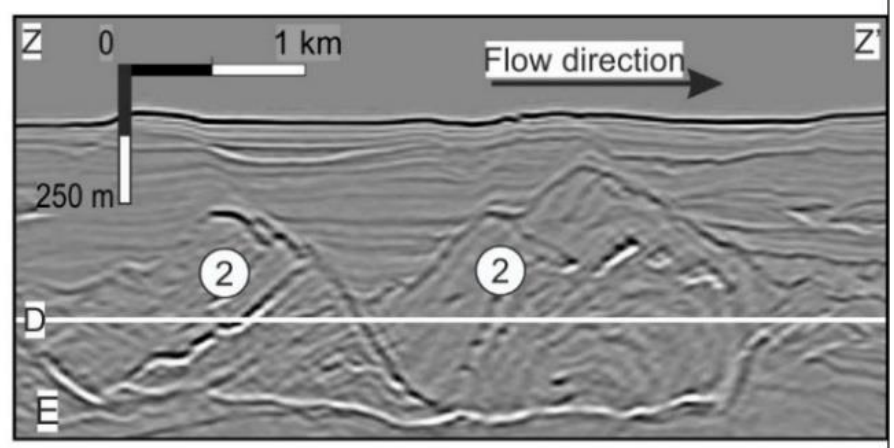

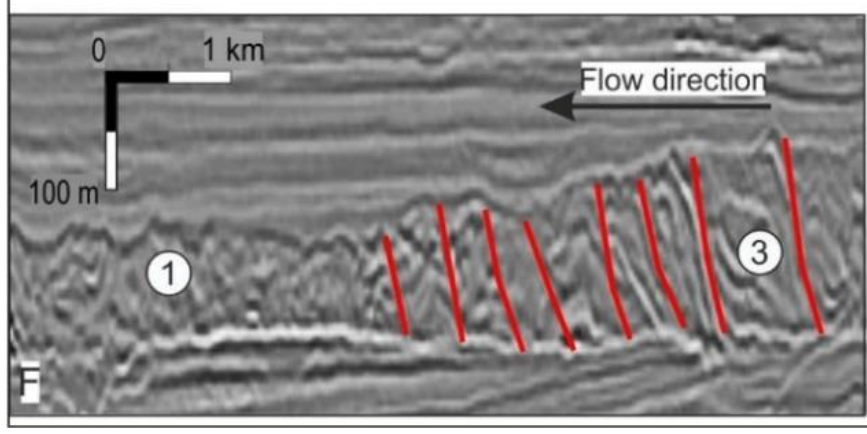

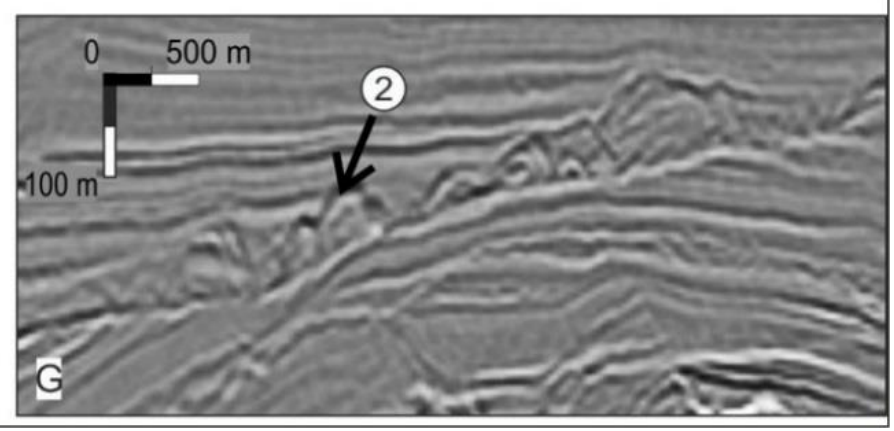

Table 5.1. MTC seismic facies. **A.** Description and interpretation of the seismic facies. **B.** Variance extraction of the upper part of an MTC (see A for intersection) showing the appearance of facies 1 and 2. **C.** Seismic line across B showing examples of facies 1 and 2. **D.** Depth-slice showing the map-view appearance of a large folded megaclast. Note the semi continuous folded reflections and the fold axis. **E.** Seismic line across D. Note the asymmetry of the folds. **F.** Seismic line across facies 1 and 3. Note the imbricate fold-and-thrust systems in facies 3. **G.** Seismic line showing facies 2.

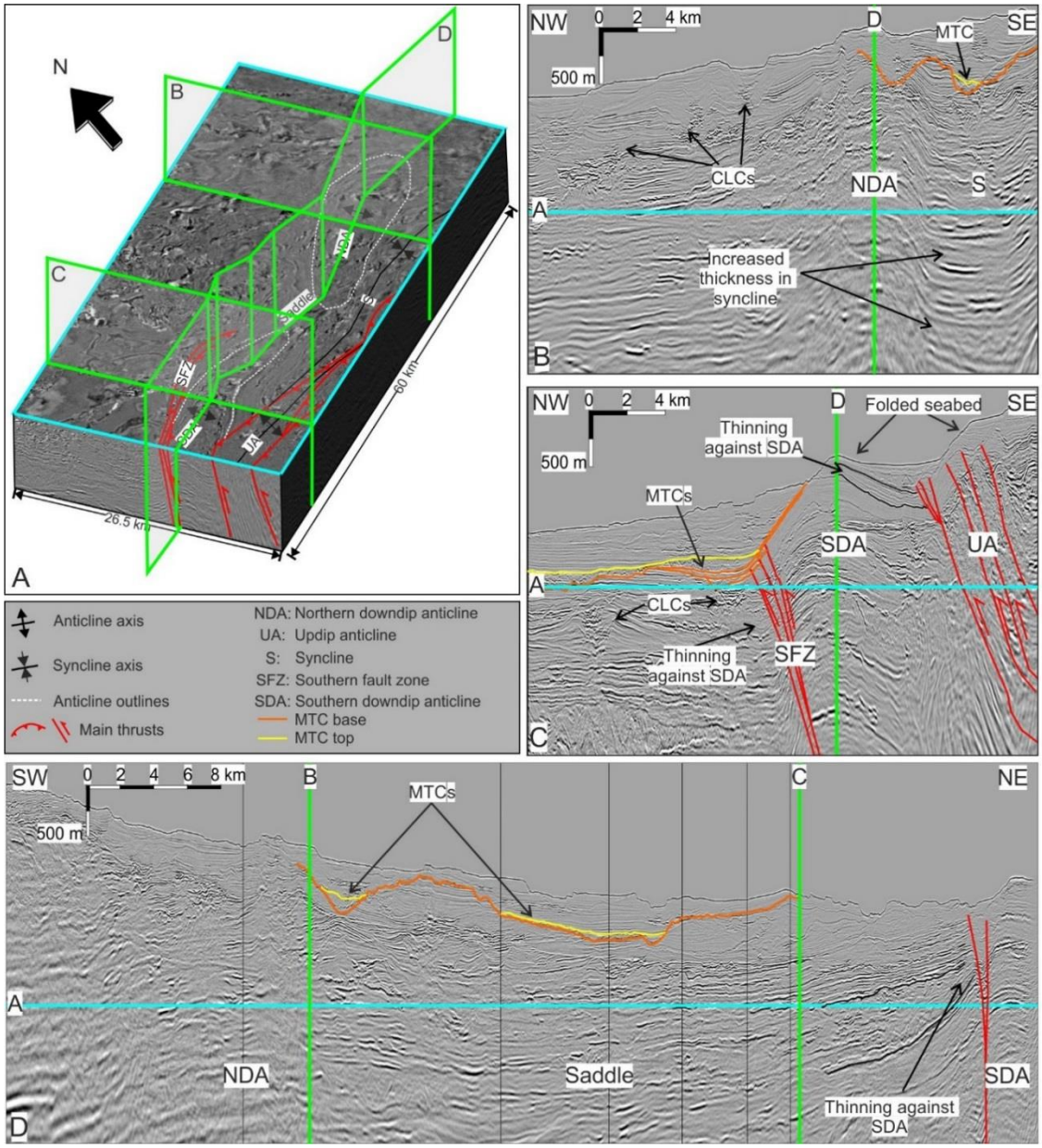

Figure 5.3. Structural elements. **A.** Three dimensional perspective view of the seismic cube (see B-D for depth intersection). The southern downdip anticline (SDA) is thrust-cored, the northern downdip anticline (NDA) is not faulted. A saddle separates the SDA and the NDA. To the E, there is a syncline (S) that separates the DA and the updip anticline (UA). **B.** Dip seismic line across the northern part of the dataset: The NDA becomes symmetric and is not faulted. There is increased sediment thickness in the syncline (S). **C.** Dip seismic line across the southern part of the dataset: The SDA is thrust-cored and asymmetric, to the E is the UA. **D.** Seismic line along the axis of the downdip anticline. There is a saddle between the SDA and NDA. Note thinning of the sedimentary packages against the SDA.

The UA is a narrow, thrust-cored, asymmetric anticline that verges to the NW with a sub-vertical to overturned frontal limb (Fig. 5.3C). The UA is expressed at the seabed, although its geometry has been modified by erosion (Fig. 5.3C). The thrust coring the

UA also curves to the east and continues to the NE, bending towards the shelf (Fig. 5.2 and 5.3A).

According to Martinez et al. (2015), the structures in the study area have experienced episodic growth since the Late Miocene. This protracted growth history is evidenced by thinning of the stratigraphic packages against the DA and UA, and increased sediment thickness in the syncline (Fig. 5.3B and C), which together indicate the presence of growth strata. Because these folds have deformed the seabed, and their underlying thrusts displace shallow stratigraphy (Fig. 5.3C), the last period of uplift of these structures is interpreted to have occurred relatively recently, and potentially coincides with the latest stage of uplift associated with the Late Pleistocene avulsion of the Magdalena River (Romero-Otero, 2009). However, the youngest MTCs and the overlying channel-levee complex sets are not faulted and onlap the downdip anticline (Fig. 5.3C). This reflects a period of local tectonic quiescence and active fan sedimentation post-dating the latest episode of fold and thrust activity.

5.5 Seismic Stratigraphy

The base and top surfaces of Unit D (*sensu* Ortiz-Karpf et al., 2015; Chapter 7) are continuous negative-amplitude reflections that can be mapped throughout the study area and bound several MTCs (Fig. 5.4). Here, the stratigraphy within Unit D can be subdivided into multiple seismic packages based on mappable surfaces. To facilitate the description of the MTCs, the area was divided into three regions based on the morphology of the erosion surface that defines the base of Unit D (Fig. 5.4): i) the *southern region*, which is located basinward of the SDA, and to the NE of two thrust sheets that terminate to the south of the dataset (Fig. 5.4A and B); ii) the *central region*, which trends SW along the axis of the syncline, NW across the downdip anticline at the saddle between the SDA and NDA, and covers the basin-low outboard of the downdip anticline (Fig. 5.4B); and (iii) the *northern region*, which traverses the NDA (Fig. 5.4B). The nomenclature adopted for the individual MTCs described below is based on the

region where they occur and on their relative age with respect to other MTCs in the same region. Thus, the MTCs in the southern region are named S1-S6, the MTC in the central region is referred to as C1, and those in the northern region are called N1 and N2. With the exception of S1-S4 and the MTC remnants underlying C1, the MTCs described below form part of Unit D of Ortiz-Karpf et al. (2015) (Chapter 7; Fig. 5.4C). Table 5.2 summarises the dimensions, seismic facies, megaclast dimensions and kinematic indicators associated with each of the MTCs.

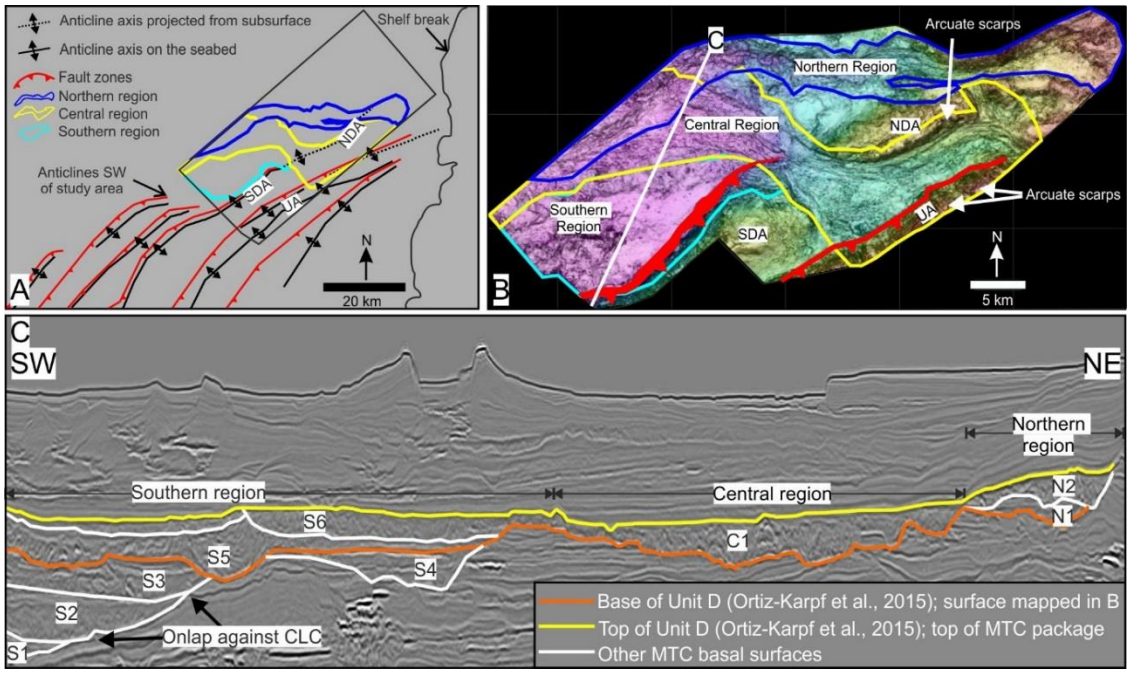

Figure 5.4. MTC Regions. **A.** Location of the MTC regions with respect to the main thrusts and folds around the area; axes of anticlines expressed on the seabed taken from Romero-Otero (2009). The black polygon indicates the location of the study area; the polygons defining the limits of the MTC regions are projected vertically onto the seabed. The southern region is to the west of the southern downdip anticline (SDA), the central region traverses the saddle between the SDA and the northern downdip anticline (NDA), and the northern region traverses the NDA. Towards the E of the dataset is the updip anticline (UA). **B.** Combined display of variance and elevation on the base surface of Unit D, the orange horizon in C (cf. Ortiz-Karpf et al., 2015). **C.** Oblique seismic line across the MTC regions; the orange horizon corresponds to the erosional surface mapped in B and the yellow horizon is the top of the MTC package. Unit D of Ortiz-Karpf et al. (2015) corresponds to the interval between the orange and yellow horizons.

		MTC	Thickness (m)	Minimum Dimensions (within study area)	Seismic facies	Size of megaclasts	Kinematic Indicators
Folded and Faulted	Detached	S1	25-150	Length: 5 km Width: 2 km Area: 9 km^2	Obscured by tectonic deformation	None identified	NE-SW elongation; progressive onlap against channel levee to the N
Folded and Faulted	Detached	S2	20-150	Length: 8 km Width: 5 km Area: 30 km^2	Facies 1 (debrites) and facies 2 (megaclasts)	Thickness: 80-130 m Area: 0.3 km^2	NE-SW elongation; progressive onlap against channel levee to the N, alignment of megaclasts
Folded and Faulted	Detached	S3	30-100	Length: 9 km Width: 5 km Area: 42 km^2	Facies 1 (debrites) and facies 2 (megaclasts)	Thickness: 50-90 m Area: 0.06-0.35 km^2	NE-SW elongation; progressive onlap against channel levee to the N, alignment of megaclasts
Folded and Faulted	Detached	S4	30-130	Length: 19 km Width: 6 km Area: 75 km^2	Facies 1 (debrites) and facies 2 (megaclasts)	Thickness: 20-70 m Area: 0.1-1.1 km^2	NE-SW elongation.
Folded and Faulted	Detached	S5	100-400	Length: 13 km Width: 11 km Area: 98 km^2	Facies 1 (debrites) and facies 2 (megaclasts)	Thickness: 70-400 m Area: 0.2-7 km^2	Vergence of folds within megaclasts, grooves & scours, onlap against levee to the N
Undeformed	Detached	S6	50-130	Length: 14 km Width: 8 km Area: 80 km^2	Facies 1 (debrites) and facies 2 (megaclasts)	Thickness: 27-90 m Area: 0.04-0.5 km^2	Widening to the SW and pinch-out against megaclasts in S5.
Undeformed	Shelf-attached	C1	50-200	Length: 40 km Width: 4-13 km Area: 300 km^2	Facies 1 (debrites) and facies 2 (megaclasts)	Thickness: 50-200 m Area: 0.06-1.6 km^2	Orientation of lateral scarps, vergence of folds and faults
Undeformed	Shelf-attached	N1	50-130	Length: 45 km Width: 3-4 km Area: 244 km^2 (base surf.)	Facies 1 (debrites)	None identified	Orientation of lateral scarps
Undeformed	Shelf-attached	N2	20-150	Length: 35 km Width: 3-4 km Area: 220 km^2 (base surf.)	Facies 1 (debrites)	None identified	Orientation of lateral scarps

Table 5.2. Summary table showing the main characteristics of the MTCs and their classification according to the interpreted source and timing with respect to the evolution of the anticlines.

5.5.1 Southern Region

The southern region contains six stacked MTCs that are mainly composed of debrites and megaclasts (Fig. 5.5, Table 5.2); these are elongate in a NE-SW direction and are the oldest MTCs in the study interval (S1-S6; Fig. 5.4 and 5.5). S1-S5 continue beyond the southwestern limit of the dataset where the southern fault zone curves to the west, and where two additional thrust sheets, located west of the downdip anticline, plunge to the north (Fig. 5.4A).

MTC S1 is located towards the southern limit of the dataset and is only locally preserved due to erosion, folding and faulting (Fig. 5.5A). Towards the north it onlaps and erodes an underlying external levee and is truncated by S2 (Fig. 5.6A). Structural deformation hinders the identification of its eastern depositional limit, seismic facies, or the transport direction.

MTC S2 overlies an erosion surface that incises S1 and is erosionally overlain by S3 (Fig. 5.6A). S2 onlaps and erodes the external levee of an underlying channel complex

set (Fig. 5.6A) extending farther north than S1 (Fig. 5.5B). S2 thins towards the north and west (Fig. 5.6C) and is folded and faulted to the SE, thinning against the frontal flank of the SDA (Fig. 5.7A and B). In the thicker central area, S2 is characterised by variable amplitudes, and towards its margins displays lower amplitudes and is more homogenous (Fig. 5.5B and 5.6C). Megaclasts in S2 are concentrated in the central part of the deposit and are aligned SW-NE, broadly sub-parallel to the margins (Fig. 5.5B and 5.6C). The megaclasts are folded but the sense of fold vergence is unclear.

MTC S3 overlies an erosion surface that incises S2 although, locally, they are separated by erosional remnants of a package with low-amplitude internal reflections (Fig. 5.6A). The top of S3 is truncated by S5 (Fig. 5.6A) and, in the north, by S4 (Fig. 5.5D). S3 onlaps and erodes the underlying external levee towards the north, and is folded and faulted to the SE where it thins against the western flank of the SDA (Figs. 5.6A and D, 5.7A and B). Amplitudes are variable towards the central area; more homogenous, lower amplitudes characterise the northern margin (Fig. 5.5C and 5.6D). Most of the megaclasts in S3 are aligned NE-SW, parallel to its northwestern margin (Fig. 5.5C and 5.6D) and are internally folded. The vergence of the folds within the megaclasts is not clear.

MTC S4 is located to the NW of S1-S3 (Fig. 5.5D and 5.6D). It overlies and incises into the axes and levee crests of two SW-trending channel-levee complex sets (Fig. 5.6A and D(i)). The southeastern external levee of one of these channel-levee complex sets separates S4 from S3 (Fig. 5.5D and 5.6D). To the NW, S4 overlies the remnant external levee that constitutes the limit between the southern and central regions (Fig. 5.5D). S4 is truncated by S5 to the SW, by S6 to the NE and truncates S3 (Fig. 5.5D-E, 5.6A and 5.8A-B). S4 can be traced updip onto the SDA, where it is folded, faulted (Fig. 5.8A) and truncated by C1 (Fig. 5.5D). S4 is composed of two packages separated by a laterally continuous, high-amplitude erosion surface that suggests the presence of two stacked deposits (Fig. 5.8A); both are composed of debrites with few megaclasts (Fig. 5.5D and

5.6D). The megaclasts are concentrated in the SW (Fig. 5.5D). The orientation of the lateral boundaries of S4, which follow the trend of underlying channel-levee complex sets, suggest deposition from a NE- or SW-directed flow (Fig. 5.6D); however there are no additional kinematic indicators to support either interpretation.

MTC S5 overlies an erosion surface that incises S3 and S4 (Fig. 5.6A). To the NW, as in S4, it is limited by the external levee deposits that define the boundary between the southern and central regions (Fig. 5.5E). To the NE, S5 thins and pinches-out against the underlying channel levee complex set and is erosionally truncated by S6 (Fig. 5.6A and 5.8A). To the east it thins against the SDA where it is folded and faulted (Fig. 5.7A and B). S5 has an irregular top that is overlain and locally eroded by channel-levee complex sets to the south (Fig. 5.7 A and B). S5 is composed of debrites towards the margins and, in its centre, by continuous reflections that form asymmetric to recumbent, NE-verging folds contained within deformed megaclasts (Figs. 5.5E and 5.7A and D). To the NE, the transition from folded megaclasts to debrites coincides with a relative shallowing of the basal surface and thinning of the deposit (Fig. 5.7C-E). Based on the orientation of the axes of the folds within the megaclasts (WNW-ESE; Fig. 5.7D), their NNE fold vergence (Fig. 5.8B), and the presence of erosional scours and grooves at the base of S5 (Fig. 5.7C), the emplacement direction of the flow depositing S5 is interpreted to be towards the NNE.

MTC S6 overlies an erosion surface that incises S5 and S4 (Fig. 5.8A and B), and is overlain by channel-levee complex sets (Fig. 5.8). As in S4 and S5, to the NW, it thins against the external levee that defines the boundary between the southern and central regions (Figs. 5.5F and 5.8D). Although an erosion surface can locally be observed between MTC S6 and MTC C1 (Fig. 5.5), it is not consistently traceable, meaning it is possible that S6 is part of C1 (Fig. 5.6A). To the SW, S6 thins and pinches-out against relief developed along the upper surface of S5 (Fig. 5.5G and 5.8). To the NE, the basal erosion surface can be traced to the tip of the southern fault zone where it overlies S4

and amalgamates with the erosion surface bounding the base of C1 (Fig. 5.5F). S6 is only offset by faults developed in the southern fault zone towards the base and is undeformed towards the top. The channel-levee complexes that overlie it are undeformed (Fig. 5.8A and B). S6 mainly comprises debrites and folded megaclasts (Fig. 5.5F and 5.8C), being c. 100 m thick towards its centre and thinning in all directions (Fig. 5.8D). The overall widening of the deposit to the SW and its southwestern termination against S5 suggest deposition from a SW-directed flow.

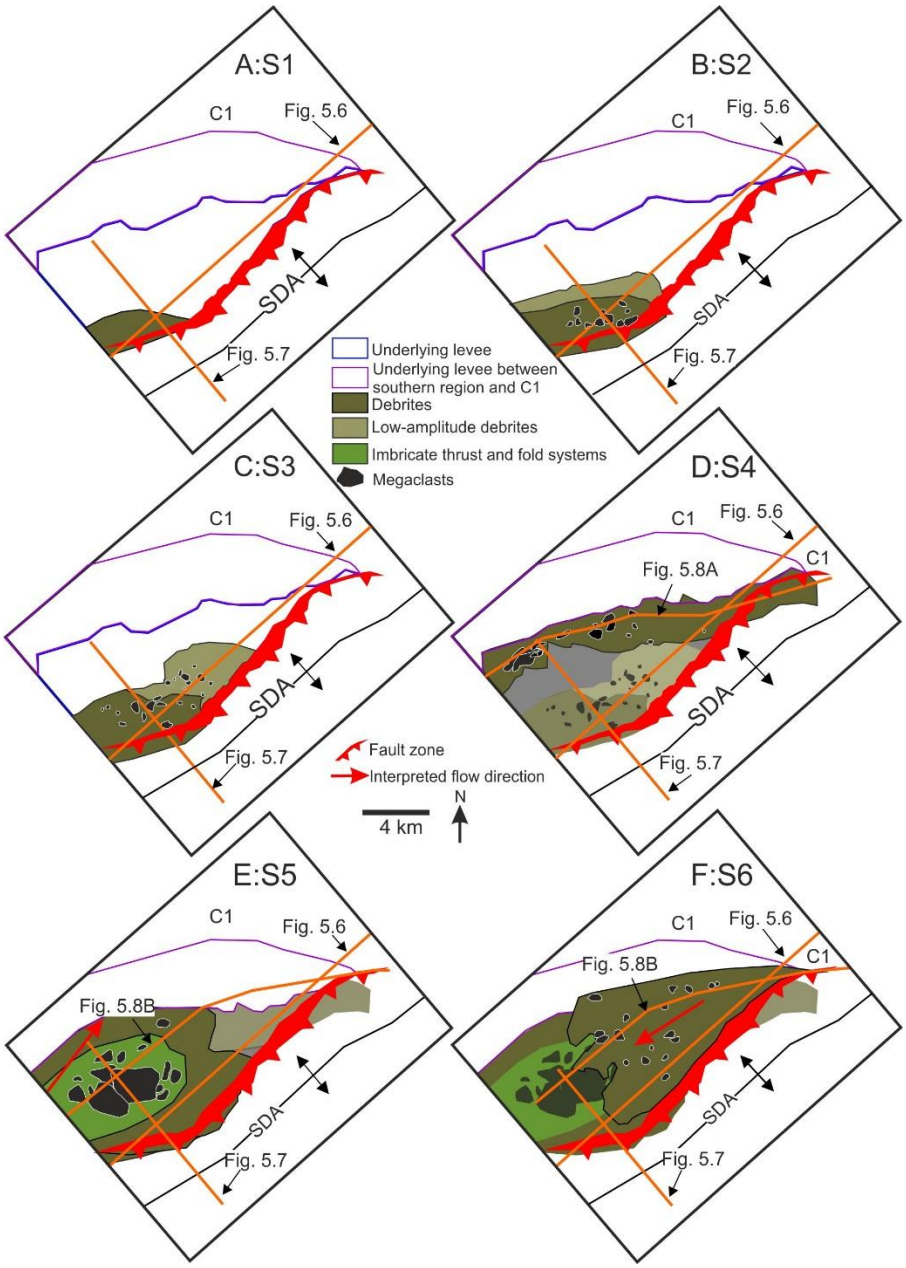

Figure 5.5. Maps showing the areal distribution, morphology and seismic facies of MTCs S1-S6. Projected vertically onto a depth slice, refer to Fig. 5.6A for intersection.

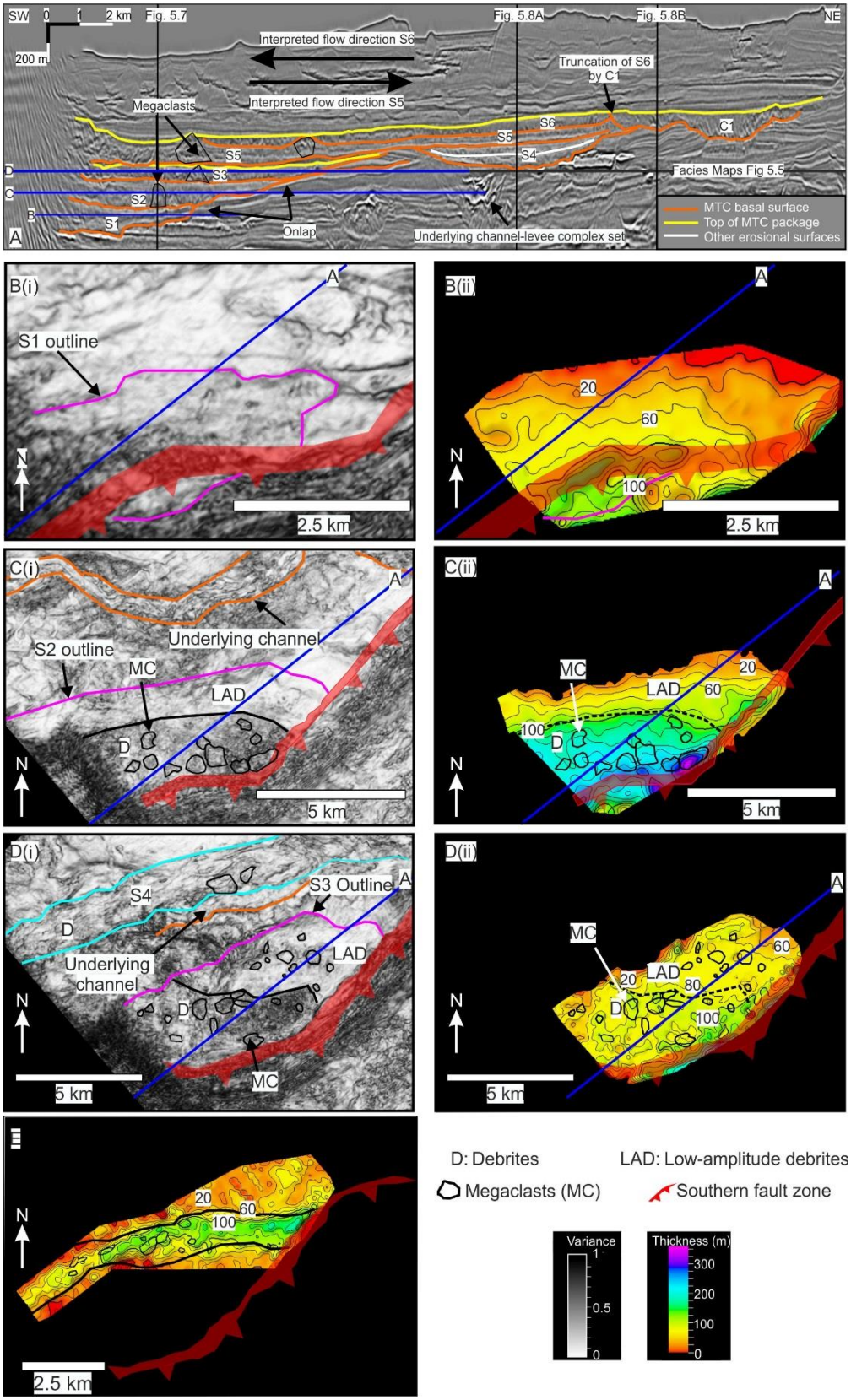

Figure 5.6. MTCs S1-S4. **A.** Strike line along the southern region, see Fig. 5.5 and 5.6B-D for location. MTCs S1-S3 onlap an underlying external levee. S4 overlies a channel-levee complex set. S5 pinches out to the north and S6 pinches out to the south against megaclasts protruding at the top of S5. **B-D**. i) Variance depth slices across MTCs S1, S2 and S3 respectively showing the distribution of the seismic facies; see A for intersection), ii) Vertical thickness maps for S1, S2 and S3. E. Vertical thickness map for MTC S4.

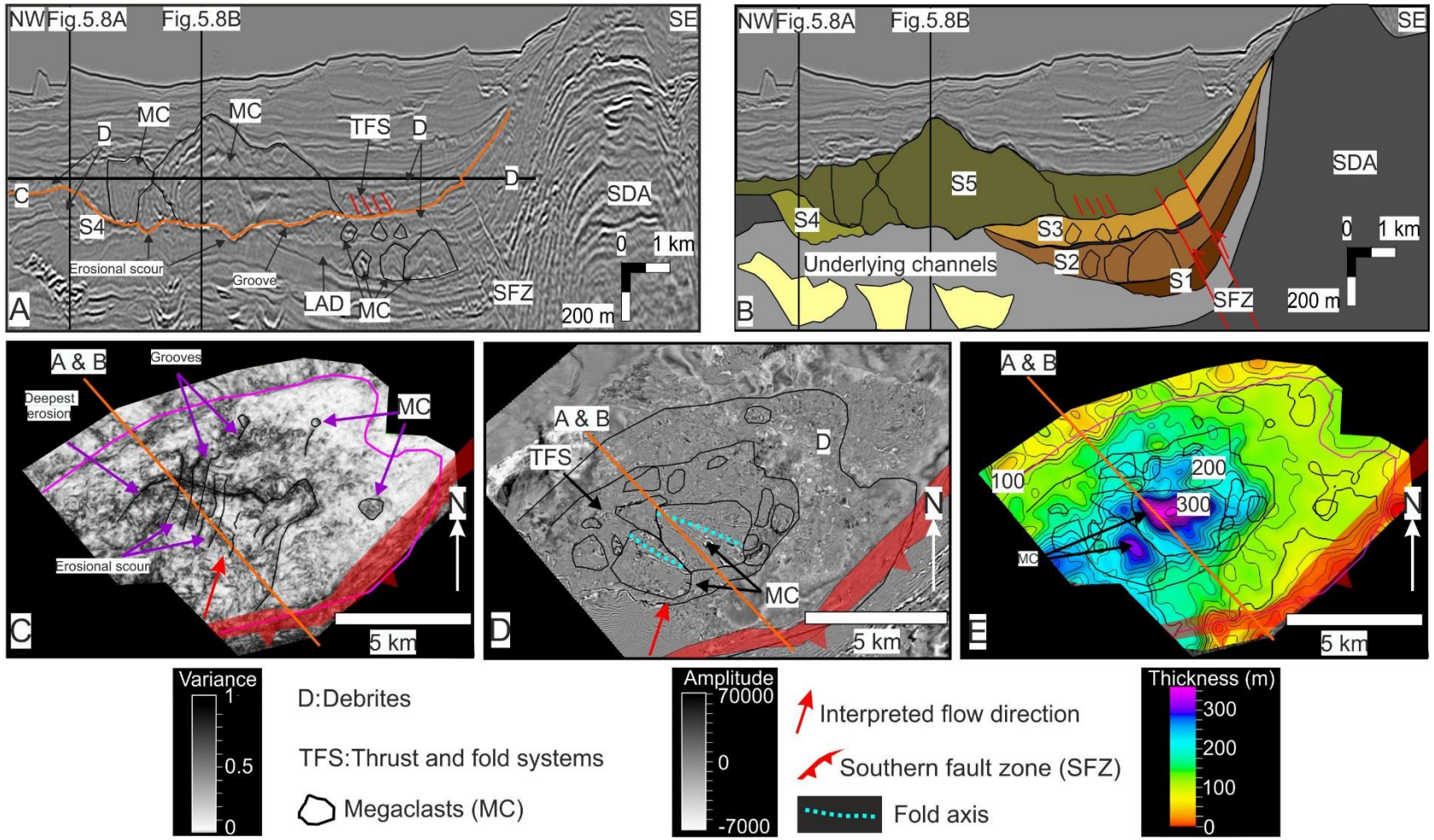

Figure 5.7. MTC S5. Seismic cross-section across S1-S5 showing examples of the seismic facies. For location refer to B-E and Fig. 5.5. **B.** Geo-seismic cross-section showing the deformation of S1-S5 by the southern fault zone (SFZ) and the western limb of the southern downdip anticline (SDA). **C.** Variance extraction at the base of S5 showing lineaments interpreted as erosional scours and grooves. **D.** Amplitude depth slice across S5 showing the distribution of the seismic facies; see A for intersection **E.** Vertical thickness map for S5.

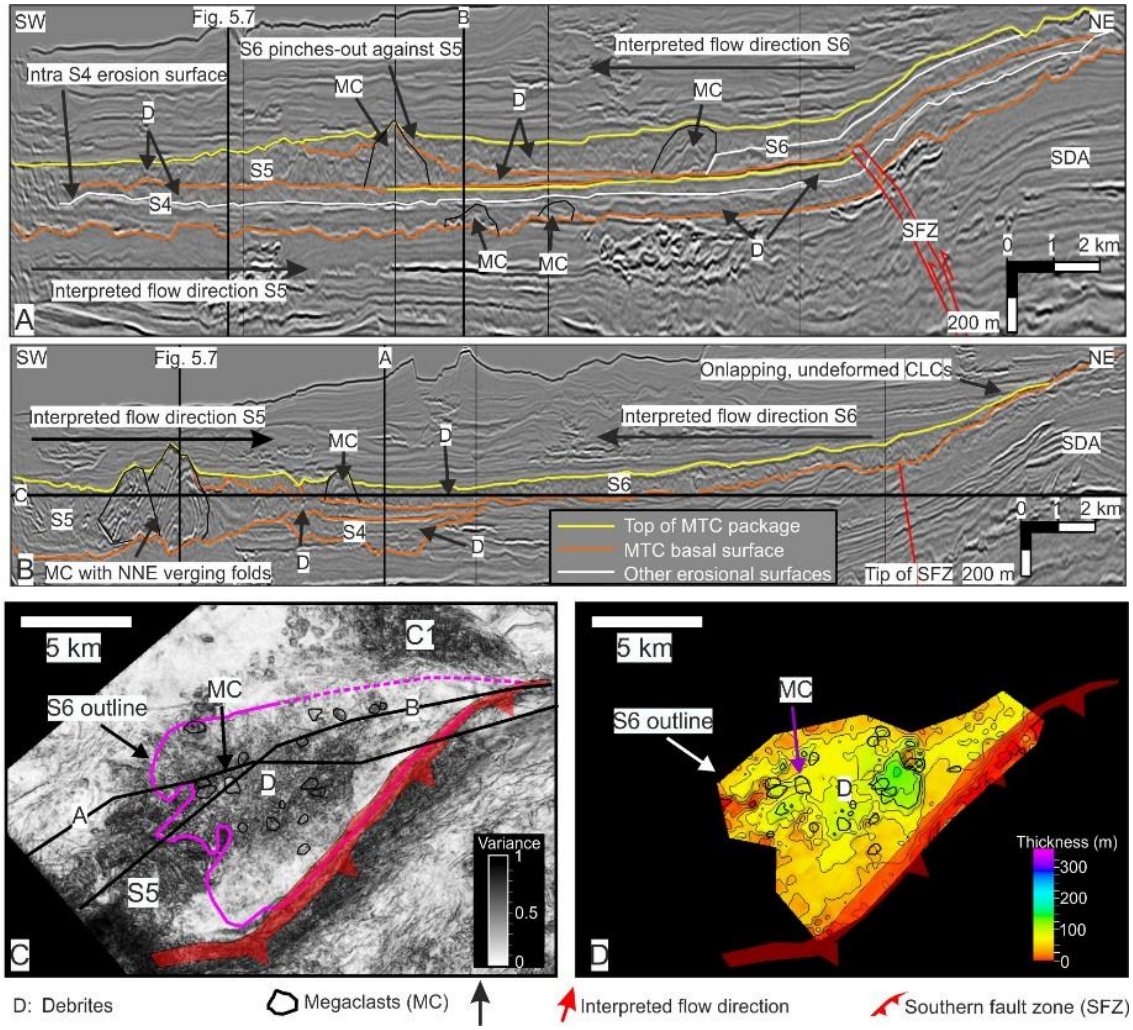

Figure 5.8. MTCs S4 and S6. **A.** Seismic line along S4 showing examples of the seismic facies. For location refer to C and 5.5D. Note the deformation of S4 across the southern fault zone (SFZ) and the western limb of the southern downdip anticline (SDA). **B.** Seismic line along S6. For location refer to C and Fig. 5.5F. S6 pinches to the south against protrusions on the top of S5; to the E it is undeformed. Note the geometry of the folded megaclasts in S5, which is used to interpret a NNE-directed flow. S6 is interpreted to have been emplaced by a SW-directed flow. CLCs are channel-levee complex sets. **C.** Variance depth slice (see B for intersection) showing the geometry and seismic facies within S6. **D.** Vertical thickness map for S6.

5.5.2 Central Region

Only one laterally extensive MTC (C1) is developed in the central region. C1 overlies a major erosion surface that trends along the syncline, cross-cuts the downdip anticline in the saddle area and extends into the basin-low to the west (Fig. 5.9A and B). In the syncline, the lateral walls to C1 are steep and formed by the back limb of the NDA and the frontal limb of the UA (Fig. 5.9D). Basinward of the downdip anticline, C1 is bounded to the SE by the external levee remnant that separates the southern and the central regions, and to the NW by the southern external levee of an underlying SW-trending

channel-levee complex set (Fig. 5.9E). C1 covers an area of c. 300 km^2 and its basal surface covers c. 400 km^2 with the height of its lateral margins decreasing in the downdip direction from c. 500 m to c. 120 m (Fig. 5.9D and E). C1 is not incorporated into or deformed by the fold-and-thrust belt, and is overlain by channel-levee complex sets that onlap the MTC and the flanking anticlines (Fig. 5.9C).

C1 is mainly composed of debrites and it is also internally deformed by imbricate thrusts and folds, which are concentrated towards the centre of the deposit where it is thickest (up to 200 m) (Fig. 5.9A-C). Towards its margins, the deposit is thinner (up to 50 m) and consists of lower-amplitude debrites (Fig. 5.9A-B). The deposit thins to ≤50 m across the downdip anticline, where it contains abundant megaclasts in a thin matrix formed by debrites (Fig. 5.9). Megaclasts are identified throughout C1 and are internally folded (Fig. 5.9B and E).

In the syncline, thrusts within C1 dip to the NE (Fig. 5.9C), suggesting emplacement by a SW-directed flow, an interpretation supported by the SW orientation of the lateral scarps (Fig. 5.9A-B). Further downdip, in the basin-low, thrusts dip to the SE (Fig. 5.9C), indicating emplacement by a broadly NW-directed flow. This inferred emplacement direction is supported by the NW-SE strike orientation of the lateral scarps, which is interpreted to be broadly parallel to the overall flow direction (*cf.* Bull et al., 2009). Further downdip, towards the western edge of the dataset, the orientation of the lateral scarps changes to WSW, suggesting C1 was emplaced by a WSW-directed flow (Fig. 5.9A). Therefore, although the overall trend of MTC C1 is roughly WNW, there were local variations in the direction of the flow.

The stratigraphy underlying C1 is folded and comprises channel-levee complex sets and MTCs (Fig. 5.9C). Towards the toe of the frontal limb of the DA, at the tip of the southern fault zone, a SW-trending erosional surface overlain by thin MTC remnants is locally preserved beneath C1 (Fig. 5.9C). Due to subsequent erosion its updip limit cannot be established. In the syncline, the strata underlying C1, thin against the flanks (Fig. 5.10B).

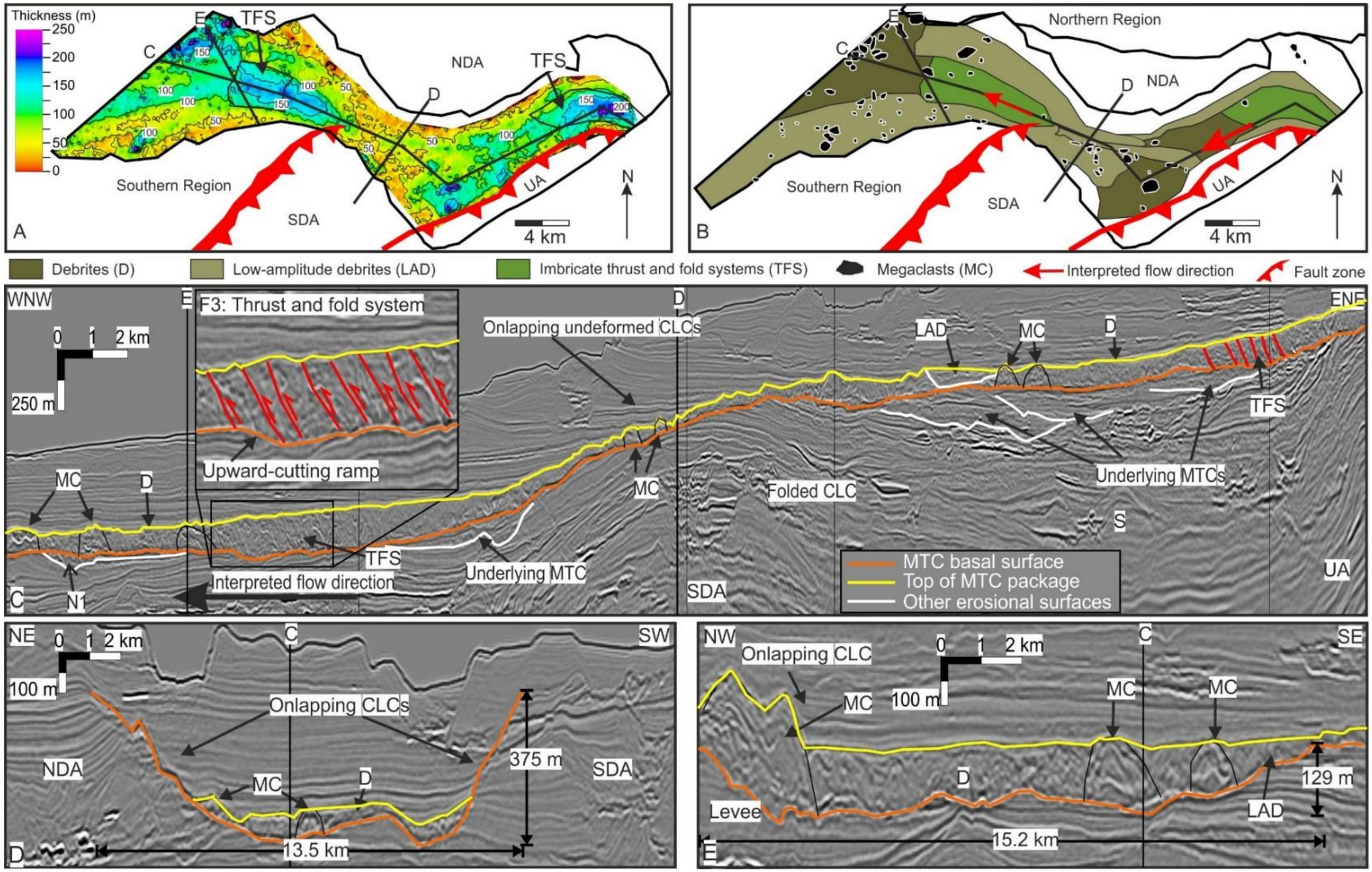

Figure 5.9. MTC C1. **A.** Thickness map of C1. Note that C1 thins towards its margins and across the downdip anticline (DA). **B.** Facies map of C1. **C.** Seismic line along C1 showing the variation of the seismic facies along strike. Note the MTC remnant underlying C1 at the toe of the SDA and the thinning across the anticline. C1 is not structurally deformed. CLCs denote channel-levee complex sets. **D.** Seismic line across the constriction of C1 showing examples of the seismic facies. The underfilled basal surface of C1 was filled by onlapping, undeformed CLCs. **E.** Oblique seismic line towards the western limit of the dataset showing examples of folded megaclasts, note the decrease in the relief of the erosion surface with respect to D.

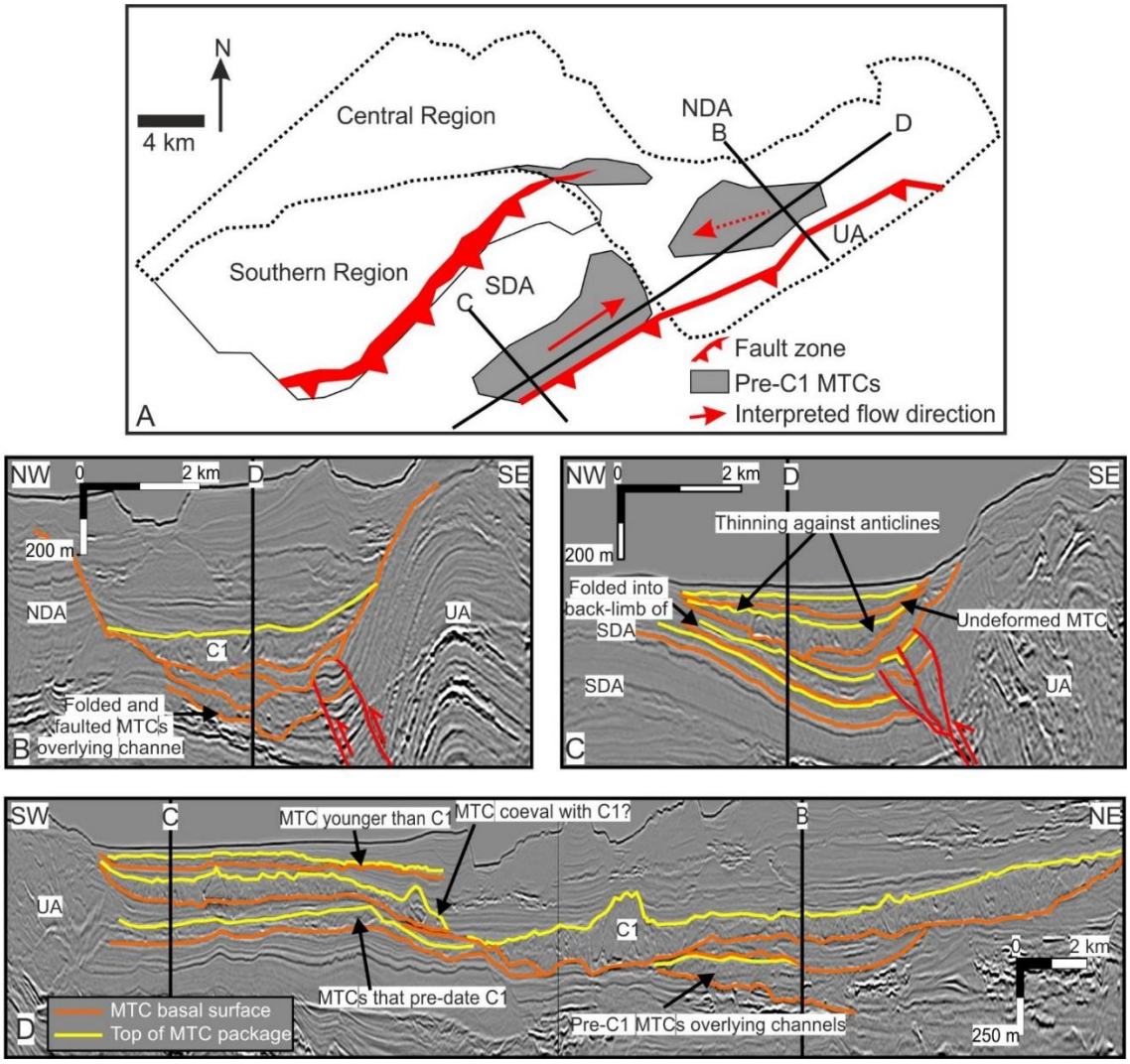

Figure 5.10. MTCs underlying C1. **A.** Map showing the distribution of the MTCs that underlie C1 (grey polygons). **B.** Seismic cross-section across the northern part of the syncline where several stacked MTCs underlie C1. They overlie a channel-levee complex set and are folded and faulted into the northern downdip anticline (NDA) and the updip anticline (UA). **C.** Seismic cross-section across the southern part of the syncline, which is filled by several MTCs. The older MTCs are faulted and folded into the SDA and the UA. The younger MTCs are undeformed. **D.** Seismic line along the syncline. The MTCs that underlie C1 in the northern part overlie a CLC and are older than those in the southern part of the syncline. The MTCs in the southern part of the syncline can be traced to the western flank of the UA. To the N, they are truncated by C1. There is also evidence of MTCs sourced from the UA in the stratigraphy overlying C1.

Updip of the NDA, folded MTC remnants underlying C1 are elongate NE-SW, and overlie and erode the axial portion of a SW-trending channel-levee complex set that is also folded (Fig. 5.10A and B). Given that the MTCs are only locally preserved their emplacement direction is uncertain. However, because the MTCs and the underlying channel-levee complex are folded and follow a similar trend, it is more likely that the MTCs were emplaced by a SW-directed flow. The southern part of the syncline contains

stacked MTCs that thin against the fold flanks and are interpreted to be younger than those in the northern part of the syncline (Fig. 5.10D). The older MTCs in the southern part of the syncline are displaced by the thrusts that core the UA and are folded into the back limb of the SDA, with the degree of stratal rotation decreasing upward (Fig. 5.10C). There are also younger, undeformed MTCs that overly C1 (Fig. 5.10D). Irrespective of their relative age, all the MTCs in the southern part of the syncline are elongate in a SW-NE direction and can be mapped to the steep frontal limb of the UA, which is thus interpreted to be their source (Fig. 5.10A and D).

5.5.3 Northern Region

The northern region traverses the NDA and contains two MTCs that overlie erosion surfaces (N1 and N2) (Fig. 5.4). N1 is truncated by N2, and thins updip where the two bounding erosion surfaces merge; no MTCs are documented above the clearly erosional basal surface, suggesting a zone of erosion and sediment bypass (e.g. Stevenson et al., 2015, Fig. 5.11B). The composite erosion surface incised c. 300 m into the northern part of the NDA and truncates several folded stratigraphic packages (Fig. 5.11B). Updip of the NDA, the composite surface directly overlies and erodes a channel-levee complex set, and across the western limb of the anticline it is bounded on either side by channel-levee complex sets (Fig. 5.11B and C). Further downdip, N1 underlies C1 and is capped by N2 (Fig. 5.11B); the downdip extent of N2 is controlled by irregular relief formed by megaclasts in C1 (Fig. 5.11B).

N1 and N2 are up to c. 90 m thick and are composed of debrites (Fig. 5.11A, Table 5.2). They contain several laterally discontinuous erosion surfaces, suggesting these deposits are the result of multiple periods of erosion and deposition. Along the northern lateral wall, arcuate scarps visible on variance extractions (Fig. 5.11A) coincide with a terrace-like geometry to the basal surface (Fig. 5.11C). These discontinuous erosion surfaces are overlain by debrites and are therefore interpreted to have been formed by

gravitational collapse of the northern lateral wall, a process that probably contributed to the southward shift and progressive widening of the basal erosion surface (Fig. 5.11C).

Based on the orientation of the lateral scarps, N1 and N2 are interpreted to have been deposited by WSW-directed flows. N1 and N2 truncate underlying folded stratigraphy; they are not folded and are overlain by onlapping, undeformed channel-levee complex sets (Fig. 5.11B). The stratigraphic packages underlying N1 and N2, which include thin (50-90 m thick) stacked MTCs, thin against the western flank of the DA (Fig. 5.11D).

5.6 Interpretation

5.6.1 MTC provenance and timing of emplacement

Figure 5.12A summarises the chronostratigraphic relationship between the different MTCs and the growth history of individual structures in the fold-and-thrust belt. In the southern region, S1-S5 are folded and displaced across the thrusts coring the SDA (Fig. 5.7A and B), indicating they were deposited before the most recent phase of faulting and folding. Furthermore, eastward thinning of S1-S5 against the western flank of the SDA suggests that some structural relief existed prior to the emplacement of MTCs S1-S5 and that they are likely syn-tectonic (Fig. 5.12A). In contrast, S6 is mostly undeformed and is overlain by largely undeformed channel-levee complex sets that passively onlap the flanking anticlines (Fig. 5.8B). Therefore, S6 was likely deposited towards the end of the last phase of uplift. In the central region, the MTCs pre-dating C1 in the syncline are folded and thin against the flanks (Fig. 5.10), and they are therefore interpreted as syn-tectonic. C1 is undeformed and is onlapped by undeformed channel-levee complex sets meaning that it was deposited at the end or after the last phase of uplift (Fig. 5.9C). In the southern part of the syncline, the transition from folded and faulted MTCs, to undeformed MTCs occurs at a similar stratigraphic level to C1 (Fig. 5.10C and D), indicating that the UA and DA were active at broadly the same time.

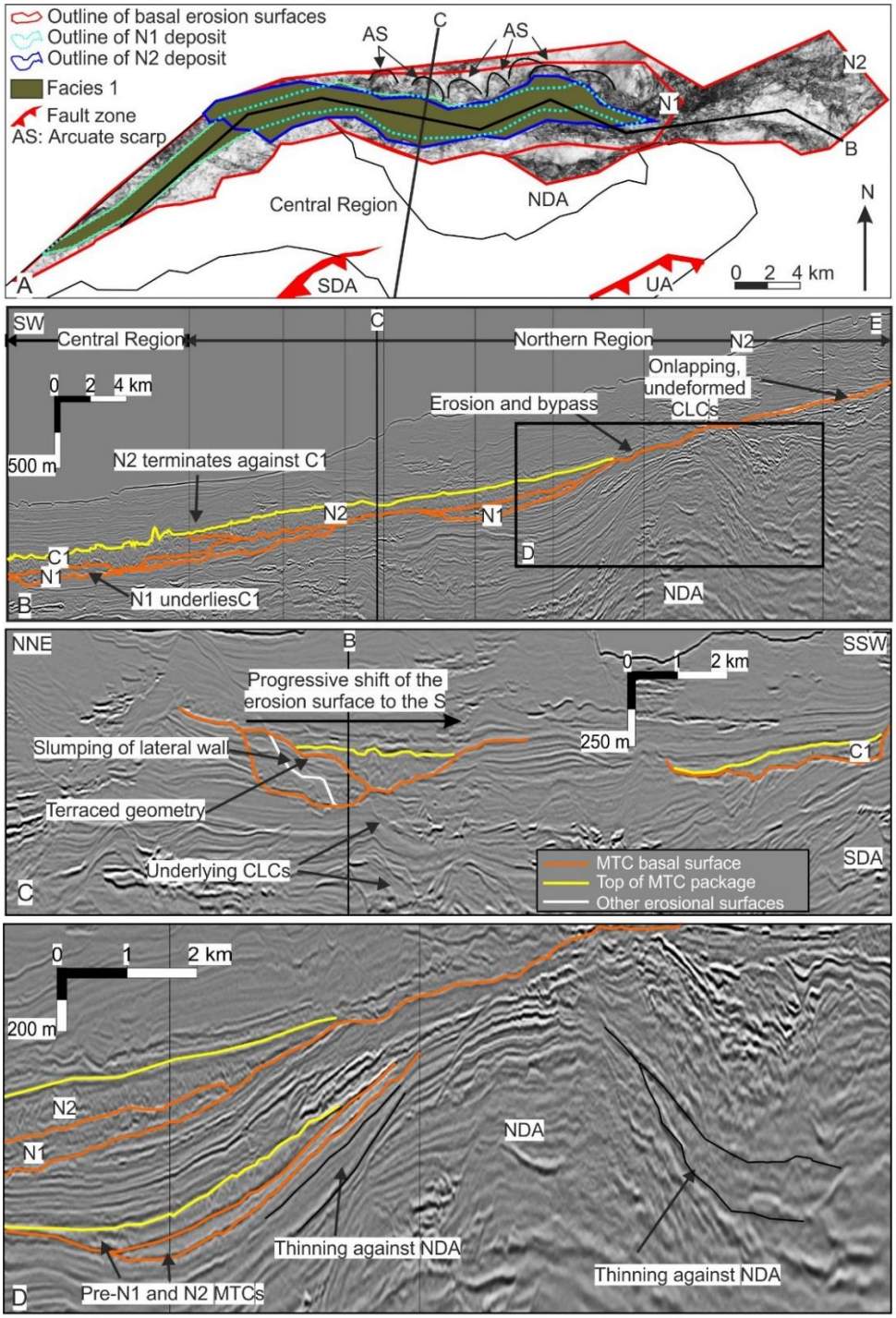

Figure 5.11. MTCs N1 and N2. **A.** Variance extraction at the base of N1 overlain by seismic facies maps for N1 and N2, which are mainly composed of facies 1. Note the arcuate scarps (AS) visible on the variance extraction. **B.** Seismic line along the northern region. N1 and N2 traverse the northern downdip anticline (NDA); the stratigraphy underlying the erosion surfaces of N1 and N2 is folded while the stratigraphy overlying them is undeformed. Note that N1 is eroded by N2 and that N1 underlies C1 while N2 overlies it. The downdip extent of N2 is controlled by protrusions at the top of C1. Updip, there is an area of bypass. **C.** Seismic line across the arcuate scarps shown in A. They coincide with a “terraced” geometry, which is interpreted to reflect slumping from the northern lateral wall. N1 and N2 overlie channel-levee complex sets (CLCs). **D.** Close up of B on the NDA showing thinning against the flanks of the anticline and MTCs that can be traced to the western limb of the NDA.

Similarly, in the northern region, N1 and N2 are underlain by folded MTCs that thin against the NDA (Fig. 5.11D). Conversely, N1 and N2 are themselves undeformed and overlain by undeformed, onlapping channel-levee complex sets (Fig. 5.11B). The age relationship between tectonically deformed MTCs in the southern, central and northern regions cannot be established with confidence.

The emplacement directions of the southern MTCs are challenging to constrain with confidence because the MTCs extend to the SW of the study area (Fig. 5.5). S5 contains the most convincing kinematic indicators, which together support an emplacement direction towards the NNE (Fig. 5.12B): NNE orientated grooves and scours at the base (Fig. 5.7C), and NE- verging folds within megaclasts (Fig. 5.8B) with WNW-ESE orientated fold axes (Fig. 5.7D). The elongate morphology of S1-S3 (Fig. 5.5), their northward onlap against the underlying levee (Fig. 5.6A) and the NE-SW alignment of the megaclasts in S2-S3 (Fig. 5.5 and 5.6B-D) also suggest a similar emplacement direction. Therefore, MTCs S1-S3 and S5 could have been sourced from local collapse of the southern part of the SDA or other anticlines to the SW of the dataset (Fig. 5.12B). MTCs S1-S3 and S5 are thus classified as detached MTCs (*sensu* Moscardelli and Wood, 2008). Estimated runout distances for MTCs S1-S3 could be c. 10, 15 and 20 km, respectively. The abrupt increase in quantity and size of megaclasts in S5 (Table 5.2) could reflect a shorter runout distance and it is more likely that S5 was sourced from the southern part of the SDA (Fig. 5.12B). Similar mass-wasting of deep-water fold-and-thrust belts has been documented south of the study area (Vinnels et al., 2010; Romero-Otero et al., 2010; Alfaro and Holz, 2014). The provenance of S4 is uncertain because there are no flow direction indicators, its northeastern portion is folded and eroded by S6 and C1 (Figs. 5.8A), and it is only partially imaged by the seismic survey. S4 may have been also sourced from the SW. Alternatively, given that it follows the trend of underlying channel-levee complex sets, it could also have been sourced from the northern part of the SDA or even further updip, depending on the structural relief of the SDA at the time

of emplacement. S6 was emplaced from the NE. It can be traced to the tip of the southern fault zone but, because it is eroded by C1, the updip limit of its headwall is not preserved (Fig. 5.8C), and it is unclear whether it was sourced from the frontal flank of the SDA or if it traversed the anticline and was sourced from further updip (Fig. 5.12B).

Based on the orientation of the lateral scarps and the vergence of the faults in the imbricate fold and thrust systems (Fig. 5.9), C1 is interpreted to have been emplaced by a broadly WNW-trending flow. C1 extends beyond the eastern limit of the dataset, where the present-day bathymetry shows arcuate scarps on the shelf break, analogous to the 'cookie-bite' features described by Moscardelli and Wood (2008; Fig. 5.12B). The shelf break thus represents the potential source area for C1, suggesting this deposit is best classified as a shelf-attached MTC (*sensu* Moscardelli and Wood, 2008). There are multiple possible sources for the syn-tectonic MTCs that underlie C1 in the syncline. Towards the southern part of the syncline, MTCs were sourced from the frontal flank of the UA and were directed to the NE (Figs. 5.10 and 5.12B). There are also some MTCs that post-date C1, indicating several stages of mass-wasting of the UA. In the northern part of the syncline, the early-tectonic MTC remnants are interpreted to have been sourced from the NE because they are elongated parallel to the syncline and the underlying SW-trending channel-levee complex sets (Fig. 5.10A). However, it is not possible to establish whether they were sourced from the shelf or from other collapses along the frontal limb of the UA. It is also unclear whether the MTCs in the syncline traversed the DA into the basin-low. However, given that these MTCs are relatively small and that there is scarce evidence of older MTCs underlying C1 in the basin-low outboard of the DA (Figs. 5.10A and 5.13A-C), it is inferred that they were confined to the small basin defined by the syncline.

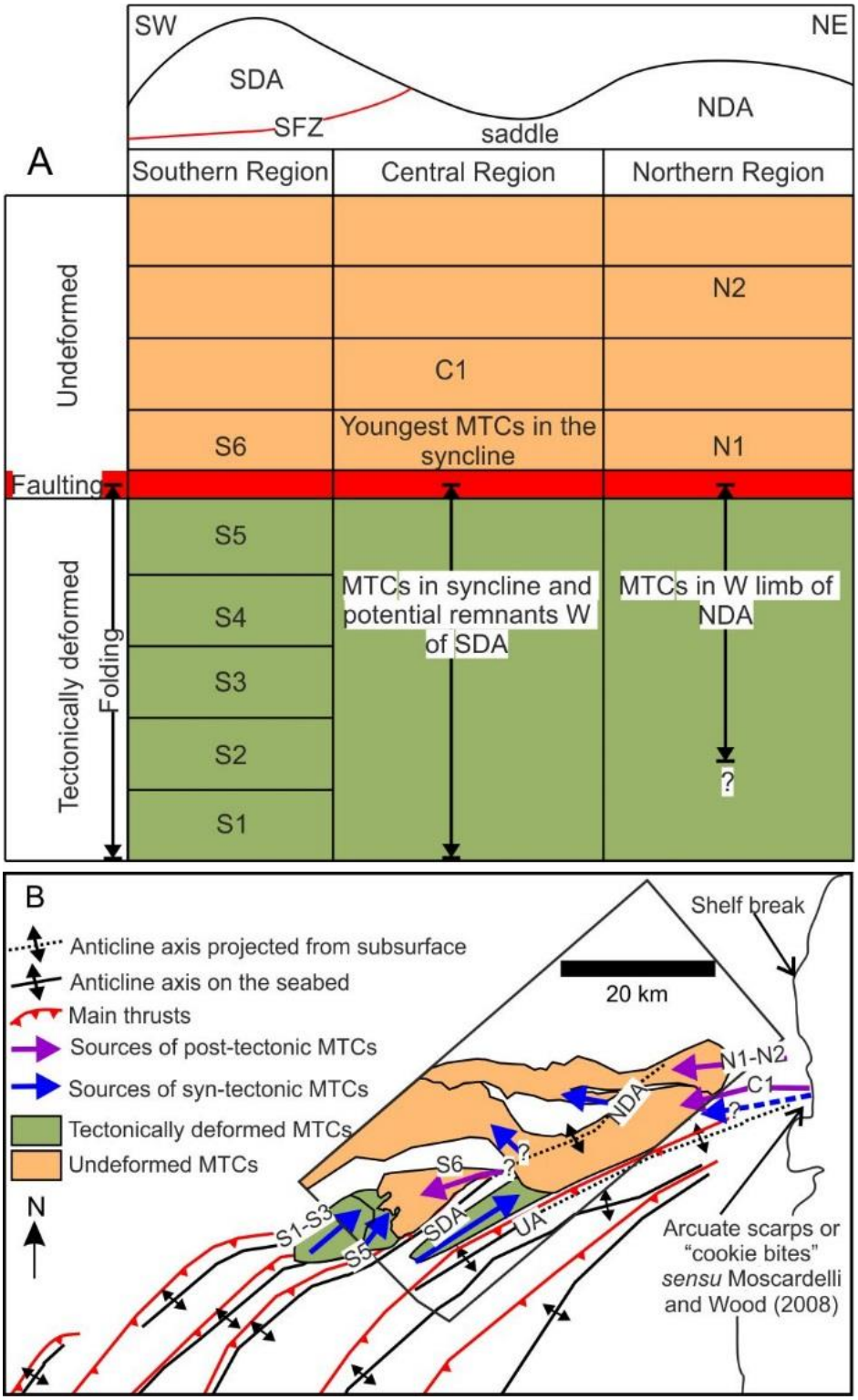

Figure 5.12. Summary of interpreted chronostratigraphy and provenance. **A.** Chronostratigraphic chart of the MTCs and their relative timing with respect to the tectonic events. In the southern region, MTCs S1-S5 and the basal part of S6 were deposited before faulting and during folding. Upper S6-N2 were deposited after folding and faulting. In the central region, the MTCs underlying C1 were deposited during folding and possibly during faulting. **B.** Map showing the interpreted source areas for MTCs S1-S5 and the MTCs underlying C1 and N1/N2), and MTCs C1, N1 and N2. Most of the earlier MTCs (S1-S5) were sourced from the flanks of the growing anticlines and are classified as detached (sensu Moscardelli and Wood, 2008), while younger MTCs (C1, N1-N2) are shelf-attached (sensu Moscardelli and Wood, 2008).

Based on the orientation of the lateral scarps, N1 and N2 are interpreted to have been deposited by WSW-directed flows and to have been sourced from the NE. Like C1, N1 and N2 are located directly downdip of the arcuate scarps on the shelf break (Fig. 5.12B); these MTCs are accordingly interpreted to have been sourced from the shelf and are classified as shelf-attached MTCs (*sensu* Moscardelli and Wood, 2008). The syn-tectonic MTCs underlying N1 and N2 (Fig. 5.11D) were likely sourced from the frontal flank of the NDA (Fig. 5.12B) and are therefore classified as detached MTCs (*sensu* Moscardelli and Wood, 2008).

5.6.2 Tectono-stratigraphic Evolution

Figure 5.13 summarises the interpreted link between growth of the deep-water fold-and-thrust belt and the emplacement of genetically-related MTCs. Before the latest phase of activity on the thrusts that core the UA and the DA, MTCs in the southern region were mostly sourced from the SW, where the flanks of the anticlines were steeper (Fig. 5.13A). As the SDA grew, S1 became folded and S2 was emplaced occupying a greater area and extending further to the NE (Table 5.2). The MTCs deposited in the syncline were mainly sourced from the UA and are interpreted to have been confined to the mini-basin bounded by the DA and UA (Fig. 5.13A). This interpretation is supported by the presence of growth strata, which indicates that the DA and UA had been uplifted and degraded to some extent, by the scarce and thin MTC remnants found at the toe of the DA (Fig. 5.9C), and by the small size of the detached MTCs that occupy the syncline (Fig. 5.10). Nonetheless, it remains possible that some flows, possibly including S6, traversed the structure prior to the emplacement of C1, potentially across the lower relief saddle between the SDA and NDA, and that the deposits associated with these flows were subsequently eroded by C1.

As the anticlines grew, the syncline and areas basinward of the DA were filled by MTCs derived from the degradation of the growing structures (Fig. 5.13B): S3 occupied a greater area and extended further north than S2 (Table 5.2, Fig. 5.12B), S4 was

emplaced to the NW of S1-S3, and syn-tectonic MTCs where sourced from the frontal limb of the DA (Fig. 5.13B).

S5 was the last and largest MTC sourced from the SW and it was likely derived from the southern part of the SDA (Fig. 5.13C). It eroded S3 and S4 and extended further to the NE. After S5 was emplaced, thin-skinned shortening and folding culminated with faulting of both fold cores (Fig. 5.13C). Faulting would have generated further instability due to steepening of the anticline frontal limbs leading to the emplacement of S6. It could have been sourced from the frontal limb of the DA or derived further updip (Fig. 5.13C). N1 was also emplaced following the latest phase of tectonic uplift in the study area, being deposited along the trend of a long-lived sediment flow-pathway defined by stacked channel-levee complex sets (Fig. 5.13C). The DA was degraded progressively by erosion of the back limb of the SDA and possibly by retrogradational collapse of the frontal limb (Fig. 5.13C).

Decreased accommodation as the syncline filled and degradation of the folds at the saddle between the SDA and NDA would have allowed larger, shelf-attached MTCs to traverse the anticline, establishing a conduit between the syncline and the deep basin (Fig. 5.13D). It is also possible that the through-going erosional surface across the anticline was established solely by the erosive power of C1. This is supported by the scale of C1, its irregular and erosional basal surface, and the presence of large megaclasts, all of which suggest that the flow was voluminous and erosive. However, progressive degradation of the DA by several erosional flows that were initially confined in the syncline is supported by the presence of folded MTC remnants that underlie C1. It is therefore likely that the connection between the shelf break and the basin-low downdip of the structures was established through a combination of progressive degradation, filling of the syncline and erosion by C1. Following the emplacement of C1, in the northern region N2 followed the trend of N1, leading to widening of the erosion surface.

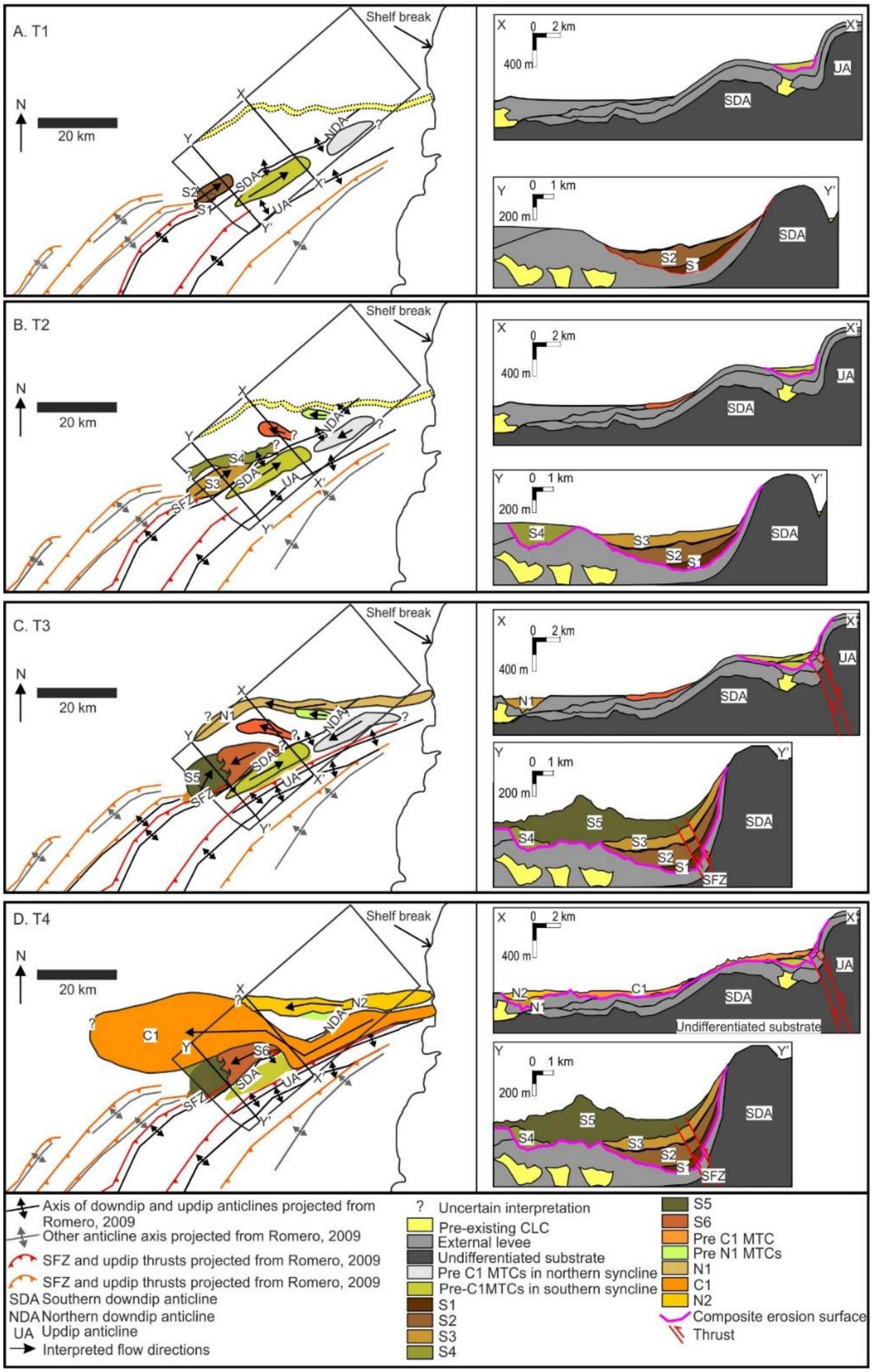

Figure 5.13. Schematic representation of the tectono-stratigraphic evolution. **A.** MTCs were potentially ponded in the syncline sourced mainly from the frontal limb of the updip anticline (UA). MTCs in the northern part of the syncline may have been sourced from the UA or the shelf. S1 and S2 were sourced from the SW of the dataset. The northern region contained a channel-levee complex set (CLC). **B.** As uplift continued S3 and S4, and more MTCs in the syncline were deposited. Stacking of the MTCs created composite basal erosion surfaces. **C.** Emplacement of S5 was followed by faulting. As structural uplift ceased, the syncline was filled by MTCs that eroded the back limb of the downdip anticline and further enlarged the composite basal surface. Back-stepping erosion of MTCs from the frontal flank may have contributed to the degradation of the DA. It is not clear if S6 was connected to the syncline or sourced from the frontal limb of the SDA. N1 exploited and widened the CLC in the northern region. **D.** C1 traversed the DA creating a through-going composite surface that connected the basin-low and the syncline. This surface amalgamated with the basal surface in the southern region creating an even larger composite surface. N2 was also sourced from the shelf.

Previous studies document similar breaching of the folds bounding mini-basins by MTCs (e.g. Vinnels et al., 2010; Geersen et al., 2011). Based on data from offshore Chile, Geersen et al. (2011) propose a model for the breaching of a thrust-cored high formed between the shelf and an offshore anticline. They propose that structural uplift led to oversteepening of the frontal flank of the anticline until a critical angle was reached, at which time mass-wasting, possibly triggered by an earthquake, smoothed the slope profile and reconnected the shelf with the slope. Vinnels et al. (2010), recognise comparable processes to the SW of the current study area associated with repeated back-stepping slope failures that connected otherwise isolated piggyback basins developed in the evolving Sinú Fold Belt.

5.7 Discussion

5.7.1 Changes in MTC distribution, source and size in response to structural uplift

Deposition of MTCs S1-S5 shifted progressively to the NE, likely reflecting changes in source area. After the last episode of uplift, which culminated in propagation of the faults that core the DA and the UA, and possibly the emplacement of S6, MTC source areas shifted towards the NE closer to the shelf-break, and shelf-attached MTCs were emplaced (MTCs C1, N1 and N2). These change could have been controlled by the evolution of the structures, or could be attributed to externally-driven, more regional controls, such as increased sediment supply, eustatic sea-level change, gas hydrate dissolution and/or seismicity (e.g. Manley and Flood, 1988; Beaubouef and Friedmann, 2000; Maslin et al., 2004; Frey Martinez et al., 2005; Grozic, 2010; Masson et al., 2010; Alfaro and Holz, 2014). Along the northern coast of Colombia, during the Pleistocene, uplift of the Sinú Fold Belt was accompanied by uplift of the northern Andes, which coincided with changes in eustatic sea-level and regional climate (Van der Hammen, 1958, 1974; Duque-Caro, 1979; Hooghiemstra and Ran, 1994; Ortiz-Karpf et al., 2015). Also, in the Plio-Pleistocene, there were nine avulsions of the Magdalena River (Romero-

Otero, 2009), which would have caused abrupt changes in sediment input and dispersal patterns. Therefore, several external forcing mechanisms can be invoked for the emplacement of the shelf-attached MTCs (Ortiz-Karpf et al., 2015). However, the UA bends to the east towards the area of the shelf where the arcuate scarps, interpreted as a possible source for the shelf-attached MTCs, are located (Fig. 5.12B). It is therefore likely that uplift associated with the propagation of the thrust that cores the UA induced the development of steep, unstable areas close to the shelf. The results of this study suggest a northward shift in the source area of the MTCs through time, coinciding with the propagation direction of the structures (e.g. Martinez et al., 2015; Bernal-Olaya, 2015). This local finding suggests that systematic shifts in MTC source areas through time could be investigated in other areas along the margin to help constrain the evolution of the entire Sinú Fold Belt. Previous studies in other basin margins also report systematic variations in the morphology and distribution of syn-tectonic sedimentary packages with continued structural uplift. In the Apennines, Festa et al. (2015) also observed systematic shifts in the occurrence of MTCs in the direction of propagation of the fold-and-thrust-belt, and an increase in the volume of the MTCs through time. In the Niger Delta, variations in the architecture, morphology and distribution of MTCs and channel-levee complex sets were also documented in a syn-tectonic stratigraphic package in the vicinity of a fold; these variations were used to constrain the evolution of the fold (Clark and Cartwright, 2012). These observations suggest that systematic, fold-belt-driven shifts in MTC source areas are reflected in the morphology, distribution and characteristics of the deposit, and that this link is common to both active and passive margins. The results presented here are thus potentially applicable to other fold-and-thrust belts around the world.

Changes in source are reflected in the size of the MTCs: S1-S5 are detached and cover areas of c. 9-100 km^2 within the study area (Table 5.2); C1, N1 and N2 are shelf-attached and have areal extents of at least 200-300 km^2 (Table 5.2). These findings are in

accordance with those of Moscardelli and Wood (2008, 2015), who found that detached MTCs have areas of tens of km^2 whereas attached MTCs can be hundreds to thousands of km^2 in area. The difference between the volumes of detached and shelf-attached MTCs can be readily explained by considering the volumes of material available at the source; these volumes are likely to be smaller along local flank collapses than on the delta-fed shelf break. However, the evolution of the seascape during degradation and sedimentation can also play an important role in the areal extent, runout distance and therefore the distribution of MTCs. For example, in the southern region, there is a progressive increase in the area and down-flow extent of S1-S5 (Table 5.2). This could be explained by the sequential steepening of the frontal limbs of the growing anticlines, which could have resulted in progressively larger failures. Also, the emplacement of earlier MTCs immediately downdip of the forelimb would have smoothed the break-in-slope contributing to the progressively longer runout distances and larger areal extents. The greater areal extents and runout distances of the shelf attached MTCs (C1, N1 and N2, Table 2) are also the result of the smoothed the slope profile through progressive degradation of the folds. The distribution, morphology and scale of the resulting MTCs therefore reflect changes in source areas induced by the combined effects of structural growth and degradation of the thrust-and-fold belt. Such changes in external MTC characteristics should also be reflected in their internal composition, impacting their ability to act as hydrocarbon reservoirs or seals (e.g. Gamboa et al., 2010; Omosanya and Alves, 2013; Alves et al., 2014).

5.7.2 Evolution and chronostratigraphic significance of MTC basal surfaces

The recent tectono-stratigraphic evolution of the fold-and-thrust belt resulted in the formation of an erosion surface that is overlain by at least 9 distinct MTCs (Fig. 5.13). This composite, surface was widened and deepened by multiple erosional flows and is therefore time-transgressive. The basal surface developed during a period dominated by thin-skinned folding and thrusting, and fold degradation, presumably over a protracted

period of time. In addition to the specific MTCs identified and described, local collapse of the lateral walls, evidenced by the arcuate scarps at the margins of the basal surfaces of N1 and N2 (Fig. 5.11C), also contributed to widening the composite basal erosion surface. Previous studies suggest that time-transgressive MTC basal surfaces are common. Using 3D seismic from offshore Israel, Frey-Martinez et al. (2005) document at least three large-scale slumps related to, and emplaced on a continuous basal shear surface. On the Exmouth Plateau, Scarselli et al. (2013) report a series of MTCs in the Late Pliocene-Recent stratigraphy, interpreting that the different orientations of grooves in the basal surface to reflect different transport directions resulting from the multi-stage evolution of the complex. The models for syn-tectonic fold degradation presented by Heniö and Davies (2006) and Geersen et al. (2011) also imply repeated episodes of mass-wasting and sedimentation. Therefore, despite the quasi-instantaneous emplacement of individual MTCs, their deposits may coalesce above composite basal surfaces that are time-transgressive. In other words, these composite basal surfaces are transferred into the rock record, but probably never were a geomorphic surface (cf. Strong and Paola, 2008). The identification of discrete MTCs is likely limited by dataset resolution. For instance, the basal surface of Unit D (Ortiz-Karpf et al., 2015), which is overlain by MTCs of various ages, is a continuous reflection that can be mapped across the study area (Fig. 5.4). At deeper burial depths the composite nature of similar erosion surfaces at the base of multiple stacked MTCs might not be resolvable, and thus be interpreted as a geomorphic surface overlain by a single MTC, obscuring the complex tectono-stratigraphic history that led to its formation. Distinguishing between single and composite basal surfaces can impact the interpretation of sedimentary basin burial histories, which are commonly used to evaluate the timing of hydrocarbon generation and expulsion. It can also influence the prediction of the characteristics and distribution of the sedimentary packages downdip of the MTCs. Furthermore, the presence of coalescing MTCs can introduce lateral facies variability and affect the prediction of sealing capacity (e.g. Gamboa et al., 2010; Omosanya and Alves, 2013; Alves et al.,

2014). Hence, this study illustrates the potential complexity of deeper subsurface examples where the development of the MTC basal surfaces and the tectono-stratigraphic history may not be resolvable.

5.8 Conclusions

Detached and shelf-attached MTCs are recognised in the northern tip of the southern Sinú deep-water fold–and-thrust belt. Detached MTCs deposited prior to last phase of folding and faulting were mostly sourced from the SW, and in the southern region have minimum areal extents of c. 9 to 100 km^2. Younger MTCs deposited after the last phase of folding and faulting are shelf-attached and cover areas in excess of 300 km^2.

The characteristics of the MTCs reflect changes in source area through time and help constrain the complex tectono-stratigraphic history of the study area. The direction in which the MTC source areas shifted through time coincides with the direction of propagation of the anticlines, suggesting that structural evolution was an important control on the distribution and characteristics of the MTCs. Similar observations in other active and passive basin margins suggest that systematic shifts in MTC source areas as fold-and-thrust-belts evolve are possibly generic and that a similar approach could be applied to help constrain the evolution of fold-and-thrust belts elsewhere.

The unconformity represented by the erosion surface at the base of the MTC package is composite and time-transgressive, forming over a protracted period of slope instability associated with the punctuated growth of the deep-water fold-and-thrust belt. Therefore, despite the quasi-instantaneous emplacement of individual MTCs, MTC basal surfaces may have longer and more complex histories in locations subject to repeated mass-flows, with implications for interpretations of burial history, the heterogeneity of the MTCs themselves and inferences regarding downdip sedimentation. The studied system may be a valuable analogue for deeper subsurface examples where the development of MTC basal surfaces and the tectono-stratigraphic evolution may not be resolvable.

6 Influence of Seabed Morphology and Substrate Composition on Mass-Transport Flow Processes and Pathways

The work in this chapter constitutes the unrevised submitted version of a manuscript accepted for publication in the Journal of *Sedimentary Research* pending major revisions.

6.1 Introduction

The basal surfaces of MTCs can be defined by deep and widespread incision (e.g. Weimer and Slatt, 2007; Posamentier and Martinsen, 2011), with the volume of entrained substrate accounting for up to 40-50% of the total volume of the deposit (e.g. Prior et al., 1984; Gee at al., 2006; Lamarche et al., 2008; Joanne et al., 2013). The morphology of an MTC basal surface depends on the capacity of the flow to erode, which in turn depends on the characteristics of the flow and of the slope over which it propagates (Dykstra et al., 2011; Iverson, 2012; Day et al., 2015). Slope profiles are commonly bathymetrically irregular due to the development of gravity and tectonically-driven structures, salt and mud diapirism, or depositional relief associated with underlying deep-water architectural elements such as channel-levee complex sets, contourites and MTCs (e.g. Nakajima et al., 1998; Migeon et al., 2001; Piper and Normark, 2001; Skene et al., 2002; Steffens et al., 2003; Frey-Martinez et al., 2006; Heiniö and Davies, 2006; Vinnels et al., 2010; Alves, et al., 2010; Ducassou et al., 2015). Substrate composition can be variable, with deep-water depositional elements having different textures and compositions, and therefore being variably susceptible to erosion and entrainment. Entrainment of different types of substrate can have implications in the rheology and structure of the flow and therefore on the resulting deposits (e.g. Iverson, 1997; 2012; Dykstra et al., 2011; Joanne et al., 2013). The heterogeneity resulting from entrainment of material with different compositions and clast sizes can potentially affect the ability of

MTCs to act as hydrocarbon seals or reservoirs (e.g. Gamboa et al., 2010; Omosanya and Alves, 2013; Alves et al., 2014).

This study uses a 3D seismic reflection volume located in the southern Magdalena Fan, offshore Colombia to investigate the effect of bathymetric relief and substrate heterogeneities on the dispersal patterns, distribution and geometries, and seismic facies of several Pleistocene MTCs. Here, tectonic structures formed due to thin-skinned shortening and multiple stacked channel-levee complex sets combine to form a complicated slope upon which several highly erosive MTCs were transported and emplaced (Ortiz-Karpf et al., 2015; Ortiz-Karpf et al., 2016). The geological setting and the high seismic resolution at shallow stratigraphic levels make it an ideal dataset to study MTC-substrate interactions in detail.

6.2 Data

This study uses a Post-Stack Depth-Migrated (PSDM) seismic survey that covers an area of 1900 km^2 and which has a bin spacing of 12.5 x 12.5 m. This study focuses on a 1 km thick stratigraphic succession immediately below the seabed; at this depth the dominant frequency is 30 Hz and the assumed sediment velocity is 1900 m/s, thus yielding a vertical and horizontal resolution of c. 10-15 m and c. 15 m respectively (Ortiz-Karpf et al., 2015; Ortiz-Karpf et al., 2016). The seabed is defined by a positive reflection represented by a black horizon in the seismic images shown herein. A few wells lie NE of the study area, but they were not available for this study.

6.3 Geological Setting

The Magdalena Fan is located in the Caribbean Sea, off the northern coast of Colombia, South America (Fig. 6.1). This is a tectonically active margin, where the Caribbean Plate subducts obliquely beneath the South American Plate resulting in the development of imbricate fold-and-thrust belts (Duque-Caro, 1979; Pindell, 1994; Meschede and Frisch, 1998; Cediel et al., 2003; Pindell and Kennan, 2009). The youngest is the Sinú Fold Belt,

which is located offshore and has experienced episodic growth since the Middle to Late Miocene (Cediel et al., 2003; Martinez et al., 2015), propagating sequentially to the north (Bernal-Olaya, 2015; Martinez et al., 2015). The Sinú Fold Belt is divided into the Southern and Northern Sinú Fold Belt, with subdued deformation and relief characterising the area between the two segments (Fig. 6.1). It is this location that the Magdalena Fan has evolved since the Late Miocene (Duque-Caro, 1979, 1984; Kolla and Buffler, 1984; Breen, 1989; Romero-Otero, 2009; Fig. 6.1).

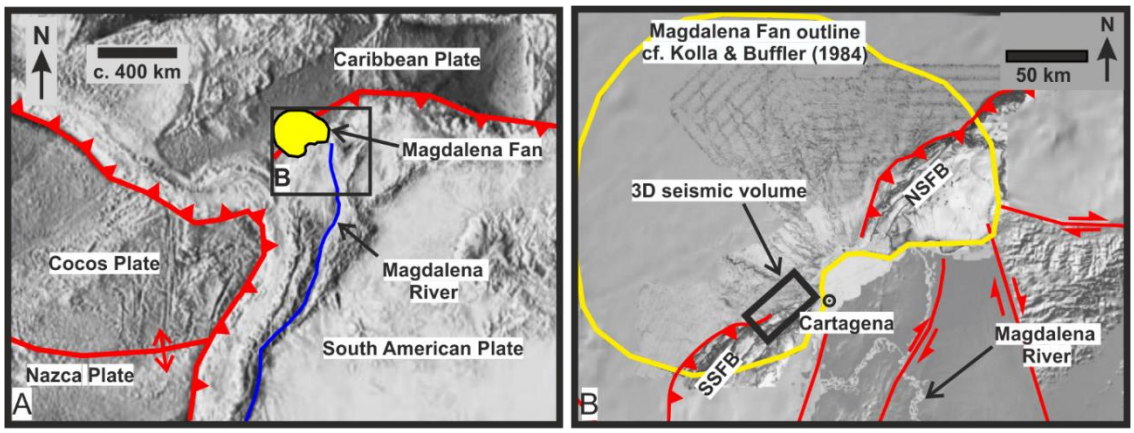

Figure 6.1. Geological setting. **A)** The Magdalena Fan is located in an active margin where the Caribbean Plate collides obliquely with the South American Plate **B)** The Magdalena Fan is located in a relatively undeformed area between the Southern Sinú Fold Belt (SSFB) and the Northern Sinú Fold Belt (NSFB). The study area, defined by the black rectangle includes the northern part of the SSFB and part of the relatively undeformed area.

The study area is defined by the outline of the three-dimensional seismic volume, which is located in the northern tip of the Southern Sinú Fold Belt (Fig. 6.1B). It images two large anticlines, referred to as the *downdip anticline (DA)* and *updip anticline (UA)* (Fig. 6.2), separated by a syncline (cf. Ortiz-Karpf et al., 2016; Fig. 6.2B-D). The DA is composed of two segments separated by a saddle (Fig. 6.2B-D). The southern segment, which is thrust-cored and asymmetric, with its steepest flank dipping to the NW, is referred to as the *southern downdip anticline (SDA)* (cf. Ortiz-Karpf et al., 2016; Fig. 6.2B and C). The northern domain is broader and more symmetric, it is not faulted and is referred to as the *northern downdip anticline (NDA)* (cf. Ortiz-Karpf et al., 2016; Fig. 6.2D). The UA is asymmetric and thrust-cored, with a steep, NW-verging frontal limb (Fig. 6.2D). To the west of these tectonic structures, the seabed is dominated by

compensationally stacked channel-levee complex sets that are c. 100-200 m high at the external levee crests. The primary depositional geometry of the channel-levee complex sets is sometimes modified by sediment waves and MTCs (Romero-Otero, 2009).

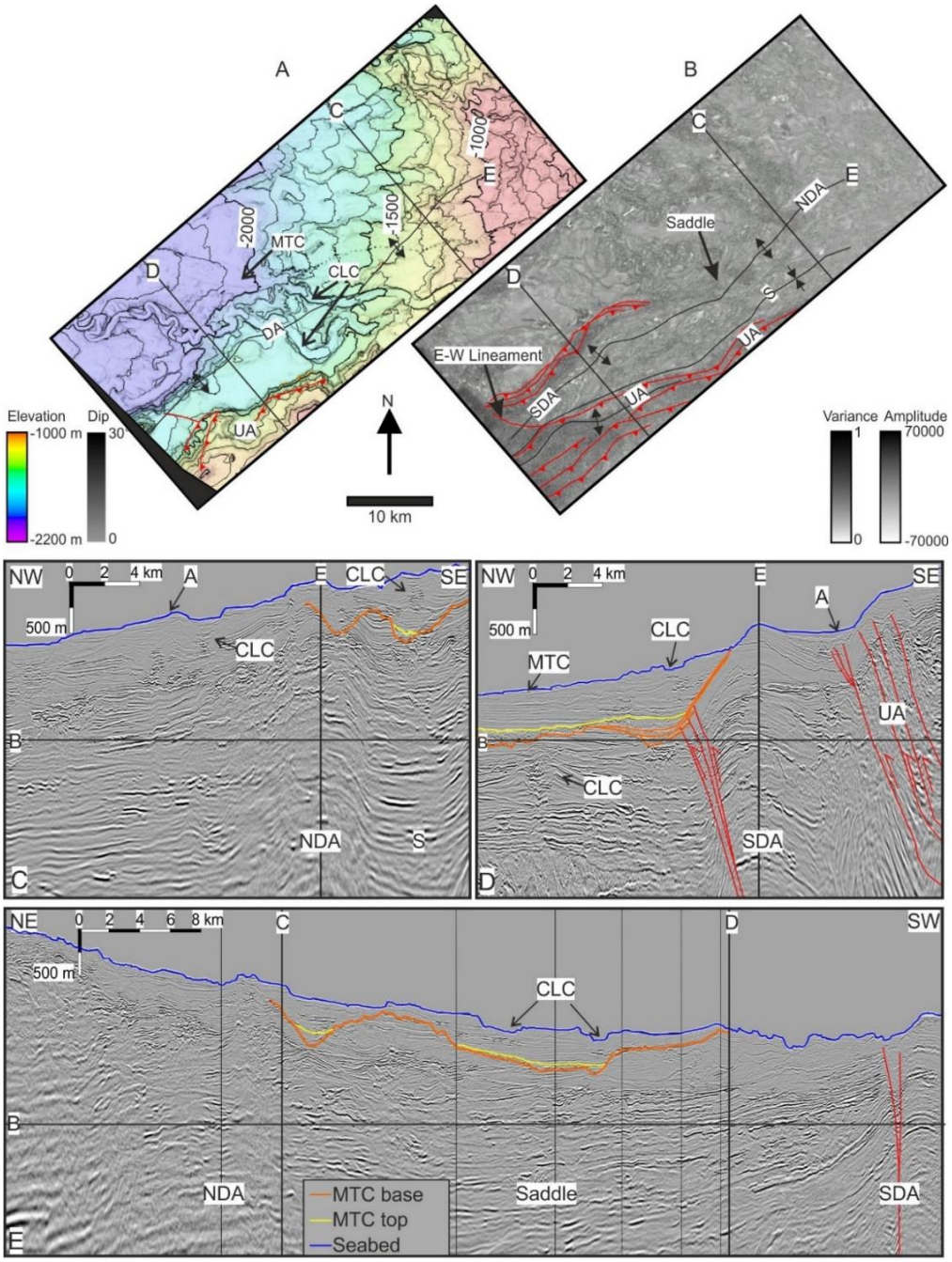

Figure 6.2. Structural elements. **A)** Seabed dip map coloured by subsurface elevation. To the SE of the study area, two thrust sheets develop, the updip anticline (UA) and the downdip anticline (DA). The northern part of the DA is not expressed on the seabed and its axis is projected from the subsurface. The rest of the study area is dominated by channel-levee complex sets (CLC). **B)** Depth slice combining variance and amplitude, see C-E for intersection. The DA is subdivided in two segments separated by a saddle, the southern downdip anticline (SDA) and the northern downdip anticline (NDA). The DA is separated from the UA by a syncline. **C)** The NDA is not faulted and is more symmetric **D)** The SDA is faulted and asymmetric. **E)** The NDA and the SDA are separated by a saddle. Several MTCs developed on these structures.

6.4 Methodology

Using the same seismic survey, Ortiz-Karpf et al. (2015) define seven seismic facies and interpret sedimentary sub-environments (i.e. channel-fill, levees, lobes and MTCs) and define seven seismic units (Chapter 7). Seismic Unit D (*sensu* Ortiz-Karpf et al., 2015) is located c. 300-500 m below the seabed, and comprises coalesced MTCs that overlie a composite basal erosion surface. In this study, Unit D is further subdivided by mapping a series of laterally extensive, intra-unit truncation surfaces. Four MTCs that underlie Unit D in the southwestern part of the dataset were also mapped. In total, nine MTCs were mapped; five within and four below Unit D. Using the seismic facies classification defined by Ortiz-Karpf et al (2015), and by mapping key, laterally continuous seismic-stratigraphic surfaces, six seismic units that underlie the MTCs were also defined. The relative chronology of the substrate units was established through their seismic-stratigraphic relationships (e.g. onlap, downlap, erosional truncation).

A separate seismic facies classification was defined for the largest MTC (Table 6.1) in order to capture its lateral variability. This approach is based on previous studies that have used lithologically-calibrated 3D seismic to characterise the internal variability of MTCs and found that the internal deformation and coherency of the deposit are accurately portrayed by the seismic images (e.g. Dykstra et al., 2011; Alves et al., 2014). Thus, seismic facies were classified based on the amplitude and lateral continuity of the reflections. Five seismic facies were defined (Table 6.1): Facies 1 is composed of discontinuous chaotic reflections interpreted as debrites (cf. Posamentier and Kolla, 2003; Gamboa et al., 2011; Olafiranye et al., 2013) and is interpreted to be composed of disaggregated material; facies 2 is composed of semi-continuous folded reflections with unclear fold vergence and is interpreted as debrites composed of partially disaggregated material; facies 3 is characterised by contractional deformation with thrusts and folds that verge down-flow and is interpreted to be composed of more coherent, less disaggregated material; facies 4 is composed of low-amplitude packages with few

internal reflectivity and is interpreted as mud-prone debrites (cf. Posamentier and Kolla, 2003); finally, facies 5 is composed of discrete packages of coherent, parallel, generally folded reflections contained in a matrix composed of facies 1-3 and is interpreted as megaclasts (cf. McGilvery et al., 2004; Bull et al., 2009; Frey-Martinez, 2010; Posamentier and Martinsen, 2011; Olafiranye et al., 2013; Jackson, 2011). In order to investigate the lateral and vertical distribution of the seismic facies, the interval defined by the top and base surfaces of the largest MTC was divided into four proportional slices using pseudo-horizons (see approach outlined by Zeng et al., 1998) and interval attribute extractions were generated. Variance and RMS amplitude were found to be the most useful attributes to define the limits between seismic facies and they were integrated observation from cross-sections and depth slices in amplitude, variance and impedance volumes to generate an MTC seismic facies map.

6.5 Seismic stratigraphy

6.5.1 Pre-MTC Stratigraphy

The MTCs in the interval of interest erosionally overlie remnants of older MTCs and channel-levee complex sets that are interpreted to have been active at different times. Most of the channel-levee complex sets are folded into the DA and UA but remain undeformed to the west of the structures. In order to assess the importance of possible variations in substrate properties, the most laterally extensive channel-levee complexes were mapped and their relative chronology was established based on seismic-stratigraphic relationships. Figure 6.3 illustrates the distribution of the main substrate units directly underlying the MTCs, with Unit I being the oldest and Unit VI the youngest.

A

Seismic Facies	Description	Interpretation
1	Discontinuous, chaotic reflections in packages that have an erosional base and irregular top (B, C). Packages are c. 50 m thick and commonly contain facies 2.	The chaotic character of facies 1 suggests that the contained material is disaggregated (cf. Dykstra, 2011) and is interpreted to represent debrites (cf. Posamentier and Kolla, 2003; Olafiranye et al., 2013).
2	Semi-continuous, variable amplitude, reflections in packages that have an erosional base and irregular top (E). Packages are c. 100 m thick and are often deformed into 200-300 m wide folds. Commonly contains facies 2.	Interpreted to represent debrites (cf. Posamentier and Kolla, 2003; Olafiranye et al., 2013) where the material is less disaggregated than in facies 1.
3	Variable amplitude, semi-continuous reflections that are folded and disrupted by imbricate thrusts (D) that bound folds that are 400-500 m wide and c. 200 m high.	Imbricate thrust and fold systems in contractionally deformed MTCs (*sensu*. Bull et al., 2009). Flow direction is generally perpendicular to the strike of the faults and folds verge in the down-flow direction (Bull et al., 2009).
4	Low-amplitude packages with few internal reflections (F, G).	Mud-prone debrites (cf. Posamentier and Kolla, 2003).
5	Discrete packages of coherent, parallel reflections set within a matrix generally composed of facies 1 or 2 (B, C). These coherent reflections occur in packages that are predominantly up to 200 m thick and cover areas of up to c.0.6 km^2. In some cases these packages are internally folded.	Megaclasts transported within the mass-flow (cf. McGilvery et al., 2004; Bull et al., 2009; Frey-Martinez, 2010; Posamentier and Martinsen, 2011; Olafiranye et al., 2013; Jackson, 2011; Alves, 2015; Ortiz-Karpf et al., 2015; *accepted*).

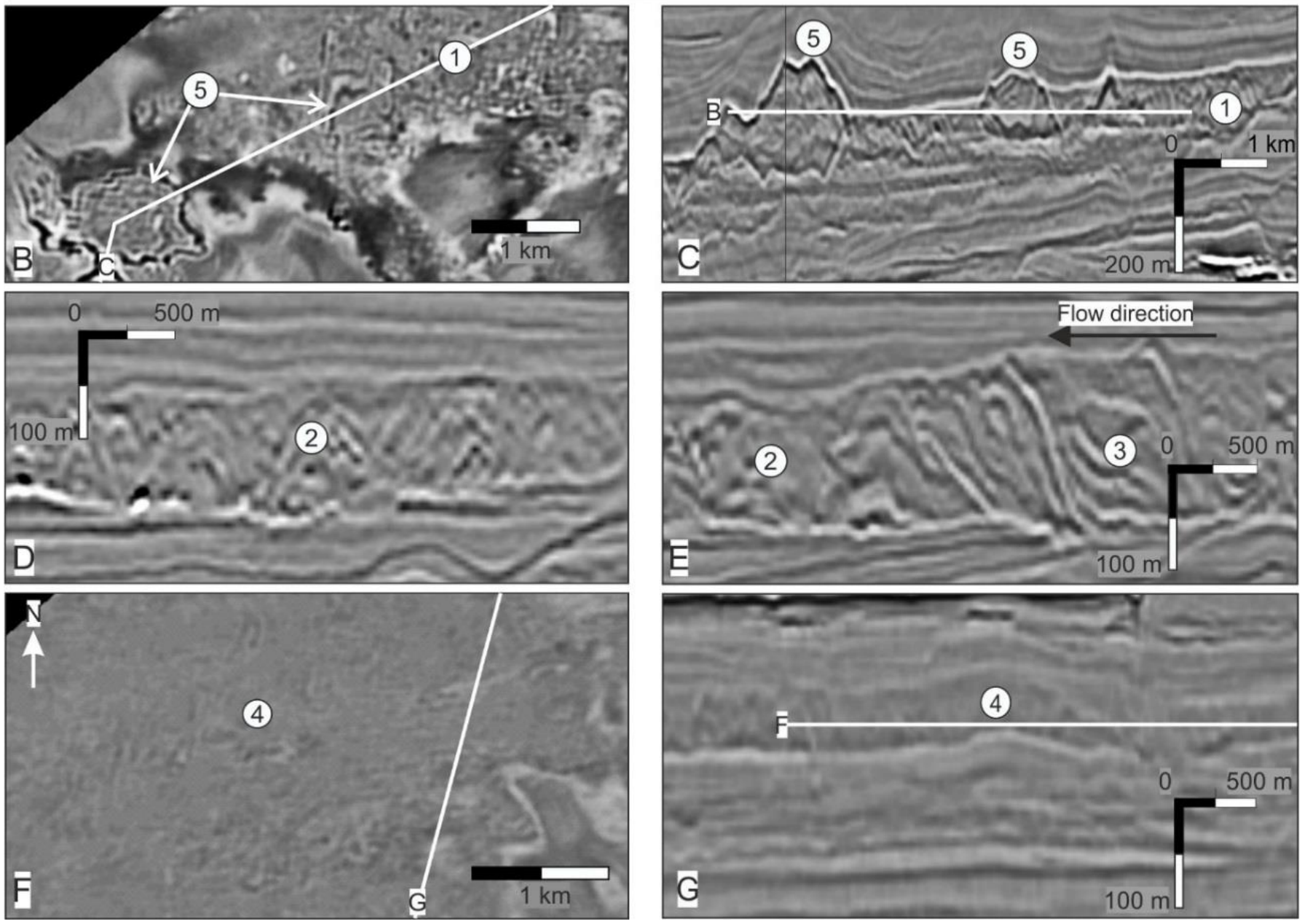

Table 6.1. MTC seismic facies classification. **A.** Description and interpretation of the seismic facies. **B.** Depth slice showing the map-view appearance of facies 5 and 1 (see C for intersection). **C.** Cross section across A showing seismic facies 1 and 5. **D.** Seismic cross section showing the appearance of facies 2. Note the semi-continuous folded reflections. **E.** Seismic cross-section showing imbricate thrust systems in facies 3. **F.** Depth slice showing the appearance of facies 4, see G for intersection. **G.** Cross-section showing facies 4. Note the low-amplitude, homogenous character.

Unit I is a SW-trending channel-levee complex set that has been incorporated into and faulted within the SDA (Fig. 6.3). The external levees are defined by low-amplitude, parallel internal reflections that downlap onto underlying strata (Fig. 6.4). The channel fill is composed of stacked packages of relatively high-amplitude discontinuous reflections (Fig. 6.4A, C and D). West of the SDA the channel-levee complex set is partially eroded by MTCs (Fig. 6.4A-C).

Unit II is a NW-trending channel-levee complex set that is folded into the DA and UA (Fig. 6.3). The basal part of the channel axis is defined by high-amplitude discontinuous reflections, with the strength of these reflections decreasing upwards; the levees are defined by very low-amplitude, parallel reflections that downlap the underlying packages (Fig. 6.4A and D). Unit II levees were partially eroded by MTCs to the north and south, whereas the channel axis is only locally eroded by MTCs (Fig. 6.3A and 6.4A).

Unit III (Unit A in Ortiz Karpf et al., 2015) is a SW-trending channel-levee complex set developed north of the main suite of MTCs (Fig. 6.3). The axis of Unit III is composed of high-amplitude discontinuous reflections towards the base and lower amplitude discontinuous reflections towards the top. (Fig. 6.4B). The external levees are predominantly composed of low-amplitude, parallel reflections (Fig. 6.4B-D). The southwestern external levee of Unit III is partially eroded by MTCs (Fig. 6.4A and B).

Unit IV is a NE-SW elongate package interpreted as a remnant of a SW-trending channel-levee complex set (Fig. 6.3A and C). It comprises variable amplitude reflections that are mostly parallel, but which are locally cut by erosional surfaces that are overlain by thin packages of low-amplitude, chaotic reflections (see lower part of Unit IV in Fig. 6.4A), and a locally preserved elongate package of high-amplitude reflections (Fig. 6.4B). The high-amplitude package is interpreted as a remnant of the axial portion of the channel-levee complex set (Fig. 6.3C), whereas the variable amplitude packages to the NW (Fig. 6.4B) are interpreted as remnants of its northern external levee. The southern levee of Unit IV is interpreted to have been mostly eroded by MTCs.

Units V is a W-trending channel-levee complex set (Fig. 6.3C) that is folded into the NDA (Fig. 6.3A and 6.4D). In the NDA, the channel axis of Unit V is preserved directly below an area of deep scouring along the base of overlying MTCs and is composed of variable amplitude discontinuous reflections (Fig. 6.4D). Its external levees are composed of low-amplitude parallel reflections (Fig. 6.4D). West of the NDA, the channel axis of unit V is completely eroded by MTCs (Figs. 6.3C and 6.4C).

Unit VI (Unit B in Ortiz-Karpf et al., 2015) is interpreted as a remnant of a W-trending channel-levee complex set (Fig. 6.3C) that follows a similar trend to that of Unit V (Fig. 6.3C and 6.4D) and is also folded into the NDA (Fig. 6.3A and 6.4D). Its channel axis was mostly eroded (Fig. 6.4D) and only a very small remnant is locally preserved in the western flank of the NDA. (Fig. 6.3C). The levees of Unit VI are characterized by continuous parallel reflections that are generally higher-amplitude than the levees in other stratigraphic units (Fig. 6.4D). In the NDA, the southern levee of Unit VI is affected by several south-dipping normal faults (Fig. 6.4D). Few of these faults affect the lower-amplitude Units V and II. In the SE of the study area, Unit I is overlain by a seismic package that is in a similar stratigraphic position to and which resembles unit VI (VI' in Figs. 6.3A and 6.4B-D); it is not possible however to establish whether they are age-equivalent.

The fact that the levees of Unit VI display higher amplitudes and are more faulted than the levees of other, lower-amplitude stratigraphic units, suggests differences in the lithological characteristics and mechanical properties of the levees. These differences probably arise from variations in the composition and texture of levees deposited by different channels, and variable degrees of compaction/lithification resulting from different burial histories. Hence, variations in the mechanical properties of levees may be reflected in their resistance to erosion and affect the morphology of the MTC basal erosion surfaces; this is further investigated below.

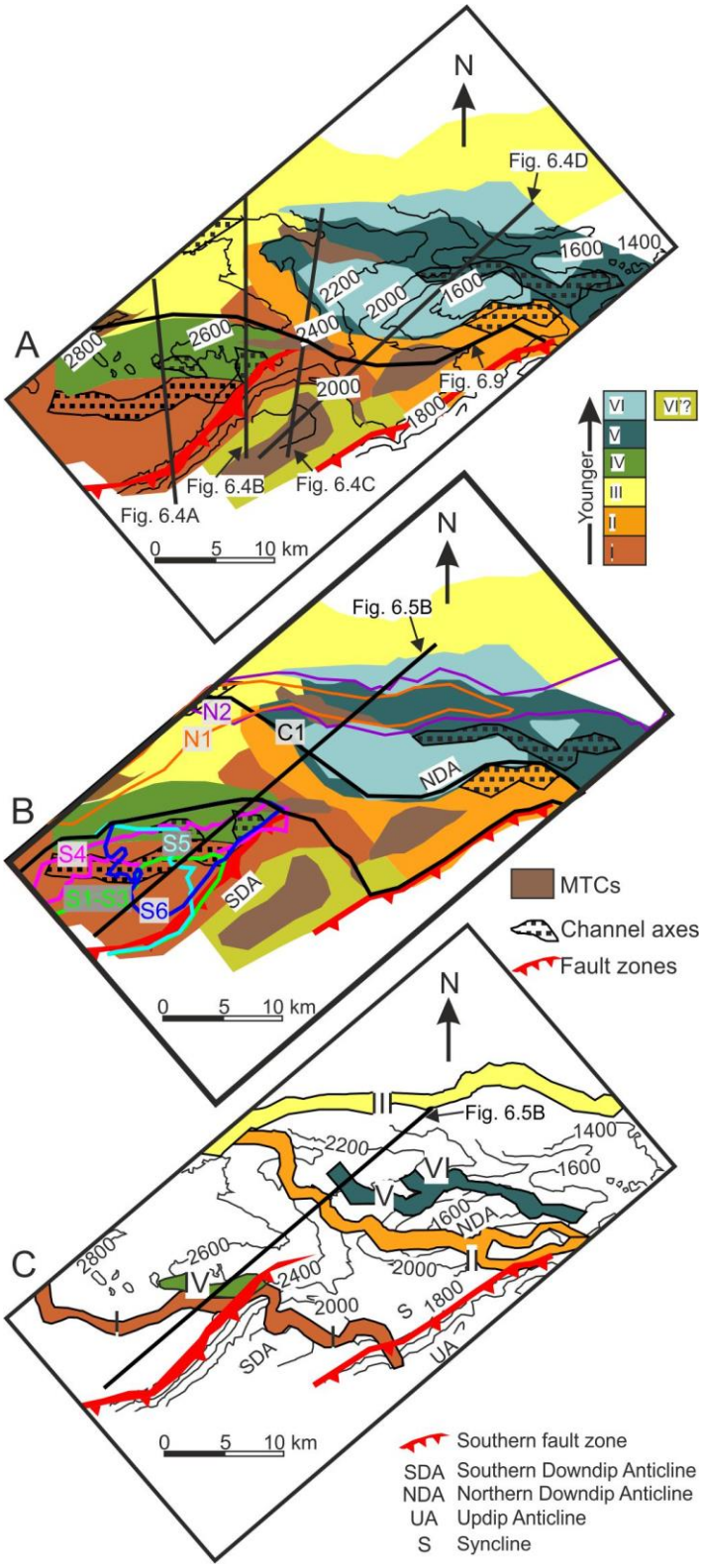

Figure 6.3. Substrate Map. **A.** Map showing the configuration of the substrate directly underlying the MTCs. Unit I is the oldest and VI the youngest. They are all composed of channel-levee complex sets. The brown polygons represent older MTCs. The black lines show the location of the cross-sections in figure 6.4 and 6.9. **B.** Substrate maps overlain with the polygons defining the outline of the MTCs. The black line indicates the location of figure 6.5. **C.** General trend of the channel axes of units I-VI. Note that the axes of units IV and VI are almost entirely eroded and the axis of Unit Vis absent outboard of the northern downdip anticline (NDA).

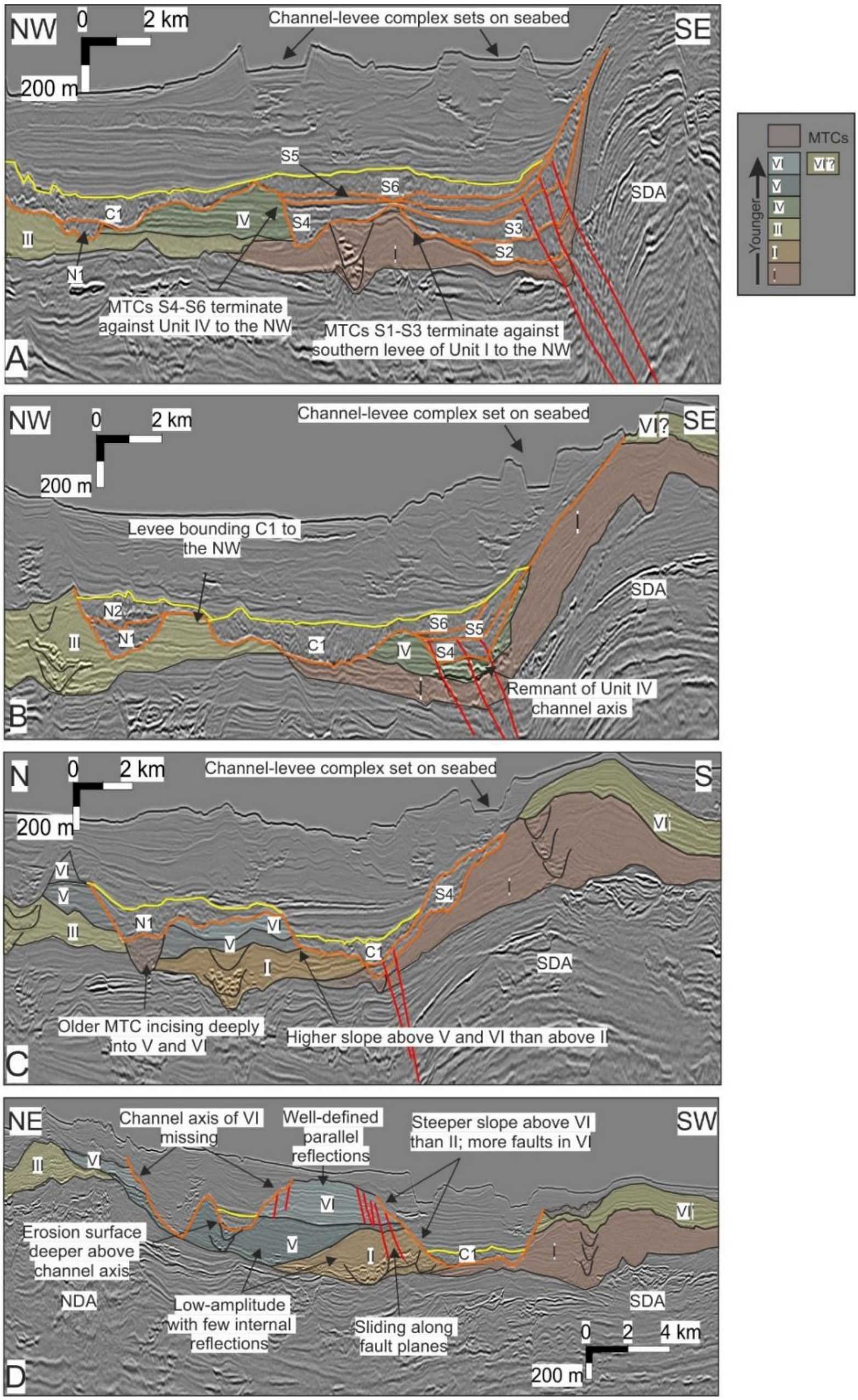

Figure 6.4. Seismic cross sections showing the morphology of the basal surfaces and the configuration of the substrate. See Figure 6.3 for location. **A.** MTC C1 is bounded to the NW by Unit III and to the SE by Unit IV. Unit IV is also eroded by MTCs S4-S6. MTCs S1-S3 onlap the levee of Unit I. **B.** Unit III separates N1 and N2 from C1. To the SE C1 overlies units I and IV. Note the high-amplitude discontinuous reflections in Unit D which are interrupted as remnants of its channel axis. **C.** N1 and N2 are bounded by units II, III, V and VI. The channel axes of units V and VI have been completely removed and there is a deeply incised MTC underlying N1. Towards the east, the basal surface of C1 is steeper across Units V and VI and flattens on Unit II. **D.** To the NE, the composite basal surface of N1 and N2 incises more deeply above the channel axis of Unit V. The axis of Unit VI was completely eroded. Unit VI is affected by faults that dip into the MTC erosion surfaces. The slope of the basal surface of C1 is steeper above Unit V than above Unit II.

6.5.2 MTCs

The nomenclature of the nine MTCs, defined by Ortiz-Karpf et al (2016) is based on their location within the study area. MTCs S1 to S6 are located towards the SW, basinwards of the SDA. MTC C1 is located towards the centre of the study area, cross-cutting the DA at the saddle developed between the southern and northern segments. MTCs N1 and N2 are located towards the NE and traverse the NDA (Fig. 6.5A). Five of the MTCs (S5, S6, C1, N1 and N2) form part of Unit D as defined by Ortiz-Karpf et al. (2015) and four underlie it (S1-S4; Fig. 6.5B).

6.5.2.1 MTCs S1-S6

S1-S6 are elongate in a NE-SW direction (Fig. 6.5A). S1-S5 extend beyond the southern limit of the seismic survey (Fig 6.5A). To the NW S1-S3 are bounded by southeastern levee of Unit I (Figs. 6.3B and 6.5B), and S4-S6 by the northwestern levee of Unit IV (Figs. 6.3B).To the SE S1-S5 and S6 are bounded by the SDA (Fig. 6.5A), while S4 is limited by the northeastern levee of Unit I (Fig. 6.5B).

Ortiz-Karpf et al., (2016) interpret S5 to have been emplaced by NNE-directed flows based on the orientation of grooves in the basal surface and on the orientation and vergence of folds contained within megaclasts. Based on the orientation of the lateral margins of S1-S3, on the NE-SW alignment of megaclasts and on the northern onlap against the southeastern levee of Unit I, Ortiz-Karpf et al., (2016*)* also inferred S1-S3 to have been emplaced by NNE-directed flows. Contrary to MTCs S1-S3 and S5, S6 is interpreted to have been sourced from the NE and emplaced by a SW-directed flow because it widens to the SW and terminates against protrusions along the top of S5 (Ortiz-Karpf et al., 2016; Fig. 6.5B). Provenance of S4 is uncertain because it continues beyond the southern limit of the dataset and its northeastern portion was eroded by S6 and C1 (Ortiz-Karpf et al., 2016*;* Fig. 6.3B).

The southern levee of Unit I, which is onlapped by S1-S3 (Fig. 6.5B) is orientated WSW, which is highly oblique to the interpreted NNE flow direction of S1-S3 (Fig. 6.3A and B). Unit I is hence interpreted to have constituted a barrier that restricted their down-flow extent. S4 overlies the channel axis of Unit I and follows its overall trend (Ortiz-Karpf et al., 2016*;* Figs. 6.3B and C and 6.5B); it is therefore is interpreted to have exploited the underlying channel. It is possible that S6 was confined between the SDA and Unit IV (Fig. 6.3B), but erosion of Unit IV makes it difficult to infer its original depositional geometry.

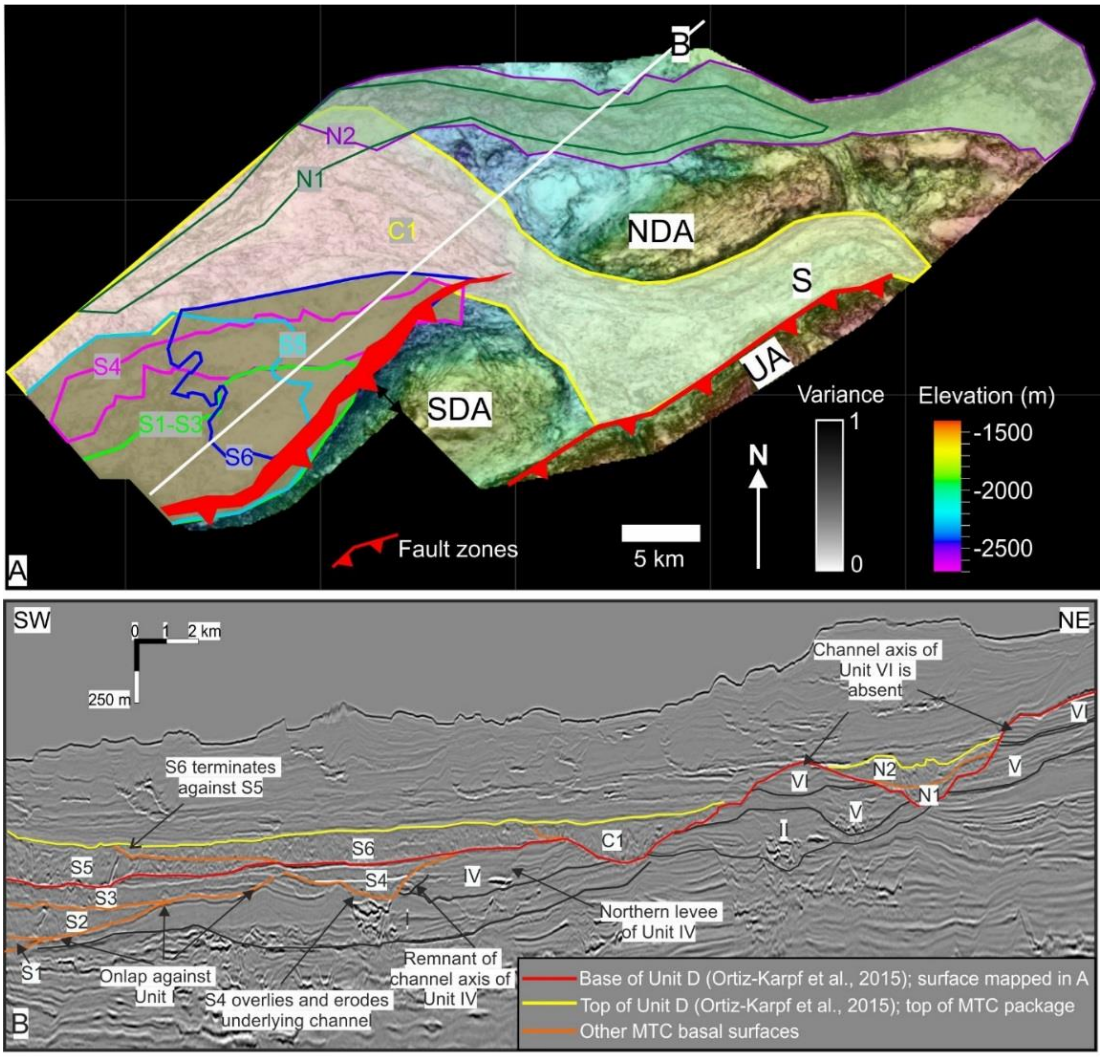

Figure 6.5 MTCs in the study area. **A.** Variance extraction coloured by subsurface elevation at the composite surface defined as Unit D by Ortiz-Karpf et al. (2015) showing the areal extent of the different MTCs that were mapped. The coloured polygons represent the outline of the MTCs. **B.** Seismic section across the MTCs showing their temporal and spatial relationship. MTCs S1-S3 onlap the southern levee of Unit I, while S4 overlies Unit I , mostly concentrated to the NW odf its northern levee. Unit IV also constitutes the northwestern limit of S5 and S6 and the southeastern limit of C1.

6.5.2.1 MTC C1

MTC C1 is the most laterally extensive MTC, extending beyond the eastern and western limits of the dataset (Fig 6.6). Based on the presence of arcuate scarps updip of the dataset, Ortiz-Karpf et al. (2016) interpret that C1 was sourced from at-or-close to the shelf-break. C1 trends along the syncline between the UA and DA and across the DA into the basin low (Fig. 6.6A). The basal surface is erosional and covers an area of c. 400 km^2 within the study area. The top surface is characterised by irregular protrusions (Fig. 6.6B) and the deposit covers an area of c. 300 km^2 within the dataset. C1 was emplaced above a bathymetrically complex seabed and eroded several stratigraphic units (Fig. 6.3B); this enables the investigation of the relationship between the geometry of the basal surface and the distribution of the seismic facies, with the form and composition of the underlying substrate. The morphology of the basal surface, its geographic relationship with the substrate units and the distribution of the seismic facies are hence described below, starting from the updip, eastern limit of the dataset and progressing towards the downdip, western limit (Fig. 6.7).

In the syncline, the basal erosion surface is c. 6 km wide and up to c. 600 m deep (Fig. 6.7C), The overlying MTC is, however, c. 100-200 m thick (Fig. 6.7B), indicating that the erosional relief in this area is severely underfilled (cf. ‘evacuated morphology’ of Eggenhuisen et al., 2010). The eastern margin of C1 is defined by the frontal flank of the UA, whereas the western margin is defined by the back limb of the NDA, which is largely composed of the southern levees of units II, V and VI (Figs. 6.3B and 6.7C). Along the syncline, C1 locally overlies the channel axis of Unit II (Figs. 6.3B and 6.7C). The lateral margins of C1 are stepped, being characterized by relatively steep slopes (c. 24°) and arcuate scarps (Figs. 6.6A and 6.7A-C). In general, the basal surface is steeper across Units V and VI and flattens above Unit II (Fig. 6.7C and D). In the back limb of the NDA, there is a NW-trending, narrow erosional trough that potentially links the basal surface of C1 with that of N1 and N2 (Figs. 6.6A, C and D). It incises through the external levees

of Unit VI and partially erodes Unit V. The channel axis of Unit VI is not present and was presumably eroded (Fig. 6.6D). The erosion surface across this trough is overlain by a thin, c. 50 m package of debrites (Fig. 6.6D).

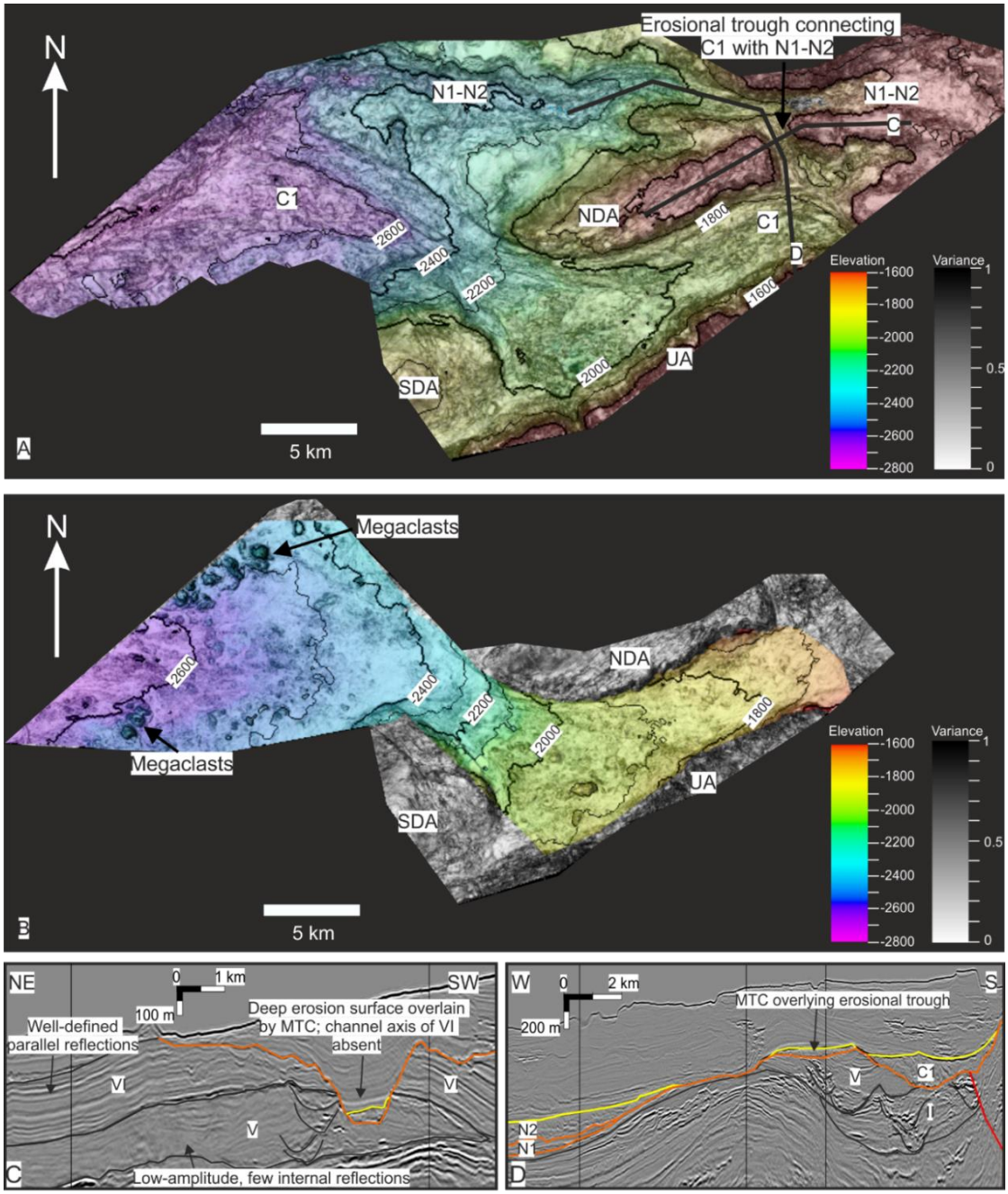

Figure 6.6. Bounding surfaces of C1. **A.** Variance extraction coloured by subsurface elevation showing the basal surface of C1 and the composite basal surface of N1 and N2. Note the trajectory of C1 and its relationship to the anticlines (SDA and NDA) and the erosional trough that connects the erosional fairway of C1 with that of N1 and N2. **B.** Variance extraction coloured by subsurface elevation at the top of MTC C1. The irregularities are related to underlying megaclasts. **C.** Cross-section across the erosional cut across the NDA connecting C1 to N1 and N2. The location of the cut possibly coincides with the location of the eroded channel axis of Unit VI. **D.** Section along the erosional cut between C1 and N1 and N2 showing an MTC remnant overlying the erosion surface.

In the syncline the deposit is thickest towards the eastern limit of the dataset (c. 200 m) where imbricate thrust and fold systems (facies 3) develop (Fig. 6.8). Thrust planes dip to the NNE (Fig. 6.8), suggesting emplacement by an overall WSW-trending flow. To the SW, the thrust and fold system transitions to facies 2, which is characterised by folding but no systematic faulting and has an average thickness of 100 m (Fig. 6.8). Updip of the saddle between the southern and NDA, a W-trending basal erosion surface incises through the entire thickness of facies 2. It is filled with low-amplitude debrites (Facies 4; Fig. 6.8), and is interpreted to be younger. The northwestern margin of the syncline and part of the southeastern margin contain chaotic debrites (Facies 1; Fig. 6.8).

C1 traverses the DA at the saddle between the southern and northern segments (Figs. 6.6A and 6.7A). Across the DA, the basal surface progressively narrows to c. 5 km (Fig. 6.7A, D and E) and the axial slope steepens from c. 2° to 6°. Here, the southern lateral scarp of C1 is composed of units I and the northern scarp by units II, V and VI (Fig. 6.7D-G). The northern lateral scarp tend to be steeper across Unit VI, which is affected by more normal faults, than across Unit II, which contains fewer faults and is less reflective (Figs. 6.4D and 6.7D). Across the anticline the thickness of the deposit decreases abruptly to <50 m (Fig. 6.8A), and comprises megaclasts (facies 5) contained in a thin (<50 m) chaotic matrix (Facies 1; Fig. 6.8). Most megaclasts are roughly aligned parallel to the lateral margins (Fig. 6.8).

Basinwards of the DA, the slopes of the lateral walls and the erosional relief of the basal surface decrease progressively (Figs. 6.7D-G). The basal surface also widens, reaching c. 10 km towards the western limit of the dataset where it is completely filled by MTC material (Fig. 6.7G). The southern margin of C1 is composed of units I and IV. The northern margin is composed by units II, V and VI directly basinwards of the anticlines, where it also tends to be steeper across units V and VI, than across Unit II (Figs. 6.7E and F); further downdip it is bounded to the NW by Unit III.

Immediately basinward of the DA, the deposit thickens progressively to >150 m (Fig. 6.8A) and is composed of imbricate thrust and fold systems (Facies 3; Figs. 6.8 and 6.9). The thrusts dip ESE and become more closely-spaced and steeper basinward (Fig. 6.9), supporting a WNW emplacement direction. The thrust and fold system terminates against a landward-dipping ramp developed at the basal erosion surface where the deposit thins from c. 150 m to c. 100 m. Downdip of this position, C1 is composed of semi-continuous, folded reflections with no systematic faulting (Facies 2; Figs. 6.8 and 6.9). Towards its lateral margins, the deposit thins to <50 m (Fig. 6.8A) and is mainly composed of debrites (facies 1) and megaclasts (facies 5; Figs. 6.8 and 6.10B).

The megaclasts in C1 are up to c. 0.6 km^2 and occur in facies 1-3 (Fig. 6.8). Internally, most megaclasts are characterized by low-amplitude, folded reflections (e.g. Fig. 6.10). In some cases, the internal reflections are contorted or chaotic and, in a few cases, they either reflection-free or contain plane-parallel reflections (Fig. 6.10B). Megaclasts are more abundant on the DA where they are aligned parallel to the lateral margins of C1 (Figs. 6.8 and 6.10A), and in the basin low to the west of the anticlines, where they tend to concentrate towards the southern and northwestern margins (Fig. 6.8). Some of the largest (c. 0.3 km^2), and more deformed megaclasts occur in the downdip area in the northwestern margin, where they overlie the southern external channel-levee of Unit III (Fig. 6.10B). At the opposite margin, c. 0.4 km^2 megaclasts are clustered above areas of increased incision of the basal erosional surface above Unit IV (Figs. 6.10B).

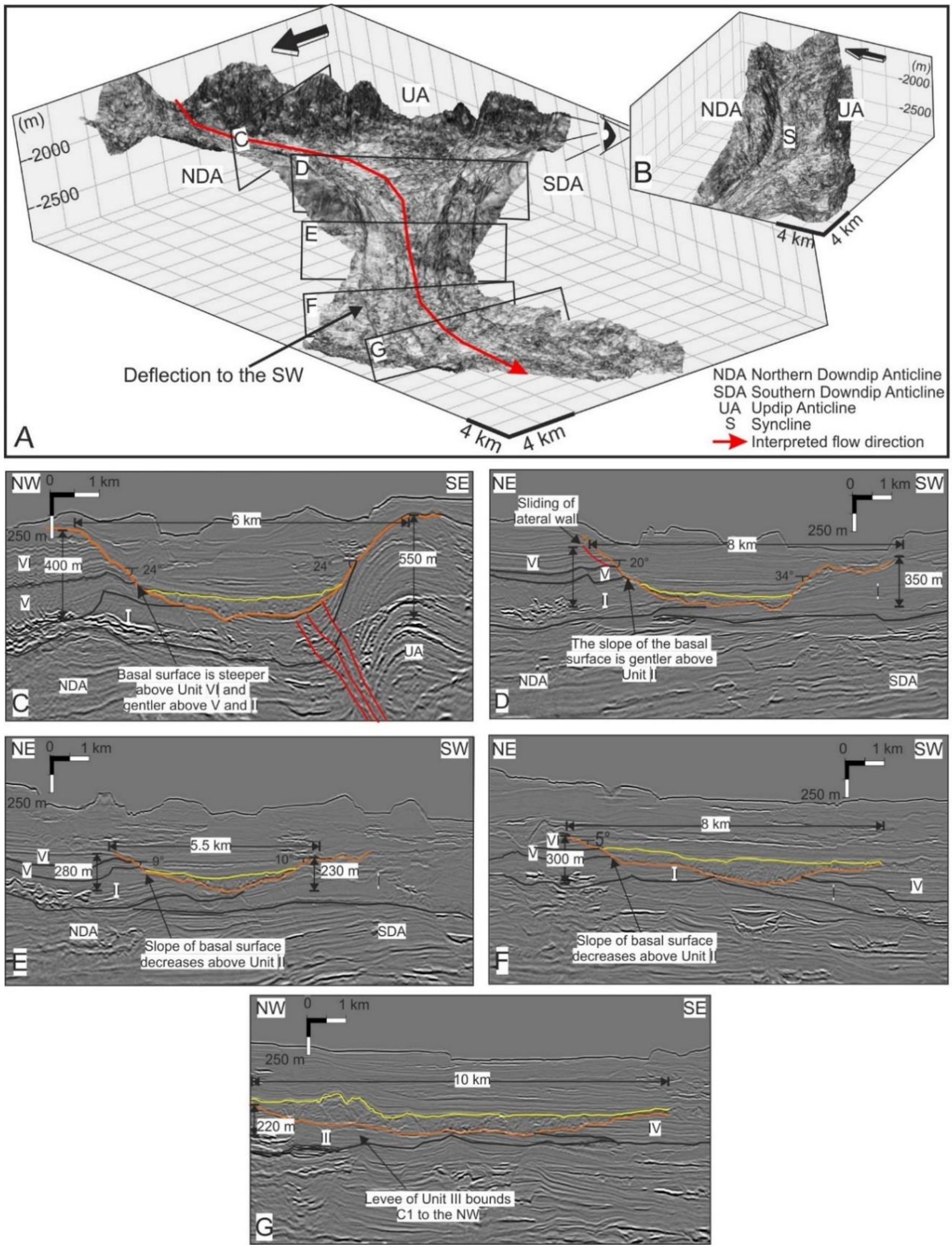

Figure 6.7. Downdip changes in the morphology of C1. **A.** Perspective view of the basal surface of C1 showing the location of the sections shown in C-G. **B.** View between the northern downdip anticline (NDA) and the updip anticline (UA) showing that C1 followed the orientation of the syncline (S). **C-G.** Seismic cross sections showing that the height and slope of the lateral walls of C1 decreases downdip and highlighting changes in the slope of the lateral margins which are sometimes related to changes in the substrate units.

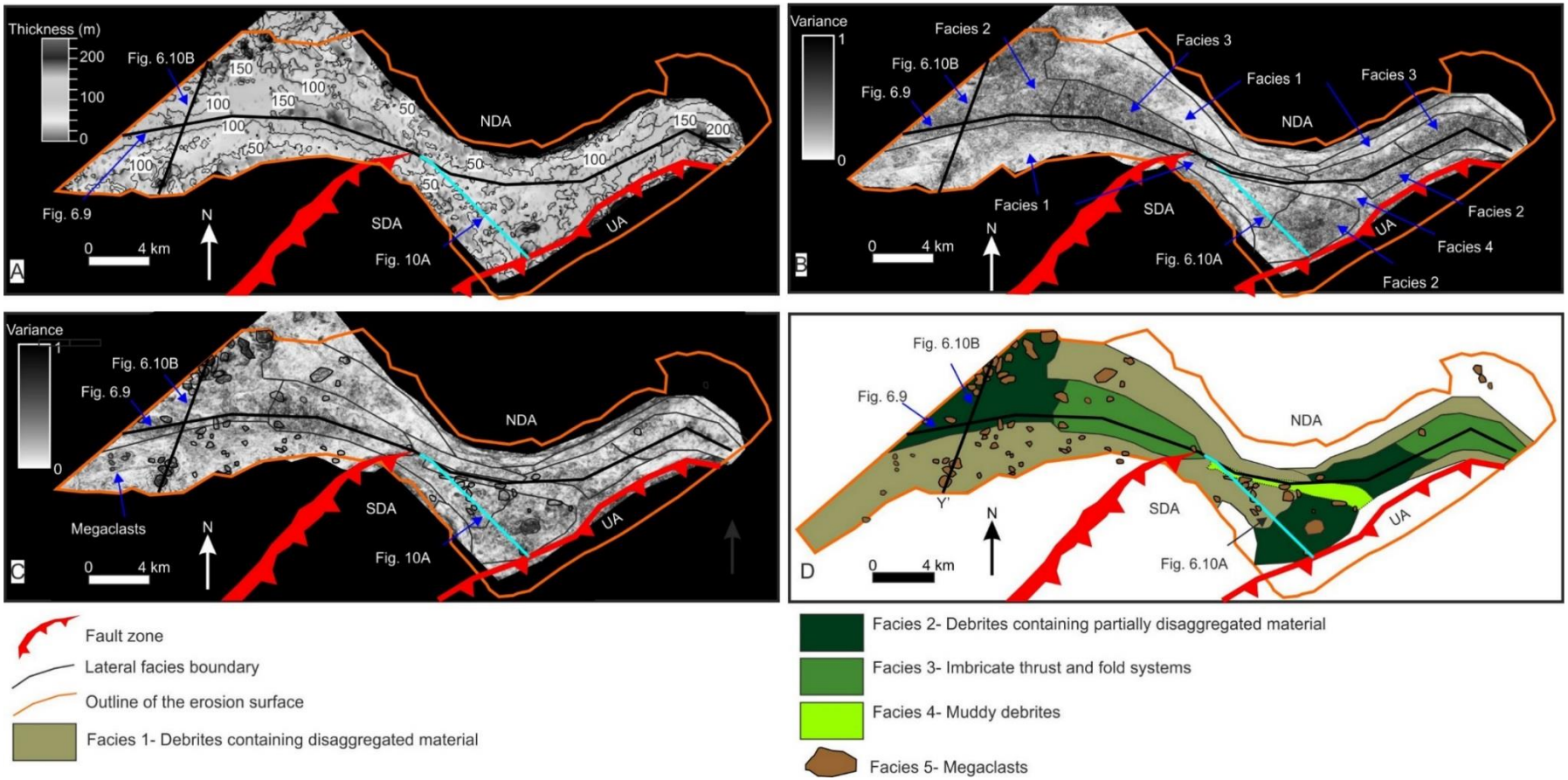

Figure 6.8. Thickness, variance and facies maps of C1. **A.** Vertical thickness map of C1. **B.** Variance extraction at the interval between 50-75% of the vertical thickness of C1 form base to top. Note the character of the seismic facies, with facies 1 having the lowest variance, facies 3 having the highest variance and facies 2 having an intermediate variance. **C.** Variance extraction of the top-quarter of C1 showing the appearance of the megaclasts. **D.** Seismic facies map of C1.

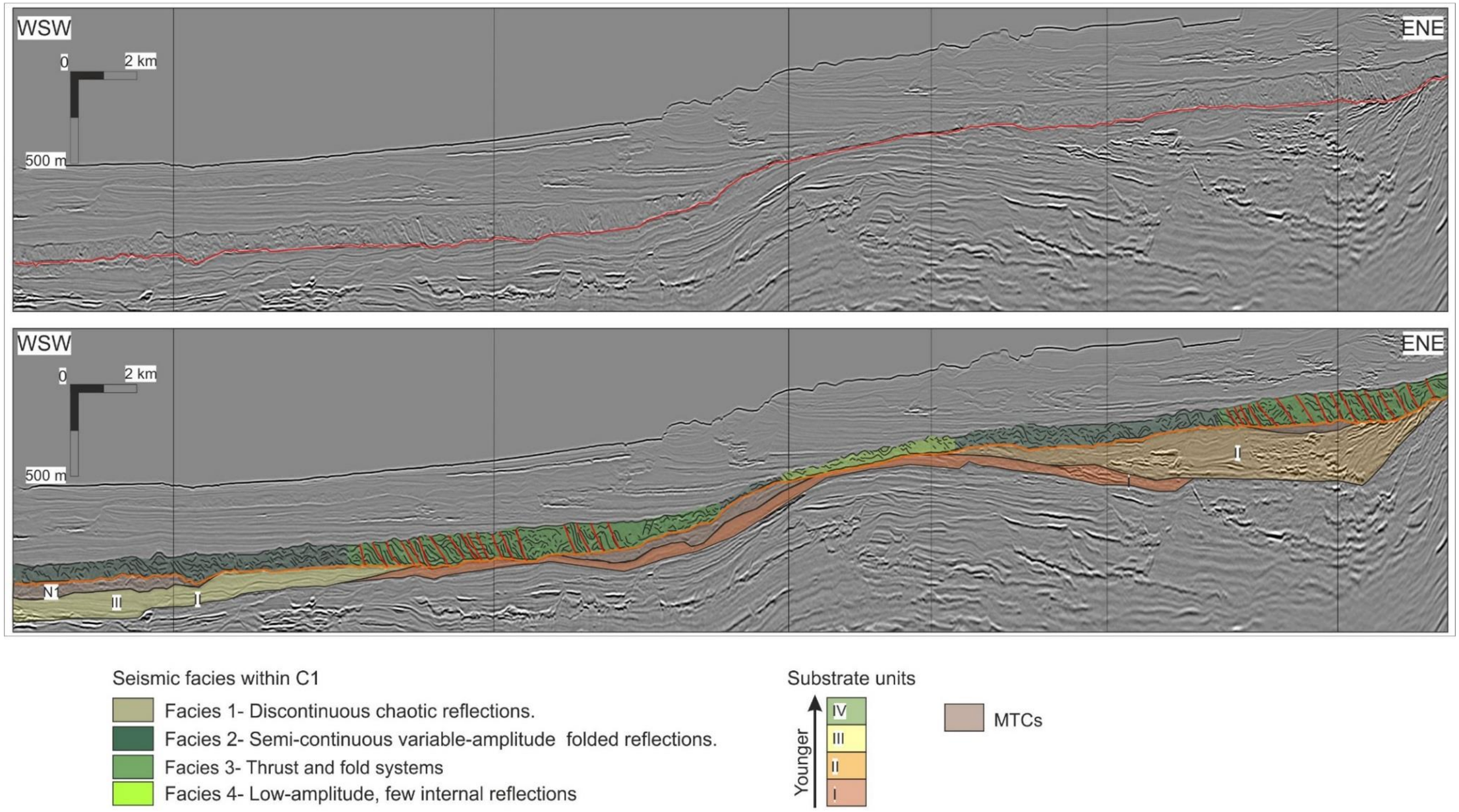

Figure 6.9. Uninterpreted and interpreted sections along the centre of MTC C1 showing the down-dip distribution of the seismic facies. See figures 6.3 and 6.8 for location.

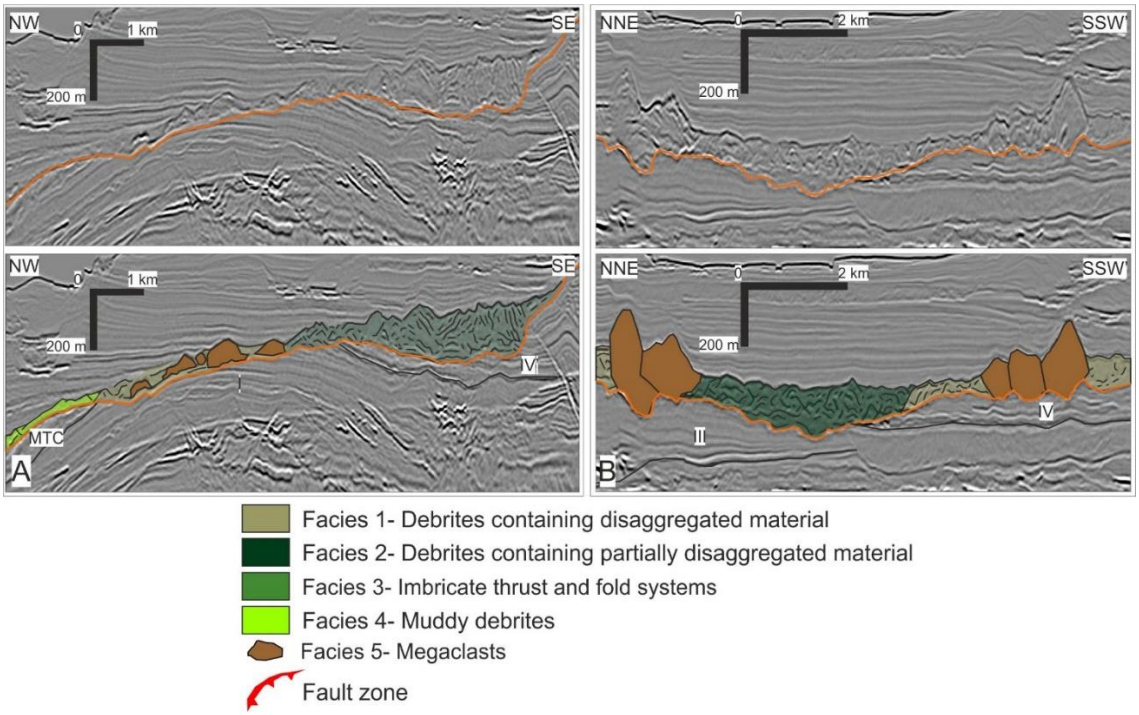

Figure 6.10. Seismic cross-sections showing the examples of the seismic facies in C1. **A.** Uninterpreted and interpreted sections across the downdip anticline. Note the change in thickness and megaclast abundance above the crest of the anticline. **B.** Uninterpreted and interpreted sections across C1 towards the down-dip limit of the dataset. Note the erosion at the base and the presence of large megaclasts.

A series of lineaments are developed along the basal surface of MTC C1. They are particularly well imaged in variance extractions (Fig. 6.11), where they are orientated sub-parallel to the lateral margins of the basal surface (Ortiz-Karpf et al., 2015; Fig 6.11A). In cross-section the lineaments appear as v-shaped erosional scours that have a similar appearance irrespective of the underlying substrate unit (Fig. 6.11B). They are interpreted as ‘grooves’ (*sensu* Bull et al., 2009) formed by megaclasts transported at the base of the flow (cf. Posamentier and Kolla, 2003; Bull et al., 2009). The orientation and downslope divergence of the grooves, together with the overall morphology of the basal surface and the vergence of the faults in the imbricate thrust and fold systems, are used to infer the MTC flow direction, which, in this case, is interpreted as being: (i) NW-directed towards the eastern limit of the dataset; (ii) south-westward in the syncline; (iii) NW-directed across and directly basinward of the DA, and (iv) SW-directed towards the western limit of the dataset (Fig. 6.11A).

The change in overall flow direction from NW to SW in the syncline was driven by the presence of the NDA, which forced the flow to follow the trend of the synclinal hinge. The MTC traversed the DA at the saddle between the southern and northern segments, indicating that the location of erosional surface across the anticline was also likely controlled by the structural configuration. Basinwards of the DA, C1 trends broadly parallel to the channel-levee complex sets in the underlying units, which constitute its northern and southern margins (Fig. 6.3B). Unit III is an exception because it trends SW and is oblique to the orientation of C1 (Fig. 6.3B). Therefore, although erosion of Unit IV obscures its original depositional geometry, it seems likely that C1 was emplaced along the bathymetric low between the northern levee of Unit IV and the southern levee of units V. Further downdip, the change in the flow direction of C1 from NW to SW is interpreted to have been driven by the southern levee of Unit III, which was orientated oblique (Fig. 6.3), and is thus interpreted to have deflected flow south-westwards (Figs. 6.6A, and 6.7A).

6.5.2.1 MTCs N1 and N2

MTCs N1 and N2 overlie a composite SW-trending erosion surface that overlies units V and VI above the NDA and Unit III towards the western limit of the seismic survey (Fig. 6.3A). Based on the morphology of the basal surface, which is parallel to the underlying channel-levee complex sets (Fig. 6.3C), N1 and N2 are interpreted to have been emplaced by SW-directed flows. Because the composite erosion surface is located downdip of scarps on the present shelf-break, N1 and N2 are interpreted to have been sourced from the shelf. In the western limb of the DA, the composite basal erosion surface of N1 and N2 incised more deeply into the channel axis of Unit V than the flanking levees; the channel axis of Unit VI was eroded completely (Fig. 6.4D). Basinwards of the NDA, the channel axes of both units are absent (Fig. 6.3 and 6.4C) and N1 overlies a debrite with a deep erosional base (Fig. 6.4C). The position of the underlying debrite is

interpreted to roughly mark the position of the eroded channel axes of units V and VI (Fig. 6.4C).

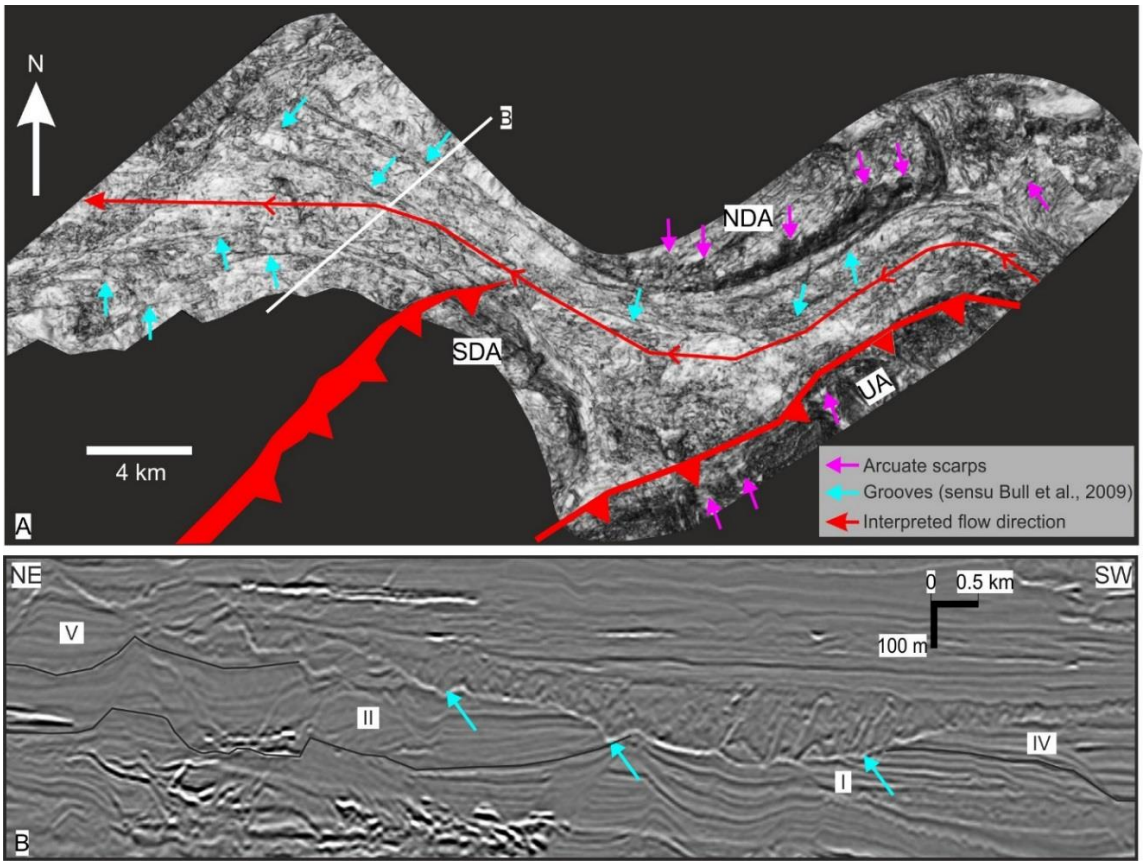

Figure 6.11. Grooves at the base of C1. **A.** Variance extraction at the base of C1 showing the presence of lineaments parallel to the lateral scarps which are interpreted as grooves. Also note the presence of lateral scarps in the margins, which are interpreted as areas of local collapse. **B.** Seismic cross-section across the grooves showing their v-shaped morphology.

6.6 Discussion

6.6.1 Substrate and Bathymetric Controls on Flow Pathways and Deposit Geometry

6.6.1.1 Substrate Controls

Deeper incision above channel axes in comparison to the surrounding levees is observed suggesting that channel-fill deposits were preferentially eroded during the emplacement of the MTCs. This is supported by the following observations: i) in the western flank of the NDA, deeper erosion under the composite basal surface of N1 and N2 is observed above the channel axis of Unit V (Fig. 6.4D); ii) west of the NDA, the channel axes of

units V and VI have been completely eroded by N1 and N2 while the levees have been preserved (Figs. 6.3B and 6.4C); and iii) the erosional trough that connects the basal erosion surface of C1 to the composite erosion surface of N1 and N2 occurs between the levees of unit V and VI and the channel axis is absent (Figs. 6.6A, C and D). Preferential erosion of the channel axis across this erosional trough suggests that lithological variations between channels and levees played an important role in determining the location of the trough and the flow pathway of C1. Deeper erosion above channel axes with respect to the adjacent levees may be explained by their different lithological characteristics. Channel-fill deposits are generally composed of coarser grained to heterolithic material (e.g. Mayall et al., 2006; Babonneau et al., 2010; Hodgson et al., 2011; Hubbard et al., 2014; Jobe et al. 2015), while levees generally contain fine-grained particles with a higher clay content (e.g. Babonneau et al., 2010; Kane and Hodgson, 2011; Morris et al., 2014; Hansen et al., 2015). The electro-chemical forces between clay particles, which lead to rapid consolidation and the development of shear strength upon sedimentation, can result in a higher resistance to erosion (Mehta et al., 1989). Another potentially important factor is the higher tendency of sandy sediments to suffer liquefaction, with respect to mud-prone sediments. Liquefaction results from pore-pressure build up within the boundary layer as it is loaded by the overriding flow (e.g. Butler and Tavarnelli, 2006; Iverson, 2012); the higher pore-fluid volume in the coarser grained sediments that typically occupy the channel-axes makes them more susceptible to liquefaction and entrainment. Differences between the composition and texture of channel axes and levee deposits may therefore be reflected in their resistance to erosion, with channel-fill sediments being more easily eroded and entrained than levees (e.g. Joanne et al., 2013). The characteristics of the substrate can therefore influence the local morphology of the basal surface, control the flow-pathways by pre-determining areas that may be more easily eroded and breached, and ultimately influence the compositional, textural and rheological flow evolution and depositional character of a mass-flow. For instance, part of flows that are focused above channel axes may cause

deeper incision and become sandier and less cohesive downslope. Comparatively, the depth of incision of parts of mass-flows passing over levees may be less and the flows may tend to become muddier and more cohesive downdip. Also, preferential erosion of the channel-fill deposits with respect to the levees suggests that buried channel axes may also be more readily eroded once they are exhumed by the overriding mass-flow.

There are more subtle changes in the morphology of the basal erosion surfaces that coincide with changes in the seismic expression and style of deformation, and thus potentially composition of underlying levee units. For example, the basal erosion surface of C1 tends to be steeper across the external levees of Unit VI and flatter above the levees of Unit II (Figs. 6.4D, 6.7C and D). This coincides with variations in the seismic character and deformation of the substrate units, with Unit VI displaying higher amplitudes than Unit II, and Unit VI containing more faults than Unit II. This suggests that despite being primarily composed by levees, there are heterogeneities in the substrate that potentially arise from variations in the mechanical properties of the levees associated with different channels, and that this variability is reflected in the morphology of the MTC basal surface.

6.6.1.2 Bathymetric Controls

The most prominent bathymetric features in the study area are the thrust anticlines, which were a primary control on the dispersal and ultimate distribution of the MTCs. This is demonstrated by the change in the interpreted flow direction of C1 NW to SW to follow the orientation of the syncline, and the fact that it traversed the DA at the saddle. Basinward of the DA, the depositional relief of the channel-levee complex sets constituted the main bathymetric perturbations. By comparison with similar channel-levee complex sets on the present seabed these buried systems could have been 100-200 m high at the external levee crests (e.g. Fig. 6.4A-C). The orientation of the channel-levee complex sets with respect to the emplacement direction of the mass-flows determined the effect that the underlying channel-levee complex sets had on the MTC

flow pathways and depositional geometries. The flow direction of MTCs N1 and N2 was sub-parallel to the orientation of the underlying channel-levee complex sets in units V and VI (Fig. 6.3B and C) and N1 and N2 are therefore interpreted to have exploited the underlying channel conduits. To the west of the DA, MTC C1 was also parallel to the underlying channel-levee complex sets and is interpreted to have been focused in the inter-channel low formed between units IV and V. Further downdip, MTC C1 was deflected to the SW by the southern levee of Unit III, which was orientated oblique to the propagation direction of C1 (Fig. 6.3B). The propagation direction of MTCs S1-S5, which is interpreted as NNE, was highly oblique to the underlying channel-levee complex set in Unit I which trends WSW (Fig. 6.3B) which, due to its depositional relief, constituted a barrier that limited its down-flow extent (Fig. 6.5B). Based on these observations four generic types of interaction between mass-flows and underlying channel-levee complex sets can be depicted and are illustrated in Figure 13. These are end-members and intermediate scenarios may occur during MTC emplacement.

6.6.1.2.1 Type 1: MTCs Overlie and Exploit Underlying Channel Conduits

This occurs when the mass-flow is parallel to the underlying channel-levee complexes and is confined within its levees (Fig. 6.12). Due to erosion of channel axis deposits, the mass-flow is likely to become entrenched, preferentially entraining the channel-fill deposits and increasing the sand content of the mass-flow. The depth of erosion above the levees is likely to be lower than above the channel axis.

6.6.1.2.2 Type 2: MTCs Confined in Inter-Channel Lows

Mass-flows focused along inter-channel lows may be entirely confined if the external levees are high relative to the thickness of the mass-flow, eroding only the levees and preserving the adjacent channel axes (Fig. 6.12). The morphology of the basal surface is likely to be influenced by variations in the properties of the underlying levees.

6.6.1.2.3 Type 3: MTCs Deflected by Levees

The presence of channel-levee complex sets orientated obliquely to the transport direction can cause the mass-flow to be diverted away from the external levee, introducing a change in the overall flow direction (Fig. 6.12). If the height of a deflecting levee is greater than the thickness of the flow and associated flow runup, the channel axis is likely to be preserved. If the mass-flow is able to erode and override the levee, it may become focused above the adjacent channel axis in a Type 1 interaction.

6.6.1.2.4 Type 4: MTCs Blocked by Levees

When the underlying channel-levee complex sets are perpendicular or highly oblique to the flow direction and the height of the external levee exceeds the flow thickness, the levee can act as a barrier that blocks the mass-flow and hinders further basinward transport and the erosion of the channel axis (Fig. 6.12).

The type of interaction between mass-flows and the underlying channel-levee complex sets determines the volume and type of substrate entrained thereby affecting the properties and dynamic evolution of the flow. Channel axes orientated parallel or subparallel to the emplacement direction of mass-flows are more likely to be eroded than those perpendicular or highly oblique because the latter are shielded by their levees (types 3 and 4; Fig. 6.12). The type of interaction can also determine the runout distance of mass-flows. Understanding these different scenarios has an important application for predicting the presence and continuity of underlying hydrocarbon reservoirs.

6.6.2 Substrate and Bathymetric Controls on the Distribution of the Seismic Facies of C1

The seismic facies distribution within C1 is interpreted to reflect the heterogeneity of the deposit, and the different facies are interpreted to represent the degree of stratal disaggregation and internal deformation incurred during transport and emplacement.

Here the possible effects of bathymetry on the flow-processes and resulting deposit are discussed.

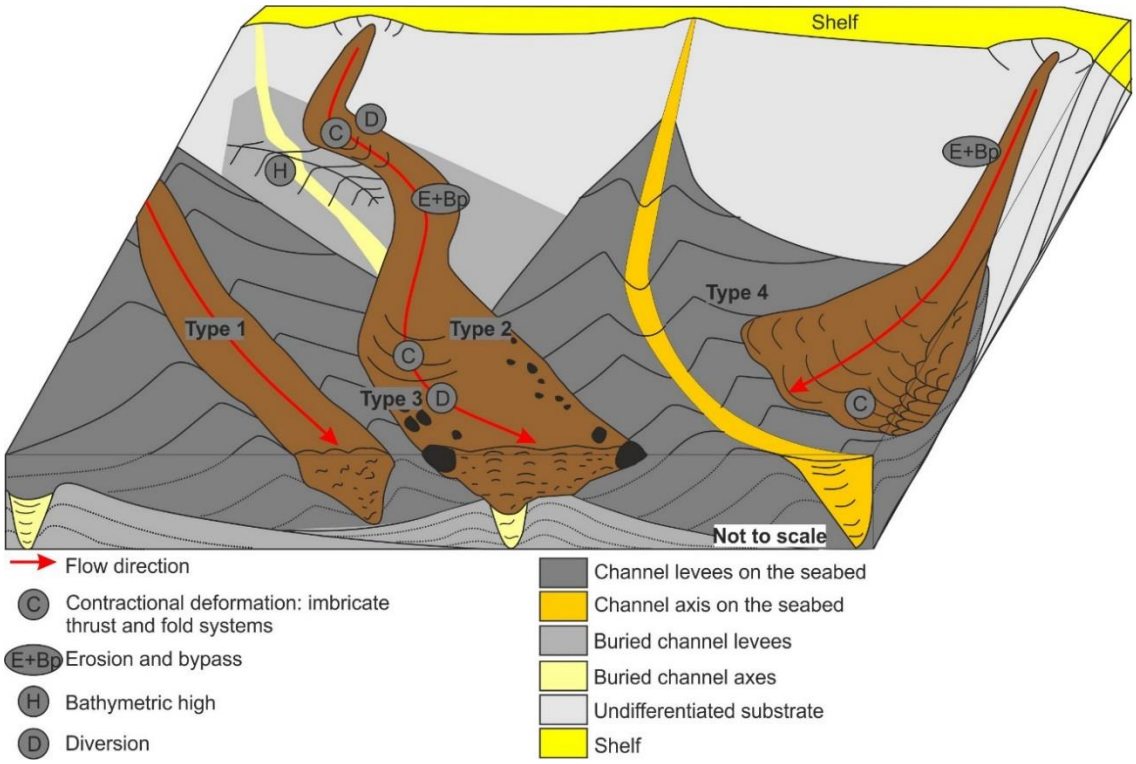

Figure 6.12. Types of interactions between MTCs and channel-levee complex sets. Simplified cartoon representation of the main bathymetric and substrate controls on MTCs. From left to right: Type 1: An MTC exploiting an underlying channel-levee complex set has incised deeply above the channel axis and widens the erosion surface by eroding the external levees less deeply. Towards the middle: Updip the MTC is diverted by a bathymetric high (H) on the seabed. Further downdip it is focused along an inter-channel low (Type 2). Farther downdip it is deflected by the channel-levee complex to the north (Type 3). Contractional seismic facies develop updip of the bathymetric highs. Erosion and by-pass dominate areas of steeper axial gradient. To the right, an MTC is blocked by a highly oblique channel-levee complex set (Type 4). Contractional seismic facies develop as the MTC is buttressed against the levee.

6.6.2.1 Distribution and Nature of the Megaclasts (facies 5)

The basal grooves at the base of C1 suggest that some megaclasts were transported for several kilometres (Fig. 6.13). Megaclasts could have been derived from the original (shelf margin) failure, entrained through erosion of the DA, or sourced from local collapse of the lateral margins. The large megaclasts that are clustered in erosional scours towards the margins (Fig. 6.13) could have been derived from local erosion and entrainment. There are therefore multiple possible sources for the megaclasts. Nonetheless, most exhibit low-amplitude seismic facies and contain parallel reflections similar to the underlying levees. The fact that they are folded and contorted and that

there is no evidence of faulting indicates ductile deformation and suggests a clay-rich composition. There is, however, evidence of channel axis erosion in the syncline where the basal surface of C1 directly overlies the channel axis of Unit II (Fig. 6.3). It is possible that the entrained channel axes, which contained higher proportions of sandy material (e.g. Mayall et al., 2006; Babonneau et al., 2010; Hodgson et al., 2011; Hubbard et al., 2014; Jobe et al. 2015) disaggregated to become part of the matrix (e.g. Dykstra et al., 2011). The more cohesive muddy material from the external levees (e.g. Babonneau et al., 2010; Kane and Hodgson, 2011; Morris et al., 2014; Hansen et al., 2015) could have been more resistant (e.g. Joanne et al., 2013) and carried as megaclasts that became folded during transport (e.g. Masson et al., 1997; Gee et al., 2006; Jackson, 2011; Alves, 2015).

There is a relatively higher abundance of megaclasts towards the margins (Figs. 6.8), this coincides with Day et al. (2015) who noted that megaclasts concentrate at MTC margins offshore Papua New Guinea. Similar observations were also made by Alves (2010) in the Espírito Santo Basin, offshore Brazil. The relative abundance of megaclasts at the margins could be explained by increased friction at the base and margins of the up-stepping erosion surface leading to local entrainment. The occurrence of large megaclasts clustered above the eroded external levee of Unit III along the northwestern margin of C1 (Figs. 6.10B and 6.13), could be explained by local entrainment resulting from increased shear stress as the levee was partially overridden by the mass-flow as it was deflected to the SW (Type 3 interaction; Fig. 6.12). Alternatively, the higher density of megaclasts towards the margins could be explained by dynamic grain-size segregation pushing larger particles towards the margins, a process which has been observed in subaerial debris flows (e.g. Major, 1997; Johnson et al., 2012).

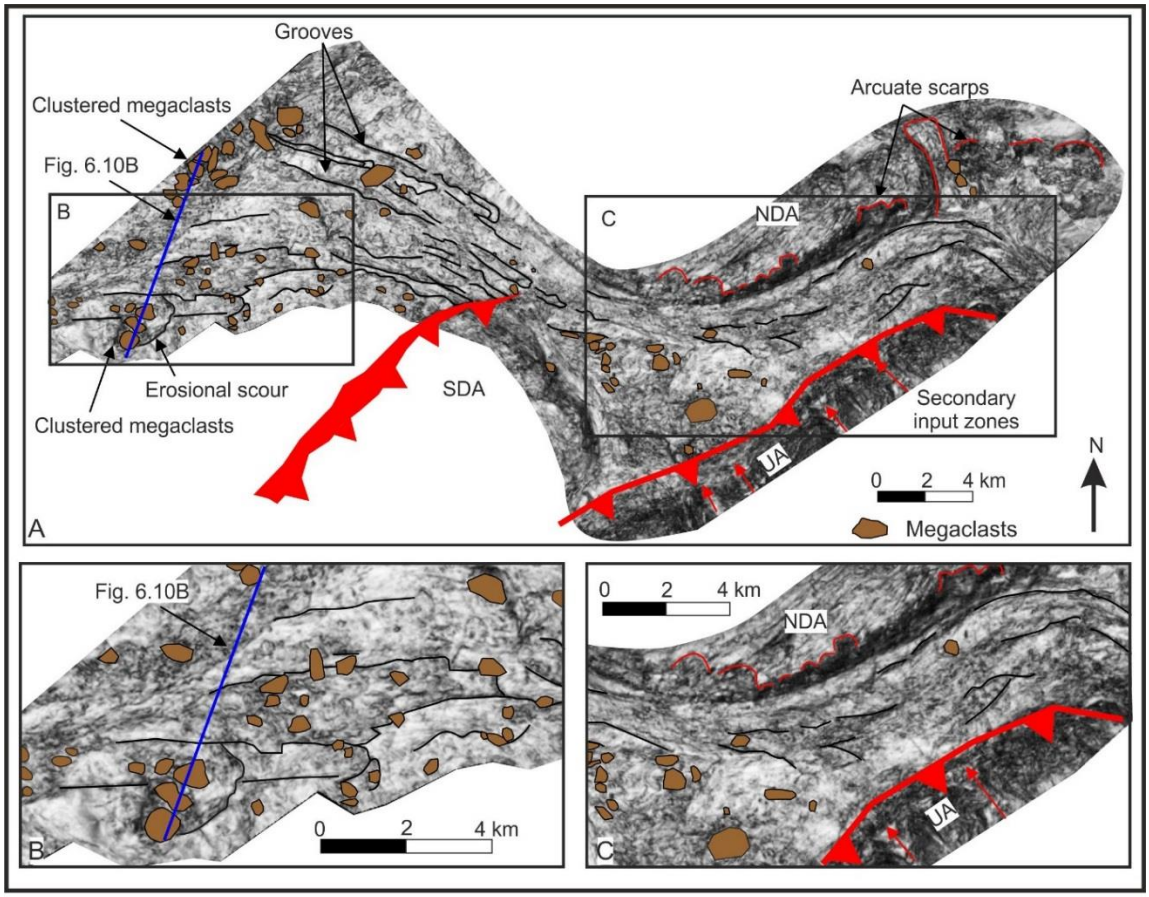

Figure 6.13. Distribution of the megaclasts with respect to the grooves on the basal surface of C1. **A.** The presence of grooves indicate that some megaclasts were transported for several kilometres, likely across the downdip anticline. **B.** Close-up on the southern downdip margin of C1 showing the occurrence of clustered megaclasts above erosional scours. **C.** Close-up on the syncline showing the presence of arcuate scarps which may have been sources of megaclasts.

6.6.2.1 Occurrence of chaotic debrites (facies 1)

Chaotic debrites (facies 1) occur towards the margins of the deposit and across the DA (Fig. 6.8). This observation is similar to Alves and Cartwright (2009) and Gamboa et al. (2011), who document the occurrence of chaotic facies in the thinner portions of MTCs offshore Brazil. The chaotic character of facies 1 could be explained by the increased shear stress at the base of the flow, caused by the shallowing of the erosion surface, and by lateral shearing against the margins, which may cause increased mixing and disaggregation of the material.

Across the DA disaggregated debrites overlie a relatively smooth basinward-facing erosion surface that truncates the crest of the underlying structure (Figs. 6.8, 6.9 and 6.10A). Here, facies 1 is thin (≤50 m) and is associated with aligned megaclasts (Fig.

6.8). Several processes are inferred to have occurred in this area: erosion and entrainment of the DA, bypass and sedimentation emplacement of megaclasts within an apparently finer-grained matrix. Erosion could have been caused by the bypassing head of the flow, prior to sedimentation. Subsequently, if deposition occurred *en-masse*, the megaclasts and the matrix would have been simultaneously emplaced. Alternatively, the megaclasts could have been deposited by the predominantly bypassing body of the flow as a lag, and the matrix could have been deposited later by a finer-grained and more disaggregated tail.

6.6.2.2 Occurrence of Semi Continuous, Folded Reflections (facies 2) and Imbricate Thrust-and-Fold Systems (facies 3)

Facies 2 and 3 predominantly occur in the central part of the deposit (Fig. 6.8). The abundance of systematically downdip-facing imbricate folds and thrusts within facies 3 suggests a higher degree of contraction with respect to facies 2, which comprises a broader range of fold styles and lacks associated thrusting (Table. 6.2; Fig. 6.9). Imbricate thrust and fold systems tend to occur updip of bathymetric highs that constituted barriers that deflected the flow. In the syncline, they develop updip of the back limb of the NDA, which is interpreted to have deflected the flow to the SW (Fig. 6.8). Basinward of the DA, they are found between the toe of the DA where the slope decreases abruptly from c. 6° to c. 3°, and the levee of Unit III, which is interpreted to have deflected the flow to the SW in a type 3 interaction (Figs. 6.8 and 6.12). The imbricate thrust-and-fold systems are interpreted to have resulted from buttressing against bathymetric highs. Similar thrust-and-fold systems could therefore develop in MTCs updip of either structural or depositional bathymetric highs that deflect or block the mass-flows in type 3 or type 4 interactions (Fig. 6.12). The folds in facies 2 also indicate contraction, but the lack of a consistent sense of vergence suggest these folds formed due to internal deformation resulting from simple shear against the basal surface, rather than buttressing resulting from downdip blockage or deflection. These folds could also

represent a transition from the more coherent (facies 3) to the disaggregated debrites (facies 1; e.g. Shanmugam et al., 1994; Stow et al., 1996; Locat and Lee, 2005; Strachan, 2008; Omosanya and Alves, 2013).

The characteristics of the flow at the time of emplacement are recorded in the seismic facies (e.g. Strachan, 2008; Dykstra et al., 2011; Alves et al., 2014) and result from the deformation, disaggregation and mixing of the original failed mass, and from the entrainment of fluid and substrate (Shanmugam et al., 1994; Strachan, 2008; Dykstra et al., 2011). The initial composition and texture of C1 would have been determined by the characteristics of the failed material. The main source area of C1 is interpreted to be located to the east of the study area, at-or-close to the shelf-edge break (Ortiz-Karpf et al., 2016); the characteristics of the protolith are therefore unknown. The widespread erosion at the base of C1 suggests that a large volume of sediment was entrained, likely increasing the volume of the flow and modifying its rheology and dynamic behaviour. Although the presence of several source areas may have contributed to the observed heterogeneity, this was exacerbated by the entrainment from at least 6 underlying units, composed mainly of channel-levee complex sets (Fig. 6.3). The different degrees of disaggregation interpreted from the seismic facies can therefore reflect 1) the different properties of the entrained units, 2) the different transport distances and strain histories experienced by sediment entrained at different points and times, and 3) the distribution of stress and strain within the flow. Despite this complicated interplay, the distribution of the seismic facies in C1 seems to correlate with the underlying bathymetry, with contraction updip of bathymetric highs, predominant bypass above higher gradient slopes, and increased disaggregation at the margins. This suggests that bathymetry was an important control on the characteristics of the deposit.

6.7 Implications of Flow-Seabed Interactions

Erosion at the base of mass-flows depends on the characteristics of the flow and the substrate (e.g. Dykstra et al., 2011; Iverson, 2012; Day et al., 2015). Because these

factors are intimately related and there is a feedback effect between them, they cannot be isolated. However, as this study demonstrates, the morphology of the seabed and the composition of the substrate can be as important as the internal composition and structure of the parent flow. Previous studies have documented the interaction between bathymetric highs and mass-flows. For example, Moscardelli et al. (2006) document MTCs focused along underlying canyons and lateral confinement by mud diapirs, which resulted in the development of imbricate thrusts and folds within the MTC where bathymetrically induced flow contraction occurred. In the Magdalena Fan, north of the present study area, Romero et al. (2010) document the presence of MTCs focused along inter-channel lows, whereas Alfaro and Holz (2014) and Vinnels et al (2010) document ponding of MTCs in piggy-back basins to the south of the study area. Although the gross impact of bathymetry on MTC dispersal has been documented, the implications of such interaction on the distribution and internal characteristics of the MTCs have not been fully addressed.

The influence of substrate composition on MTCs has received even less attention. Previous contributions have noted the presence of ramps and flats on the basal surfaces of MTCs and attributed them to pre-existing weaknesses in the underlying substrate (e.g. Frey-Martinez et al., 2005; Bull at al., 2009). The effect of substrate entrainment on the compositional and rheological evolution of mass-flows was discussed by Dykstra et al. (2011), who document shearing of sand from entrained megaclasts into the matrix of an MTC. They note, for example, that MTCs propagating over sandy substrates may become sandier downslope. Dykstra et al. (2011) also observed superimposition of extensional and contractional deformation, and ductile and brittle strain, and attributed it to a complicated distribution of stress and strain within the flow (see also Jackson, 2011). However, such variations may also reflect the different mechanical properties of the entrained units and the different transport distances and strain histories experienced by sediment entrained at different points and times. The composition of the substrate could

also determine whether the material entrained is incorporated to the matrix or transported as megaclasts.

Simplified MTC depositional models are useful in conveying the key characteristics of the bounding surfaces and internal character of MTCs (e.g. Prior et al., 1984; Weimer and Slatt, 2004; Frey-Martinez et al., 2005; Bull et al., 2009). However, they assume a layered, homogenous substrate, which, in many if not most cases, does not adequately represent the slope stratigraphy encountered in deep-water settings. For example, the slope in some active and passive continental margins is complicated by tectonic, gravity and salt-driven structures (e.g. Steffens et al., 2003; Moscardelli et al., 2006; Heniö and Davies, 2006; Gee et al., 2007; Gamboa et al., 2010; Clark and Cartwright 2009, 2012; Vinnels et al., 2010). In areas lacking major structures, depositional relief associated with channel-levee complexes, MTCs and/or contourites can produce bathymetric irregularities that can influence the flows that propagate above them (e.g. Nakajima et al., 1998; Migeon et al., 2001; Piper and Normark, 2001; Skene et al., 2002; Frey-Martinez et al., 2006; Jackson and Johnson, 2009; Alves, et al., 2010; Kneller, et al., 2015; Ducassou et al., 2015; Ortiz-Karpf et al., 2015). Moreover, differences in the compositional and textural characteristics of the various deep-water architectural elements result in lithological heterogeneities, which can also influence subsequent flows. This is particularly significant for larger MTCs that cover areas of hundreds to thousands of squared kilometres. The flow-pathways and dynamic evolution of mass-flows, which is ultimately recorded in the deposits, is therefore expected to be greatly influenced by the morphology and composition of the seabed upon which they propagate. Therefore, although there are commonalities amongst MTCs, there is likely to be an important influence imposed by the local morphology and composition of the slope.

6.8 Conclusions

The bathymetrically and lithologically complex seabed, above which the mass-flows propagated, influenced the flow behaviour, routing, depositional geometry and internal characteristics of the MTCs. In particular:

The geometry of the basal surfaces of the MTCs was influenced by the properties of the underlying stratigraphic units, which are mainly composed of channel-levee complex sets of different ages. Changes in the slope of the basal surface or depth of erosion coincide with changes in the lithology of underlying units. Deeper erosion above channel axes suggests preferential erosion of the sandier, less cohesive channel-fill deposits in relation to the more cohesive, mud-prone levees. Changes in the morphology of the basal surfaces across different levee units are interpreted to represent differences in composition and/or lithification.

The orientation of the channel-levee complexes with respect to the MTC flow direction, together with the height of the levee with respect to the thickness of the mass-flow, determine whether the flow is blocked or deflected by perpendicular to oblique bathymetric barriers of depositional origin, or confined by underlying channel levee complex-sets and/or parallel inter-channel lows. Therefore, the style of MTC-channel-levee complex set interaction can influence mass-transport flow-pathways and runout distances, the preservation of channel axes, the type of substrate over which the mass-flow propagates and the compositional, textural and rheological evolution of the mass-flow. This impacts the prediction of presence and continuity of underlying hydrocarbon reservoirs and the sealing capacity of MTCs.

The widespread erosion at the base of C1 resulted in the entrainment of at least six underlying units composed of channel-levee complexes and underlying MTCs. The entrained substrate would have increased the volume of the flow and modified its rheology and dynamic behaviour. The heterogeneity observed in the deposit, with

different degrees of disaggregation and internal deformation therefore resulted from the combined effect of the different mechanical properties of the entrained units, the different transport distances and strain histories experienced by sediment entrained at different points and times and the distribution of stress and strain within the flow.

Seabed topography at the time of mass-flow emplacement was an important control on the distribution of the seismic facies in MTC C1, which displays contraction updip of bathymetric highs, predominant erosion and bypass above higher gradient slopes, and increased disaggregation towards the margins. In this case, the seismic facies apparently reflect the non-uniformity of the debris flow immediately prior to deposition. This relationship should be tested across other systems.

7 The role of mass-transport complexes in controlling channel avulsion and the subsequent sediment dispersal patterns on an active margin: the Magdalena Fan, offshore Colombia

The work in this chapter is published in:

Ortiz-Karpf, A., Hodgson, D.M., McCaffrey, W.D. (2015). The role of mass-transport complexes in controlling channel avulsion and the subsequent sediment dispersal patterns on an active margin: the Magdalena Fan, offshore Colombia. *Marine and Petroleum Geology*, v. 64, p. 58–75.

7.1 Introduction

The avulsion of submarine channels is a fundamental process that shapes sediment dispersal patterns through time, and therefore the evolution and growth of submarine fans (Pirmez and Flood, 1995). An avulsion node is the locus of a change in channel orientation. Avulsion lobe deposits, which form at the start of an avulsion cycle, can be sand-rich and in reflection seismic data have been associated with high-amplitude seismic reflection packages (HARPS) found towards the base of channel-levee complexes (e.g. Flood et al., 1991; Pirmez et al., 1997).

Previous studies on the causes of channel avulsion have focused on passive margins and have interpreted the most common trigger mechanism to be increased in-channel aggradation and/or peak volume flows (Kolla, 2007; Armitage et al., 2012). According to Kolla (2007), the probability of avulsion in sinuous submarine channels is determined by the relationship between the degree of instability of the channel-levee complex and the magnitude of the flows. Stable channel-levee complexes are likely to require high-volume turbidity currents to breach the levee and cause avulsion, while unstable channel-levee complexes do not necessarily require large volume flows to force a breach (Kolla, 2007). Channel-levee complexes may become unstable due to several factors, whose effects

may be additive (Kolla, 2007). Triggers invoked for avulsions include changes in sinuosity, changes in slope, in-channel aggradation and reduced channel relief, levee breaching by MTCs or channel plugging and levee slumping (Posamentier and Kolla, 2003; Kolla, 2007; Armitage et al., 2012; Brunt et al., 2013). Armitage et al. (2012) assessed the effects of in-channel aggradation upon the probability of avulsion in the Niger Delta slope, interpreting avulsion to be triggered by turbidity currents that were relatively oversized with respect to the channel's cross-sectional area. Radial avulsion patterns have been shown to develop in response to gradient changes in the Niger Delta, and the Southern Zaire, Indus and Bengal fans (Kolla, 2007; Armitage et al., 2012). Although levee collapse or failure has been mentioned as a possible mechanism for avulsion (Pirmez and Flood, 1995; Pirmez et al., 1997; Kolla, 2007; Armitage et al., 2012), few cases have been documented. Kolla (2007) considers that the collapse of levees is a random process that can trigger an avulsion, but it is not significant in submarine fans on passive margins.

This study used detailed mapping and interpretation of a three-dimensional seismic volume in the southern Magdalena Fan, offshore Colombia, an active basin margin. The objective was to investigate the role of a pre-existing MTC deposit on the later levee collapse and on the subsequent sediment dispersal patterns of an avulsion lobe complex–set. The almost complete preservation of lobe complexes enables the entire cycle of avulsion from the breaching of the levee to the establishment of a new channel to be described and interpreted.

7.2 Geological setting

The Magdalena Fan is located in the Caribbean Sea off the northern coast of Colombia, South America, where the Caribbean Plate is subducting under the South American Plate (Fig. 7.1). The interaction of the Cocos and Caribbean plates causes the latter to collide obliquely against the South American Plate (Cediel et al., 2003), resulting in a transpressional structural style characterised by a series of imbricate thrust structures

that propagate basinward and are transferred to the north by a series of strike-slip fault zones.

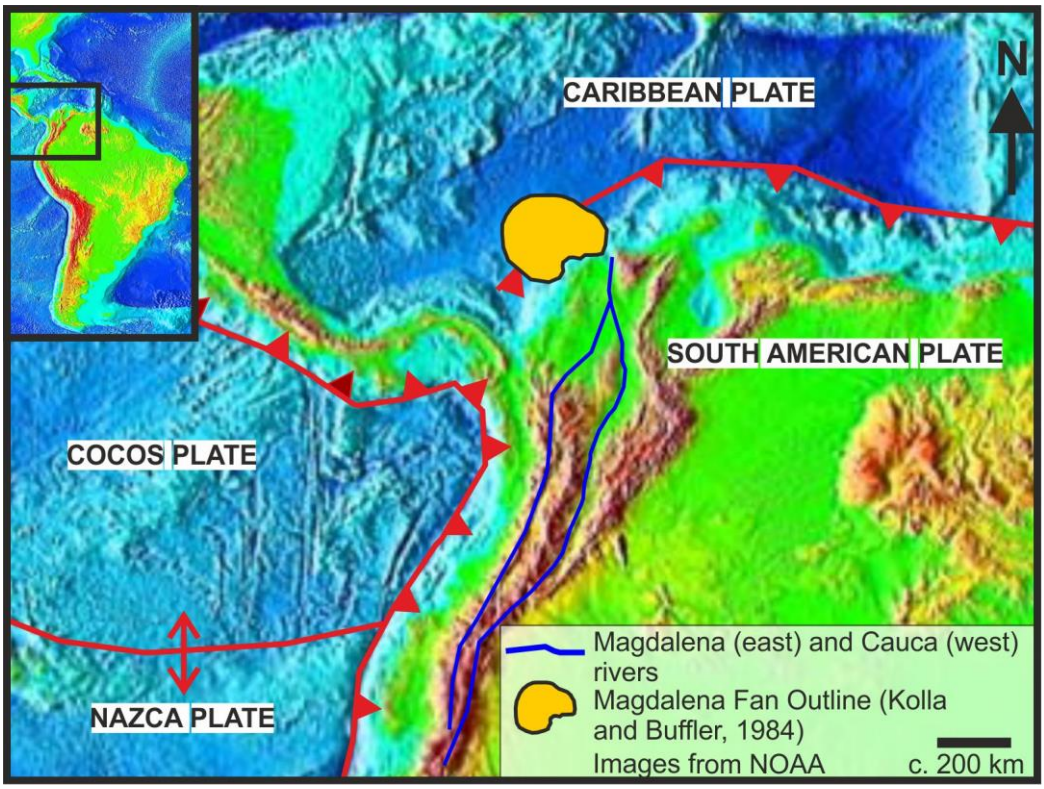

Figure 7.1. General location and tectonic setting of the study area. The Magdalena Fan is in the Caribbean Sea, off the northern coast of Colombia. It is located on a subduction zone where the Caribbean Plate collides obliquely with the South American Plate.

The Magdalena Fan lies on the offshore extension of the Sinú Fold Belt. The central part of the fan lies in a relatively undeformed area between the northern and southern fold belts, where the deformation front bends towards the continent (Fig. 7.2). The southern and northern parts of the fan are within the deformed areas and are characterised by canyons and gullies that feed mini basins between the structural highs (Ercilla et al., 2002; Romero-Otero et al., 2009). The recurrent collapse of steep scarps reincorporates sediment into the system and modifies sediment pathways (Ercilla et al., 2002; Romero-Otero et al., 2010; Vinnels et al., 2010; Alfaro and Holz, 2014). The undeformed central part of the fan is characterised by channel- levee complex–sets (*sensu* Sprague, 2005), large scale MTCs and sediment wave fields (Ercilla et al., 2002; Romero-Otero et al.,

2010). The study area is located in the transition zone between the southern deformed and the central undeformed provinces (Fig. 7.2).

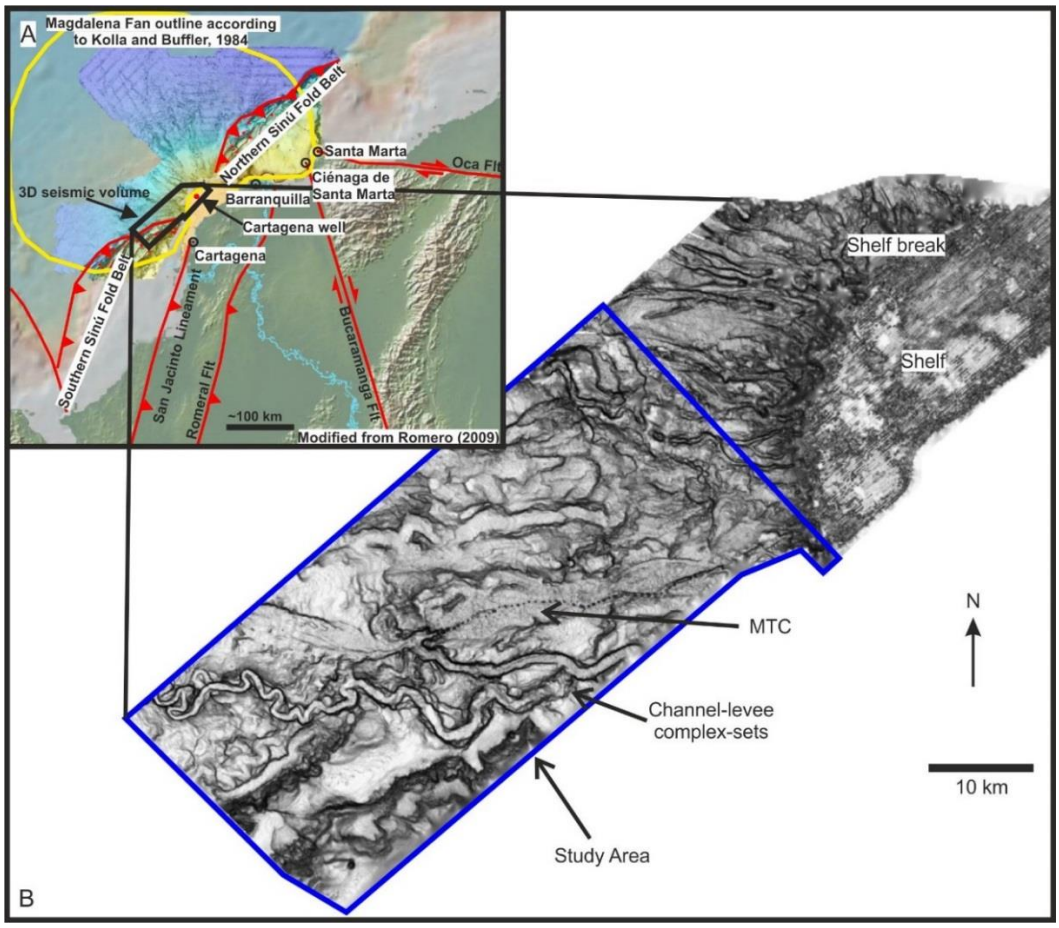

Figure 7.2. Subregional setting and study area. **A.** The Magdalena Fan is located in the offshore extension of the Sinú Fold Belt. Its apex coincides with a zone of subdued deformation between the southern and northern segments of the deformed fold belt. The area is characterised by transpressional tectonics with a combination of thrusts and strike-slip faults. The seismic volume is located in the southwestern part of the fan and includes the tip of the southern Sinú Fold Belt. **B.** Seabed dip map from the 3D seismic volume. The study area is defined by the blue box which is located to the southwest of the present-day continental shelf. The seabed displays a network of slope channel-levee complex-sets, MTCs and lobes.

The Magdalena Fan has an area of 53,000 km^2 (Ercilla et al., 2002) and is fed by the Magdalena River, which currently is 1,600 km long with a drainage basin area of 260,000 km^2 (Restrepo and Kjerfve, 2000). The sedimentation of the Magdalena Fan is inferred to have started in the Middle Miocene following the Oligocene-Miocene Proto-Andean Orogeny (Duque-Caro, 1979; Kolla and Buffler, 1984; Martinez et al., 2015). During the Plio-Pleistocene, the first peak of uplift of the Sinú Fold Belt took place, coinciding with the Andean Orogeny (Van der Hammen, 1958; Duque- Caro, 1979). Since the Miocene,

repeated avulsions of the Magdalena River have led to the river mouth being positioned in multiple locations between the cities of Cartagena and Santa Marta (Romero-Otero, 2009; Fig 7.2). Romero-Otero (2009) identified eleven different positions of the Magdalena River mouth and its corresponding delta. Nine shifts occurred during the Plio-Pleistocene, with the last major changes taking place in the Late Pleistocene when onshore uplift caused the river to avulse from just north of the city of Cartagena to the Ciénaga de Santa Marta. Subsequently, it switched to the west in the Holocene to its present-day river mouth position.

The stratigraphic interval studied correlates with the uppermost c.500-1000 m of the c. 3000 m of Pleistocene-Recent sediments drilled by one of the Cartagena wells (Rincón et al, 2007), located to the northeast to the study area (Fig. 7.2A). Also, the most recent activity of the Magdalena Fan in the area occurred in the Late Pliocene-Pleistocene (Romero-Otero, 2009); therefore the interval studied here is likely Pleistocene.

7.3 Study area and data

The study area is defined by a 1900 km^2 3D seismic volume located 26 km northwest of the city of Cartagena, Colombia (Fig. 7.2). Here, the upper to mid slope fan deposits are distributed in a series of submarine channel-levee complex-sets, the youngest of which have a prominent seabed expression (Fig. 7.2B). Intercalated with the channel-levee complex-sets are mass-transport complexes that range in scale from a few square kilometres to several hundreds of square kilometres in area (Ercilla et al., 2002; Romero-Otero et al., 2010). The southeastern part of the study area is within the northern tip of the southern Sinú Fold Belt where the deformation front bends to the east towards the continent (Fig. 7.2). A northeast-southwest trending anticline, referred to as the Downdip anticline (DA), is subdivided in two segments by a saddle. These are referred to as the *Southern Downdip Anticline (SDA)* and the *Northern Downdip Anticline (NDA;* Fig. 7.3*)*.

The 3D seismic volume was acquired in 2008, and is a Post Stack Depth Migrated (PSDM) volume, which for the first 1000 m contains a maximum frequency of 45 Hz and a dominant frequency of 30 Hz, yielding a vertical resolution of approximately 10-15 m assuming a sediment velocity of 1900 m/s. The bin spacing is 12.5 X 12.5 m and the horizontal resolution is approximately 15 m.

7.4 Seismic units

Seven dominant seismic facies were identified based on descriptive parameters such as: the amplitude, continuity and geometry of seismic reflections, the geometry of the units representing a specific seismic facies, and their stratal relationship with other seismic facies (Table 7.1). In the absence of lithological calibration from wells, the interpretation of these seismic facies and facies associations as sedimentary sub-environments is based on comparisons with previously published and widely cited seismic-based studies of deep-water systems (e.g. Mitchum et al., 1977; Pirmez et al., 1997; Abreu et al., 2003; Deptuck et al., 2003; Posamentier and Kolla, 2003; Gee et al., 2007; Cross et al., 2009; Catterall et al., 2010), and on the broader understanding of the regional setting.

Seismic facies 1 is composed of variable-amplitude, parallel, discontinuous reflections within a confining surface, interpreted as slope channel-fill (cf. Abreu et al., 2003; Deptuck et al., 2003; Posamentier and Kolla, 2003). Facies 2 is found on either side of facies 1 and is composed of parallel, continuous reflections that form wedge-shaped packages and is interpreted as external levee deposits (cf. Deptuck et al., 2003; Nakajima and Kneller, 2013). Facies 3 is made of sub-parallel, wedge-shaped reflections that are found within a confining surface; it is found next to facies 1 and 2 and is interpreted as internal levees (*sensu* Kane and Hodgson 2011), or terrace deposits (cf. Deptuck et al., 2003; Babonneau et al., 2004). Channel-levee complex-sets (*sensu* Sprague et al., 2005) are commonly formed by c.100-200 m thick and 1-2 km wide packages of stacked facies 1 and 3, that are bounded on either side by c.3.4 km wide

packages of facies 2 (Table 7.1B and C). Facies 4 is made of packages of chaotic reflections (Table 7.1D) that may contain discrete blocks with internal reflections that may be parallel or folded and commonly protrude above the top of the package. Facies 4 is interpreted as MTCs that can comprise deposits from a range of cohesive mass-flow processes including debris flows, slumps and slides (e.g. Carter, 1975; Masson et al., 1997; Pickering and Corregidor, 2005; Moscardelli et al., 2006; Bull et al., 2009). The discrete blocks are interpreted as large clasts (cf. Masson et al., 1997; Jackson, 2011; Olafiranye et al., 2013). Facies 5 is characterised by sub-parallel, dipping reflections interpreted as rotated blocks of sediment affected by sliding; when found within the confining surfaces they are interpreted as slides of internal levee, or inner external levee deposits (*sensu* Kane and Hodgson, 2011) (Table 7.1B and C), and when found at the margins of MTCs they are interpreted as slides (Table 7.1D) (cf. Masson et al., 1997; Pickering and Corregidor, 2005; Moscardelli et al., 2006; Bull et al., 2009). Facies 6 is composed of parallel, variable-amplitude reflections that thin away from a central point and display convex shapes in cross-section and lobate shapes in map view; it is interpreted as lobe deposits fed by channelized conduits (Table 7.1F and G) (cf. Posamentier, 2003; Posamentier and Kolla, 2003; Saller and Dharmasamadhi, 2012). Facies 7 contains parallel, low-amplitude, continuous reflections that drape the underlying bathymetry and are interpreted as background sedimentation (Table 7.1A) (cf. Stow and Piper, 1984; Stow and Mayall, 2000).

A

Facies	Description	Interpretation
① Parallel, discontinuous reflector facies	Parallel, discontinuous reflectors (continuous for ~1 km) that can be flat, inclined, undulated or concave. The seismic amplitudes are variable but they are generally high, especially towards the base. Facies 1 is elongate and sinuous in map view, and is bounded on either side by facies 2.	Slope channel-fill (cf. Mitchum et al., 1977; Pirmez et al., 1997; Abreu et al., 2003; Deptuck et al., 2003; Posamentier and Kolla, 2003; Gee et al., 2007; Cross et al., 2009)
② Parallel, wedge-shaped reflector facies	Parallel, inclined, continuous, low-amplitude reflectors that form wedge-shaped packages (max thickness 50-300 m) that pinch out over a maximum distance of ~4 km. The reflectors downlap or onlap older packages and are found on either side of facies 1. Facies 2 is elongate in map view and trends parallel to facies 1.	External levees (cf. Deptuck et al., 2003; Nakajima and Kneller, 2013).
③Confined, sub-parallel, wedge-shaped reflector facies	Sub-parallel, continuous, low-amplitude reflectors that form ~100 m thick packages that are traceable for ~1-2 km. They thin and dip towards an incision surface at an angle that decreases upwards. The reflectors may be down-thrown and rotated across discontinuities that dip into the confining surface. Facies 3 is found between facies 1 and the confining surface, trending parallel to both in map view.	Internal levees (sensu Kane and Hodgson 2011) or terrace deposits (cf. Deptuck et al., 2003; Babonneau et al., 2004;)
④ Chaotic reflector facies	Chaotic, discontinuous reflectors that dip in different directions and at different angles. The packages are ~50-200 m in thickness with areal extents of 10s -100s of km^2. The packages have erosional bases and irregular tops. They contain discrete ~50-250 m thick packages of coherent reflectors that commonly protrude above the top of the package and cover areas of up to ~7 km. The seismic amplitudes are generally low.	Mass-transport complexes (MTC) including debris flows, slumps and slides (cf. Carter, 1975; Moscardelli et al., 2006; Bull et al., 2009), containing megaclasts (cf. Masson et al., 1997; Jackson, 2011; Olafiranye et al., 2013; Alves, 2015).
⑤ Sub-parallel, dipping reflector facies	Sub-parallel, dipping reflectors that are rotated with respect to the surrounding packages. They are found within channel-confining surfaces outboard of facies 1 in packages that are ~100 m thick and ~700-1500 m wide. They are rotated across a fault that dips into the channel. They are also found at the margins of facies 4 in packages that are ~100 m thick and ~3 km wide overlying normal faults. Facies 5 is elongate in map view.	Blocks of sediment affected by sliding. Internal or inner external levees (*sensu* Kane and Hodgson, 2011) when adjacent to the channel-fill. Slide blocks when at the margins of the chaotic facies (cf. Pickering and Corregidor, 2005).
⑥ Parallel, variable amplitude reflector facies	Parallel, reflectors that are found as single reflectors or in packages of a few reflectors (~15-80 m thick). They are parallel and continuous over ~3-7 km. They downlap or onlap older packages and thin in both directions from a central point resulting in a convex shape. The seismic amplitudes are variable. The higher amplitudes follow elongate pathways to lobate geometries that cover areas up to 10 km^2.	Lobe deposits fed by channelized conduits. (cf. Posamentier, 2003; Posamentier and Kolla, 2003; Saller and Dharmasamadhi, 2012)
⑦ Parallel, low-amplitude, continuous reflector facies	Parallel, continuous reflectors that drape pre-existing bathymetry. They can be traced for up to 10km. The seismic amplitudes are generally low.	Background sedimentation (cf. Stow and Piper, 1984;Stow and Mayall, 2000).

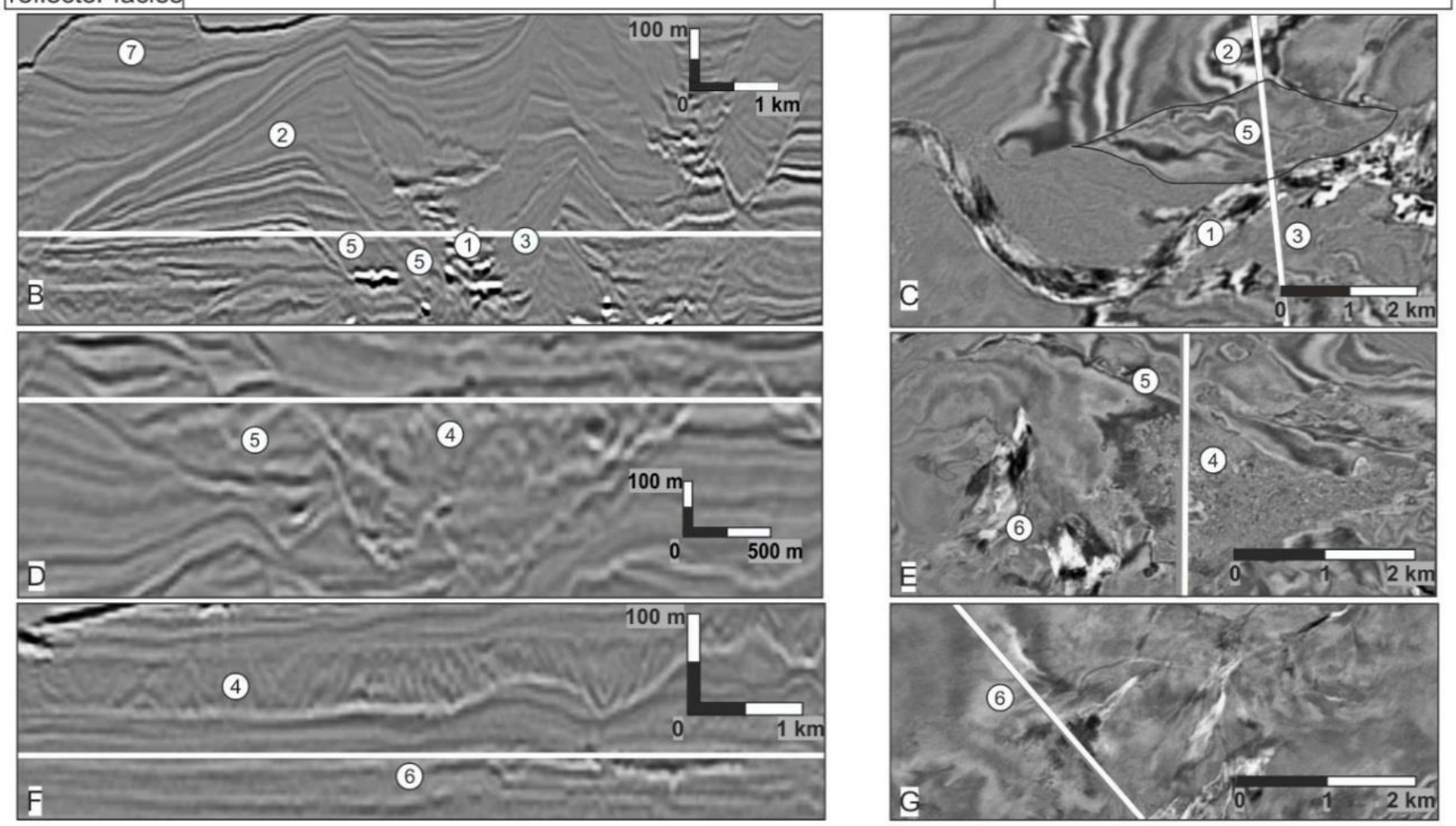

Table 7.1. Seismic facies classification. **A.** Descriptions and interpretations of the seismic facies defined in this study. **B-G.** Representative examples of the seismic facies are shown in seismic cross-sections (left) and on depth slices (right), with the white lines indicating the *loci* of intersection.

Eight surfaces of seismic-stratigraphic significance were defined based on reflection terminations such as onlap, truncation and downlap and on changes in the seismic facies associations. The surfaces that define the seismic units were mapped with a line spacing of 10 to 20 lines depending on the continuity of the seismic reflections. In addition, seismic attribute extractions were used to investigate their internal geometries and distributions. The seismic units are named A to G, A being the oldest and G the youngest (Figs. 7.3 and 7.4). To assist in their description, the study area has been divided into three areas based on the architecture of Unit E. These are referred to as the upper, middle and lower reaches (Fig. 7.3).

7.4.1 Seismic Unit A: Channel-levee complex-set (CLC) 1

Seismic Unit A is composed of the oldest channel-levee complex-set in the stratigraphic interval studied which will be referred to as CLC1. The base of Unit A is defined by the basal erosion surface of CLC1 and the top surface is defined by the bases of the channel-levee complex-sets in Units C and E. The basal erosion surface of CLC1 incises below the basal external levee surface and is c. 3 km wide and c. 300 m deep, from the remnant levee crest to the deepest point in the incision. The levees are c. 200 m thick at the crest and c. 3.4 km wide; they are truncated on either side. At least three erosional surfaces can be recognized within the channel which contains c. 70- 150 m of facies 1 (parallel, discontinuous reflections) and 110-140 m of facies 4 (chaotic) interpreted as a channel-confined MTC. The presence of at least two channel-levee complexes and an MTC within the confining surface suggests that this was a long lived sediment pathway repeatedly utilized by turbidity currents and debris flows.

7.4.2 Seismic Unit B: Erosional remnant

Unit B is predominantly located to the south of Unit A (Fig. 7.3). It has a maximum thickness of c. 100 m and comprises seismic facies 2 (parallel, wedge shaped reflections) in the upper reach, and seismic facies 5 (sub-parallel, dipping) and facies 4 (chaotic) in the middle and lower reaches (Fig. 7.3). In the upper reach, the wedge-

shaped package of Unit B onlaps the southern levee of CLC1 and is overlain by Unit E. To the south, the package is truncated by the base of Unit D. Unit B is interpreted as the northern external levee of a channel complex-set that was later eroded.

In the middle reach, seismic Unit B overlies Unit A with an irregular basal surface that down-steps to the southwest (Fig. 7.4). It is overlain by Unit E and is composed of seismic facies 5 (parallel, dipping reflections) with thicknesses ranging from c. 70-130 m, and is interpreted as slide blocks of external levee deposits. Towards the lower reach it forms a c. 90 m thick package of seismic facies 4 (chaotic) interpreted as an MTC, and is overlain by Unit D with an erosional contact (Fig. 7.4). The bounding surfaces of Unit B can be traced from the lower to the upper reaches and it is therefore interpreted as a single sedimentary package that was affected by post-depositional slumping.

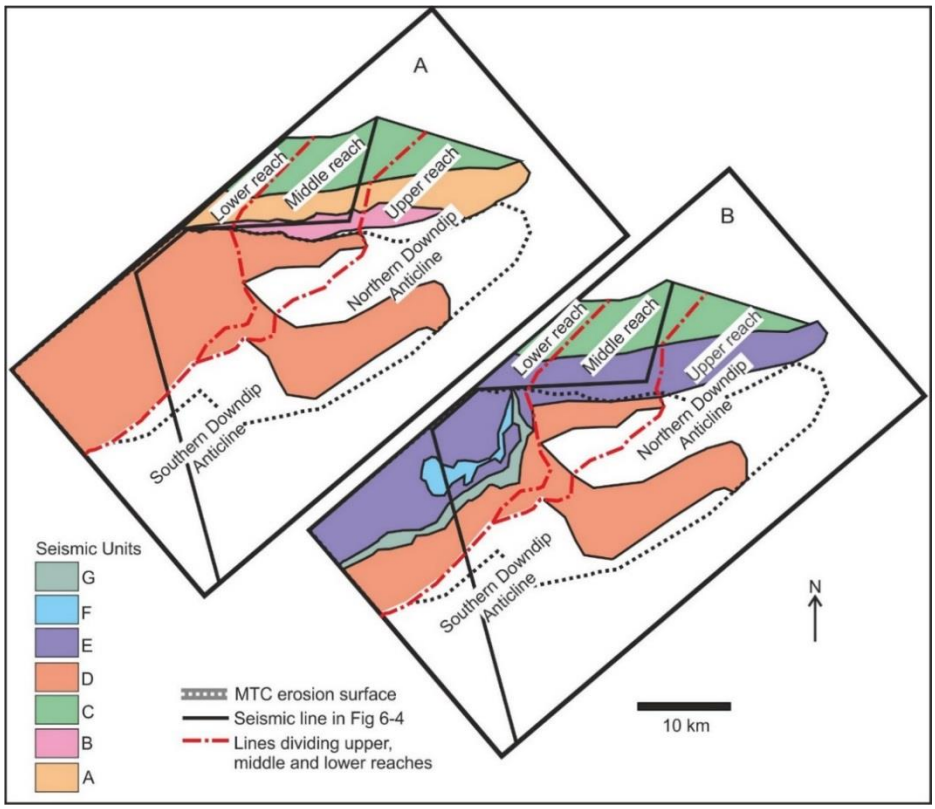

Figure 7.3. Areal distribution of the seismic units. **A.** Map showing the distribution of seismic units A-D within the data set. Note that Unit C overlies Unit A; however to allow the illustration Unit A it has only been shaded to the north. Note the narrow remnant ridge of Unit B in the middle and lower reaches. **B.** Map showing the distribution of seismic units D-G. Although Unit E overlies Unit C, Unit C is shown for illustration purposes. The levees of CLC4 in Unit G have not been shaded to visualize the relationship between the CLC4 channel-levee complex-set and Unit F. Likewise, only part of Unit F has been shaded. The black line indicates the location of the seismic line in Fig. 7.4.

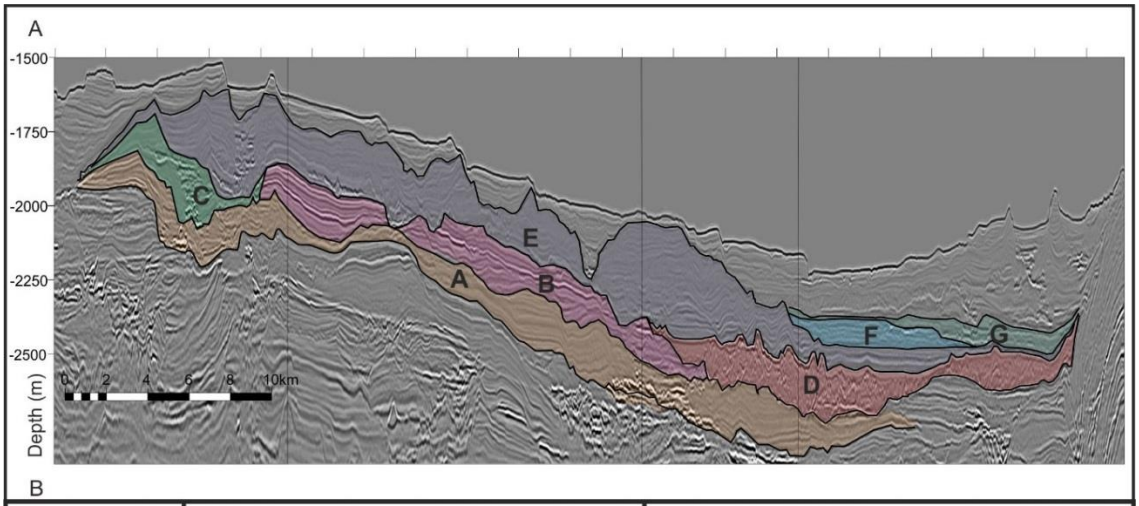

Seismic Unit	Seismic Facies Association	Interpretation
G	Facies 1 and 2	Channel-levee complex-set (CLC4) developed from the consolidation of the CLC3 avulsion
F	Facies 6	Avulsion lobe complex-set derived from the avulsion of CLC3
E	Facies 1, 2 and 3	Channel-levee complex-set (CLC3).
D	Facies 4	MTC: Debrites with megaclats that protrude above the top surface.
C	Facies 1, 2 and 3	Channel-levee complex-set (CLC2).
B	Facies 2 in the upper reach and facies 5 in the middle and lower reaches	Remnant levee deposits that have been affected by sliding and slumping in the middle and lower reaches.
A	Facies 1, 2 and 3	Channel levee complex-set (CLC1).

Figure 7.4. Seismic Units. **A.** Composite seismic line showing the interpreted seismic units. The location of the seismic line is shown in Fig. 7.3 **B.** Facies associations and interpretations of the seismic units.

7.4.3 Seismic Unit C: Channel-levee complex-set (CLC) 2

Unit C has an erosive base that incises into Unit A and follows a similar map view trend in the upper reach. In the middle reach, it diverges from CLC1 and trends to the northwest (Fig. 7.3). At the top, it is erosionally truncated and/or downlapped upon by Unit E. This package is interpreted as a channel-levee complex-set (CLC2) composed of c. 150-200 m of stacked high-amplitude, discontinuous reflections, overlain by c.100 m of parallel low-amplitude reflections. It is c. 2 km wide between levee crests and it is bounded by 2.4 km wide and c. 100-200 m high external levees. In the middle and lower reaches, sediments from the southern levee of CLC2 occupy the under-filled incision of CLC1 and

underlie Unit E. Therefore, CLC2 is younger than CLC1 and Unit B and older than Unit E.

7.4.4 Seismic Unit D: MTC

Seismic Unit D is composed of seismic facies 4 (chaotic) and is interpreted as a package of MTCs. The base of Unit D is defined by a continuous, negative-amplitude reflection that truncates older channel-levee deposits creating an erosional trough (Fig. 7.5). The depth of the basal incision surface ranges from c. 500 m in the upper reach to c. 250 m in the lower reach and the package covers an area of c.470 km^2 within the study area. The erosional surface is overlain by c.100-200 m of chaotic reflections (facies 4) interpreted as debrites, and discrete blocks, interpreted as megaclasts. In the upper and middle reaches, the northwestern lateral margin of the MTC truncates Unit B. In the lower reach, towards the limit of the dataset, the MTC erodes Unit B completely and incises into the southern external levee of CLC1 (Fig. 7.3A).

A coherency extraction along the MTC basal surface shows sub-parallel lineations that can be traced for up to 7 km (Fig. 7.6A). In cross-section, the lineations coincide with zones some 200-500 m in width where the basal surface incises c. 20-30 m deeper than in the surrounding substrate. The top surface is an irregular negative-amplitude reflection characterised by prominent bathymetric highs that commonly coincide with megaclasts that are c. 50-250 m thick (Fig. 7.7). The protruding megaclasts generally lie directly above the basal erosion surface and are thicker than the surrounding deposit. Some are internally deformed (Fig. 7.7B and E) while others display parallel internal reflections (Fig. 7.7C and D). Towards the northwest, three megaclasts are aligned parallel to the basal lineations, interpreted as the flow direction, resulting in variable amounts of incision of the basal shear surface and a highly irregular MTC top surface (Fig. 7.7B). The largest megaclasts are located towards the south, where the incision of the basal shear surface is c. 100 m deeper than in the surrounding area, while the top surface is at least 150 m higher.

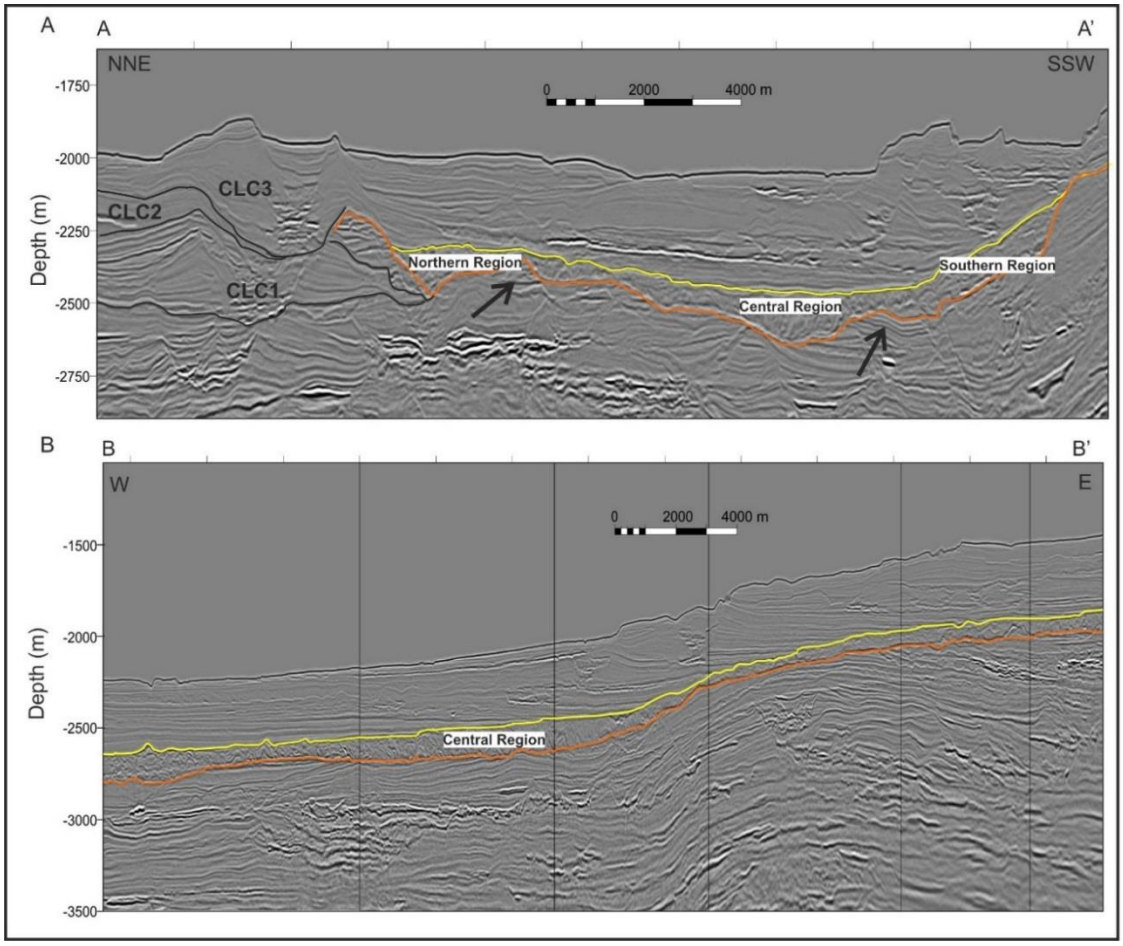

Figure 7.5. Architecture of the MTC in Unit D. **A.** NNE-SSW seismic line showing the top and base horizons of the MTC. The MTC is bounded to the SSW by the downdip anticline and to the SSE by stacked channel-levee complex-sets (CLC1 and CLC3). Arrows point to the erosional remnants that constitute the ridges separating the three MTC regions (Southern, Central and Northern regions) shown in Fig. 7.6A. **B.** W-E composite seismic line along the axis of the main MTC incision. Note the irregularities on the MTC top surface to the west and the eroded anticline crest to the east. The location of the lines is shown in Fig. 7.6.

The deep erosional depression was not entirely filled by the overlying MTC, resulting in the creation of a significant amount of accommodation through net seascape degradation (Fig. 7.5A and 7.6A). It is therefore likely that the remaining volume of the MTC is deposited downdip of the study area. The lineations on the basal shear surface are interpreted as grooves or drag marks and are used as kinematic indicators (cf. Bull et al., 2009) that show that there are at least three MTC regions with different transport directions (Fig. 7.6A). The presence of arcuate-shaped scarps along the lateral margins of the MTC and the forelimb of the structures (Fig. 7.6A), as well as rotated blocks of substrate at the margins of the MTC (facies 5), suggests that some megaclasts may have originated during the passage of the flow via entrainment of the older channel-levee

complex sets that formed the substrate. Because the megaclasts are not floating in a matrix and some are internally deformed, they are interpreted to have been transported by a shearing, laminar flow rather than in a plug flow.

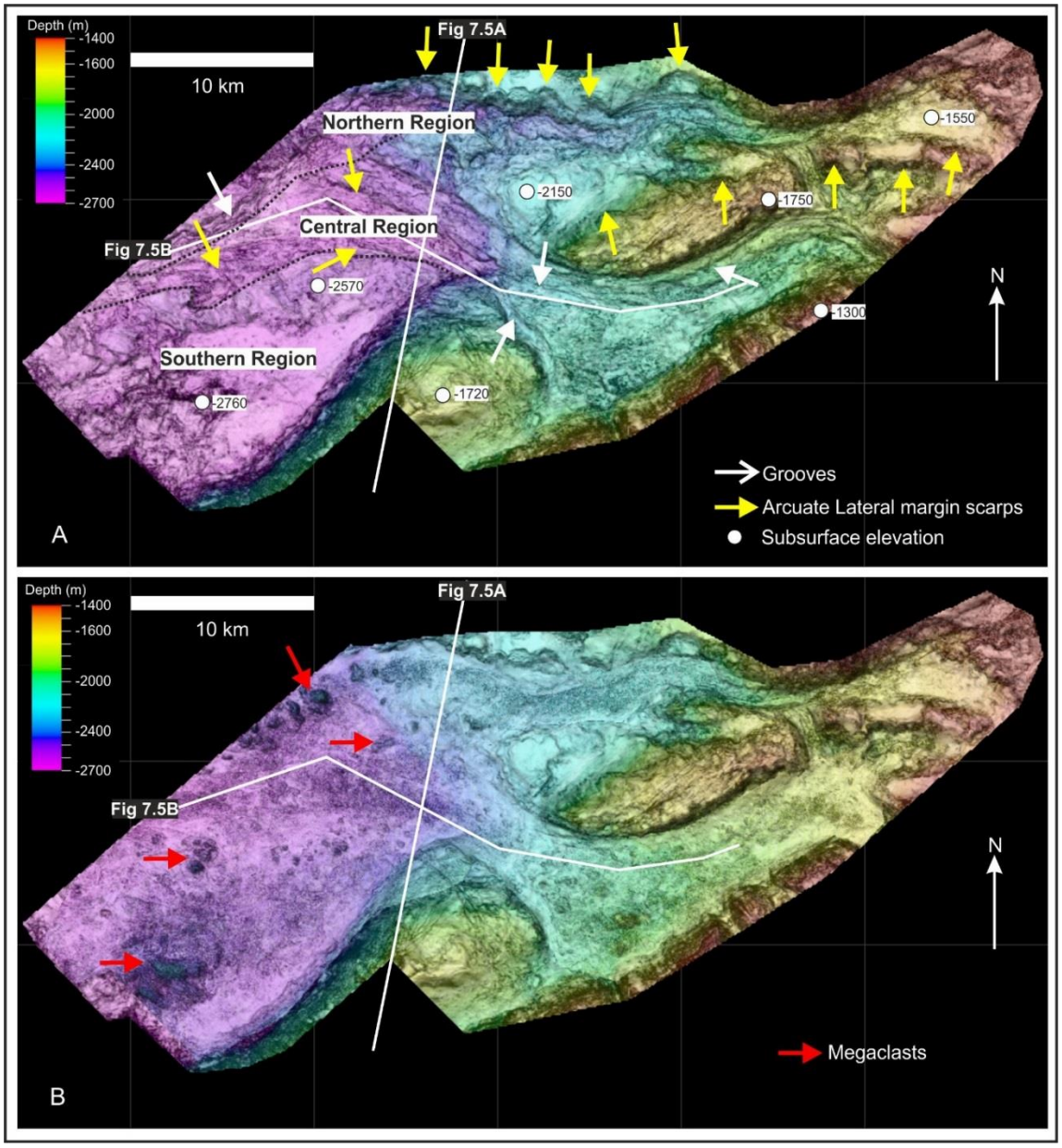

Figure 7.6. Characteristics of the MTC in Unit D. **A.** Variance extraction on the MTC basal surface coloured by subsurface elevation; the white circles indicate depth values. Three separate MTC regions (Southern, Central and Northern regions) can be discriminated based on the interpretation of the lateral and head wall scarps and grooves. **B.** Combined display of a variance extraction on the MTC top, coloured by subsurface elevation and a variance extraction on the basal MTC surface, coloured by subsurface elevation. The red lines point to bathymetric highs on the top MTC surface interpreted as protruding megaclasts. The white lines show the location of the seismic lines in Fig. 7.5.

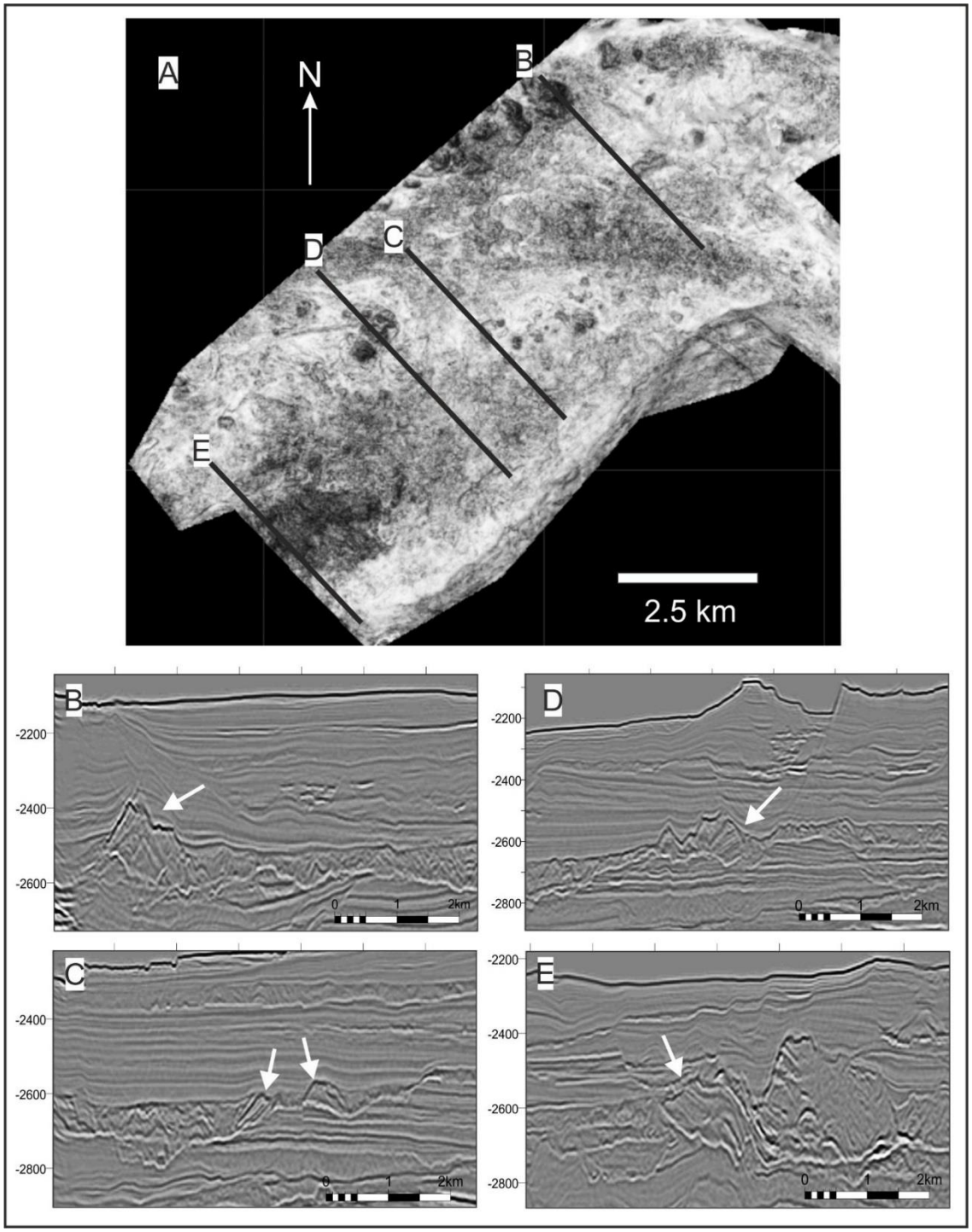

Figure 7.7. Megaclasts protruding on the MTC top surface. **A.** Variance extraction on the top MTC surface. The darker, rounded shapes are interpreted as megaclasts. The lines indicate the location of the seismic sections in figures B-E. **B.** Internally deformed megaclast underlying the levee of CLC3. **C** and **D.** Internally layered tilted blocks that clearly exhibit a different seismic character from the surrounding chaotic seismic facies, they are interpreted as relatively undeformed megaclasts. **E.** Internally deformed megaclasts that protrude above the MTC top surface.

7.4.5 Seismic Unit E: Channel-levee complex-set (CLC) 3

This unit has an erosional base that incises into CLC1 and CLC2. In the upper reach, its top surface is well expressed on the present-day seabed geomorphology and in the lower reach it is overlain by Units F and G (Fig. 7.3B). It is interpreted as a channel-levee complex-set (CLC3) that trends in approximately the same direction as CLC1 in Unit A. The channel complex set is c. 1.5-2 km wide and c. 250-370 m thick and it contains stacked channel complexes that are c. 40-50 m thick and c. 600-800 m wide. The northern levee of CLC3 onlaps the southern levee of CLC2; it is c. 300-400 m thick, and its cross-sectional width is c. 2.3 km. The southern levee is c. 700 m to 2 km wide and c.100-200 m thick in the middle reach, and increases in size to c. 4 km in width and c. 250-300 m in thickness in the lower reach.

Along the middle and lower reaches, the geometry of CLC3 changes. In the middle reach, the basal portion of the southern levee is confined by the levee remnants of Unit B, and the younger portion downlaps onto Unit B and the MTC (Fig. 7.8B and C). In figure 7.8B the levee reflections are locally truncated along a steep surface and in figure 7.8C they appear internally deformed. In the middle and lower reaches, the narrow erosional remnants of Unit B confine the basal southern levee. The younger reflections override them with a mounded geometry that is persistent for over 100 m above the levee basal surface (Fig. 7.8D and E).

In the lower reach, the southern levee is almost entirely absent and the remaining levee sediments above the MTC are overlain by four or five parallel high-amplitude troughs (Fig. 7.9B). In figure 7.9C and F, the levee reflections are steeply inclined towards the MTC and the levee package at the toe of the remnants of Unit B is thicker. Farther downdip, the southern levee abruptly thins against the aligned megaclasts in Unit D (Fig. 7.9D). To the southwest, CLC3 is no longer visible within the dataset but the deposits of the eastern levee thin towards the structural trend covering the MTC almost entirely and displaying similar morphological features that relate to underlying bathymetric highs (Fig.

7.9E). The internal deformation features, and the local absence of the southern levee of CLC3 suggest it was unstable.

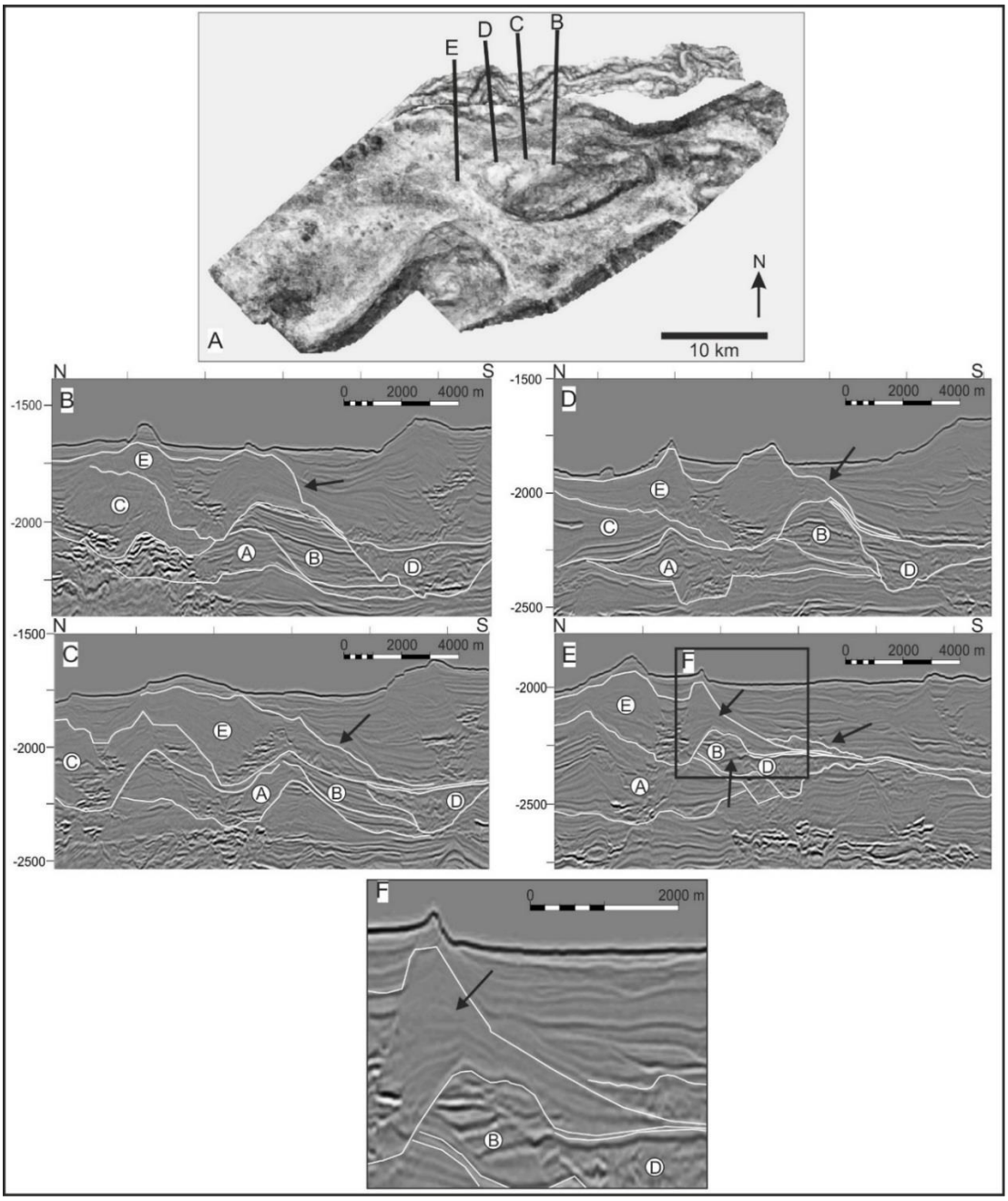

Figure 7.8. Down-flow changes in architecture through the middle reach of CLC3 in response to its position relative to the MTC. The circled letters denote the seismic units. **A.** Combined map of: A variance extraction at the MTC top, a variance extraction at the MTC basal surface, and a variance extraction at the CLC3 top. The black lines show the location of the seismic cross-sections in B-E. **B.** The steep slope of the southern levee made it unstable and prone to collapse. **C.** The chaotic facies in the southern levee are indicative of collapse. **D.** The remnant of Unit B separating CLC3 from the MTC is narrowed by the erosion of CLC3 and the MTC. The geometry of the southern CLC3 levee is altered by the ridge. **E.** The remnants of Unit B are incorporated into the MTC and form a bathymetric anomaly that leads to a consistent discontinuity in the overlying levee reflections. Instability is evidenced by the slumped levee deposits. The rectangle indicates the location of F. **F.** Close-up of the seismic section in E showing the discontinuity in the levee reflections above the erosional remnant of Unit B.

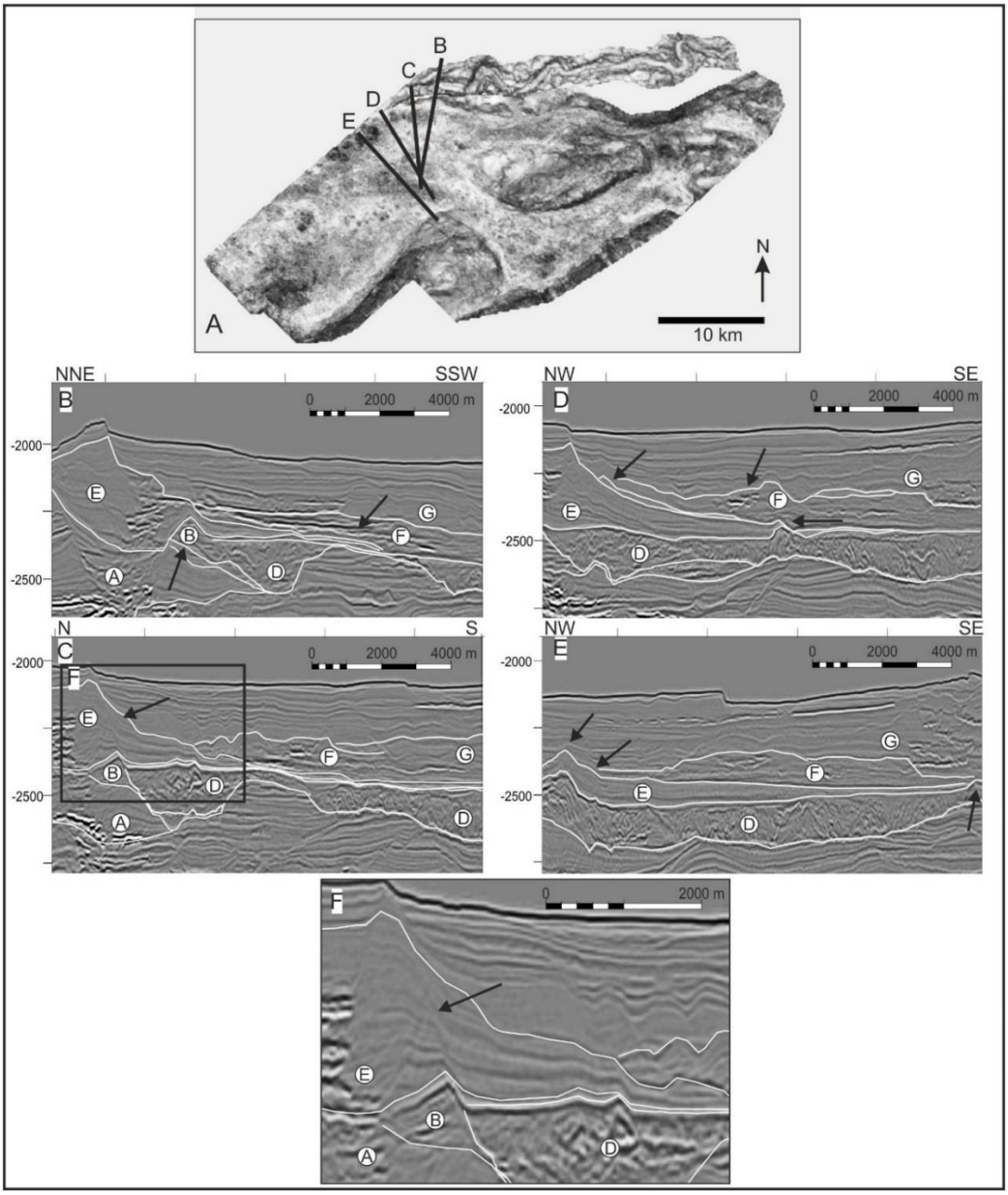

Figure 7.9. Down-flow architectural changes in the lower reach of CLC3 in response to its position relative to the MTC. The circled letters denote the seismic units. **A.** Combined map of: A variance extraction at the MTC top, a variance extraction at the MTC basal surface, and a variance extraction at the CLC3 top. The black lines show the location of the seismic cross-sections in B-E. **B.** The entrained Unit B remnant becomes narrower and the southern levee collapses leading to the avulsion lobes in Unit F. **C.** A discontinuity that vertically offsets the levee reflections is aligned with the bathymetric anomaly on the MTC top. The rectangle indicates the location of F. **D.** The bathymetric anomalies on the MTC top limit the lateral extent of the levee. The instability is evidenced by a collapsed portion of the levee. The lobe deposits in Unit F become channelized. **E.** The irregularities on the MTC top surface alter the geometry of the CLC3 levee and the underlying bathymetry limits the distribution of the avulsion lobes in Unit F. **F.** Close-up of the seismic section in C showing the discontinuity in the levee reflections above the remnant ridge of Unit B. Note the increased levee thickness at the toe of the ridge.

7.4.6 Seismic Unit F: Avulsion Lobes

Seismic Unit F mainly comprises variable-amplitude, parallel reflections at the base, and relatively higher amplitude, parallel reflections towards the top. The reflections are inclined and onlap the southern levee of CLC3 to the west. At the top they are overlain and locally truncated by the basal surface of Unit G to the east (Fig. 7.10). The package has a maximum thickness of c. 150 m.

Three reflections were mapped in detail (Fig. 7.10 horizons 1, 2, 3). The basal package (Fig. 7.10-horizon 1) is represented by a single reflection and has an area of c. 33 km^2. It dips to the east and onlaps the top of the CLC3 levee to the west. The middle package (Fig. 7.10 horizon-2) has a maximum thickness of c. 55 m and covers an area of c. 51 km^2 thinning in all directions with a convex-up shape to the south. The middle package extends farther in all directions with respect to the lower package and its western limit coincides with the aligned megaclasts in Unit D (Fig. 7.11B).

The upper package (Fig. 7.10-horizon 3) is made of four variable-amplitude reflections that onlap the levee of CLC3 to the west and are erosionally truncated by Unit G to the east (Fig. 7.10). The package has a maximum thickness of c. 80 m, and it contains discontinuous, high-amplitude, parallel reflections towards the centre and parallel, low-amplitude reflections towards the fringes. It covers an area of c. 66 km^2. It thins to the south becoming a single high-amplitude trough and to the north it onlaps the levee and channel axis of CLC3.

Amplitude extractions from an interval 10 m above and below the mapped horizons show that the basal package has relatively low amplitudes with respect to the overlying packages (Fig. 7.11A). The highest amplitudes have an area of c. 0.8 km^2 and are located at the toe of the levee against a bathymetric high related to an underlying megaclast. Here, several narrow (c. 200 m wide) threads of slightly higher amplitudes originate; they diverge and fade downdip after c. 4 km. In the middle package, the high amplitudes at the toe of the levee are c. 3 km^2 (Fig. 7.11B) and can be traced for c. 4 km along a thread

of high amplitudes to the axis of CLC3. Downdip, c. 10 km of elongate high amplitudes are interpreted as channelized deposits that terminate in a c. 5 km^2 high-amplitude lobe complex. In the upper package, elongate high amplitudes extend for c. 12 km to the south of CLC3, terminating in a c. 11 km^2, high-amplitude lobe to the south of the aligned megaclasts (Fig. 7.11C). The southern limit of the package coincides with the presence of an underlying megaclast. Unit F is interpreted as an avulsion lobe complex-set that developed at a high angle to CLC3.

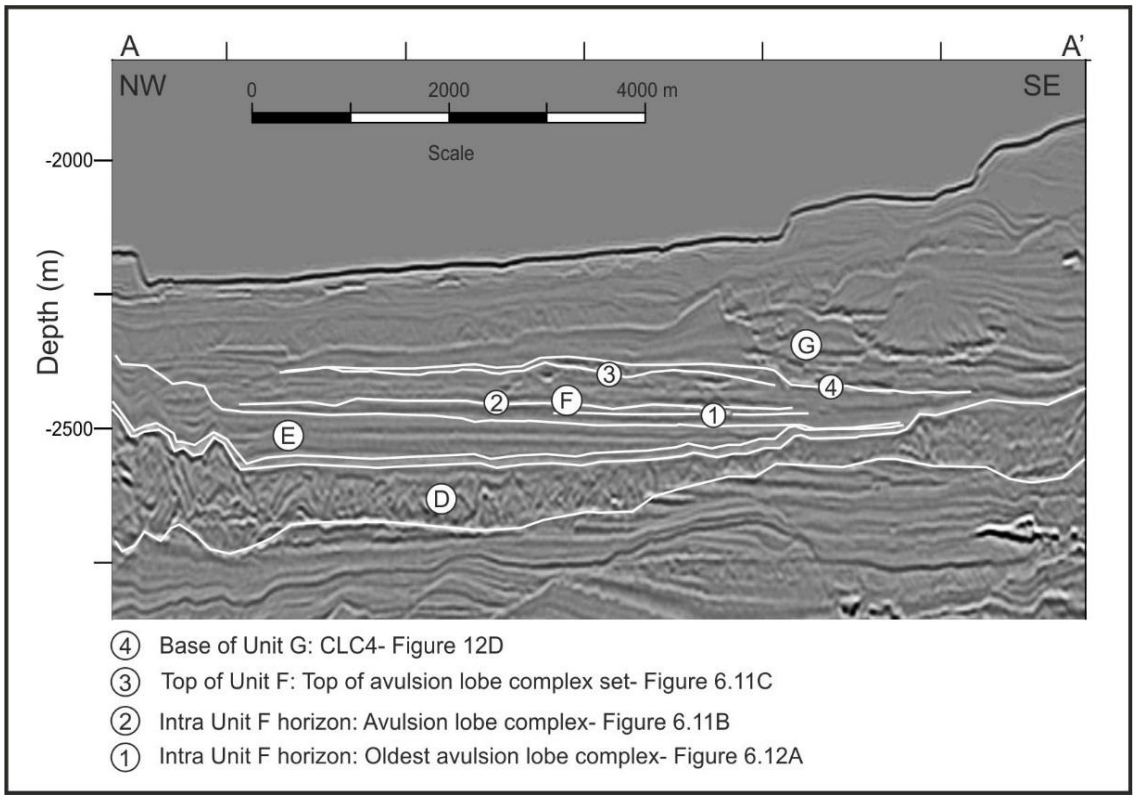

Figure 7.10. Detailed seismic line to indicate the stratigraphy of the avulsion lobe deposits that overlie CLC3. The location of the line is shown in Fig. 7.11A.

7.4.7 Seismic Unit G: Channel-levee complex-set (CLC) 4

Unit G is composed of a channel-levee complex-set (CLC4) that overlies, and partly erodes, the avulsion lobe complex-set in Unit F to the west, and the top of the southern CLC3 levee to the north. It is overlain and eroded by a younger channel-levee complex-set that is not considered in this study.

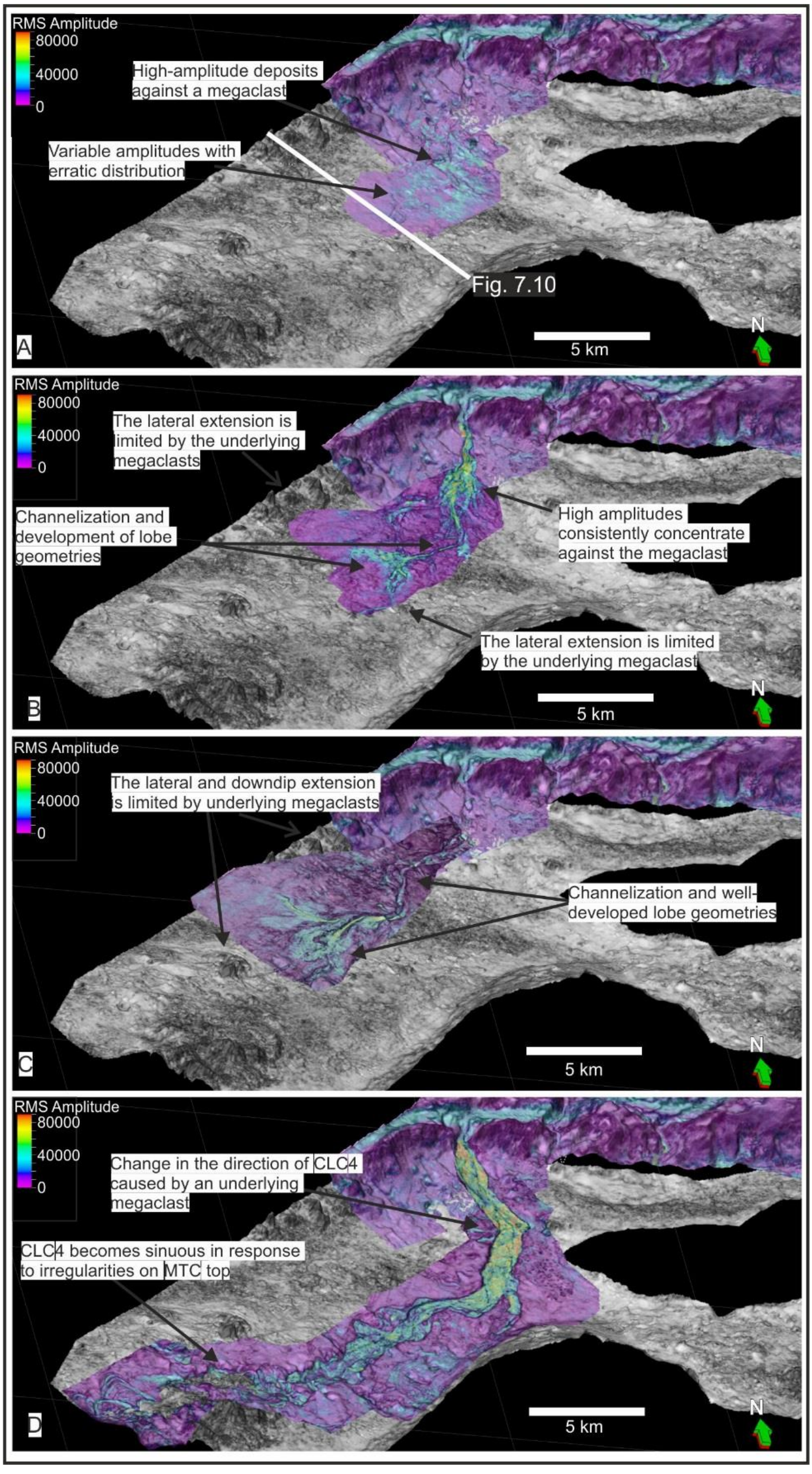

Figure 7.11. North-facing perspective views of RMS amplitude extractions 10 m above and below the reflections 1, 2, 3 and 4 in figure 7.10, overlain on variance extractions on the MTC top surface. **A.** The amplitude distribution of the oldest deposit is erratic and amorphous. **B.** At this stage a channelized segment develops before terminating in a high-amplitude lobe. **C.** High amplitudes become increasingly channelized and form well-developed lobes. The lateral extent and distribution is controlled by the position of underlying bathymetric highs. **D.** A new channel-levee complex-set (CLC4) develops to the east of the lobe complex-set. The channel orientation is controlled by the underlying bathymetry. Downstream, the increased Sinúosity and branching is related to the presence of protruding megaclasts.

CLC4 originates from CLC3, trending to the southeast before an abrupt change in direction to southwest (Fig. 7.11D). The southeastern levee of CLC4 is limited by the west-facing flank of the southern anticline. The northwestern levee terminates against the avulsion lobe complex-set (Unit F) and the CLC3 levee. From its intersection with CLC3 until c.10 km downdip, CLC4 is c. 1.5 km wide and c. 75 m thick. Its bounding levees have been partially eroded by subsequent channelized elements; the maximum levee thickness preserved is c. 150 m, and the maximum cross-sectional extent is c. 3 km. The channel-fill is composed of one or two high-amplitude reflections (c. 25 m) that are overlain and truncated by c. 50 m of chaotic reflections interpreted as a channel-confined MTC. Downdip, CLC4 is characterised by a series of channel complexes (c. 400 m wide and c. 50 m thick) that stack laterally and have sinuous planform geometries (Fig. 7.12). The sinuosity increases and the channel complexes become thinner (c. 30-40 m) as they approach a c. 9 km^2 irregular bathymetric high on the MTC top surface (Fig. 7.12). CLC4 is interpreted to be the culmination of the phase of avulsion when a channel-levee complex-set of a similar scale to CLC3 was established.

7.5 Discussion

7.5.1 Possible causes for shelf/slope instability

There are many MTCs in the top 1000 m of the stratigraphic succession of the Magdalena Fan in the study area, indicating that mass-wasting is a recurrent process. Most of them are confined to pre-existing channel-levee complex-sets (e.g. CLC1) or limited to the inter-channel lows and tend to be less than 100 m thick and limited in area. The MTC package in Unit D is considerably thicker (c .200 m) and covers an area of more than c. 470 km^2. The presence of three different headwalls suggests multiple episodes of mass-wasting; the absence of hemipelagites deposited between them, suggests that limited time elapsed between episodes and that they are related to a period of increased slope or shelf instability.

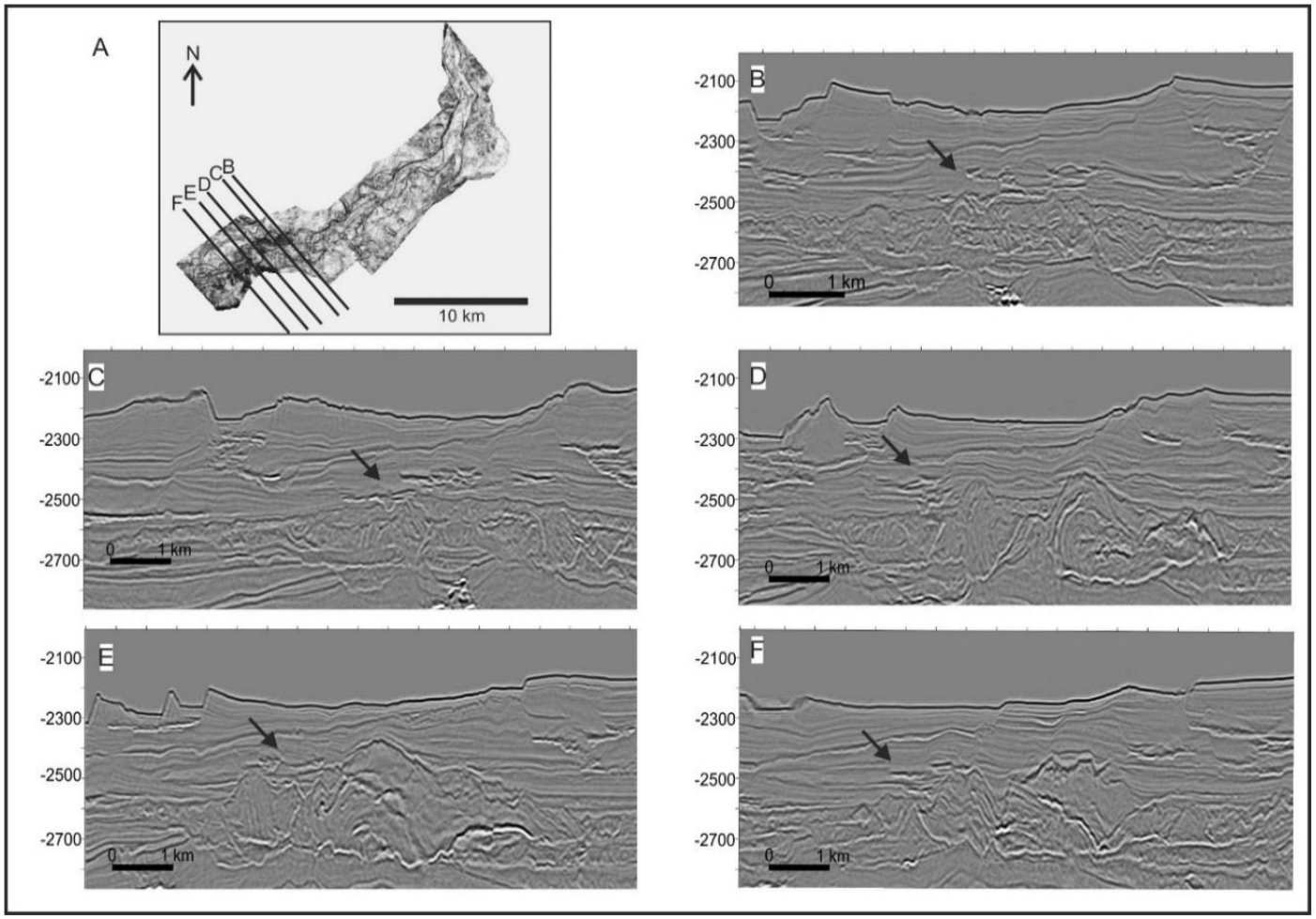

Figure 7.12. Changes in the response of CLC4 to the underlying bathymetric anomalies. **A.** Amplitude map overlain on a variance extraction at the base of CLC4. The updip segment is characterised by a consistent, relatively straight conduit, while the lower segment is increasingly Sinuous. The lines indicate the location of the seismic sections. **B-E.** Seismic sections showing the marked changes in the architecture of CLC4 in response to the underlying bathymetric highs. Arrows indicate the location of CLC4.

A number of different controls have been invoked to account for periods of slope instability, including increased sediment supply (e.g. Beaubouef and Friedmann, 2000; Manley and Flood, 2000; Dugan and Stigall, 2010; Masson et al., 2010), eustatic sea-level changes (e.g. Maslin et al., 1998, 2004; Masson et al., 2010), gas hydrate dissolution (e.g. Manley and Flood, 2000; Maslin et al., 2004; Grozic, 2010), seismicity (e.g. Frey Martinez et al, 2005; Alfaro and Holz, 2014; Vargas and Idárraga-García, 2015) and combinations of these controls. In Colombia, during the Pleistocene, uplift of the northern Andes and of the Sinú Fold Belt (Van der Hammen, 1958; Duque-Caro, 1979; Kolla and Buffler, 1984; Romero-Otero et al., 2010), were accompanied by high-amplitude eustatic and climatic changes (Van der Hammen, 1974; Hooghiemstra and Ran, 1994). Any combination of these factors could have potentially triggered the mass-wasting events that deposited the MTC in Unit D.

7.5.2 Channel avulsion

In the lower reach, the southern levee of CLC3 (Unit E) is almost entirely absent and it is overlain by a series of avulsion lobes (Unit F) that prograde at a high angle to the main direction of CLC3, and evolved into a channel-levee complex-set (CLC4, Unit G). The possible causes for channel instability in this location include: changes in sinuosity, changes in slope, in-channel aggradation and reduced channel relief, levee breaching by MTC erosion or channel plugging and levee slumping (Posamentier and Kolla, 2003; Kolla, 2007; Armitage et al., 2012; Brunt et al., 2013). In the study area, there is no evidence of CLC3 external levee erosion or channel plugging. The overall slope angle and the planform geometry of CLC3 remain constant through time and the avulsion is located in a relatively straight segment of the channel (Fig. 7.11). Therefore, changes in the channel sinuosity or the slope are not considered causes. However, the data available in this study only image a portion of CLC3 and it is unknown whether there were any foregoing significant changes in the channel's architecture, or avulsions downdip of the study area. However, if the avulsion documented here was the

consequence of downdip modifications in the architecture of the channel, changes in the channel-fill and a decrease in the channel cross-sectional area prior to the avulsion might be expected. Yet, no significant changes can be observed in the fill of the channel either updip or downdip of the avulsion point prior to the avulsion. This also suggests that the characteristics of the flows, which could reflect allogenic controls, remained relatively stable. Furthermore, downdip of the avulsion node, the post-avulsion channel-fill is composed of c. 175 m of parallel dim amplitude reflections interpreted to represent the abandonment of the complex, suggesting that at the time of the avulsion the channel was underfilled. Also, both updip and downdip of the avulsion node the levee crests are sub-vertically aligned meaning that the cross-sectional area of the channel had not been reduced before the avulsion.

It can be noted, however, that, the architecture of the CLC3 southern levee varies in response to the underlying bathymetry. A physiographic feature on the seabed after emplacement of the MTC in the middle and lower reaches was a downstream tapering ridge formed by a remnant of Unit B (Figs. 7.8, 7.9 and 7.13). In the middle reach, the remnant ridge of Unit B separated CLC3 (Unit E) from the bathymetrically lower top surface of the MTC (Unit D) (Fig. 7.8). Onlap of the basal reflections of the southern levee of CLC3 against the remnant ridge of Unit B indicate that initially, the levee was confined by the remnant ridge of Unit B. Later it overstepped the narrow ridge and built out into the bathymetric depression generated by the MTC (Fig. 7.13D). The geometry of the CLC3 southern levee indicates that it had to steepen into the low as it built outwards. Locally, a discontinuity in the reflections within the levee package can be traced from the cusp of the irregular underlying deposits to the crest of the levee (Figs. 7.8F, 7.9F and 7.13). Farther downdip, a package of chaotic reflections overlies the top levee surface, indicating local collapse of the levee (Fig. 7.8E). In figure 7.9B the ridge of Unit B is less than 500 m wide and the southeastern levee of CLC3 is almost entirely absent; local remnants of the CLC3 levee are overlain by the younger avulsion lobe

complex-set in Unit F. Downdip of the avulsion, the discontinuity in the levee reflections is also present (Fig. 7.9C-F) and there is evidence of levee collapse (Fig. 7.9D).

The observations of the seismic stratigraphy suggest that the discontinuity in the levee acted as slip surface above which it collapsed towards the bathymetric low above the MTC (Fig. 7.13). Therefore, the most-likely cause for the location of the channel avulsion is interpreted as levee instability and collapse due to an unstable levee geometry that was imposed by underlying bathymetric anomalies. This pre-disposition of the levee to collapse effectively pre-determined the location of the avulsion node.

An additional contributory mechanism towards the levee instability and collapse is considered to be the composition of the substrate. At the location of the point of avulsion, the inner external southern levee (*sensu* Kane and Hodgson, 2011) was deposited onto CLC1 and the erosional remnant of Unit B whereas the outer external levee was deposited onto the MTC (Fig. 7.13D). Differential compaction of the rapidly deposited debrites with respect to the channel-levee deposits in Unit B and CLC1 could have caused syn-sedimentary steepening of the outer external levee leading to levee collapse. However, the increased thickness of the basal levee deposits outboard of the remnant of Unit B (Figs. 7.9F and 7.13D) suggests that Unit B was a bathymetric high on the seabed at the time that CLC3 started to deposit. Therefore, although the different substrate characteristics may have contributed to the instability, the principal cause for the irregular levee geometry is likely the irregular underlying bathymetry.

Previous studies have suggested that levee collapse is not a significant cause of channel avulsion and it has been considered to be a random process (Kolla, 2007). In this example, the relationship between the inherent instability of the levee and the bathymetric anomalies demonstrates that levee collapse and subsequent avulsion are not spatially random processes, particularly when the bathymetry beneath the external levee is irregular.

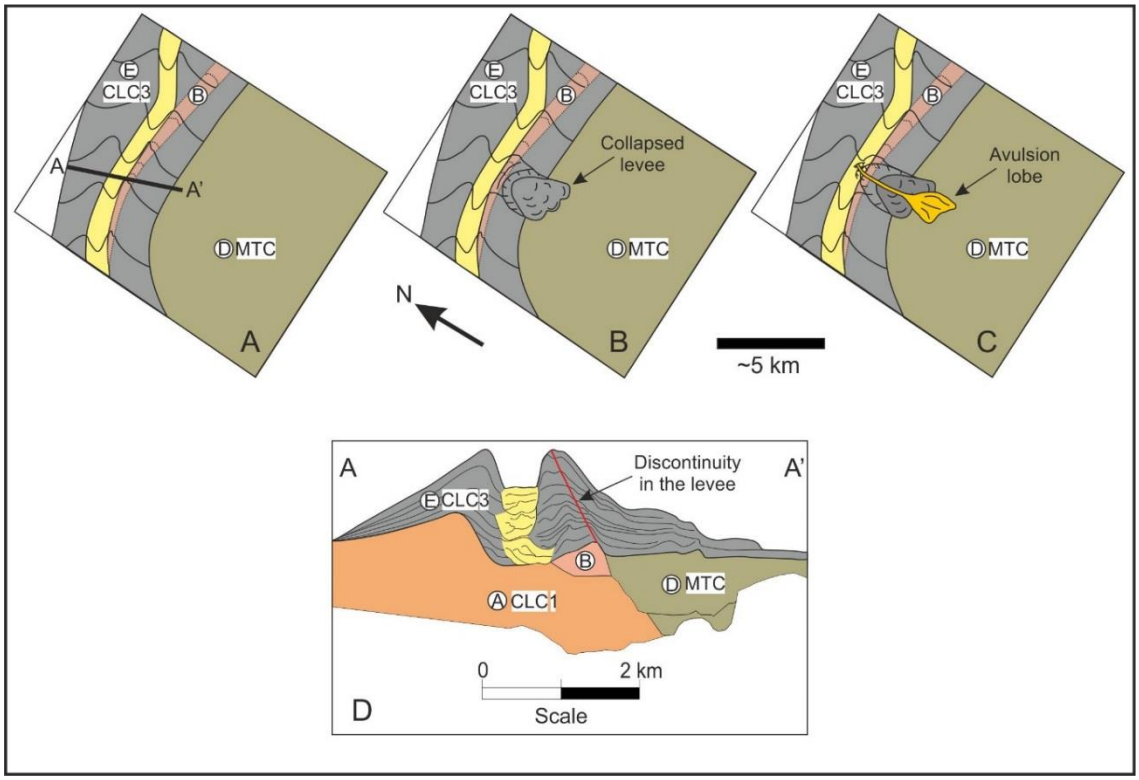

Figure 7.13. Schematic line drawings summarising the evolution of the CLC3 levee collapse and the initiation of avulsion. The circled letters denote the seismic units. **A.** Map view cartoon showing the configuration of CLC3 before the collapse of the levee. Note the location of the underlying Unit B remnant ridge. **B.** Initial levee collapse. **C.** Updip erosion and channel avulsion. **D.** Cross-section representing the interpreted configuration of the channel-levee complex-set prior to collapse and avulsion. The location of the line of section is shown in A. The remnant of Unit B caused a discontinuity in the overlying levee which developed into a slip surface along which the levee collapsed.

7.5.3 Evolution of the avulsion lobe complex-set

The emplacement of the MTC primed the system for a cycle of channel avulsion and a major change in sediment dispersal patterns. The collapse of the CLC3 levee led to the development of a series of avulsion lobe complexes, and ultimately the construction of a new channel levee complex-set (CLC4), which developed at a high angle to the parent channel complex-set (Fig. 7.11). The avulsion lobe complex-set was deposited above the partially healed, but irregular top MTC surface. The downdip reach and the strength of the amplitude response of the avulsion lobes increases through time (Fig. 7.11). In the absence of well penetrations we infer that higher, brighter amplitudes are a reasonable proxy for sand content while lower, dimmer amplitudes represent mud-prone facies. A similar approach has been taken by many authors where well calibration is not available

(e.g. Abreu et al., 2003; Deptuck et al., 2003; Posamentier and Kolla, 2003; Gee et al., 2007; Cross et al., 2009; Catterall et al., 2010). In this study, this reasoning is supported by the clear physiographic expression of the high-amplitude areas that are concentrated within channelized conduits and that are connected to well-defined lobate features (Figs. 7.11A-C).

The avulsion lobe complex-set (Unit F) starts with a single cycle reflection that onlaps the southeastern levee of CLC3 to the north. Internally, seismic amplitudes are low and only a few slightly higher amplitude streaks can be seen to originate from a higher amplitude cluster at the toe of the levee (Fig. 7.11A). Using the amplitude response as a guide, these early deposits are probably mud-rich and/or contain mud clasts through the entrainment of the fine grained material from the collapsed levee. Most of the sediment load is thought to have been deposited at the toe of the levee in response to the abrupt gradient change (Fig. 7.13). These deposits could perhaps share similarities with the matrix-rich packages interpreted by Terlaky and Arnott (2014) and Terlaky et al. (2016) as avulsion splay deposits in the Neoproterozoic Kaza Group, Canada.

As the avulsion cycle progressed sediments were transported farther away from the parent channel as indicated by the higher amplitudes in the form of channelized features that fed lobes (Figs. 7.11B and C, and 7.13). The higher amplitudes are interpreted as sand-rich sediments close to the mouth of the feeder conduit, and the surrounding lower amplitudes are interpreted as mud-rich deposits that concentrate at the fringes of the lobes (e.g. Prélat et al., 2009). The high-amplitude, sand-prone deposits in figure 7.11 are similar to HARPs, first described from the Amazon Fan and interpreted to be proximal deposits laid down early in an avulsion cycle (Pirmez et al., 1997). As the avulsion cycle continued to develop, a single channel conduit fed a high-amplitude avulsion lobe complex that comprises at least three lobes (*sensu* Prélat et al., 2009), and formed downdip of the aligned megaclasts (Fig. 7.11C). This avulsion lobe complex has a

thickness of c. 40 m and the high amplitudes have an area of c.11 km^2 yielding a rock volume of c. $440x10^6$ m^3.

The latest stage of the avulsion cycle is marked by the formation of a new channel-levee complex-set that was similar in scale to CLC3. At the point of avulsion, the new channel is bounded by the older unrelated levee of CLC3. A similar configuration of a channel complex-set cutting through the levee of another system at high angle has been reported from outcrop (Brunt et al. 2013). The bathymetric configuration guided the channel-levee complex-set to the southeast meaning that the avulsion lobe complex-set is well preserved (Fig. 7.14D). Down-flow, the channel encountered a 9 km^2 irregular bathymetric high; at this point there is an associated increase in channel sinuosity, a tendency for frequent lateral migration and ultimately a deflection of the channel to the west (Figs. 7.11D and 7.12).

The slope from the collapsed levee to the area above the MTC would have evolved from an initial out-of-grade profile towards a smooth equilibrium profile through increased sedimentation at the toe of the collapsed levee, enabling the flows to increase their run-out distance (Fig.7.13). The inferred increase in the amount of sand in successive avulsion lobe complexes is thought to be in part related to the healing of the avulsion node and the updip incision and entrainment of the sand-prone axis of the parent channel-levee complex-set (Fig. 7.13).

The onlap patterns and the map view geometries indicate that the irregularities present on the seabed, which were inherited from the rugose top surface of the MTC, played an important role in defining the location, and geometry of the avulsion lobes. Figure 7.14 shows the position of the underlying megaclasts that are interpreted to have influenced the sedimentation patterns of the avulsion lobes. The northernmost arrows in figure 7.14A and B show that the concentration of high amplitudes at the toe of the collapsed levee was influenced by the presence of several megaclasts protruding from the underlying MTC top surface as well as by the abrupt change in slope gradient.

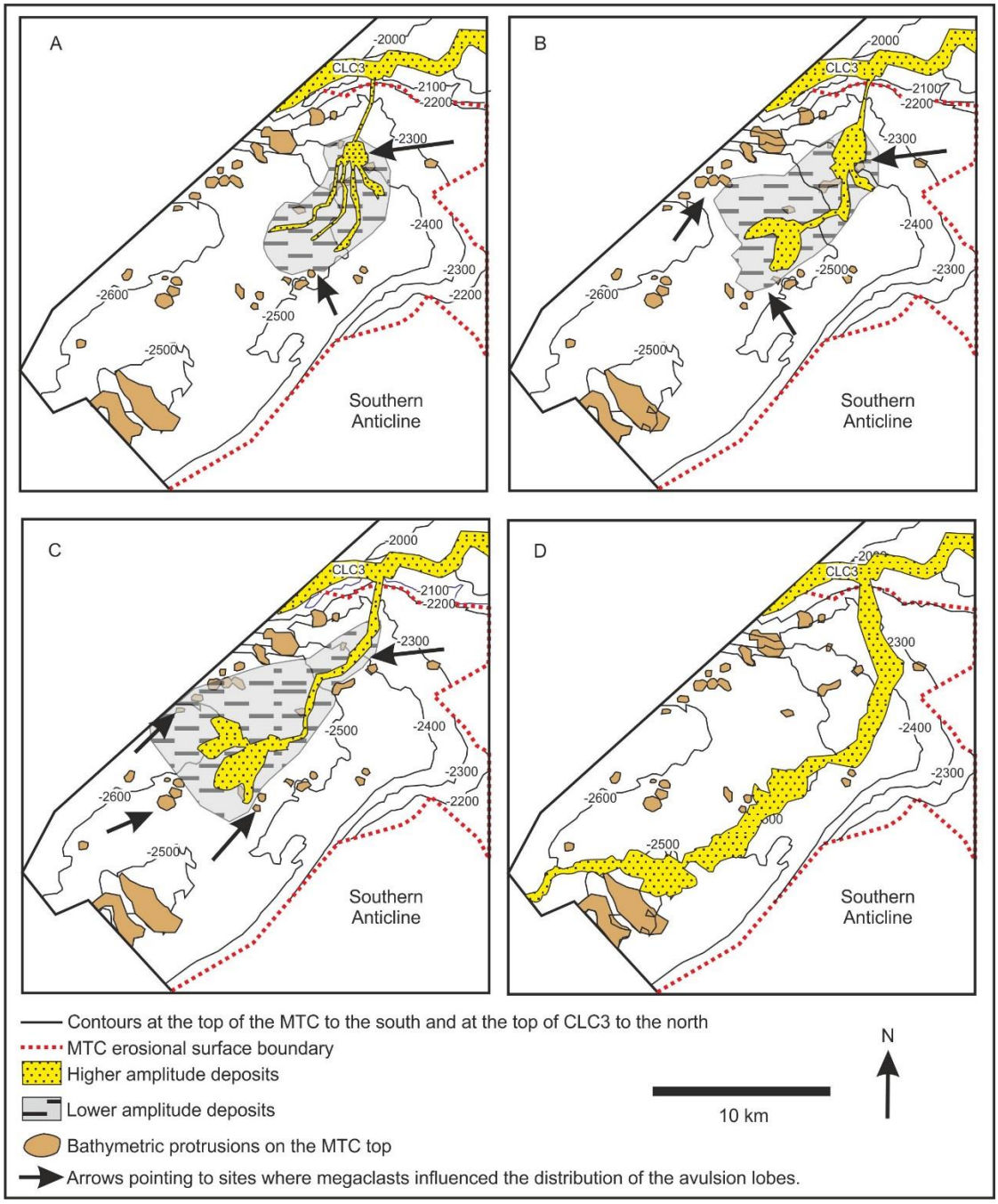

Figure 7.14. Cartoon highlighting the interaction between the avulsion lobe deposits and the underlying bathymetric anomalies. **A-D)** Stages of evolution of the CLC3 avulsion. The contours are elevation at the top of the MTC and CLC3 and constitute a proxy to the bathymetry underlying the lobes; however this had been partially healed by the CLC3 southern levee. The arrows point to the areas influenced by the bathymetric anomalies discussed in Section 7.5.3.

In figure 7.14B, the channelized conduit is located between two megaclasts. Downdip, the extent of the avulsion lobe deposits is influenced by a subtle increase in the elevation of the underlying surface and by a series of aligned megaclasts (Fig. 7.14A-C). The southeastern limit of the lobe complexes remains relatively constant through time and

the younger deposits extend to the southwest and northwest where they are limited by a series of aligned megaclasts at the toe of the CLC3 levee (Fig. 7.14B and C). The aligned megaclasts to the south of the youngest lobe complex (Fig. 7.14C) seem to have influenced the deflection of the resulting lobe deposits to the northwest. Also, the position of the transition between the channelized segment and the lobes may have been influenced by the decrease in the size and frequency of the underlying megaclasts towards the western edge of figure 7.14C.

7.5.4 Implications

MTCs can comprise as much as 90% of the overall stratigraphy of submarine slope systems (Posamentier and Martinsen, 2011). They are particularly significant in number and size on active margins where large scale MTCs may be triggered by tectonic activity (Frey Martinez et al., 2005; Moscardelli et al., 2006). MTCs can modify the seascape and create accommodation. They can also alter sediment dispersal patters as illustrated by the CLC3 avulsion cycle with the formation of an avulsion lobe complex-set and a channel-levee complex-set almost perpendicular to the direction of the parent channel and the regional downdip direction. Also, the irregular top surfaces of MTCs influence the distribution and evolution of the subsequent deposits (e.g. Frey Martinez, 2005; Pickering and Corregidor, 2005; Jackson and Johnson, 2009; Alves, 2010; Olafiranye et al., 2013). This is shown by the association between the morphology and distribution of the avulsion lobe deposits in Unit F and the location of the protruding megaclasts in the underlying Unit D.

The relationship proposed in this case study between the irregular seabed bathymetry resulting from MTC erosion and emplacement and the levee collapse and subsequent channel avulsion, suggests a link between the probability of channel avulsion in active tectonic margins and the irregular substrates produced by large-scale MTCs. However, more studies are required to test the applicability of this relationship to other areas.

Avulsion lobe complexes can be important hydrocarbon reservoir targets on submarine slopes otherwise dominated by sediment bypass. These could stack to form significant thicknesses in bathymetric depressions such as those created by MTC erosion. If there is a link between MTC emplacement and channel avulsion on active margins, avulsion lobe complexes could be important targets in such settings. The changes in amplitude and morphology suggest that there is an evolution of the avulsion lobes from mud-prone to sand-prone that may record the decrease in the amount of fines available to be entrained during the healing of the avulsion node. In this case, the youngest avulsion lobes are likely to exhibit the best reservoir quality sandstones.

7.6 Conclusions

Mass-transport complexes (MTCs) can quasi-instantaneously modify the seascape, leading to widespread changes in sediment dispersal patterns (e.g. Frey Martinez et al., 2005; Moscardelli et al., 2006; Moscardelli and Wood, 2008; Vinnels et al., 2010; Brunt et al., 2013; Olafiranye et al., 2013). Their irregular top surfaces influence the distribution and the evolution of subsequent deposits (e.g. Frey Martinez et al., 2005; Olafiranye et al., 2013).

This study has described the relationship between the emplacement of an MTC and the location and evolution of a subsequent channel avulsion and its associated lobe complex-set. The substrate entrainment by the MTC resulted in the development of a narrow remnant of older stratigraphy that formed a bathymetric anomaly, above which a steep levee succession grew. The resulting instabilities led to the development of an internal discontinuity from the crest of the levee to the cusp of the bathymetric high which acted as a slip surface above which the levee collapsed towards the bathymetric low above the MTC, thereby establishing the location of the avulsion node.

The geometries and the amplitude responses of the avulsion lobes indicate that they were initially mud-rich. They were probably charged with fine grained sediment through

the entrainment of in-situ and collapsed levee material in the early stages of avulsion. The younger avulsion lobe complexes are more sand-rich due to the entrainment of the sandy channel-axis sediment in the channel reach above the avulsion point as the mature, post-avulsion axial gradient was progressively established. The distribution, morphology and evolution of the avulsion lobe complex-set, as well as the subsequent development of the channel-levee complex-set, is the consequence of the interaction of the sediment gravity flows with the underlying bathymetric anomalies as the channel system adjusted to the breach of the levee.

Channel avulsions driven by autogenic processes alone do not adequately explain avulsion patterns on highly irregular slopes that are prone to mass-wasting processes. Tectonic activity has been linked to the emplacement of large scale MTCs (Frey Martinez et al., 2005; Moscardelli et al., 2006), so MTC-related channel avulsion processes may be a common and important process on active plate margins. This study indicates that the points of avulsion on active margins are possible sites for the development of sand-prone intervals in relatively proximal locations. However, the wider occurrence of this sediment distribution pattern on tectonically active margins needs to be established by further study.

8 Discussion and Conclusions

8.1 How does seabed bathymetry influence the emplacement processes and architecture of MTCs, channel-levee complex sets and avulsion lobes?

8.1.1 Bathymetric effects on channel-levee complex sets and avulsion lobes

Seabed bathymetry has been widely recognised as an important influence on the emplacement processes of turbidity currents and sedimentary architecture of turbidite successions (e.g. Piper and Normark, 1983; Kneller and McCaffrey, 1999; Haughton, 2000; Pirmez et al., 2000; Prather, 2003; Amy et al., 2004; McCaffrey and Kneller, 2004; Smith, 2004; Hodgson and Haughton, 2004; Jolly, 2014; Kneller et al., 2015; Patacci et al., 2015). Numerous studies on the interaction between submarine channels and syn-sedimentary tectonic deformation have documented the effect of structural relief on the architecture and evolution of submarine channels (e.g. Haughton, 2000; Prather, 2003; Heniö and Davies, 2006; 2007; Gee and Gawthorpe, 2006; Gee et al., 2007b; Clark and Cartwright 2010, 2012; Mayall et al., 2010; Jones et al., 2012; Jolly, 2014). These studies have found that submarine channels can be blocked or deflected by structural highs and diapirs, become ponded in synclines or salt-or-shale-withdrawal basins (e.g. Booth et al., 2003; Prather, 2003; Gee and Gawthorpe, 2006; Clark and Cartwright, 2009, 2011; Vinnels et al., 2010; Jones et al., 2012) and aggrade laterally as they shift away from growing structures (Mayall, 2010; Clark and Cartwright, 2009, 2011; Kane et al., 2010; Jones et al., 2012). In this study, a similar effect is observed in the study area, with channel-levee complexes concentrating towards the northern part of the study area after emplacement of Unit IV, likely under the influence of the evolving structural relief (Fig. 8.1A-E). The effect of smaller-scale bathymetric features has received less attention; with most studies focusing on MTC-related relief, such as bathymetric lows created by

slide scars and irregular relief at the top of MTCs (e.g. May et al., 1983; Mutti et al., 1988; Brami et al., 2000; Lowe, 2004; Moscardelli et al., 2006; Jackson and Johnson, 2009; Kertznus, 2009; Alves, 2010; Olafiranye et al., 2013; Kneller 2015; see Section 8.2). In this study, bathymetric highs resulting from MTC erosion and sedimentation are shown to have affected the evolution of channel-levee complex sets basinwards from growing tectonic structures (Chapter 7). The architecture of the southern levee of Unit E is interpreted to have been influenced by a c. 20 km long and c. 1 km wide erosional remnant (Unit B) that was left after the emplacement of the MTCs in Unit D (S5-S6, C1 and N1-N2). This erosional remnant mostly affected the over-spilling flows that constructed the levees; these fine-grained, highly depositional, waning flows (cf. Straub and Mohrig, 2008; Kane and Hodgson, 2011; Hansen et al., 2015) draped the ridge and healed its bathymetric expression. The resulting architecture of the levee was irregular and unstable, leading to levee collapse and channel avulsion (Fig. 7.13). Therefore, even though the bathymetric anomaly was relatively small its effect on the overspilling flows that constructed the levee was significant.

Subsequently, the emplacement processes, architecture and evolution of the avulsion lobes in Unit F (Chapter 7) were themselves influenced by the underlying rugose relief of Unit D. Initially, these unconfined flows were mostly emplaced at the toe of the collapsed levee (Fig. 7.11A), reflecting a change in the axial gradient that led to rapid sedimentation (cf. Kneller; McCaffrey and Kneller, 2004). As this slope was healed, subsequent flows propagated farther onto MTC C1 where they were influenced by relief associated with megaclasts protruding at the MTC top (Figs. 7.11B and C and 7.14). Despite being relatively small (protruding some 80-100 m above the surrounding deposit and being no more than 1.6 km^2 in area), some megaclasts affected the geometry and distribution of the avulsion lobes because they were aligned forming a composite bathymetric high that limited the lateral lobe extent (Figs. 7.14 and 8.1C). The post-avulsion channel-levee complex set in Unit F, was also greatly affected by the underlying

bathymetry. In this case, structural relief to the east and depositional relief to the west determined the flow-pathway of Unit G, which was perpendicular to the overall slope direction for over 24 km (Fig. 8.1C). This channel developed anomalous internal architectures resulting from increased sinuosity and multiple bifurcations as it interacted with megaclasts protruding from the top of MTC S5 (Fig. 7.11D and 7.12).

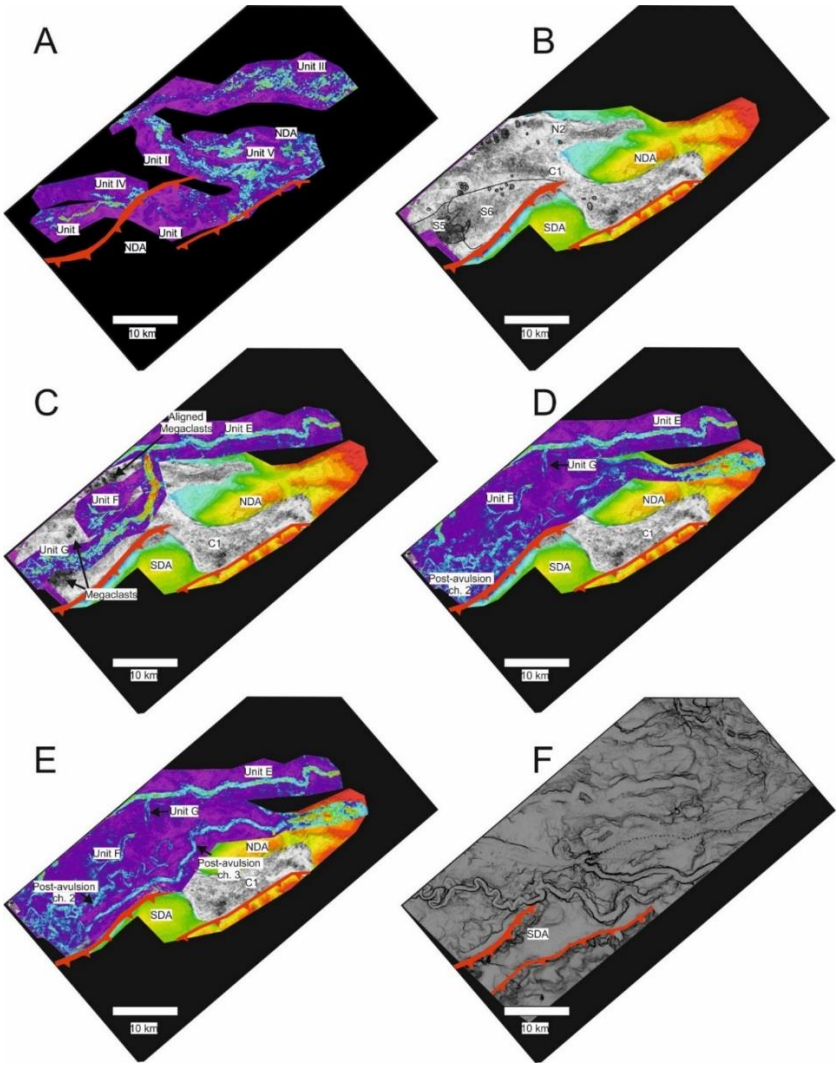

Figure 8.1. Channel location and evolution in the study area. **A.** Amplitude extractions for the six channel-levee complex sets that underlie MTCs S1-S6, C1 and N1-N2. Note that Units I and IV are located to the south and are folded into the SDA, Unit III is to the north of the NDA and Units V and VI traversed the NDA. **B.** Variance map at the composite top surface of MTCs S6, C1 and N2 overlain on a depth map of the basal surface of Unit D. **C.** Amplitude extractions of units E, F and G overlain on B. Note that Unit E followed a similar path to Unit III and that the avulsion lobes were affected by megaclasts to the NW and SW and the orientation of Unit G, which flowed almost perpendicular to the downslope direction, and its high Sinúosity above megaclasts protruding from S5. **D.** Amplitude map of the channel-levee complex set that developed after Unit G (Post-avulsion channel 2). Note that it followed the path of MTCs N1-N2. **E.** Amplitude map showing the third post-avulsion channel which was located to the E of Unit G and the post avulsion channel 2. It also followed the path of MTCs N1-N2. **F.** Seabed dip map showing channel levee complex sets that occupied the underfilled erosion surface of C1, healing it and degrading the NDA.

8.1.2 MTCs

The effects of seabed bathymetry on mass-flows have been documented by previous studies; it is widely accepted that MTCs are associated with degradation of bathymetric highs such as volcanic islands, diapirs, and salt and tectonic structures (e.g. Moore et al., 1989; Gee et al., 2006; Heniö and Davies, 2006; Alves and Cartwright, 2009; Vinnels et al., 2010; Jones et al., 2012; see Section 8.3). Also, in areas of active structural seabed deformation, the distribution and magnitude of the resulting MTCs usually change with the development of structural uplift (e.g. Clark and Cartwright, 2012; Festa et al., 2015; Pérez et al., 2016). Moreover, MTCs have been recognised to be laterally confined by tectonic structures, diapirs, submarine channels and inter-channel lows (e.g. Masson et al., 1997; Brami et al., 2000; Moscardelli et al., 2006; Alves and Cartwright, 2010; Georgiopoulou et al., 2010; Romero-Otero et al., 2010; Vinnels et al., 2010; Jones et al., 2012), ponded within piggy-back or salt-withdrawal basins (e.g. Vinnels et al., 2010; Jones et al., 2012; Alfaro and Holz, 2014; Jones et al., 2012), or blocked against structural highs (Jones et al., 2012). Despite a plethora of evidence of the influence of bathymetry on mass-flows in the literature, previous studies have not implicitly addressed the effects of the interaction between mass-flow processes and bathymetric features on the architecture of MTCs. In Chapter 6, changes in the flow direction of MTC C1 are shown to have been caused by the configuration of the structures, with C1 following the orientation of the syncline, and the breach of the downdip anticline occurring at the saddle between the two segments of the structure. This shows that similar to submarine channels, mass-flows interact with structural highs, and that their flowpaths and distribution can be influenced by them. Changes in source areas and distribution of MTCs (which are reflected in the characteristics of the deposits, and are interpreted to have been influenced by growth and along-strike propagation of the structures) are documented in Chapter 5 and are further discussed in Section 8.4.

To the west of the structural highs, the depositional relief of channel-levee complex sets was an important control on the flow-pathways and internal architecture of MTCs (Chapter 6). Four types of interactions between MTCs and channel levee complex sets, which represent end-members of a continuum, are documented (Fig. 6.12): Type 1 refers to mass-flows that overlie and exploit channel-levee complex sets, such as N1-N2, becoming entrenched along the channel axis and confined within the external levees. Similar interactions have been documented offshore NW Africa in the Sahara Landslide (Georgiopoulou et al., 2010) and the Canary Debris Flow (Masson et al., 1997), both of which exploited underlying channels. Type 2 corresponds to mass-flows that propagate along inter-channel lows, such as C1 directly basinward of the downdip anticline (DA); this type of interaction was also observed by Romero et al., 2010 to the north of the study area. Type 3 occurs when the direction of mass-flows is oblique to the orientation of the underlying channel-levee complex sets and the mass-flows are deflected, such as in the northwestern limit of C1 where it was deflected by the underlying levee of Unit III. In a similar way, offshore NW Africa, Georgiopoulou et al. (2010) noted that MTCs were locally deflected around “small bathymetric highs”. Finally, Type 4 occurs when the direction of the mass-flow is perpendicular or highly oblique and the height of the levee exceeds the thickness of the mass-flow so that the latter is blocked by the levee. This is interpreted to have occurred in MTCs S1-S3 which onlap the southern levee of Unit I to the north.

In C1, the occurrence of contractional deformation updip of the bathymetric highs is interpreted to have resulted from flow deceleration as it was diverted by the NDA and by the underlying levee to the NW (Fig. 6.12). Conversely, acceleration of the flow across the higher gradient slope and the constriction above the western flank of the DA is represented by erosion of the anticline and drastic thinning of the deposit, which is formed by megaclasts in a sparse low-amplitude matrix (Fig. 6.8 and 6.10A). Georgiopoulou et al. (2010) also observed thinning of the Sahara Slide and increased

erosion at the base across a bathymetric constriction. Towards the margins of C1, increased disaggregation is observed (Fig. 6.8) and is interpreted to have resulted from increased friction against the shallowing erosional surface. This is consistent with observed increases in disaggregation towards the margins of MTCs offshore Brazil (Gamboa et al., 2011; Alves and Cartwright, 2009). Increased friction against the margins is also interpreted to have caused local entrainment of large megaclasts that occur in clusters overlying erosional scours (Fig. 6.11). Therefore, the configuration of the seabed over which C1 propagated, which was dominated by structural highs to the east and high-relief levees to the west, is interpreted as a key control on its distribution, flow-pathways and internal characteristics. The distribution and flow pathways of S1-S6 and N1-N2 are interpreted to have been controlled mainly by the depositional relief of the underlying channel-levee complex sets. The interaction between the mass-flows and the seabed is also likely to have influenced their runout distances and rheological evolution (see Chapter 6 and Section 8.3).

Interactions between sediment gravity-flows and bathymetric perturbations depend on the height, areal extent and orientation of the bathymetric features with respect to the thickness and character of the flow. Strongly depositional, unconfined flows associated with the emplacement of levees and avulsion lobes are more likely to be affected by smaller bathymetric irregularities such as small erosional remnants or megaclasts (as well as larger bathymetric elements); while more powerful erosional flows such as channelized turbidity currents and large erosional mass-flows are more likely to be affected only by larger bathymetric features like tectonic structures and high-relief levees. However, it is important to note that the dimensions of the bathymetric features do not necessarily determine their importance for the overall evolution of sediment dispersal patterns. This is illustrated by the fact that relatively small bathymetric highs resulting from MTC erosion and emplacement influenced the avulsion of Unit E and controlled the

distribution, geometries and architecture of units F and G, thereby causing significant and long-term changes in the system (Fig. 8.1).

This study has contributed to our understanding of the effects of seabed bathymetry on the emplacement processes and architecture of MTCs, channel-levee complexes and avulsion lobes by demonstrating that: i) the architecture, geometries and distribution of MTCs, channel-levee complex sets and avulsion lobes, are affected by bathymetric irregularities on the seabed at various scales; ii) the interaction between channelized and unconfined turbidity currents with MTC-related bathymetric highs (i.e. megaclasts and erosional remnants) can determine the distribution of the overlying deposits (channel axes, levees and avulsion lobes) and result in anomalous geometries and stacking patterns; iii) mass-flows interact with structural highs and channel-levee complex sets, and this interaction is reflected in the morphology, distribution and internal characteristics of MTCs; iv) the stratigraphic evolution of slope settings dominated by MTCs and channel-levee complex sets, is characterised by a feedback effect, in which the bathymetric expression of MTCs influences the emplacement processes and architectures of channel-levee complex sets and vice-versa.

Given that continental slope profiles are commonly irregular and dynamic, with active or inherited tectonic structures, salt and mud diapirs, channel-levee complexes, MTCs and contourites (Manley and Flood, 1988; Nakajima et al., 1998; Migeon et al., 2001; Piper and Normark, 2001; Skene et al., 2002; Steffens et al., 2003; Frey-Martinez et al., 2006; Heniö and Davies, 2006; Moscardelli et al., 2006; Gee et al., 2007; Clark and Cartwright 2009, 2012; Jackson and Johnson, 2009; Alves, et al., 2010; Gamboa et al., 2010; Romero-Otero et al., 2010; Vinnels et al., 2010; Alves et al., 2014b; Kneller, et al., 2015; Ducassou et al., 2015) it is expected that similar interactions between seabed roughness and sediment gravity flows occur on all continental margins. Hence, even though generalised models of the emplacement processes and resulting architectures of channel-levee complexes (e.g. Deptuck et al., 2003; 2007; Mayall et al., 2006; Hodgson

et al., 2011), avulsion lobes (e.g. Kolla, 2007; Armitage et al., 2012; Terlaky and Arnott, 2014; Terlaky et al., 2016) and MTCs (e.g. Prior et al., 1984; Weimer and Slatt, 2004; Frey-Martinez et al., 2005; Bull et al., 2009) constitute a powerful tool in the prediction of the presence, geometries, continuity and quality of reservoirs and seals, the local seabed morphology can induce important variations. Therefore a thorough understanding of the slope physiography at the time of sediment transport and deposition is crucial.

8.2 How can MTC emplacement influence the evolution of subsequent deep-water systems?

Mass-wasting events can remobilise large volumes of sediment, and therefore can cause major modifications to the seascape, both through erosion and deposition. In the evacuated headwall domain (*sensu* Bull et al., 2009), composite slide scars can create significant accommodation (e.g. May et al., 1983; Mutti et al., 1988; Lowe, 2004; Kertznus, 2009; Lonke et al., 2009; Kneller et al., 2015). Along the translational domain (*sensu* Bull et al., 2009), mass-flows can cause deep erosion, also modifying the seascape (Masson et al., 1997; Prior et al., 1984; Gee et al., 2006; Heniö and Davies, 2006; Lamarche, 2008; Alves and Cartwright, 2009; Morley, 2009; Joanne et al., 2013). In the toe domain, MTCs can be tens to hundreds of metres thick (Frey-Martinez, 2005; 2006; Moscardelli and Wood, 2008, 2015) and due to their internal heterogeneity they often have irregular tops that can affect the sedimentation patterns of subsequent deposits (e.g. Brami et al., 2000; Moscardelli et al., 2006; Armitage et al., 2009; Jackson and Johnson, 2009; Alves, 2010; Alves and Cartwright, 2010; Olafiranye et al., 2013; Kneller et al., 2015; Section 8.1). As noted above, this study has demonstrated that bathymetric irregularities resulting from erosional remnants left after the emplacement of C1, and N1 and N2, resulted in an abnormal geometry of the southern levee of channel-levee complex in Unit E. Also, megaclasts protruding at the top of MTCs C1 and S5 affected the geometries and distribution of the avulsion lobes and the architecture of channel-levee complex G (Chapter 7; Section 8.1). The relationship between the MTC-

related bathymetry and the collapse of the levee and subsequent avulsion of the channel, demonstrates that the influence of MTC topography can have a larger-scale and longer-term implication on the overall evolution deep-water systems.

In the study area, mass-wasting degraded the anticlines, and thus changes in MTC source areas occurred as the structures propagated to the north and new areas of the slope were uplifted and steepened (Chapter 5). By degrading the high and steep frontal flanks of the DA (downdip anticline) and the UA (updip anticline), and depositing in the lows represented by the syncline and the basin-low to the west, detached MTCs (S1-S5 and MTC remnants underlying C1 and N1) progressively smoothed the slope profile (Fig. 5.13). Northward propagation of the anticlines and the faults coring the DA and UA (Bernal-Olaya; Martinez et al., 2015) formed uplifted, unstable areas close to the shelf break and enabled the development of shelf-attached MTCs (C1, N1 and N2). The propagation of MTC C1 across the DA was likely facilitated by the fact that the anticline had already been degraded to some extent and that the syncline had been filled by syn-tectonic MTCs (Fig. 5.13). Similar processes in which degradation of the frontal limbs of anticlines have led to linking of isolated basins has been observed to the south of the study area by Vinnels et al. (2010), offshore Chile (Geersen et al., 2011), NW Borneo (Gee et al., 2009; Morley, 2009) and in the Niger delta slope (Heniö and Davies., 2006). The creation of this flow-path across the DA did not immediately lead to the capture of the turbidite fairway. Instead, following the development of Unit G (Fig. 8.1C) two channel-levee complex sets exploited the flow-path inherited from MTCs N1 and N2 and to the west of the DA continued almost perpendicular to the downslope direction (Fig. 8.1D and E). It was only in the latest stage of fan sedimentation in the study area that channel-levee complex sets exploited the flow-pathway that was inherited from C1 (Fig. 8.1F). These channels continued to degrade the folds and healed the erosion surface of C1. Re-establishment of channel-levee complex sedimentation across the DA could have been driven by updip avulsion or by back-stepping erosion at the headwall of C1.

Retrogradational failures connecting the shelf to failure scars has been documented in the East Breaks slide in the Gulf of Mexico, the Rosetta slide offshore Egypt and the Storegga slide offshore Norway (Piper and Behrens, 2003; Haflidason et al., 2004; Kertznus, 2009; Loncke et al., 2009).

This study has shown MTC emplacement can influence the evolution of subsequent deep-water systems at various scales; from local changes in the architecture of the overlying deposits as in units E, F and G, to fold degradation and sub-regional smoothing of the slope profile as seen across the DA, and to regional re-routing of turbidite fairways through capture of shelf-derived sediments. There are important implications in understanding for the sedimentary and petroleum systems in the Colombian Caribbean margin where structural growth, mass-wasting and turbidite sedimentation have been intimately related since Miocene times (Kolla and Buffler, 1984; Duque-Caro, 1979, 1984; Romero-Otero, 2009; Romero-Otero et al., 2010; Martinez et al., 2015). Moreover, these observations are potentially applicable to other basin margins where MTCs and turbidites co-occur.

8.3 How does substrate composition influence the evolution, facies and geometries of MTCs?

Erosion by mass-flows is a widely recognised process, with some flows gaining a large proportion of their volume through substrate erosion and entrainment (e.g. Prior et al., 1984; Gee et al., 2006; Lamarche et. al., 2008; Weimer and Slatt, 2007; Posamentier and Martinsen, 2011, Joanne et al., 2013). The ability of a mass-flow to erode depends on the characteristics of the substrate upon which it translates and on the characteristics of the flow, such as volume, velocity, rheology, clast support-mechanism, stress and strain distribution, and internal structure (Dykstra et al., 2011; Iverson, 2012; Day et al., 2015). Several studies have aimed to characterise the dynamics of mass-flows and it is widely accepted that mass-flows undergo transformations as they translate downslope either through sediment and fluid entrainment or sedimentation (e.g. Shanmugam et al.,

1994; Stow et al., 1996; Strachan, 2008; Georgiopoulou et. al., 2010; Omosanya and Alves, 2013). However, the role of substrate on MTC emplacement processes and its implications on deposit character is an understudied facet of mass-flow evolution. This probably reflects the fact that there is a complicated interaction between flow dynamics, erosion, sedimentation and fluid entrainment, and that isolating individual controls is therefore challenging.

Chapter 6 shows that the morphology of the basal erosion surface of MTC C1 may relate to changes in the lithology inferred for the substrate (Figs. 6.4 and 6.7). The depth of MTC erosion in several locations is deeper above channel axes than above the surrounding levees and more subtle changes were observed across levees related to different channels (Fig. 6.4). Moreover, variations in the lithology of the substrate also affected the flow-pathway of C1 by pre-determining the location of a breach in its lateral wall (Fig. 6.6). These findings suggest that different substrate types are variably susceptible to entrainment by overpassing MTCs. The higher clay content in levees (e.g. Babonneau et al., 2010; Kane and Hodgson, 2011; Morris et al., 2014; Hansen et al., 2015) can make them more cohesive. Rapid consolidation upon sedimentation due to electrochemical forces acting between clay particles can also make them more resistant to erosion (e.g. Mehta et al., 1989). Conversely, sandier channel axes (e.g. Mayall et al., 2006; Babonneau et al., 2010; Hodgson et al., 2011; Hubbard et al., 2014; Jobe et al. 2015) can be less cohesive and may contain higher pore-fluid volumes that make them more susceptible to liquefaction upon pore-pressure pressure increase as they are overridden by voluminous mass-flows. This process is invoked by Georgiopoulou, et al. (2010) to explain erosion and entrainment of a vocaniclastic sand layer underlying the Sahara Slide offshore NW Africa. Offshore New Zealand, Joanne et al. (2013) calculate that 40% of the volume of the Matakaoa debris flow corresponds to entrained material and propose that the high entrainment rates relate to the sandy nature of the substrate, which makes it more prone to MTC entrainment. Variable resistance to erosion may also

explain the absence of high-amplitude clasts within C1, despite local erosion of underlying channel axes. It is possible that sandy material liquefied and was incorporated as loose sand, or that due to their weak nature, sandy clasts were rapidly disaggregated and incorporated to the matrix. The later process was observed by Dykstra et al. (2011) in an outcrop in northwestern Argentina, where sandstone streaks originating from a megaclast surface were interpreted to record shearing of sand grains into the matrix of a debrite.

Given that substrate entrainment can change flow rheology, the previous observations imply that mass-flows that translate above sandy substrates may incorporate more sediment and become less cohesive than those translating above muddy substrates (e.g. Georgiopolou et al., 2010; Dykstra et al., 2011). Therefore, if we imagine debrites with identical compositions and flow structures, translating above a slope characterised by channel-levee complex sets, three hypothetical end-members could be defined: i) debrites that propagate above the channel axes would become entrenched, entraining sandy sediment and becoming less cohesive, possibly transforming into hybrid flows or into turbidity currents and propagating farther into the basin (Fig. 8.2A); ii) debrites propagating above levees (Fig. 8.2B), would become more cohesive, possibly freezing en-mass and having shorter runout distances and relatively simple basal surface geometries; and iii) debrites propagating above channel axes and levees would entrain different volumes and types of sediment at different locations, resulting in deposits with increased lateral heterogeneity and irregularly shaped basal surfaces (Fig. 8.2C). These simplified end-members are unlikely to represent MTCs developed in real slope settings because they disregard the effects of bathymetry (see Section 8.1) and inherent downslope changes in flow dynamics. They do, however, illustrate the importance of substrate characteristics on sediment flow pathways, runout distances and flow evolution, which are key to assessing hazard potential and the presence and continuity of underlying reservoirs, and in turn help to determine the characteristics of the resulting

deposits, which are key to predicting the ability of MTCs to act as hydrocarbon seals or reservoirs.

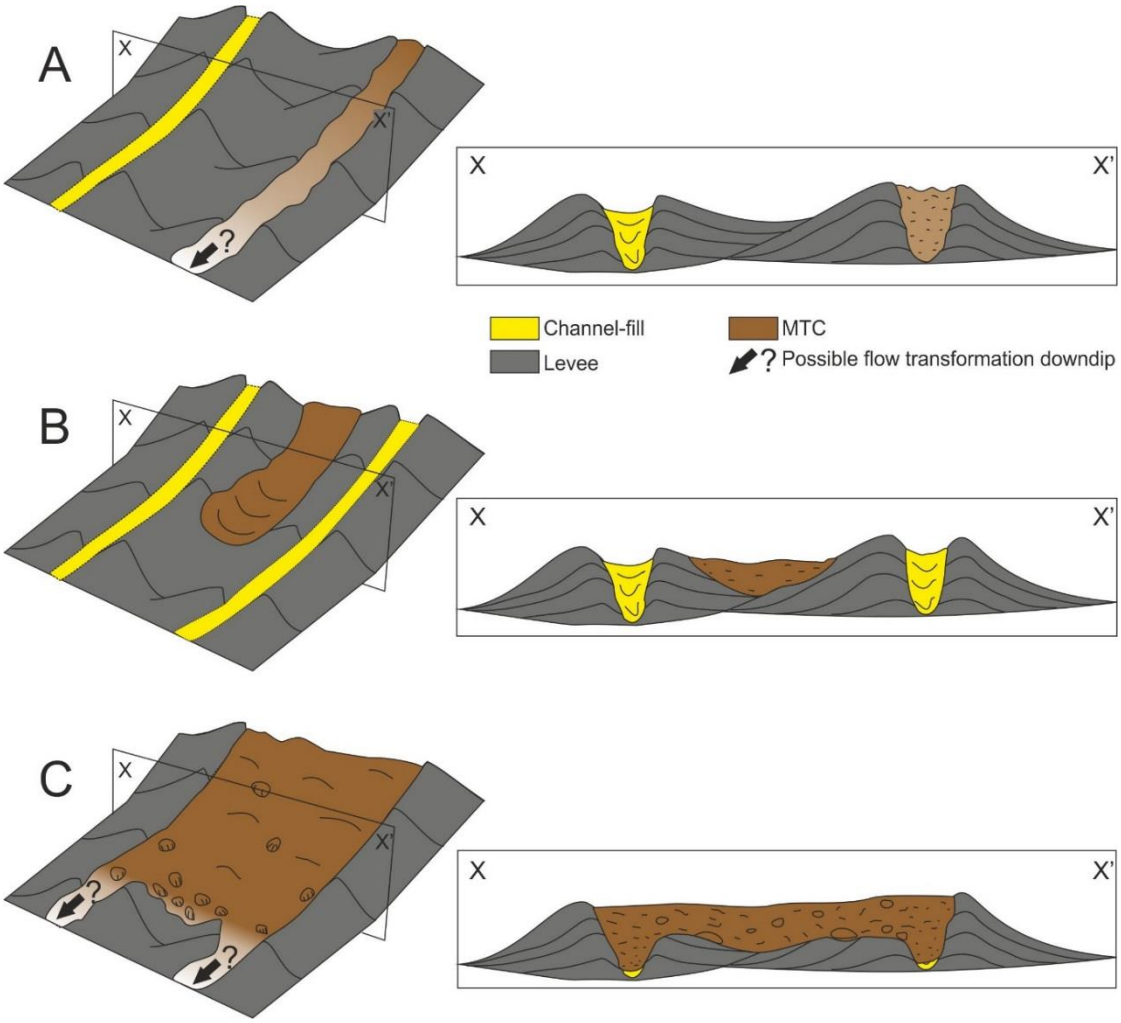

Figure 8.2. Schematic diagram illustrating the effect of substrate composition on mass-flow emplacement processes and the distribution, geometries and characteristics of the resulting deposits. **A.** MTC developed above an underlying channel axis. Note the deep, entrenched erosion surface. The debris flow would potentially become less cohesive downslope achieving longer runout distances and possibly transforming into a hybrid flow or turbidity current. **B.** Debrite developed along an inter-channel low. The emplacing flow would probably become more cohesive downslope resulting in shorter runout distances. Note the relatively simple basal surface, which displays subtle changes in geometry across different levees. **C.** Debrite developed above channel axes and levees. The emplacing flow would entrain different volumes and types of sediment at different locations, resulting in increased lateral heterogeneity and an irregular basal surfaces.

8.4 How can MTCs be used as a record of the style and timing of dynamic seabed deformation?

Within growth sequences, changes in the distribution, geometries and architecture of submarine channels have been used to establish the relative timing of structural uplift and turbidite sedimentation (Clark and Cartwright, 2009, 2011, 2012; Mayall et al., 2010; Jones et al., 2012; Alves et al., 2014b; Jolly, 2014). Because mass-wasting constitutes an important agent in the degradation deep-water fold-and-thrust belts (Heniö and Davies, 2006; Alves and Cartwright, 2009; Gamboa et al., 2010; Alves and Lourenço, 2010; Alves et al., 2014b), they can record periods of slope instability that in some cases can be related to dynamic seabed deformation (e.g. Alves and Lourenço, 2010; Clark and Cartwright, 2012; Alves et al., 2014b; Festa et al., 2015; Geersen et al., 2015; Pérez et al., 2016). However, there are only few studies that have used MTC emplacement as a tool to reveal the style and timing of seabed deformation and constrain the tectonostratigraphic evolution. Thus Clark and Cartwright (2012) reconstructed the evolution of the Bobo fold in the fold-and-thrust-belt in the Niger Delta using the distribution and architecture of MTCs and submarine channels. Alves et al. (2014b) demonstrate the effect of fold degradation and sediment bypass on the kinematic evolution of thrust-cored anticlines in the Nankai accretionary wedge offshore SE Japan, and correlated the development of an MTC with a period of increased deformation. In the Northern Italian Apennines, Festa et al. (2015) document systematic lateral and temporal shifts in the occurrence of MTCs along the Ligurian accretionary wedge and use this to constrain the tectonic evolution of the margin. More recently, Pérez et al., (2016) used the dimensions, and the vertical and lateral density of 1020 MTCs in several basins along the Scotia-Antarctic plate-margin to infer periods of increased slope instability and establish the timing of major tectonic events, thereby constraining the regional tectonic history.

In the study area, the distribution and size of MTCs S1-S6, C1 and N1-N2, is interpreted to have been controlled by the dynamic evolution of the structures (Chapter 5). Relative timing of folding and thrusting is interpreted based on the tectonic deformation of MTCs. MTCs S1-S5 (Fig. 5.7) are interpreted to have been emplaced during folding but before faulting, while S6 was most likely deposited during or towards the end of the last phase of faulting. The fact that MTCs C1, N1 and N2 are not folded or faulted suggests that they were deposited at the end of the last phase of tectonic uplift or in the subsequent period of tectonic quiescence, which is recorded by undeformed channel-levee complex sets (Figs. 5.8, 5.9 and 5.11). These observations are used to propose a model for the tectonostratigraphic evolution of the area (Fig. 5.13), demonstrating that MTCs can be an important tool for constraining the history of seabed deformation in time and space. The documented northward shift of MTC source areas, which coincides with the direction of structural propagation, suggests a structural control for MTC distribution. Given that the youngest MTCs (C1, N1 and N2) are not folded and are shelf-attached, there is some uncertainty regarding the controls on MTC emplacement and the relative importance of structural uplift with respect to other controls such as climate and eustatic sea level changes. Nonetheless the fact that possible sources for the shelf-attached MTCs occur at-or-close to the inferred location of the fault that cores the UA (updip anticline; Fig. 5.12B), suggests that structural uplift was an important control. The local observation that MTC source areas shifted in the direction of structural propagation, coincides with subregional (Festa et al., 2015) and regional (Pérez et al., 2016) studies elsewhere. This broader pattern of occurrence may suggest that systematic and generic shifts in mass-wasting activity occur as deformation fronts propagate, and that the source areas, distribution, flow-pathways and internal characteristics of MTCs could help constrain seabed deformation across different settings and scales. A similar approach could therefore be applied to constrain the evolution of the entire Sinú Fold Belt, with implications to the tectonic history of the Caribbean. Having a better constraint on the evolution of seabed relief can improve our ability to predict temporal and spatial changes

in mass-transport and turbidite fairways, and hence the presence, quality and continuity of hydrocarbon reservoirs and sealing capacity of MTCs.

8.5 Interaction of Controls

In this study, the interplay of several controls was observed. Turbidites, represented by channel-levee complex sets and avulsion lobes were shown to be affected by bathymetric features, which in this case are tectonic structures, erosional remnants and megaclasts contained within MTCs. MTCs were in turn shown to be affected by the underlying bathymetry, namely tectonic structures and channel-levee complex sets, and by the composition of the substrate. Depositional flows were found to be more affected by small-scale bathymetric features compared to more powerful flows. There are therefore three main factors that control erosion and sedimentation and are reflected in the resulting deposits: flow properties (i.e. composition, structure, and velocity), bathymetry and substrate (Fig. 8.3). The properties of the flow determine its erosional or depositional character, which in turn is influenced by the bathymetry; the latter is related to the substrate. Because bathymetry determines flow-pathways, it also influences the substrate upon which the flow translates and consequently the rheological evolution of the flow. Interactions between gravity flows and the underlying seafloor are therefore recorded in the distribution, morphology and internal characteristics of the deposit.

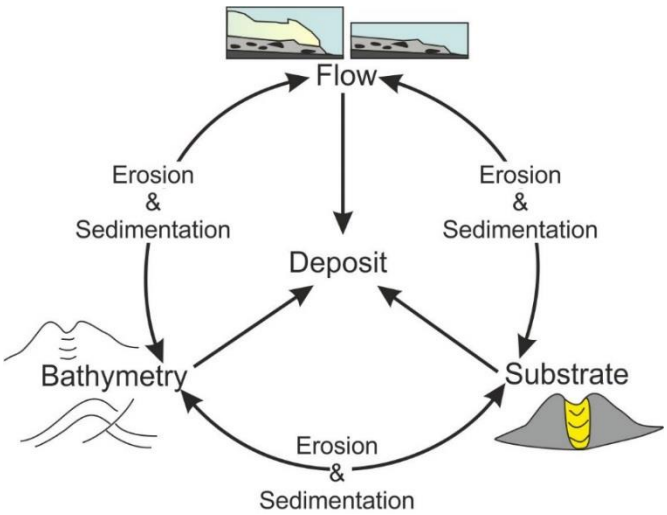

Figure 8.3. Influence of the interaction between gravity flows and the underlying seabed on the resulting deposits

8.6 Recommendations for Future Work

8.6.1 MTCs as markers of seabed deformation

In this study, changes in the provenance, distribution and characteristics of MTCs through time were found to conform to the regional direction of propagation of the Sinú Fold Belt (e.g. Martinez et al., 2015; Bernal-Olaya, 2015). Similar relationships have been documented at local, subregional and regional scales (Clark and Cartwright, 2012; Festa et al., 2015; Pérez et al., 2016). This suggests that MTCs can provide a powerful tool to constrain tectonostratigraphic histories at a variety of scales. Given that MTCs have been reported along the entire Colombian Caribbean margin (Ercilla et al., 2002; Romero-Otero, 2009; Romero-Otero et al., 2010; Vinnels et al., 2010; Alfaro and Holz, 2014; Idárraga-García and Vargas 2014; Vargas and Idárraga-García 2014), similar studies could help to constrain the regional tecno-stratigraphic history of the Colombian margin, which in turn could help constrain the tectonic history of the Caribbean.

8.6.2 Relationship between MTC-related relief and channel avulsions

This study has demonstrated that MTC-related relief can result in abnormal levee geometries that increase the probability and determine the location of channel avulsion. Future detailed studies to investigate the geometries and stacking patterns of channel-levee complexes that develop above irregular MTC tops are required to determine whether the relationship between MTC-related relief, anomalous levee geometries and channel avulsions is generic and can be applied to other basin margins.

8.6.3 Relationship between bathymetry and substrate heterogeneities with the internal characteristics of MTCs

The interpretations in this study are solely based on seismic-facies that are not calibrated to wells. Similar studies that integrate seismic interpretation with lithological descriptions and well-log interpretations could provide better constraints on the seismic facies of MTCs and the properties of the substrate. Lithological calibration is also

necessary to test the proposed evolution of the avulsion lobes from mud-prone disorganised packages to well-defined sandy lobes.

8.6.4 Detailed Architecture and Evolution of the Channel-levee Complex-Sets.

The seismic volume used in this study provides a high-quality image of the shallow stratigraphy. This provides an excellent opportunity to study the internal architecture and evolution of the channel-levee complex sets. Detailed, cycle-by-cycle mapping and attribute analysis of the fill of these channel-levee complex sets would provide new insights into the architecture, stacking patterns and lateral continuity of the reflections, thereby improving predictions on reservoir presence, quality and continuity. It could also provide a better understanding of the evolution of these channel-levee complex sets, enabling the assessment of the importance of avulsion on the evolution of individual channel-levee complexes and on the entire Magdalena Fan.

9 LIST OF REFERENCES

Abreu, V., Sullivan, M., Pirmez, C., Mohrig, D. (2003). Lateral accretion packages (LAPs): An important reservoir element in deep water sinuous channels. *Marine and Petroleum Geology*, 20, 631–648.

Adams, E. W., Schlager, W. (2010) Basic types of submarine slope curvature. *Journal of Sedimentary Research*, 70 (4), 814-828.

Alfaro, E., Holz, M. (2014). Seismic geomorphological analysis of deepwater gravity-driven deposits on a slope system of the southern Colombian Caribbean margin. *Marine and Petroleum Geology*, 57, 294-311.

Alfaro, E., Holz, M. (2014b). Review of the chronostratigraphic charts in the Sinú-San Jacinto Basin based on new seismic stratigraphic interpretations, *Journal of South American Earth Sciences*, 56, 139–169.

Alves, T.M. (2010). 3D Seismic examples of differential compaction in mass-transport deposits and their effect on post-failure strata: *Marine Geology,* 271, 212-224.

Alves, T. (2015). Submarine slide blocks and associated soft-sediment deformation in deep-water basins: A review. *Marine and Petroleum Geology*, 67, 262-285.

Alves, T.M., Cartwright, J.A. (2009). Volume balance of a submarine landslide in the Espírito Santo Basin, offshore Brazil: quantifying seafloor erosion, sediment accumulation and depletion. *Earth and Planetary Science Letters*, 288, 572-580.

Alves, T.M., Cartwright, J.A. (2010). The effect of mass-transport deposits on the younger slope morphology, offshore Brazil. *Marine and Petroleum Geology*, 27, 2027-2036.

Alves, T. M., Kurtev, K., Moore, G. F., Strasser, M. (2014). Assessing the internal character, reservoir potential, and seal competence of mass-transport deposits using seismic texture: A geophysical and petrophysical approach. *AAPG Bulletin*, 98 (4), 793-824.

Alves, T.M., Strasser, M., Moore, G.F. (2014b). Erosional features as indicators of thrust fault activity (Nankai Trough, Japan). *Marine Geology*, 356, 5-18.

Alves, T.M., Lourenço, S.D.N. (2010). Geomorphologic features related to gravitational collapse: Submarine land sliding to lateral spreading on a Late Miocene–

Quaternary slope (SE Crete, eastern Mediterranean). *Geomorphology,* 123, 13-33.

ANH, Universidad de Caldas. 2009. Estudio integrado de los núcleos y registros obtenidos de los pozos someros tipo “slim holes” en la Cuenca Sinú. Consultancy report.

Armitage, D.A., Romans, B.W., Covault, J.A., Graham, S.A. (2009). The influence of mass-transport-deposit surface topography on the evolution of turbidite architecture: The Sierra Contreras, Tres Pasos Formation (Cretaceous), southern Chile. *Journal of Sedimentary Research*, 79, 287-301.

Armitage, D. A., McHargue, T., Fildani, A., Graham, S. A. (2012). Postavulsion channel evolution: Niger Delta continental slope. *AAPG Bulletin*, 96(5), 823–843.

Baas, J.H., Van Kesteren, W., Postma, G. (2004) Deposits of depletive high-density turbidity currents: a flume analogue of bed geometry, structure and texture. *Sedimentology*, 51, 1053–1088.

Babonneau, N., Savoye, B., Cremer, M., Bez, M. (2004). Multiple terraces within the deep incised Zaire Valley (ZaiAngo Project): are they confined levees? In S. A. Lomas & P. Joseph (Eds.), *Confined Turbidite Systems*, vol. 222, 91–114.

Barley, B. (1999). Deepwater problems around the world*. Leading Edge,* 18, 488–494.

Beaubouef, R.T. & Friedmann, S.J. (2000). High resolution seismic/sequence stratigraphic framework for the evolution of Pleistocene intra slope basins, western Gulf of Mexico: depositional models and reservoir analogs. In: P, Weimer, R.M. Slatt, J. Coleman, N.C. Rosen, H. Nelson, A.H Bouma, M.J. Styzen, and D.T. Lawrence (Eds.), *Deep-water Reservoirs of the World*, Gulf Coast Section SEPM 20th Annual Research Conference, 40-60.

Bernal-Olaya, R., Sanchez, J., Mann, P., Murphy, M. (2015). Along-strike crustal thickness variations of the subducting Caribbean Plate produces two distinctive styles of thrusting in the offshore South Caribbean Deformed Belt, Colombia. In: C. Bartolini and P., Mann (Eds.), *Petroleum geology and potential of the Colombian Caribbean margin,* AAPG Memoir, 108, 295-322.

Birman, V., Meiburg, E., Kneller, B. (2009). The shape of submarine levees: exponential or power law? *Journal of Fluid Mechanics*, 619, 367-376.

Booth, J.R., Dean, M., DuVernay, A.E III, Styzen, M.J. (2003). Paleo-bathymetric controls on the stratigraphic architecture and reservoir development of confined fans in the Auger Basin: central Gulf of Mexico slope. *Marine and Petroleum Geology*, 20, 563-586.

Bouma, A.H. (1962) Sedimentology of Some Flysch Deposits: A Graphic Approach to Facies Interpretation. Elsevier, Amsterdam/New York, 168 pp.

Brami, T. R., C. Pirmez, C. Archie, Holman, K. (2000). Late Pleistocene deep-water stratigraphy and depositional processes, offshore Trinidad and Tobago, In: P. Weimer, R. M. Slatt, J. Coleman, N. C. Rosen, H. Nelson, A.H. Bouma, M. J. Styzen, and D. T. Lawrence (Eds.), *Deep-water reservoirs of the world,* Gulf Coast Section SEPM 20th Annual Research Conference, 104–115.

Breen, N. A. (1989). Structural effect of Magdalena fan deposition on the northern Colombia convergent margin. *Geology,* 17 (1), 34–37.

Brunt, R.L., Di Celma, C.N., Hodgson, D.M., Flint, S.S., Kavanagh, J.P., Van der Merwe, W.C. (2013). Driving a channel through a levee when the levee is high: an outcrop example of submarine down-dip entrenchment. Marine and Petroleum Geology, 41, 134-145.

Bull, S., Cartwright, J., Huuse, M. (2009). A review of kinematic indicators from mass-transport complexes using 3D seismic data. *Marine and Petroleum Geology*, 26(7), 1132–1151.

Bull, S., Cartwright, J. (2010). Small-Scale Insights into Seismic-Scale Slumps: A Comparison of Slump Features from the Waitemata Basin, New Zealand, and the Møre Basin, Off-Shore Norway. In: D.C. Mosher, R.C. Shipp, L. Moscardelli, J.D. Chaytor, C.D.P. Baxter, H.J. Lee, and R. Urgeles (Eds.), *Submarine Mass Movements and Their Consequences*, Springer, Netherlands, 257–266.

Buttler, R.W.H., McCaffrey, W.D. (2010). Structural evolution and sediment entrainment in mass-transport complexes: outcrop studies from Italy. *Journal of the Geological Society,* London, 167, 617-631.

Butler, R.W.H., Tavarnelli, E. (2006). The structure and kinematics of substrate entrainment into high-concentration sandy turbidites: a field example from the Gorgoglione ‘flysch’ of southern Italy: *Sedimentology*, 53, 655-670.

Cadena, A.F., Romero, G., Slatt, R. (2015). Application of stratigraphic grade concepts to understand basin-fill processes and deposits in an active margin setting,

Magdalena submarine fan and associated fold-and-thrust belts, offshore Colombia. In: C. Bartolini and P., Mann (Eds.), *Petroleum geology and potential of the Colombian Caribbean margin*, AAPG Memoir, 108, 323-344.

Cardona, A., Montes, C., Ayala, C., Bustamante, C., Hoyos, N., Montenegro, O., Ojeda, C., Niño, H., Ramírez, V., Valencia, V., Rincón, D., Veervoort, J., Zapata, S. (2012). From arc-continent collision to continuous convergence, clues from Paleogene conglomerates along the southern Caribbean–South America plate boundary. *Tectonophysics*, 580, 58-87.

Carter, R.M. (1975). A discussion and classification of subaqueous mass-transport with particular application to grain flow, slurry-flow and fluxoturbidites. *Earth Science Reviews*, 11, 145-177.

Cattaneo, A., Babonneau, N., Dan, G., Déverchère, J., Domzig, A., Gaullier, V., Lepillier, B., De Lépinary, B.M., Nouguès, A., Strzerzynski, P., Sultan, N., Yelles, K. (2010). Submarine landslides along the Algerian margin: A review of their occurrence and potential link with tectonic structures. In: D.C. Mosher, R.C. Shipp, L. Moscardelli, J.D. Chaytor, C.D.P. Baxter, H.J. Lee, and R. Urgeles (Eds.), *Submarine Mass Movements and Their Consequences*, Springer, Netherlands, 515–525.

Catterall, V., Redfern, J., Gawthorpe, R., Hansen, D., Thomas, M. (2010). Architectural style and quantification of a submarine channel–levee system located in a structurally complex area: offshore Nile Delta. *Journal of Sedimentary Research*, 80(11), 991–1017.

Cediel, F., Shaw, R. P., Cáceres, C. (2003). Tectonic assembly of the northern Andean block. In: Bartolini, C., Buffler, R. T., Blickwede, J. (Eds.), *The Circum-Gulf of Mexico and the Caribbean: Hydrocarbon habitats, basin formation and plate tectonics, AAPG Memoir*, 79, 815–848.

Cerón, J.F. (2008). Crustal architecture of the Colombian Caribbean basin and margins. PhD thesis, University of South Carolina.

Clark, I.R., Cartwright, J.A. (2009). Interactions between submarine channel systems and deformation in deepwater fold belts: Examples from the Levant Basin, Eastern Mediterranean sea. *Marine and Petroleum Geology*, 26, 1465–1482.

Clark, I.R., Cartwright, J.A. (2011). Key controls on submarine channel development in structurally active settings. *Marine and Petroleum Geology*, 28, 1333-1349.

Clark, I.R., Cartwright, J.A. (2012). Interactions between coeval sedimentation and deformation from the Niger delta deepwater fold belt. In: B. E. Prather, M. E. Deptuck, D. Mohrig, B. van Hoorn and R. B. Wynn (Eds.), *Application of the Principles Seismic Geomorphology to Continental Slope and Base-of-Slope Systems*: *Case Studies from Seafloor and Near-Seafloor Analogues*, SEPM Special Publication, 99, 243-267.

Clark, J.D., Kenyon, N.H., Pickering, K.T. (1992). Quantitative analysis of the geometry of submarine channels: implications for the classification of submarine fans. *Geology*, 20, 633–636.

Clark, I.R., Pickering, K.T. (1996). Architectural Elements and Growth Patterns of Submarine Channels: Application to Hydrocarbon Exploration. *AAPG Bulletin*, 80(2), 194-221.

Coussot, P. (1997) Mudflow Rheology and Dynamics. IAHR Monograph, Balkema, Rotterdam, 272 pp.

Covault, J. A., Kostic, S., Paull, C. K., Ryan, H. F., Fildani, A. (2014). Submarine channel initiation, filling and maintenance from sea-floor geomorphology and morphodynamic modelling of cyclic steps. *Sedimentology*, 61(4), 1031-1054.

Cronin, B.T., Hurst, A., Celik, H., Türkmen, I. (2000). Superb exposure of a channel, levee and overbank complex in an ancient deep-water slope environment. *Sedimentary Geology*, 132, 205-216.

Cross, N. E., Cunningham, A., Cook, R. J., Taha, A., Esmaie, E., El Swidan, N. (2009). Three-dimensional seismic geomorphology of a deep-water slope-channel system: The Sequoia field, offshore west Nile Delta, Egypt. *AAPG Bulletin,* 93(8), 1063–1086.

Dailly, G.C. (1982). Slope readjustment during sedimentation on continental margins. In: *Studies in Continental Margin Geology,* 593-604.

Dalla Valle, G., Gamberi, F., Foglini, F., Trincardi, F. (2015). The Gondola Slide: A mass transport complex controlled by margin topography (South-Western Adriatic Margin, Mediterranean Sea). *Marine Geology*, 366, 97-113.

Damuth, J.E., Embley, R. (1981). Mass-Transport Processes on Amazon Cone: Western Equatorial Atlantic. *AAPG Bulletin*, 65(4), 629-643.

Dan, G., Sultan, N., Cattaneo, A., Déverchère, J., Yelles, K. (2010). Mass-transport deposits on the Algerian margin (Algiers area): Morphology, lithology and sedimentary processes. In: D.C. Mosher, R.C. Shipp, L. Moscardelli, J.D. Chaytor, C.D.P. Baxter, H.J. Lee, and R. Urgeles (Eds.), *Submarine Mass Movements and Their Consequences*, Springer, Netherlands, 527–539.

Day, S., Llanes, P., Silver, E., Hoffmann, G., Warb, S., Driscoll, N. (2015). Submarine landslide deposits of the historical lateral collapse of Ritter Island, Papua New Guinea: *Marine and Petroleum Geology*, 67, 419-438.

DeMets, C., Jansma, P.E., Mattioli, G.S., Dixon, T.H., Farina, F., Bilham, R., Calais, E., Mann, P. (2000). GPS geodetic constraints on Caribbean-North America Plate Motion. *Geophysical Research Letters*, 27(3), 437–440.

Dennielou, B., Huchon, A., Beaudouin, C., Berné, S. (2006). Vertical grain-size variability within a turbidite levee: Autocyclicity or allocyclicity? A case study from the Rhône neofan, Gulf of Lions, Western Mediterranean. *Marine Geology*, 234 (1), 191-213.

Deptuck, M. E., Steffens, G. S., Barton, M., Pirmez, C. (2003). Architecture and evolution of upper fan channel-belts on the Niger Delta slope and in the Arabian Sea. *Marine and Petroleum Geology*, 20(6–8), 649–676.

Deptuck, M.E., Sylvester, Z., Pirmez, C., O'Byrne, C. (2007). Migration–aggradation history and 3-D seismic geomorphology of submarine channels in the Pleistocene Benin-major Canyon, western Niger Delta slope. *Marine and Petroleum Geology*, 24, 406-433.

Di Celma, C.N., Brunt, R.L., Hodgson, D.M., Flint, S.S. and Kavanagh, J.P. (2011). Spatial and temporal evolution of a Permian submarine slope channel–levee system, Karoo Basin, South Africa. *Journal of Sedimentary Research*, 81(8), 579-599.

Dott, R.H Jr. (1963). Dynamics of Subaqueous Gravity Depositional Processes. *AAPG Bulletin,* 47 (1), 104-128.

Draganits, E., Schlaf, J., Grasemann, B., Argles, T. (2008). Giant submarine landslide grooves in the Neoproterozoic/Lower Cambrian Phe Formation, northwest Himalaya: Mechanisms of formation and palaeogeographic implications. *Sedimentary Geology*, 205, 126-141.

Ducassou, E., Fournier, L., Sierro, F. J., Zarikian, C. A., Lofi, J., Flores, J. A., Roque, C. (2015). Origin of the large Pliocene and Pleistocene debris flows on the Algarve margin: *Marine Geology*, 377, 58-76.

Dugan, B., Stigall, J. (2010). Origin of Overpressure and slope failure in the Ursa region, northern Gulf of Mexico. In: D.C. Mosher, R.C. Shipp, L. Moscardelli, J.D. Chaytor, C.D.P. Baxter, H.J. Lee, and R. Urgeles (Eds.), *Submarine Mass Movements and Their Consequences*, Springer, Netherlands, 167–178.

Duque-Caro, H. (1979). Major structural elements and evolution of northwestern Colombia. Geological and Geophysical Investigations of Continental Margins: *AAPG Memoir*, 29, 329–351.

Duque-Caro, H. (1984). Structural style, diapirism, and accretionary episodes of the Sinú-San Jacinto terrane, southwestern Caribbean borderland, *Geological Society of America Memoir*, 162, 303–316.

Duque-Caro, H. (1990). Neogene stratigraphy, paleoceanography and paleobiogeography in northwest South America and the evolution of the Panama seaway. *Palaeogeography, Paleoclimatology, Palaeoecology*, 77, 203-234.

Duque-Caro, H., Guzmán G., Hernández, R. (1996). Mapa geológico de la plancha 38 Carmen de Bolívar. *INGEOMINAS*, Santafé de Bogotá, Colombia.

Dykstra, M., Garyfalou, K., Kertznus, V., Kneller, B., Milana, J.P., Molinaro, M., Szuman, M. and Thompson, P. (2011). Mass-transport deposits: Combining outcrop studies and seismic forward modelling to understand lithofacies distributions, deformation, and their seismic stratigraphic expression. In: *Mass Transport Deposits in Deepwater Settings*. SEPM, Special Publication 96, 293-310.

Edgar, N.T., Saunders, J. B., Bolli, H. M., Boyce, R. E., Donnelly, T. W., Hay, W. W., Maurrasse, F., Prell, W. P., I. P. Silva, Riedel, W. R., Schneidermann, N. (1973). *Initial reports of the Deep Sea Drilling Project 15*: U.S. Government Printing Office.

Eggenhuisen, J.T., McCaffrey, W.D., Haughton, P.D.W., Butler, R.W.H, Moore, I. (2010). Reconstructing large-scale remobilisation of deep-water deposits and its impact on sand-body architecture from cored wells: The Lower Cretaceous Britannia Sandstone Formation, UK North Sea. *Marine and Petroleum Geology*, 27, 1595-1615.

Elliot, C.G., Williams, P.F. (1988). Sediment slump structures: a review of diagnostic criteria and application to an example from Newfoundland. *Journal of Structural Geology*, 10(2) 171-1852.

Elverhøi, Issler, D., De Blasio, F.V., Ilstad, T., Harbitz, C.B., and Gauer, P. (2005). Emerging insights into the dynamics of submarine debris flows. *Natural Hazards and Earth System Sciences*, 5, 633-648.

Ercilla, G., Alonso, B., Estrada, F., Chiocci, F. L., Baraza, J. (2002). The Magdalena Turbidite System (Caribbean Sea): Present-day morphology and architecture model. *Marine Geology*, 185(3), 303–318.

Escalona, A., Mann, P. (2011) Tectonics, basin subsidence mechanisms, and paleogeography of the Caribbean-South American plate boundary zone. *Marine and Petroleum Geology,* 28(1), 8–39.

Farrell, S.G. (1984). A dislocation model applied to slump structures, Ainsa Basin, South Central Pyrenees. *Journal of Structural Geology*, 6(6), 727-736.

Farrell, S.G., Eaton, S. (1988). Foliations developed during slump deformation of Miocene marine sediments, Cyprus. *Journal of Structural Geology*, 10 (6), 567-576.

Festa, A., Ogata, K., Pini, G.A., Dilek, Y., Codegone, G (2015). Late Oligocene-early Miocene olistostromes (sedimentary mélanges) as tectonostratigraphic constraints to the geodynamic evolution of the exhumed Ligurian accretionary complex (Northern Apennines, NW Italy), *International Geology Review*, 57 (5-8), 540-562.

Fisher, R.V. (1982). Flow transformations in sediment gravity flows. *Geology*, 11(5), 273-274.

Flinch, J. F. (2003). Structural evolution of the Sinú-Lower Magdalena area (northern Colombia). In: C. Bartolini, R. T. Buffler, and J. Blickwede (Eds.), *The Circum-Gulf of Mexico and the Caribbean: Hydrocarbon habitats, basin formation, and plate tectonics.* AAPG Memoir, 79, 776–796.

Flood, R. D., Manley, P. L., Kowsmann, R. O., Appi, C. J., Pirmez, C. (1991). Seismic facies and late Quaternary growth of Amazon submarine fan. In Weimer, P. and Link, M. H. (Eds.), Seismic facies and sedimentary processes of submarine fans and turbidite systems: New York (Springer), pp. 415–433.

Frey-Martinez, J. (2010). 3D Seismic interpretation of mass transport deposits: Implications for basin analysis and geohazard evaluation. In: Mosher, D.C., Shipp, R.C., Moscardelli, L., Chaytor, J.D., Baxter, C.D.P., Lee, H.J., and Urgeles, R. (Eds.), *Submarine Mass Movements and Their Consequences*, Springer, Netherlands, 553-568.

Frey Martinez, J., Cartwright, J., Hall, B. (2005). 3D seismic interpretation of slump complexes: examples from the continental margin of Israel. *Basin Research*, 17, 83–108.

Frey-Martinez, J., Cartwright, J., James, D. (2006). Frontally confined versus frontally emergent submarine landslides: A 3D seismic characterisation. *Marine and Petroleum Geology*, 23, 585–604.

Galindo, P. (2016). Transtension and transpression in an oblique subduction setting: Evolution of the Bahia Basin, Colombian Caribbean margin. PhD thesis, Imperial College, London.

Gamboa, D., Alves, T.M. (2015). Three-dimensional fault meshes and multi-layer shear in mass-transport blocks: Implications for fluid flow on continental margins. *Tectonophysics*, 647-648, 21-32

Gamboa, D., Alves, T., Cartwright, J., Terrinha, P. (2010). MTD distribution on a 'passive' continental margin: the Espírito Santo Basin (SE Brazil) during the Palaeogene. *Marine and Petroleum Geology*, 27 (7), 1311-1324.

Gamboa, D., Alves, T.M., Cartwright, J. (2011). Distribution and characterization of failed (mega) blocks along salt ridges, southeast Brazil: Implications for vertical fluid flow on continental margins. *Journal of Geophysical Research*, 116, B08103.

Gee, M.J.R., Gawthorpe, R.L. (2006). Submarine channels controlled by salt tectonics: Examples from 3D seismic data offshore Angola*. Marine and Petroleum Geology*, 23, 443-548.

Gee, M.J.R., Gawthorpe, R.L., Friedmann, S.J. (2006). Triggering and evolution of a giant submarine landslide, offshore Angola, revealed by 3d seismic stratigraphy and geomorphology, *Journal of Sedimentary Research*, 76, 9-19.

Gee, M. J. R., Gawthorpe, R. L., Bakke, K., Friedmann, S. J. (2007). Seismic geomorphology and evolution of submarine channels from the Angolan continental margin. *Journal of Sedimentary Research*, 77(5), 433–446.

Gee, M.J.R., Uy, H.S., Warren, J., Morley, C.K., Lambiase, J.J. (2007b). The Brunei slide: A giant submarine landslide on the North West Borneo Margin revealed by 3D seismic data: *Marine Geology,* 246, 9-23.

Geersen, J., Völker, D., Behrmann, J.H., Reichert, C., Krastel, S. (2011). Pleistocene giant slope failures offshore Arauco Peninsula, Southern Chile. *Journal of the Geological Society,* London, 168, 1237–1248.

Georgiopoulou, A., Masson, D.G., Wynn, R., Krastel, S. (2010). Sahara Slide: Age, initiation, and processes of a giant submarine slide. *Geochemistry, Geophysics, Geosystems*, 11, Q07014.

Gervais, A., Mulder, T., Savoye, B., Migeon, S., Cremer, M. (2001). Recent processes of levee formation on the Zaire deep-sea fan. *Comptes Rendus de l'Academie des Sciences-Series IIA-Earth and Planetary Science*, 332 (6), 371-378.

Goldfinger, C., Kulm, L.V.D., McNeil, L.C., Watts, P. (2000). Super-scale failure of the southern Oregon Cascadia margin. *Pure and Applied Geophysics*, 157, 1189–1226.

Grozic, J.L.H. (2010). Interplay between gas hydrates and submarine slope failure. In: D.C. Mosher, R.C. Shipp, L. Moscardelli, J.D. Chaytor, C.D.P. Baxter, H.J. Lee, and R. Urgeles (Eds.), *Submarine Mass Movements and Their Consequences*, Springer, Netherlands, 11-30.

Guzmán, G. (2007). Stratigraphy and sedimentary environment and implications in the Plato Basin and the San Jacinto Belt northwestern Colombia. PhD thesis, Université de Liège, 487 p.

Haflidason, H., Sejrup, H. P., Nygard, A., Mienert, J., Bryn, P., Lien, R., Forsberg, C. F., Berg, K., Masson, D. (2004). The Storegga Slide: Architecture, geometry and slide development: *Marine Geology*, 213, 201–234

Hansen, L.A.S., Callow, R.H.T., Kane, I.A., Gamberi, F., Rovere, M., Cronin, B.T., Kneller, B.C. (2015). Genesis and character of thin-bedded turbidites associated with submarine channels. *Marine and Petroleum Geology*, 67, 852–879.

Haughton, P.D.W. (2000). Evolving turbidite systems on a deforming basin floor, Tabernas, SE Spain. *Sedimentology*, 47, 497-518.

Haughton, P., Davis, C., McCaffrey, W., Barker, S. (2009). Hybrid sediment gravity flow deposits: classification, origin and significance, *Marine and Petroleum Geology*, 26, 1900–1918.

Heiniö, P., Davies, R.J. (2006). Degradation of compressional fold belts: deep-water Niger Delta. *AAPG Bulletin*, 90, 753–770.

Heniö, P., Davies, R.J. (2007). Knickpoint migration in submarine channels in response to fold growth, western Niger Delta. *Marine and Petroleum Geology*, 24, 434-449.

Heiniö, P., Davies, R.J. (2009). Trails of depressions and sediment waves along submarine channels on the continental margin of Espírito Santo Basin, Brazil: *Geological Society of America, Bulletin,* 121(5-6), 698-711.

Hesse, S., Back, S., Franke, D. (2010). The structural evolution of folds in a deepwater fold and thrust belt–a case study from the Sabah continental margin offshore NW Borneo, SE Asia. *Marine and Petroleum Geology*, 27 (2), 442-454.

Hiscott, R. N., Hall, F. R., Pirmez, C. (1997). Turbidity-current overspill from the Amazon Channel: texture of the silt/sand load, paleoflow from anisotropy of magnetic susceptibility, and implications for flow processes. In: *Proceedings of the Ocean Drilling Program*, scientific results. National Science Foundation, 53-78.

Hodgson, D.M., Di Celma, C.N., Brunt, R.L., Flint, S.S. (2011). Submarine slope degradation, aggradation and the stratigraphic evolution of channel–levee systems. *Journal of the Geological Society, London*, 168, 625–628.

Hodgson, D. M., Kane, I. A., Flint, S. S., Brunt, R. L., Ortiz-Karpf, A. (2016). Time-Transgressive Confinement on the Slope and the Progradation of Basin-Floor Fans: Implications for the Sequence Stratigraphy of Deep-Water Deposits. *Journal of Sedimentary Research*, 86(2), 73-86.

Hooghiemstra, H., Ran, E.T. (1994). Late and middle Pleistocene climatic change and forest development in Colombia: pollen record Funza II (2-158 m core interval). *Paleogeography, Paleoclimatology, Paleoecology,* 109 (2), 211-246.

Hsu, S.K., Kuo, J., Lo, C.L., Tsai, C.H., Doo, W.B., Ku, C.Y., Sibuet, J.C. (2008). Turbidity currents, submarine landslides and the 2006 Pingtung earthquake off SW Taiwan. *Terrestrial Atmospheric and Ocean Science*, 19, 767–772.

Hubbard, S.M., Covault, J.A., Fildani, A., Romans, B.W. (2014). Sediment transfer and deposition in slope channels: deciphering the record of enigmatic deep-sea processes from outcrop. *Geological Society of America, Bulletin*, 126, 857–871.

Idárraga-García, J., Vargas, C.A. (2014). Morphological Expression of Submarine Landslides in the Accretionary Prism of the Caribbean Continental Margin of Colombia. In: S. Krastel, J.H. Behrmann, M. Stripp, C. Berndt, R. Urgeles, J. Chaytor, K. Huhn, M. Strasser and C. Bonnevie Harbitz (Eds.), *Submarine Mass Movements and Their Consequences*, Springer International Publishing, Switzerland.

Ilstad, T., Elverhøi, A., Issler, D., Marr, J. (2004). Subaqueous debris flow behaviour and its dependence on the sand/clay ratio: a laboratory study using particle tracking. *Marine Geology*, 213, 415-438.

Iverson, R. (1997). The physics of debris flows. *Reviews of Geophysics*, 35 (3), 245-296.

Iverson, R. (2012). Elementary theory of bed-sediment entrainment by debris flows and avalanches. *Journal of Geophysical Research*, 117, F03006.

Jackson, C. A. L. (2011). Three-dimensional seismic analysis of megaclast deformation within a mass transport deposit; implications for debris flow kinematics. *Geology*, 39(3), 203–206.

Jackson, C.A.L., Johnson, H. (2009). Sustained turbidity currents and their interaction with debrite-related topography; Labuan Island, offshore NW Borneo, Malaysia. *Sedimentary Geology*, 219, 77-96.

Janocko, M., Cartigny, M.B.J., Nemec, W., Hansen, E.W.M. (2013). Turbidity current hydraulics and sediment deposition in erodible sinuous channels: Laboratory experiments and numerical simulations. *Marine and Petroleum Geology*, 41, 222-249.

Joanne, C., Lamarche, C., Collot, J.-Y. (2013). Dynamics of giant mass transport in deep submarine environments: The Matakaoa Debris Flow, New Zealand. *Basin Research*, 25, 471-488.

Jobe, Z.R., Sylvester, Z., Parker, A.O., Howes, N.C., Slowey, N., Pirmez, C. (2015). Rapid adjustment of submarine channel architecture to changes in sediment supply: *Journal of Sedimentary Research*, 85, 729–753.

Johnson, C. G., Kokelaar, B. P., Iverson, R., Logan, M., Lahusen, R. G., Gray, J. M. N. T. (2012). Grain-size segregation and levee formation in geophysical mass flows: *Journal of Geophysical Research: Earth Surface*, 117(1), F01032.

Jolly, B.A. (2014). The interaction between deepwater channel systems and growing thrusts and folds, toe-thrust region of the deepwater Niger Delta. PhD Thesis, Imperial College London.

Jones, O.T. (1939). The geology of the Colwyn Bay district: study of submarine slumping during the Salopian Period. *Quarterly Journal of the Geological Society,* London, 95, 335-382.

Jones, G., Mayall, M., Lonergan, L. (2012). Contrasting depositional styles on a slope system and their control by salt tectonics: through-going channels, ponded fans, and mass transport complexes. *GCSSEPM*, 503 – 533.

Kane, I.A., Kneller, B.C., Dykstra, M., Kassem, A., McCaffrey, D. (2007). Anatomy of a submarine channel–levee: An example from Upper Cretaceous slope sediments, Rosario Formation, Baja California, Mexico. *Marine and Petroleum Geology*, 24, 540-563.

Kane, I.A., McCaffrey, W.D., Peakall, J. (2008). Controls on sinuosity evolution within submarine channels. *Geology*, 36(4), 287-290.

Kane, I. A., Catterall, V., McCaffrey, W. D., Martinsen, O. J. (2010). Submarine channel response to intrabasinal tectonics: The influence of lateral tilt. *AAPG Bulletin*, 94(2), 189-219.

Kane, I., McCaffrey, W.D., Peakall, J., Kneller, B. (2010b). Submarine channel levee shape and sediment waves from physical experiments. *Sedimentary Geology*, 223, 75-85.

Kane, I. A., Hodgson, D. M. (2011). Sedimentological criteria to differentiate submarine channel levee subenvironments: Exhumed examples from the Rosario Fm. (Upper Cretaceous) of Baja California, Mexico, and the Fort Brown Fm. (Permian), Karoo Basin, S. Africa. *Marine and Petroleum Geology*, 28(3), 807–823.

Keevil, G.M., Peakall, J., Best, James, L., Amos, K.J. (2006). Flow structure in sinuous submarine channels: Velocity and turbulence structure of an experimental submarine channel. *Marine Geology*, 229, 241-257.

Keevil, G.M., Peakall, J., Best, J. L. (2007). The influence of scale, slope and channel geometry on the flow dynamics of submarine channels. *Marine and Petroleum Geology*, 24, 487-503.

Kertznus, V. (2009) Stratigraphic development of delta-fed slope systems: Offshore Ebro and Nile Deltas, Ph.D. thesis, University of Aberdeen, Aberdeen, United Kingdom.

Kneller, B. (1995). Beyond the turbidite paradigm: physical models for deposition of turbidites and their implications for reservoir prediction. *Geological Society, London, Special Publications,* 94(1), 31-49.

Kneller, B., Dykstra, M., Fairweather, L., Milana, J.P. (2015). Mass-transport and slope accommodation: Implications for turbidite sandstone reservoirs. *AAPG Bulletin*, 100 (2), 213-235.

Kneeler, B. C., Branney, M. J. (1995). Sustained high density turbidity currents and the deposition of thick massive sands. *Sedimentology*, 42, 607- 616.

Kolla, V. (2007). A review of Sinuous channel avulsion patterns in some major deep-sea fans and factors controlling them. *Marine and Petroleum Geology*, 24(6), 450–469.

Kolla, V., Buffler, R. T. (1984). Morphologic, acoustic, and sedimentologic characteristics of the Magdalena Fan. *Geo- Marine Letters*, 3, 85- 91.

Kuenen, P.H. (1950). Turbidity currents of high density. Report 18th *International Geology Congress*, Part 8, London. 44–52.

Lamarche, G., Joanne, C., Collot, J. Y. (2008). Successive, large mass-transport deposits in the south Kermadec fore-arc basin, New Zealand: The Matakaoa Submarine Instability Complex. *Geochemistry, Geophysics, Geosystems*, 9, Q04001.

Leeder, M. (1999). Sedimentology and sedimentary basins: from turbulence to tectonics. 2nd ed., Oxford: Blackwell Science.

Legros, F. (2002). Can dispersive pressure cause inverse grading in grain flows? *Journal of Sedimentary Research*, 72, 166–170.

Locat, J., Lee, H. (2005). Subaqueous debris flows. In: Jakob, M. and Hungr, O (Eds.), *Debris-flow Hazards and Related Phenomena*, Springer, Berlin, 203-245.

Loncke, L., Gaullier, V. Droz, L., Ducassou, E., Migeon, S. Mascle, J. (2009). Multi-scale slope instabilities along the Nile deep-sea fan, Egyptian margin: A general overview: *Marine and Petroleum Geology*, 26, 633–646,

López-Gamundí, O.R. (1993). Pebbly mudstones in the Cretaceous Pigeon Point Formation, western California: a study in the transitional stages from submarine slumps to cohesive debris flows. *Sedimentary Geology*, 84, 37-50.

Lewis, K.B. (1971). Slumping on a continental slope inclined at 1–4º. *Sedimentology,* 16, 97–110.

Lowe, D.R. (1976). Subaqueous liquefied and fluidised sediment flows and their deposits. *Sedimentology*, 23, 285–308.

Lowe, D.R. (1982) Sediment gravity flows. Depositional models with special reference to high density turbidity currents. *Journal of Sedimentary Petrology*, 52, 279–298.

Lowe, D. R. (2004). Deep-water sandstones: Marine canyon to basin plain, Western California: *AAPG Special Publication,* 79, 44–51.

Major, J. T. (1997). Processes in large-scale debris-flow experiments. *The Journal of Geology*, 105 (3), 345-366.

Maier, K.L., Fildani, A., Paull, C.K., Graham, S.A., McHargue, T.R. Caress, D.W., McGann, M. (2011). The elusive character of discontinuous deep-water channels: New insights form the Lucia Chica channel system, offshore California. *Geology*, 39(4), 327-330.

Manica, R. (2012). Sediment Gravity Flows: Study Based on Experimental Simulations. In: Hydrodynamics-Natural Water Bodies. In: H. Schulz, H., Simões, A. and Lobosco, R. (Eds.), *Hydrodynamics-Natural Water Bodies*, 263-286.

Manley, P.L., Flood, R.D. (1988). Cyclic deposition within Amazon deep-sea fan. *AAPG Bulletin*, 72, 912-925.

Marr, J.G., Harff, P.A., Shanmugam, G., Parker, G. (2001). Experiments on subaqueous sandy gravity flows: the role of clay and water content in flow dynamics and depositional structures. *Geological Society of America, Bulletin*, 113, 1377–1386.

Martinez, J., Castillo, J., Ortiz-Karpf, A., Rendon, L., Mosquera, J.C., Vega, V. (2015), Deep Water Untested Oil-Play in the Magdalena Fan, Caribbean, Colombian Basin. In: C. Bartolini and P., Mann (Eds.), *Petroleum geology and potential of the Colombian Caribbean margin*, AAPG Memoir, 108, 251-260.

Maslin, M., Mikkelsen, N., Vilela, C., Haq, B. (1998). Sea-level–and gas-hydrate–controlled catastrophic sediment failures of the Amazon Fan. *Geology*, 26(12), 1107-1110.

Maslin, M., Owen, M., Day, S., & Long, D. (2004). Linking continental-slope failures and climate change: testing the clathrate gun hypothesis. *Geology*, 32 (1), 53-56.

Masson, D.G., Van Niel, B., Weaver, P.P.E. (1997). Flow processes and sediment deformation in the Canary Debris Flow on the NW African Continental Rise. *Sedimentary Geology*, 110, 163-179.

Masson, D.G., Harbitz, C.B., Wynn, R.B., Pedersen, G., Løvholt, F. (2006) Submarine landslides: processes, triggers and hazard prediction. *Philosophical Transactions of the Royal Society of London,* 364, 2009–2039.

Masson, D.G., Wynn, R.B., Talling, P.J., (2010). Large landslides on passive continental margins: processes, hypotheses and outstanding questions. In: D.C. Mosher, R.C. Shipp, , L. Moscardelli, , J.D. Chaytor, , C.D.P., Baxter, H.J. Lee, and R. Urgeles (Eds.), *Submarine Mass Movements and Their Consequences*, Springer, Netherlands, 153-166.

May, J. A., Warme, J. E., Slater, R. A. (1983) Role of submarine canyons on shelfbreak erosion and sedimentation: Modern and ancient examples. In: D. J. Stanley and G. T. Moore (Eds.), *The shelfbreak*: *Critical interface on continental margins,* SEPM Special Publication 33, 315–332

Mayall, M., Jones, E., Casey, M. (2006). Turbidite channel reservoirs: Key elements in facies prediction and effective development. *Marine and Petroleum Geology*, 23, 821-841.

Mayall, M., Lonergan, L., Bowman, A., James, S., Mills, K., Primmer, T., Pope, D., Rogers, L., Keene, R. (2010). The response of turbidite slope channels to growth-induced seabed topography. *AAPG Bulletin*, 94(7), 1011-1030.

McAdoo, B.G., Pratson, L.F., Orange, D.L. (2000). Submarine landslide geomorphology, US continental slope. *Marine Geology*, 169, 103-136.

McCaffrey, W.D., Gupta, S., Brunt, R. (2002). Repeated cycles of submarine channel incision, infill and transition to sheet sandstone development in the Alpine Foreland Basin, SE France. *Sedimentology*, 49, 623-635.

McCaffrey, W.D., Kneller, B.C. (2004). Scale effects of non-uniformity on deposition from turbidity currents with reference to the Grès d'Annot of SE France. In: Joseph, P. and Lomas, S.A., *Deep-Water Sedimentation in the Alpine Basin of SE France. New perspectives on the Grès d'Annot and related systems*. Geological Society, London, Special Publications, 221, 301-310.

McGilvery, T. A., Haddad, G., Cook, D. L. (2004). Seafloor and shallow subsurface examples of mass transport complexes, offshore Brunei. In: *Offshore Technology Conference,* Offshore Technology Conference.

McHargue, T., Pyrcz, M.J., Sullivan, M.D., Clark, J.D., Fildani, A., Romans, B.W., Covault, J.A., Levy, M., Posamentier, H.W., Drinkwater, N.J. (2011). Architecture of turbidite channel systems on the continental slope: patterns and predictions: *Marine and Petroleum Geology*, 28, 728–743.

Mehta, A. J., McAnally Jr, W. H., Hayter, E. J., Teeter, A. M., Schoellhamer, D., Heltzel, S. B., Carey, W. P. (1989). Cohesive sediment transport. II: Application. *Journal of Hydraulic Engineering*, 115(8), 1094-1112.

Meiburg, E., Kneller, B. (2010). Turbidity currents and their deposits. *Annual Review of Fluid Mechanics*, 42, 135-156.

Meschede, M., Frisch, W. (1998). A plate-tectonic model for the Mesozoic and early Cenozoic history of the Caribbean plate. *Tectonophysics*, 296 (3), 269–291.

Middleton, G.V., Hampton, M.A. (1973) Sediment gravity flows: mechanisms of flow and deposition: In: *Turbidites and Deep-Water Sedimentation,* SEPM Pacific Section, Short course lecture notes, 1–38.

Migeon, S., Savoye, B. Zanella, E., Mulder, T., Faugères, J.-C., Weber, O. (2001). Detailed seismic-reflection and sedimentary study of turbidite sediment waves on the Var Sedimentary Ridge (SE France): Significance for sediment transport and deposition and for the mechanisms of sediment-wave construction. *Marine and Petroleum Geology*, 18, 179-208.

Minisini, D., Trincardi, F., Asioli, A., Canu, M., & Foglini, F. (2007). Morphologic variability of exposed mass-transport deposits on the eastern slope of Gela Basin (Sicily channel). *Basin Research*, 19, 217–240.

Mitchum Jr, R. M., Vail, P. R., Sangree, J. B. (1977). Stratigraphic interpretation of seismic reflection patterns in depositional sequences. In: Payton, C. E. (Ed), *Seismic stratigraphy- Applications to Hydrocarbon Exploration*. AAPG Memoir 26, 117-133.

Mohrig, D., Elverhøi, A., Parker, G. (1999). Experiments on the relative mobility of muddy subaqueous and subaerial debris flows, and their capacity to remobilize antecedent deposits. *Marine Geology*, 154(1), 117-129.

Moore, D.G., Curray, J.R., Emmel, F.J. (1976). Large submarine slide (olistostrome) associated with Sunda Arc subduction zone, northeast Indian Ocean. *Marine Geology*, 21, 211–226.

Morley, C.K. (2009). Growth of folds in a deep-water setting. *Geosphere*, 5(2), 59-89.

Morris, E.A., Hodgson, D.M., Brunt, R.L., Flint, S.S. (2014). Origin, evolution and anatomy of silt-prone submarine external levees. *Sedimentology,* 61, 1734–1763.

Moscardelli, L., Wood, L. (2008). New classification system for mass transport complexes in offshore Trinidad. *Basin Research*, 20(1), 73–98.

Moscardelli, L., Wood, L. (2015). Morphometry of mass-transport deposits as a predictive tool. *Geological Society of America Bulletin*, B31221 -1.

Moscardelli, L., Wood, L., Mann, P. (2006). Mass-transport complexes and associated processes in the offshore area of Trinidad and Venezuela. *AAPG Bulletin*, 90(7), 1059–1088.

Mulder, T., Alexander, A. (2001). The physical character of subaqueous sedimentary density flows and their deposits. *Sedimentology*, 48, 269–299.

Mutti, E. (1992). Turbidite sandstones. Instituto di Geologia Universita di Parma & AGIP, San Donato Milanese, 275 p.

Mutti, E., Normark, W.R. (1987). Comparing examples of modern and ancient turbidite systems: problems and concepts, In: Leggett, J.K., and Zuffa, G.G. (Eds.), *Deep Water Clastic Deposits: Models and Case Histories*: London, Graham and Trotman, 1-38.

Mutti, E., Seguret, M., Sgavetti, M. (1988). Sedimentation and deformation in the Tertiary Sequences of the Southern Pyrenees: Field trip 7. In*:* Special *Publication of the*

Institute of Geology: AAPG Mediterranean Basins Conference, University of Parma, Nice, France, 157 p.

Nakajima, T., Kneller, B. C. (2013). Quantitative analysis of the geometry of submarine external levees. Sedimentology, 60(4), 877–910.

Nakajima, T., Satoh, M. and Okamura, Y. (1998) Channel-levee complexes, terminal deep-sea fan and sediment wave fields associated with the Toyama Deep-Sea Channel system in the Japan Sea. *Marine Geology*, 147, 25–41.

Nardin, T.R., Hein, F.J., Gorsline, D.S., Edwards, B.D. (1979). A review of mass movement processes, sediment and acoustic characteristics, and contrasts in slope and base of slope systems versus canyon-fan-basin floor systems. In: L.J. Doyle and O.H. Pilkey, (Eds.), *Geology of Continental Slopes*, SEPM Special Publication, 27, 61-73.

Nemec, W. (1990) Aspects of sediment movement on steep delta slopes. In: Colella and D.B. Prior (Eds.), *Coarse-Grained Deltas*, Special Publications International Association of Sedimentologists, 10, 29-73.

Niño, C. H. (2005). Sistemas Petrolíferos da parte norte da Bacia de Sinú-San Jacinto Colombia: Umaavaliacao geológica e geoquímica integrada. Thesis pos graduaçao de engenharia-Mestreem Ciencias (M.Sc.) da Universida de Federal do Rio de Janeiro, Rio de Janeiro, Brasil, 198 p.

Nissen, S.E., Haskell, N.L., Steiner, C.T., Coterill, K.L. (1999). Debris flow outrunner blocks, glide tracks, and pressure ridges identified on the Nigerian continental slope using 3-D seismic coherency. *The Leading Edge,* 18, 595–599.

O'Byrne, C.J., Prather, B.E, Sylvester, Z., Pirmez, C., Couzens, B., Smith, R., Barton, M., Steffens, G.S., Willson, J., 2007. Architecture of a deep-water levee avulsion, Silla Oja Mesa, Parque Nacional Torres del Paine, Chile. In: Nielsen, T.H., Shew, R.D., Steffens, G.S., Studlick, J.R.J (Eds.), *Atlas of Deep-Water Outcrops: AAPG Studies in Geology*, 56, 143-147.

Olafiranye, K., Jackson, C. A.-L., Hodgson, D. M. (2013). The role of tectonics and mass-transport complex emplacement on upper slope stratigraphic evolution: A 3D seismic case study from offshore Angola. *Marine and Petroleum Geology*, 44, 196–216.

Omosanya, K. O., Alves, T. M (2013). A 3-dimensional seismic method to assess the provenance of mass-transport deposits (MTDs) on salt-rich continental slopes (Espírito Santo Basin, SE Brazil). *Marine and Petroleum Geology*, 44, 223-239.

Ortiz-Karpf, A., Hodgson, D. M., McCaffrey, W. D. (2015). The role of mass-transport complexes in controlling channel avulsion and the subsequent sediment dispersal patterns on an active margin: The Magdalena Fan, offshore Colombia. *Marine and Petroleum Geology,* 64, 58-75.

Ortiz-Karpf, A., Hodgson, D. M., Jackson, C. A.-L., McCaffrey, W. D. (2016). Mass-transport complexes as markers of deep-water fold-and-thrust belt evolution: Insights from the southern Magdalena Fan, offshore Colombia. *Basin Research*, Accepted Author Manuscript, doi:10.1111/bre.12208.

Patacci, M., Haughton, P.D.W., McCaffrey, W.D. (2015). Flow behaviour of ponded turbidity currents. *Journal of Sedimentary Research*, 85, 885-902.

Peakall, J., McCaffrey, W.D., Kneller, B. (2000). A process model for the evolution, morphology, and architecture of sinuous submarine channels. *Journal of Sedimentary Research*, 70, 434-448.

Pérez, L. F., Bohoyo, F., Hernández-Molina, F.J., Casas, D., Galindo-Zaldívar, J., Ruano, P., Maldonado, A (2016). Tectonic activity evolution of the Scotia-Antarctic Plate boundary from mass transport deposit analysis. *Journal of Geophysical Research: Solid Earth*, 121, 2216–2234.

Pickering, K. T., Clark, J. D., Smith, R. D. A., Hiscott, R. N., Lucchi, F. R., Kenyon, N. H. (1995). Architectural element analysis of turbidite systems, and selected topical problems for sand-prone deep-water systems. In: *Atlas of deep water environments,* Springer Netherlands, 1-10.

Pickering, K., Corregidor, J (2005). Mass transport complexes and tectonic control on confined basin-floor submarine fans, Middle Eocene, south Spanish Pyrenees. In: D.M. Hodgson and S.S. Flint (Eds.), *Submarine Slope Systems: Processes and Products.* Geological Society, London, Special Publications, 244, 51-74.

Pindell, J. L. (1994). Evolution of the Gulf of Mexico and the Caribbean: In: S.K., Donovan and T.A. Jackson (Eds.), *Caribbean geology. An introduction*, University of the West Indies Publisher's association, 13–39.

Pindell, J. L., Cande, S. C., Pitman, W. C., Rowley, D. B., Dewey, J. F. Labrecque, J., Haxby, W. (1988). A plate-kinematic framework for models of Caribbean evolution. *Tectonophysics*, 155(1–4), 121–138.

Pindell, J. L., Kennan, L. (2009). Tectonic evolution of the Gulf of Mexico, Caribbean and northern South America in the mantle reference frame: An update. *Special Publication Geological Society,* London, 328 (1), 1–55.

Piper, J. N., Behrens, E. W. (2003). Downslope sediment transport processes and sediment distributions at the East Breaks, northwest Gulf of Mexico. *In:* H. H. Roberts, N. C. Rosen, R. H. Fillon, and J. B. Anderson (Eds*.), Shelf margin deltas and linked down slope petroleum systems: Global significance and future exploration potential.* Gulf Coast Section SEPM 23rd Annual Research Conference, 359–385.

Piper, D.J.W., Cochonat, P, Morrison, M.L. (1999). The sequence of events around the epicenter of the 1929 Grand Banks earthquake: initiation of the debris flows and turbidity current inferred from side scan sonar. *Sedimentology*, 46, 79–97.

Piper, D.J.W., Normark, W.R. (2001). Sandy fans—from Amazon to Hueneme and beyond. *AAPG Bulletin,* 85(8), 1407-1438.

Piper, D.J.W. and Normark, W.R. (2009). Processes that initiate turbidity currents and their influence on turbidites: a marine geology perspective. *Journal of Sedimentary Research*, 79, 347–362.

Pirmez, C., Beaubouef, R. T., Friedmann, S. J., Mohrig, D. C. (2000). Equilibrium profile and base level in submarine channels: examples from Late Pleistocene systems and implications for architecture in deepwater reservoirs. In: P. Weimer, R. M. Slatt, J. Coleman, N. C. Rosen, H. Nelson, A. H. Bouma, M. J. Styzen, & D. T. Lawrence (Eds.), *Deep-water reservoirs of the world*, GCS-SEPM foundation, 20th Annual Bob F. Perkins Research Conference.

Pirmez, C., Flood, R. D. (1995). Morphology and structure of Amazon Channel. In Proceedings of the Ocean Drilling Program. Initial Reports, 155, 23–45.

Pirmez, C. Imran, J. (2003). Reconstruction of turbidity currents in the Amazon Channel. *Marine and Petroleum Geology*, 20, 823-849.

Pirmez, C., Hiscott, R. N., Kronen, J. D. (1997). Sandy turbidite successions at the base of channel-levee systems of the Amazon Fan revealed by FMS logs and cores:

Unravelling the facies architecture of large submarine fans. In *Proceedings of the Ocean Drilling Program. Scientific results*, 155, 7–33.

Posamentier, H. W., Kolla, V. (2003). Seismic geomorphology and stratigraphy of depositional elements in deep-water settings. *Journal of Sedimentary Research*, 73(3), 367–388.

Posamentier, H. W., Martinsen, O. J. (2011). The character and genesis of submarine mass-transport deposits: insights from outcrop and 3D seismic data. In Mass-Transport Deposits in Deepwater Settings. *SEPM Special Publication*, 96, 7–38.

Prather, B.E. (2003). Controls on reservoir distribution, architecture and stratigraphic trapping in slope settings. *Marine and Petroleum Geology*, 20, 529-545.

Prather, B. E., Booth, J. R., Steffens, G. S., Craig, P. A. (1998). Classification, lithologic calibration and stratigraphic succession of seismic facies from intraslope basins, deep water Gulf of Mexico, USA. *AAPG Bulletin*, 82 (5), 701–728.

Prélat, A., Hodgson, D. M., Flint, S. S. (2009). Evolution, architecture and hierarchy of distributary deep-water deposits: a high-resolution outcrop investigation from the Permian Karoo Basin, South Africa. *Sedimentology*, 56(7), 2132–2154.

Prior, D. B., Bornhold, B. D., Johns, M. W. (1984). Depositional Characteristics of a Submarine Debris Flow. *The Journal of Geology*, 92(6), 707-727.

Reading, H. G. (1996). Sedimentary Environments: Processes, Facies and Stratigraphy. 688p.

Restrepo-Correa, I.C., Ojeda, G.Y. (2010). Geologic controls on the morphology of La Aguja submarine canyon. *Journal of South American Earth Sciences*, 29, 861-870.

Restrepo, J. D., Kjerfve, B. (2000). Magdalena river: interannual variability (1975–1995) and revised water discharge and sediment load estimates. *Journal of Hydrology*, 235(1–2), 137–149.

Restrepo, J. D., López, S.A. (2008). Morphodynamic of the Pacific and Caribbean deltas of Colombia, South America. *Journal of South American Earth Sciences*, 25, 1-21.

Rincon, D., Arenas, J. E., Cuartas, C. H., Molinares, C., Caicedo, C., Jaramillo, C. (2007), Eocene-Pliocene planktonic foraminifera biostratigraphy from the continental margin of the southwest Caribbean: *Stratigraphy*, 4(4), 261–311.

Rogers, K.G., Goodbred, S.L. (2010). Mass failures associated with the passage of a large tropical cyclone over the Swatch of No Ground submarine canyon (Bay of Bengal). *Geology*, 38, 1051–1054.

Romero-Otero, G. A. (2009). Deepwater sedimentary processes in an active margin, Magdalena submarine fan, offshore Colombia: PhD Thesis, University of Oklahoma.

Romero-Otero, G.A., Slatt, R.M., Pirmez, C. (2010). Detached and shelf-attached mass transport complexes on the Magdalena deepwater fan. In: Mosher, D.C., Shipp, R.C., Moscardelli, L., Chaytor, J.D., Baxter, C.D.P., Lee, H.J., and Urgeles, R. (Eds.), *Submarine Mass Movements and Their Consequences*, Springer, Netherlands, 153-166.

Ross, W. C., Halliwell, B. A., May, J. A., Watts, D. E., Syvitski, J. P. M. (1994). Slope readjustment: a new model for the development of submarine fans and aprons. Geology, 22, 511–514.

Ruiz, C., Davis, N., Bentham, P., Price, A., Carvajal, D. (2000). Structure and tectonic evolution of the South Caribbean Basin, southern offshore Colombia: A progressive accretionary system: Extended abstract, *VII Simposio Bolivariano Exploración Petrolera en las Cuencas Subandinas*: Asociación Colombiana de Geólogos y Geofísicos del Petróleo (ACGGP), 334–340.

Saller, A., Dharmasamadhi, I.N.W. (2012). Controls on the development of valleys, canyons, and unconfined channel-levee complexes on the Pleistocene Slope of East Kalimantan, Indonesia. *Marine and Petroleum Geology*, 29, 15-34.

Sawyer, D. E., Flemings, P. B., Nikolinakou, M. (2014). Continuous deep-seated slope failure recycles sediments and limits levee height in submarine channels. *Geology*, 42(1), 15–18.

Scarselli, N., McClay, K., Elders, C. (2013). Submarine Slide and Slump Complexes, Exmouth Plateau, NW Shelf of Australia, In: Keep, M. & Moss, S.J (Eds.), *Western Australian Basins Symposium 2013,* Aug 18-21 2013 Perth, Petroleum Exploration Society of Australia.

Shanmugam, G. (2002). Ten turbidite myths. *Earth Science Reviews*, 58, 311–341.

Shanmugam, G., Lehtonen, L.R., Straume, T., Syvertsen, S.E., Hodgkinson, R. J., Skibeli, M. (1994). Slump and Debris-Flow Dominated Upper Slope Facies in the

Cretaceous of the Norwegian and Northern North Seas (61–67°N): Implications for Sand Distribution. *AAPG Bulletin.* 78 (6), 910-937.

Skene, K., Piper, D. J.W., Hill, P.A. (2002). Quantitative analysis of variations in depositional sequence thickness from submarine channel levees. *Sedimentology*, 49, 1411-1430.

Sobiesiak, M.S., Kneller, B., Alsop, G.I., Milana, J.P. (2016). Internal deformation and kinematic indicators within a tripartite mass transport deposit, NW Argentina. *Sedimentary Geology*.

Sprague, A.R., Garfield, T.R., Goulding, F.J., Beaubouef, R.T., Sullivan, M.D., Rossen, C., Campion, K.M., Sickafoose, D.K., Abreu, V., Schellpeper, M., Jensen, G.N., Jennette, D. C., Pirmez, C., Dixon, B.T., Ying, D., Ardill, J., Mohrig, D.C., Porter, M.L., Farrell, M.E., Mellere, D. (2005). Integrated slope channel depositional models: the key to successful prediction of reservoir presence and quality. In: offshore West Africa (abstract): *Colegio de Ingenieros Petroleros de Mexico, cuarto E-Exitep 2005*, Veracruz, Mexico, 1–13.

Spychala, Y. T., Hodgson, D. M., Flint, S. S., Mountney, N. P. (2015). Constraining the sedimentology and stratigraphy of submarine intraslope lobe deposits using exhumed examples from the Karoo Basin, South Africa. *Sedimentary Geology*, 322, 67-81.

Steffens, G.S., Biegert, E.K., Sumner, H.S, Bird, D. (2003). Quantitative bathymetric analyses of selected deepwater siliciclastic margins: receiving basin configurations for deepwater fan systems. *Marine and Petroleum Geology*, 20, 547-561.

Stevenson, C., Jackson, C.L., Hodgson, D.M., Hubbard, S. M, Eggenhuisen, J. (2015). Deep-water sediment bypass. *Journal of Sedimentary Research*, 85, 1058-1081.

Stow, D.A.V., Mayall, M. (2000). Deep-water sedimentary systems: New models for the 21st century. *Marine and Petroleum Geology*, 17, 125-135.

Stow, D.A.V., Piper, D.J.W. (1984). Deep-water fine-grained sediments: facies models. *Geological Society, London,* Special Publications, 15(1), 611-646.

Stow, D. A. V., Reading, H. G., Collinson, J. D. (1996). Deep seas. In: Reading, H. G. (Ed.), *Sedimentary Environments*, 3rd ed., Blackwell Science, 395-454.

Strachan, L. (2008). Flow transformations in slumps: a case study from the Waitemata Basin, New Zealand. *Sedimentology*, 55, 1311-1332.

Straub, K.M., Mohrig, D., McElroy, B., Buttles, J. (2008). Interactions between turbidity currents and topography in aggrading sinuous submarine channels: A laboratory study. *Geological Society of America Bulletin*, 120 (3-4), 368-385.

Strong, N., Paola, C. (2008). Valleys that never were: time surfaces versus stratigraphic surfaces: *Journal of Sedimentary Research*, 78, 579-593.

Talling, P.J. (2013). Hybrid submarine flows comprising turbidity current and cohesive debris flow: Deposits, theoretical and experimental analyses, and generalized models. *Geosphere*, 9(3), 460-488.

Talling, P.J. (2014). On the triggers, resulting flow types and frequencies of subaqueous sediment density flows in different settings. *Marine Geology*, 352, 155-182.

Talling, P.J., Sumner, E.J., Masson, D.G., Malgesini, G. (2012). Subaqueous sediment density flows: depositional processes and deposit types. *Sedimentology*, 59, 1937-2003.

Terlaky, V., Arnott, R. W. C. (2014). Matrix-rich and associated matrix-poor sandstones: Avulsion splays in slope and basin-floor strata. *Sedimentology*, 61(5), 1175-1197.

Terlaky, V., Rocheleau, J., Arnott, R. W. C. (2016). Stratal composition and stratigraphic organization of stratal elements in an ancient deep-marine basin-floor succession, Neoproterozoic Windermere Supergroup, British Columbia, Canada. *Sedimentology*, 63(1), 136-175.

Torelli, L., Sartori, R., Zitellini, N. (1997). The giant chaotic body in the Atlantic Ocean off Gibraltar: New results from a deep seismic reflection survey. *Marine and Petroleum Geology*, 14, 125–138.

Trenkamp, R., Kellogg, J.N., Freymueller, J.T., Mora, H.P. (2002). Wide plate margin deformation, southern Central America and northwestern South America, CASA GPS observations. *Journal of South American Earth Sciences*, 15(2), 57–171.

Trincardi, F., Argnani, A. (1990). Gela submarine slide: A major basin-wide event in the Plio-Quaternary foredeep of Sicily. *Geo-Marine Letters*, 10, 13–21.

Tripsanas, E. K., Piper, D. J., Jenner, K. A., Bryant, W. R. (2008). Submarine mass-transport facies: New perspectives on flow processes from cores on the eastern North American margin. *Sedimentology,* 55(1), 97-136.

Van der Hammen, T. (1958). Estratigrafía del Terciario y Maestrichtiano continentales y tectogénesis de los Andes Colombianos. *Boletín Geológico Ingeominas*, 6 (1- 3), 67–128.

Van Der Hammen, T. (1974). The Pleistocene changes of vegetation and climate in tropical South America. *Journal of Biogeography*, 3-26.

Van Der Merwe, W. C., Hodgson, D. M., Flint, S. S. (2011). Origin and terminal architecture of a submarine slide: a case study from the Permian Vischkuil Formation, Karoo Basin, South Africa. *Sedimentology*, 58(7), 2012-2038.

Vargas, C.A., Idárraga-García, J. (2014). Age Estimation of Submarine Landslides in the La Aguja Submarine Canyon, Northwestern Colombia. In: S. Krastel, J.H. Behrmann, M. Stripp, C. Berndt, R. Urgeles, J. Chaytor, K. Huhn, M. Strasser and C. Bonnevie Harbitz (Eds.), *Submarine Mass Movements and Their Consequences,* Springer International Publishing, Switzerland, 629-637.

Vinnels, J. S., Butler, R. W. H., McCaffrey, W. D., Paton, D. A. (2010). Depositional processes across the Sinú accretionary prism, offshore Colombia. *Marine and Petroleum Geology*, 27(4), 794–809.

Weimer, P. (1990). Sequence stratigraphy, seismic geometries, and depositional history of the Mississippi Fan, deep Gulf of Mexico*. AAPG Bulletin*, 74, 425-453.

Weimer, P. and Pettingill, H.S. (2007) A global overview of fields and discoveries in deep-water deposits. In: T. Nielsen, R.D. Shew, G.S. Steffens and J.R.J. Studlick (Eds.), *Atlas of Deepwater Outcrops*, AAPG Studies in Geology, 56, Shell Exploration and Production and AAPG, 12–16.

Weimer, P., Slatt, R. M. (2007). Deepwater reservoir elements: Mass-transport deposits and slides. In*: Introduction to the petroleum geology of deepwater settings,* AAPG Studies in Geology, 57(8), 9-419.

Weimer, P., Shipp, C. (2004). Mass transport complex: musing on past uses and suggestions for future directions. In: *Offshore Technology Conference*. Offshore Technology Conference.

Wynn, R. B., Cronin, B. T., Peakall, J. (2007). Sinuous deep-water channels: Genesis, geometry and architecture. *Marine and Petroleum Geology*, 24(6), 341-387.

Woodcock, N.H. (1976). Structural style in slump sheets: Ludlow Series, Powys, Wales. *Journal of the Geological Society,* London, 132, 399-415.

Yarbuh, I., Contreras, J. (2015). The interplay between deformation, erosion and sedimentation in the deep-water Mexican Ridges fold belt, western Gulf of Mexico basin. *Basin Research*, doi:10.1111/bre.12157

Zeng, H., Henry, S. C., Riola, J. P. (1998). Stratal slicing, part II: Real 3-D seismic data. *Geophysics,* 63(2), 514-522.

APPENDIX A

Quantitative Seismic Facies Analysis

Based on the methodology outlined by Tiago et al. (2014) to assess the seismic character of MTCs, a quantitative analysis of the characteristics of the seismic facies defined in Chapter 6 was performed. The objective was to confirm whether the variations on reflection continuity and structure identified through qualitative descriptions, was reflected in the magnitudes of seismic attributes.

Using Petrel®, three pseudo-horizons, separating four intervals of equal thicknesses within MTC C1 were created (Fig. A.1). Attribute extractions on each interval were calculated using RMS amplitude, maximum variance, average consistent dip angle, average local structural dip and average local structural azimuth. Rectangular polygons covering c. 10 km^2 and orientated approximately parallel to the interpreted flow direction were created on MTC seismic facies 1, 2 and 3 (Fig. A.2). In the case of seismic facies 2 and 3, polygons in the syncline and in the basin-low were created. These polygons were then subdivided by lines spaced every 400 m. Points every 100 m were created along these lines (Fig. A.2).

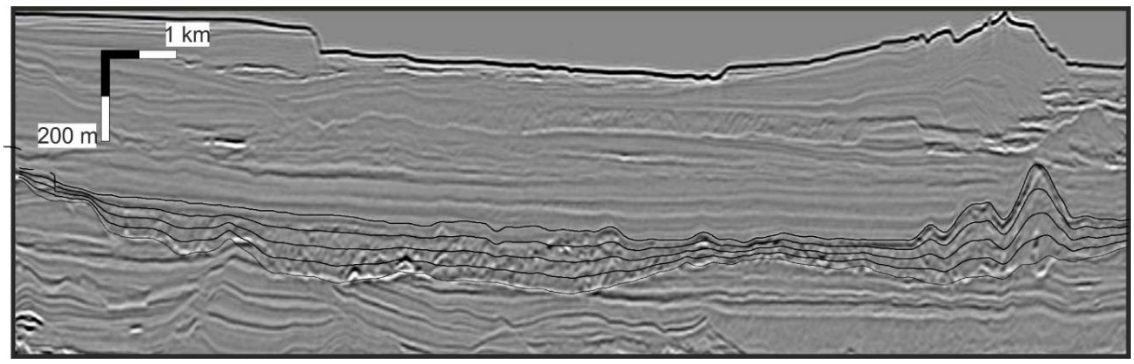

Figure A1. Pseudo-horizons in MTC C1 used to compute interval attribute extractions.

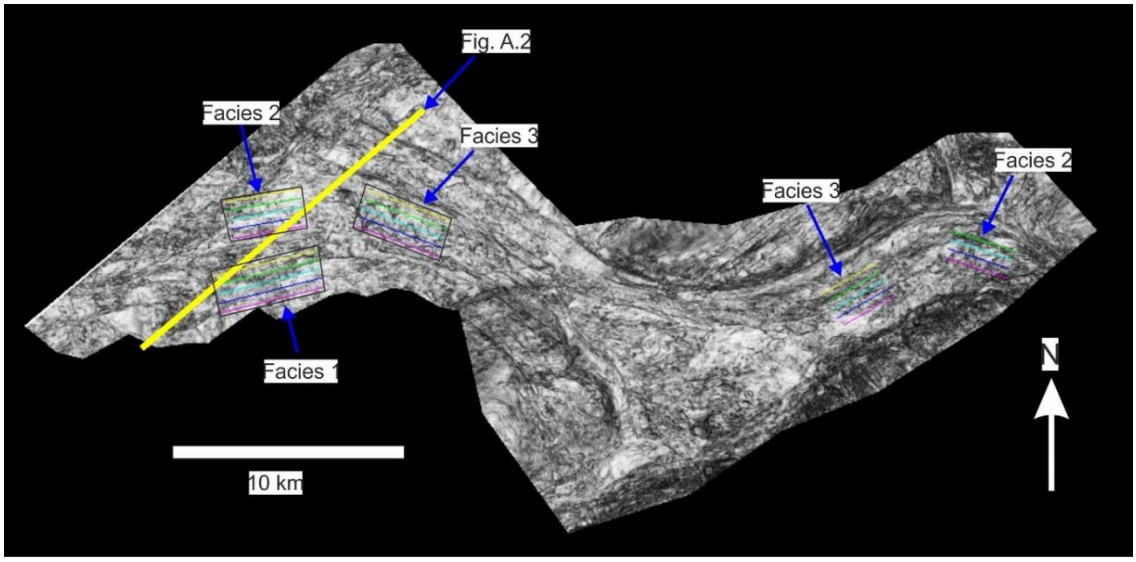

Figure A2. Polygons subdivided by equally-spaced lines in in which attribute values were extracted every 100 m.

For each of the stratigraphic sub-divisions, the value of each of the seismic attributes at every point along the parallel lines was computed. These values were then exported to Origin® where they were normalised and plotted on triangular plots (Fig. A.3).

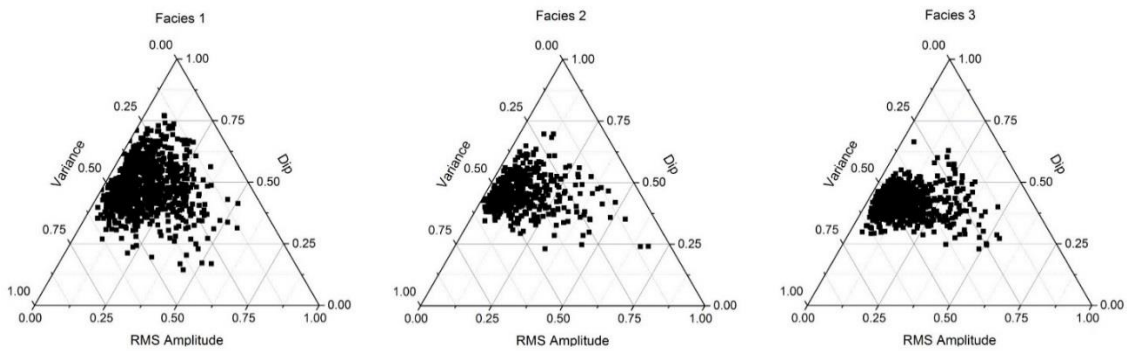

Figure A3. Ternary diagrams showing normalised values of variance, RMS amplitude and dip for facies 1, 2 and 3.

The range of values for RMS amplitude, variance and dip are similar for the three seismic facies. However, it is apparent that in facies 1 the values are more scattered confirming the more chaotic character defined through visual inspection. This probably reflects a higher degree of mixing and disaggregation (cf. Alves, 2014). Facies 2 (debrites with semi-continuous to discontinuous folded reflections) and 3 (imbricate

thrust and fold systems) display similar amplitude ranges but the amplitudes in facies 2 are more clearly skewed towards lower values. In facies 3, values of variance and dip are more clearly concentrated towards the middle of the vertical axis, while in facies 2 they are more scattered. This analysis therefore confirms that facies 3 contains more continuous, consistently dipping reflections than facies 2 and that facies 1 is the most chaotic and possibly most disaggregated seismic facies.